Molecular determinants of astrocyte morpho-functional changes in Alzheimer's disease

by

Norah Elisa Ulzheimer

A thesis submitted in partial fulfilment of the requirements for the degree of
Doctor of Philosophy at the University of Central Lancashire

June 2019

STUDENT DECLARATION FORM

Type of Award   **Doctor of Philosophy**

School   **Pharmacy & Biomedical Sciences**

1.   Concurrent registration for two or more academic awards

I declare that while registered as a candidate for the research degree, I have not been a registered candidate or enrolled student for another award of the University or other academic or professional institution

2.   Material submitted for another award

I declare that no material contained in the thesis has been used in any other submission for an academic award and is solely my own work

3.   Collaboration

Where a candidate's research programme is part of a collaborative project, the thesis must indicate in addition clearly the candidate's individual contribution and the extent of the collaboration. Please state below:
N/A

4.   Use of a Proof-reader

No proof-reading service was used in the compilation of this thesis.

Signature of Candidate

Print name: Norah Elisa Ulzheimer

Abstract

As people are living longer, neurodegenerative disorders such as Alzheimer's disease (AD) are becoming more prevalent but the pursuit for treatments has yet to deliver satisfactory results. By the time AD is diagnosed, the typical hallmarks of neurofibrillary tangles and senile plaques are present and cognitive decline has occurred, pointing future research towards the early stages of the disease. Indeed, recent research has unearthed cell-autonomous atrophy of astrocytes in the early stages of AD, characterised by decreased cell size and loss of processes. This aberrant astrocyte morphology was present in both sporadic and familial AD models and manifests independently of senile plaques. These findings challenge the neuron-centric view of AD, granting glial cells an undeniable role in neurodegeneration. The exact mechanisms underlying aberrant astrocyte morphology are entirely unexplained. This thesis explores how the Cas-proteins, previously identified by genome-wide association studies as genetic risk-factors for late-onset AD, NEDD9 and CASS4 act as regulators of astrocyte morphology and function. This could potentially unearth mechanisms that lead to astrocyte atrophy in AD.

This was achieved by transiently transfecting primary human cortical astrocytes *in vitro* with vectors mediating the overexpression or siRNA-induced knock-down of either NEDD9 or CASS4. Concurrent expression of GFP, which localised throughout the entire cell, permitted the visualisation of complete cellular morphologies, including fine processes. Morphological analysis by visual binning into morphological subtypes or 3D reconstruction followed by morphometric quantifications (e.g. surface area, volume) revealed that overexpression or knock-down of either NEDD9 or CASS4 induced significant changes in astrocyte morphology compared to controls and, specifically, depletion of the proteins lead to astrocyte atrophy, mimicking a phenotype previously

found in other studies of AD models. Moreover, manipulation of Cas-protein levels induced altered expression and sub-cellular distribution of key astrocyte functional markers, including glial fibrillary acid protein (GFAP) and the calcium-binding protein, S100B; further mimicking the pathological phenotype reported in human iPSC astrocyte models of AD.

Hence, it appears that both NEDD9 and CASS4 are capable of inducing morphological and functional changes in human astrocytes and may therefore contribute to astrocyte pathology in AD. This implies that the Cas-proteins or binding partners are potentially contributing to astrocyte atrophy in AD. This thesis delivers ample grounds for further research which could identify yet unexplored pathways, which could be used for new early diagnostic tests or therapeutic measures.

Table of contents

List of Figures

List of Tables

List of abbreviations

1321N1	Human stage 2 astrocytoma cell line
3xTg AD	Triple transgenic mouse model of AD
Aβ	Amyloid beta
Abl	Abelson murine leukaemia kinase
AD	Alzheimer's disease
APP	Amyloid precursor protein
AURKA	Aurora-A kinase
BBB	Blood brain barrier
BSA	Bovine Serum Albumin
CASS4	CAS Scaffolding Protein Family Member 4/HEF1-EFS-p130Cas-like protein
CMV	Cytomegalovirus (promoter)
CNS	Central nervous system
copGFP	Green fluorescent protein 2 from the copepod (*Pontellina plumata*)
Crk	Proto-oncogene c-Crk
DAPI	4' 6-diamidino-2-phenylindole
dH$_2$O	De-ionised Water
DMEM	Dulbecco's Minimum Essential Medium
EGFP	Enhanced Green Fluorescent Protein
EOAD	Early-onset alzheimer's disease
FAK	Focal adhesion kinase
GFP	Green Fluorescent Protein
GOI	Gene of interest
GWAS	Genome-wide association studies
HEF-1	Human Enhancer of Filamentation 1
HeLa	Human epithelial cervical adenocarcinoma cell line
HEPL	HEF1-EFS-p130Cas-like
IL-6	Interleukin 6

IPSC	Induced pluripotent stem cells
LIF	Leukaemia inhibitory factor
LOAD	Late-onset alzheimer's disease
MAPK	Mitogen-activated protein kinase
mRNA	Messenger RNA
NF-κB	Nuclear factor kappa-light-chain-enhancer of activated B cells
NHA	Normal human astrocytes
NEDD9	Neural precursor cell expressed developmentally downregulated protein 9
PBS	Phosphate Buffered Saline
PSEN1	Presilinin 1
PSEN2	Presilinin 2
PTK2B	Protein tyrosine kinase 2 beta
qRT-PCR	Real-Time Quantitative Reverse Transcription PCR
RT-PCR	Real time polymerase chain reaction
S100B	S100 calcium-binding protein B (human)
S100β	S100 calcium-binding protein B (mouse)
SDS-PAGE	Sodium Dodecyl Sulphate – Polyacrylamide Gel Electrophoresis
SH3	Src homology 3
STAT3	Signal transducer and activator of transcription 3
SVGp12	Human foetal astrocyte cell line
siRNA	small interfering Ribonucleic Acid
TF	Transcription factor
v/v	Volume per Volume
WB	Western Blot
WHO	World Health Organisation
w/v	Weight per Volume

Acknowledgements

This is by far the hardest page to write. How does a scientist, who is now 'skilled' in the reporting of cold hard facts, write about thanksgiving and emotional stuff? Apologies in advance for my attempt at clumsily stringing sentences together and a rather poor choice of words – I shall give it my best shot.

Starting with an easy one, I would like to express my gratitude to the School of Pharmacy and Biomedical Sciences and UCLan for the funding of this project, for always making me feel welcome, and giving me a sense of belonging in a place far away from home.

No matter how this page is supposed to be structured, the first person I thought of whilst writing the word 'acknowledgements' at the top of this page, is my supervisor Dr Vicky Jones. You have been an incredible mentor and I owe absolutely every bit of 'what makes me a scientist' to you. Your passion for the subject and the dedication to your students is second to none and I can only dream of filling those big boots one day.

Furthermore, I would like to give huge thanks to my other supervisors, Dr Chris Smith and Dr Lisa Shaw for their continuing support and all the inspiration they have given me. Together, all three of you have been a smashing supervisory team and I have been very lucky to have had the chance to work with you.

Naturally, I would like to thank absolutely everyone in the faculty, far too many to mention, who helped me with this project and supported me during my PhD. Special thanks go out to Dr Clare Lawrence, Dr Julie Burrows and Dr Sarah Dennison, your support and guidance have been invaluable. I would also like to thank all the cleaning and maintenance staff in Darwin building, firstly for keeping our labs and offices clean and secondly for always having a smile for me when I got to the lab – it made every day start that bit better.

I would also like to thank all my colleagues who had to put up with me over the years, particularly Zenab Butt, you have been a fantastic listener and a true friend - Western blotting will never be the same without you. You still owe me some jalebi though!

Special thanks go to Dr Catherine Coxon, my 'wicked sister', confidante and voice of reason – you have been an invaluable friend and made every horrible day bearable with your wit, humour and cups of tea. I know how much you hate the gushy stuff, but this is my thesis, so suck it up buttercup.

This is way longer than I had planned (apologies to the reader at this point), I shall try to keep the rest brief. I would like to thank Clare Hayes, my very first true friend in the UK, who encouraged me and pushed me to apply to university in the first place.

I would like to thank my Mama for passing her grit and determination on to me - believe me, it's what got me through this PhD. Thanks to my Papa who always believed in me, gave me the strength to stand up tall, and who has been readily on the other end of the phone during the entire process of this thesis. Thanks to my Oma who has been my biggest fan and encouraged me even when she had no clue what I was talking about. I know you would love to see your name in a book one day, so here it is.

Last, but not least, I want to thank the man who had to endure it all, the hair-pulling, the crying, the feet-stamping, the shouting and the crying again – the lot. Geoff, you made me laugh EVERY SINGLE DAY and I cannot think of anything that helped me more than this. Proper mate.

Chapter 1
Introduction

1 Chapter 1 – Introduction

1.1 Alzheimer's disease

Alzheimer's disease (AD), first described by Alois Alzheimer (Alzheimer, 1910), is a progressive neurodegenerative disorder and the leading cause of dementia worldwide (Feigin 2019). The World Health Organisation (WHO) reported 81.1 million cases of Alzheimer's disease last year and estimates 152 million people will be suffering from dementia by 2050 (Patterson, 2018). These figures and the associated cost of health care demonstrate the need for continuing research into AD.

AD in its familial or sporadic form manifests over several years; ranging from short-term memory loss to severe cognitive decline, ultimately leading to complete loss of bodily functions and thus death. Pathophysiologically, AD is characterised by synaptic dysfunction, accumulation of β-amyloid (Aβ) aggregates ("senile plaques") and intracellular neurofibrillary tangles of hyperphosphorylated tau, and eventual neuronal loss (Braak *et al.*, 1989, Hardy and Selkoe, 2002, Holtzman *et al.*, 2011). Neurodegeneration arises in the entorhinal cortex, advances to the hippocampus and finally manifests in the frontal, temporal and parietal lobes, leading to extensive loss of grey matter (Karas *et al.*, 2004, Thompson *et al.*, 2003, Janke *et al.*, 2001).

Hypotheses on how exactly AD begins and progresses are plentiful, with most centred on the archetypical hallmark of extracellular Aβ plaques. This aberrant protein interferes with cell signalling, particularly intracellular calcium signalling, and protein synthesis, ultimately leading to inflammatory and stress responses and thus cell death (Abramov *et al.*, 2003). The amyloid hypothesis posits that Aβ aggregates trigger the onset of AD.

First suggested by Glenner in 1984, this hypothesis was widely accepted (Glenner *et al.*, 1984, Masters *et al.*, 1985, Hardy and Allsop, 1991) and over three decades, research has focused on senile plaques as a therapeutic target (Braak *et al.*, 1989, Chen *et al.*, 2000, Haass and Selkoe, 2007, Hsiao *et al.*, 1996). Unfortunately, treatments targeted to Aβ have yet to yield satisfactory clinical results, prompting criticism within the field that a shift in the focus of AD research is necessary and overdue (Golde *et al.*, 2011, Castello *et al.*, 2014, Moreno-Treviño *et al.*, 2015, Kametani and Hasegawa, 2018).

There are several pitfalls with amyloid deposits as diagnostic and therapeutic targets for AD. Aβ plaques are also found in the healthy aging brain, in the absence of pathologies, diminishing diagnostic value of amyloid plaques (Davis *et al.*, 1999, Fagan *et al.*, 2009). Furthermore, the appearance of senile plaques correlates poorly with cognitive decline; hence the anti-Aβ treatments developed to date have only been used at the symptomatic stage, when cognitive decline has already occurred, hence limiting their curative potential (Rygiel, 2016, Kametani and Hasegawa, 2018). Moreover, it has been suggested that plaque formation might actually be a protective mechanism to corral the highly toxic soluble Aβ species to a larger insoluble mass (Gandy *et al.*, 2010, Lublin and Gandy, 2010); and prevention of this mechanism might actually exacerbate AD pathology.

The second hallmark of AD, tau neurofibrillary tangles (NFT) appear to provide a superior diagnostic and therapeutic target. Tau is a soluble phosphoprotein predominantly, but not exclusively, found in neurons of the healthy brain (Weingarten *et al.,* 1975), where it interacts with and stabilises microtubules. Tau activity is regulated by splicing (six isoforms) and post translational modifications, such as phosphorylation (Lindwall and Cole, 1984, Alonso *et al*., 1994, Wray *et al*., 2008). In AD, tau is hyperphosphorylated, which is believed to induce insoluble aggregates (Bancher *et al.,* 1989, Hanger *et al*., 1991, Kopke *et al.,* 1993). Hyperphosphorylated tau is not only a

hallmark of AD but occurs in several neurodegenerative diseases (tauopathies), such as Pick disease, progressive supranuclear palsy and Parkinsonism with fronto-temporal dementia (Irwine, 2017, Goetz *et al.,* 2018). Hyperphophorylated tau is believed to propagate from cell to cell in a prion-like manner (Clavaguera *et al.*, 2009, Nonaka *et al.*, 2010, Goedert and Spillantini, 2017) and correlates with cognitive impairment (Braak and Braak, 1991, Bejanin *et al.*, 2017), giving tau accumulation superior diagnostic value than Aβ. Although significant progress has been made, the exact mechanisms involved in the generation of aggregated tau remain unknown, hampering efforts to utilise tau as a therapeutic target (Himmelstein *et al.*, 2012, Kametani and Hasegawa, 2018).

The microtubule associated protein tau (*MAPT*) gene encodes tau and several tauopathies can be traced back to mutations in the *MAPT* gene, such as Pick's disease (Pollock *et al.,* 1986, Sergeant *et al.,* 2005). Although abnormal phosphorylation of tau is an early hallmark of neurodegeneration, AD is the most common secondary tauopathy with no known mutations of *MAPT* (Simic *et al.,* 2016, Terry, RD., 1996). Moreover, the exact mechanisms leading to these hallmarks are yet to be fully elucidated. Hence, there is a renewed research focus on understanding the causes and pathogenesis of AD in a bid to reveal alternative therapeutic and diagnostic targets.

1.2 Established risk genes of Alzheimer's disease

The vast majority of cases of AD are of a sporadic or late (>65 years) onset (LOAD) in nature. Much of what is known is based on the familial or early-onset form of AD (EOAD), which accounts for less than 2% of AD cases (Rosenthal and Kamboh, 2014). Almost all cases of EOAD are familial in nature and can be traced to several known mutations within three genes, *APP* (amyloid precursor protein), *PSEN1* and *PSEN2*

(presenilins 1 and 2) (Bagyinszky *et al.*, 2016, Lanoiselee *et al.*, 2017, Sherrington *et al.*, 1995, Campion *et al.*, 1999). Previously thought to be idiopathic, it is now understood that late-onset Alzheimer's disease (LOAD) also entails a genetic component and several genes which confer increased risk of developing the disease have been identified (Bertram *et al.*, 2008, Piaceri *et al.*, 2013).

The most widely established and strongest genetic risk for LOAD is the ε4 allele of the *APOE* gene. Encoding apolipoprotein E (ApoE), a vital component and regulator of lipid metabolism and involved in Aβ clearance. The ε4 allele has been shown to correlate with an increased risk of both familial/early and sporadic/late forms of AD (Chartier-Harlin *et al.*, 1994, Kim *et al.*, 2009, Corder *et al.*, 1993, Morris *et al.*, 2010). While this is a major advancement for our understanding of LOAD risk, only around half of individuals developing LOAD carry the APOE ε4 allele (Huang *et al.*, 2004, Naj *et al.*, 2011), raising the question of the aetiology in the rest of LOAD cases.

1.3   Emerging Alzheimer's disease risk genes

In a quest to elucidate the pathogenesis of LOAD, genome-wide association studies (GWAS) were used to search for LOAD risk genes (Lambert *et al.*, 2009; Harold *et al.*, 2009; Seshadri *et al.*, 2010; Naj *et al.*, 2011; Hollingworth *et al.*, 2011; Lee *et al.*, 2011; Reitz *et al.*, 2013) These studies have led to the identification of almost 30 susceptibility loci harbouring single nucleotide polymorphisms (SNPs) which correlate with an enhanced risk of developing LOAD. Since the identification of these risk genes, very few studies have attempted to define how they might actually influence LOAD development. Those which have been published have focused on functions and pathways known to be affected or altered in LOAD. These include genes implicated with the immune system,

CD33, CR1, HLA-DRB1-DRB5, MS4A, MEF2C, TREM2 (Bradshaw *et al.*, 2013, Kok *et al.*, 2011, Lambert *et al.*, 2013, Antúnez *et al.*, 2011, Tang *et al.*, 2016, Jonsson *et al.*, 2013); lipid transport and cholesterol metabolism, *ABCA7, CLU, PLD3, SORL1* (Hollingworth *et al.*, 2011, Harold *et al.*, 2009, Cruchaga *et al.*, 2014, K *et al.*, 2008) and endocytosis *BIN1, PICALM, CD2AP, EPHA1, SLC24A4/RIN3* (Chapuis *et al.*, 2013, Harold *et al.*, 2009, Chen *et al.*, 2015, Lambert *et al.*, 2013, Rosenthal and Kamboh, 2014).

Among the identified LOAD risk loci are polymorphic variants within *NEDD9* (Neural precursor cell expressed developmentally down-regulated protein 9) and *CASS4* (Cas Scaffolding Protein Family Member 4) (Li *et al.*, 2008, Lambert *et al.*, 2013). Follow-up studies showed that one SNP in *NEDD9* (rs760678) and three SNPs in *CASS4* (rs7274581, rs16979934 and rs6024870) had the strongest association with LOAD development (Li *et al.*, 2008, Fu *et al.*, 2012, Xing *et al.*, 2011, Wang *et al.*, 2012, Rosenthal and Kamboh, 2014). These polymorphisms appear in non-coding regions of NEDD9 and CASS4, including transcription factor binding sites and intron splice sites, hence it is predicted that these SNPs confer altered (likely reduced) expression of these proteins in carrier individuals (Beck *et al.*, 2014).

Interestingly, both NEDD9 and CASS4 are members of the same Cas-proteins family, one which has not previously been linked to AD. That both of these paralogous proteins, together with a shared interacting partner in the form of Protein Tyrosine Kinase 2 Beta (PTK2B), were identified by multiple groups working independently is intriguing and would be expected to generate significant interest. However very few studies have focused on NEDD9 or CASS4 involvement in LOAD or its functions in normal brain physiology. This may be owed to low frequencies of the risk variants in populations, as

NEDD9 rs760678 occurs with an average frequency of 34% and *CASS4* variants are even less common with rs7274581 (10%), rs16979934 (5%), and rs6024870 less than 1% (Wang *et al.,* 2012, Xing *et al*., 2011, Laumet *et al.,* 2010, Lin *et al*., 2017). Although more studies are needed, so far, *NEDD9* and *CASS4* SNPs have been shown to correlate with only a low risk of developing LOAD (Chaudhry *et al*., 2015, Rosenthal *et al.,* 2014, Wang *et al.,* 2015) and are less frequently found than other risk variants, such as *APOE*. However, at the beginning of this thesis, the Cas-proteins were the only proteins, implicated as LOAD 'risk genes', involved in cell morphology and hence of interest in the investigation of astrocyte atrophy.

1.4 Cas-proteins

The Cas-protein, NEDD9/CasL/Hef1 (Law *et al.*, 1996, Minegishi *et al.*, 1996), CASS4/HEPL (Singh *et al.*, 2008), p130Cas/BCAR1 (Sakai *et al.*, 1994) and EFS/Sin (Ishino *et al.*, 1995) make up a family of scaffolding proteins and are highly involved in signalling pathways, acting as central 'nodes' for various processes including cell growth, cell survival, migration and adhesion (Beck *et al.*, 2014).

Although lacking enzymatic activity, Cas-proteins harbour four distinct domains, including the SH3 (Src homology 3) which facilitates the binding of protein substrates such as the tyrosine kinases protein tyrosine kinase 2 Beta (PTK2B) and focal adhesion kinase (FAK), Figure 1.1 (Tikhmyanova *et al.*, 2010). Adjacent to the SH3 domain is a highly conserved largely unstructured substrate binding domain containing varying numbers of YxxP motifs, which create binding sites upon phosphorylation for partners with SH2 domains; predominantly adaptor molecules such as the proto-oncogene Crk (Roselli *et al.*, 2010, Sawada *et al.*, 2006), Next is a highly variable four-helix bundle which provides further docking sites for other interacting partners such as molecular chaperones and signalling adaptor proteins (Briknarova *et al.*, 2005, Vuori *et al.*, 1996).

Finally, at the C-terminus is highly conserved and might mediate homo- or heterodimerization with other Cas-proteins (Law *et al.*, 1999) and is predicted to mediate binding to a raft of other proteins including those containing helix-loop-helix domains and E3 ubiquitin ligases (Tikhmyanova *et al.*, 2010, Singh *et al.*, 2007).
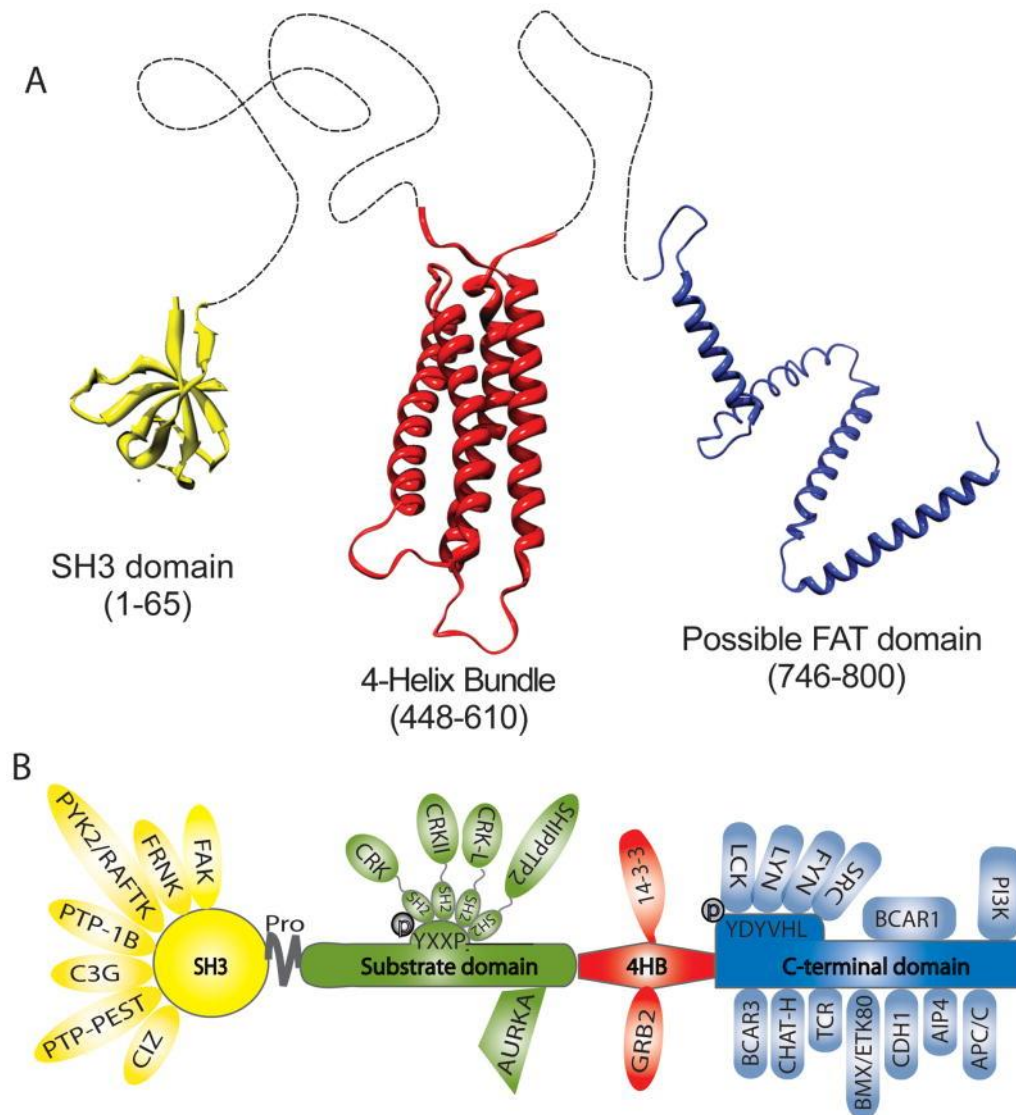
Figure 1.1 General structure of the Cas-proteins family members

> *All Cas-proteins comprise four distinct similarly structured domains including an SH3 domain, unstructured substrate binding domain, four-helix bundle and C-terminal domain (A). B indicates where some of the key Cas-proteins interacting partners have been found to bind. Note, while CASS4 and NEDD9 retain this overall domain structure, not all identified binding proteins are known to interact with these two family members. (Tikhmyanova et al., 2010)*

Despite their overall structural similarities, the individual domains do vary somewhat between Cas-protein family members and hence so do their ability to bind other proteins. Moreover, their varied tissue-specific expression and subcellular localisations suggests that each of the Cas-protein may be capable of contributing to distinct cellular processes (Law *et al.*, 1996, Singh *et al.*, 2008, Tikhmyanova *et al.*, 2010).

1.4.1 Neural precursor cell expressed developmentally down-regulated protein 9 (NEDD9)

NEDD9 (also known as HEF1) is abundantly expressed in many tissues (Fashena *et al.*, 2002, Minegishi *et al.*, 1996, Aquino *et al.*, 2008, Chang *et al.*, 2012), although expression levels are thought to vary greatly (Law *et al.*, 1998). NEDD9 (isoform 1) has a molecular weight of 93kDa, which occurs as two larger, phosphorylated versions of 105kDa and 115kDa (Singh *et al.*, 2007) and three cleaved isoforms of the protein 65, 55 and 28kDa have been identified and (Law *et al.*, 2000); expression of these isoforms is cell cycle dependant (Fashena *et al.*, 2002, Singh *et al.*, 2007).

Similar to other Cas-proteins, NEDD9 functions as a scaffold protein and regulates the assembly of signalling molecules in a number of cellular signalling cascades (Law *et al.*, 1996, Law *et al.*, 1998, Pugacheva and Golemis, 2005, Manie *et al.*, 1997). Binding partners of NEDD9 include kinases, such as aurora kinase A (AURKA), FAK and PTK2B; involved in apoptosis, adhesion, invasion and migration (Beck *et al.*, 2014, Singh *et al.*, 2007, Tikhmyanova *et al.*, 2010). Kinase activation depends on NEDD9 expression levels, which themselves are cell cycle regulated (Law *et al.*, 1998). Increased expression leads to phosphorylation of NEDD9 motifs by the proto-oncogene tyrosine-protein kinase, Src, to create additional docking sites for SH2 domain-containing partner proteins,

such as Crk. This results in the assembly of signalling complexes, capable of structurally rearranging the cytoskeleton (Aquino *et al.*, 2008, Deneka *et al.*, 2015, Manie *et al.*, 1997). Furthermore, believed to be anchored to focal adhesions and the cytoskeleton, NEDD9 has been shown to be sensitive to mechanical forces via its C-terminus; exposing yet more binding domains in response to cell stretching (Tamada *et al.*, 2004). As such, NEDD9 is essential for the maintenance of structural plasticity (Dent, 2017, Haseleu *et al.*, 2013) and plays an important role in translating internal and external signals to alterations in cellular morphology via regulation of the cytoskeleton (Law *et al.*, 1998).

Previously believed to be primarily cytoplasmic, NEDD9 is active in several cellular compartments (including the nucleus, Golgi and endoplasmic reticulum) and hence plays a role in coordinating signalling between them (O'Neill and Golemis, 2001, Singh *et al.*, 2007, Law *et al.*, 1998). Evidence has been found that NEDD9 is able to couple cell cycle regulation to morphological alterations, notably adhesion and migration (Law *et al.*, 1998, Dadke *et al.*, 2006, Rousseau *et al.*, 2015). Unsurprisingly therefore, NEDD9 has received a great deal of attention in regard to its role in cancer.

By far the majority of published studies on NEDD9 have centred on its role in the progression of various cancers, revealing this Cas-protein to be a major determinant of cancer metastasis (Nikonova *et al*, 2014). Overexpression of NEDD9 has been shown to promote cancer cell migration and invasion (Gabbasov *et al.*, 2018, Feng *et al.*, 2015, Li *et al.*, 2011, Izumchenko *et al.*, 2009), and induce the growth of cellular processes in epithelial-derived cancer cells (Bargon *et al.*, 2005). Related to the brain, NEDD9 has been identified as a regulator of invasion in glioblastoma, where a high expression of the protein correlates with a decrease in progression-free survival (Speranza *et al.*, 2012). Other studies have also confirmed a correlation between high NEDD9 expression and

poor survival in glioma and neuroblastoma; whereby NEDD9 depletion decreases cell migration (Zhong *et al.*, 2014, McLaughlin *et al.*, 2014, Kondo *et al.*, 2012).

Outside of cancer, NEDD9 has been shown to regulate neural crest cell migration during embryogenesis, a process vital for proper brain development (Aquino *et al.*, 2008, Merrill *et al.*, 2004). Additionally, the same study proposed NEDD9 expression as a master switch for cell morphology; inducing cell rounding when depleted and elongation when highly expressed (Aquino *et al.*, 2008), implicating NEDD9 expression in cell morphology. Moreover, via its activation of AURKA, NEDD9 plays a role in both centrosome formation and primary cilia disassembly (Pugacheva and Golemis, 2005, Pugacheva *et al.*, 2007). Taken together, these studies clearly implicate NEDD9 as a major regulator of cell morphology determination.

1.4.2 Cas Scaffolding Protein Family Member 4 (CASS4)

CASS4 (also known as HEPL) is the most recent addition to the Cas-proteins family (Singh *et al.*, 2008). Sharing some structural homology with its paralogues, its activity is believed to be dependent on the presence of other Cas-protein, although this is not yet conclusively proven (Deneka *et al.*, 2015). There are three known isoforms of CASS4 87kDa (isoform 1), 74kDa (isoform 2) and 38kDa (isoform 3). It is not known if highly phosphorylated or cleaved isoforms, comparable to paralogue NEDD9, exist or if these are also cell cycle related. Very little is known about the biological functions of CASS4, but it is assumed to act in a similar manner to its paralogues. As for NEDD9, overexpression of CASS4 has been suggested to correlate with tumour severity and poor prognosis in cancers, although direct mechanistic studies are lacking (Li *et al.*, 2016, Miao *et al.*, 2013). Determination of discrete roles for CASS4 is complicated by the abundant cellular expression of other Cas-proteins, such as NEDD9 and BCAR1. Nonetheless, its

subcellular localisation implies CASS4 activity at focal adhesions, and interactions between CASS4 and FAK and Src kinases have been experimentally confirmed, despite CASS4 lacking a common site found in other Cas-proteins which facilitates Src binding (Hassan *et al.*, 2018, Singh *et al.*, 2008, Tikhmyanova *et al.*, 2010). Furthermore, overexpression of CASS4 has been demonstrated to be sufficient to induce FAK phosphorylation, leading to cell spreading, albeit to a lesser degree than for NEDD9 (Li *et al.*, 2016, Singh *et al.*, 2008). Interestingly, CASS4 exerted a bimodal effect on cell migration; enhancing migration in a subset of cells, while impeding it in another. While the reason for this has not been explored, it may suggest that CASS4's effects might depend upon the relative amounts of other Cas-proteins in each cell, further supporting the idea of cell type-specific roles.

During the initial identification of CASS4, real-time PCR (RT-PCR) revealed high expression of CASS4 mRNA in spleen and lungs as well as in leukaemia and ovarian cancer cells (Singh *et al.*, 2008). CASS4 mRNA expression, and particularly the protein expression has since been described in other tissues, including neuronal cells in the cerebral cortex and hippocampus (Kim *et al.*, 2014) and in microglia (Skene and Grant, 2016). Notwithstanding, a lack of basic knowledge regarding CASS4 tissue expression levels remains.

1.4.3 NEDD9 and CASS4 in Alzheimer's disease

Although a recent study employing the expression weighted cell-type enrichment method, found that CASS4 was the only protein with a lower expression in glial cells than expected in AD brain samples (Skene and Grant, 2016), there is no empirical data to confirm the expression levels of CASS4 in glial cells in LOAD.

CASS4 has been implicated as a modulator of tau in a drosophila model (Dourlen *et al.*, 2016) and meta-analysis of neuropathologic features of AD found CASS4 to be associated with tau neurofibrillary tangles in brains with AD (Beecham *et al.*, 2014), which was confirmed in a population study of 601 participants (Makela *et al.*, 2018).

One recent study investigated the effect of NEDD9 on brain function using NEDD9 knock-out mice (Knutson *et al.*, 2016). These mice suffer extensive dendritic spine loss in the dentate gyrus and CA1 regions of the hippocampus and hence display significant deficits in learning ability in the Morris water maze test, mimicking some of the deficits usually seen in AD transgenic mouse models (Martinez-Coria *et al.*, 2015, Stimmell *et al.*, 2019). The study concluded that NEDD9 is essential for hippocampal spine maintenance, a role which is heavily influenced by astrocytes.

Very few studies have explored the role of NEDD9 and CASS4 in LOAD and there is no knowledge of the Cas-protein expression or role in astrocytes. This thesis is the first attempt to establish NEDD9 and CASS4 expression in astrocytes, to identify a possible role of the proteins in cell morphology and how the risk variants may contribute to LOAD pathology.

1.5   Astrocytes

Astrocytes (also known as astroglia) are among the most heterogenous cells in the human brain. This subset of glial cells has several roles in the central nervous system (CNS). Astrocytes are critical during development, as they modulate synapse formation (Casse *et al.,* 2018). These cells continue to support, maintain and influence synaptic function (Fields *et al.*, 2015, Nishida and Okabe, 2007), they enwrap pre- and postsynaptic membranes, building a functional unit termed the tripartite synapse (Perrera *et al.*, 2009),

which permits control of homeostasis in the neural tissue (Mohamet *et al.*, 2018). Furthermore, these cells are part of the glymphatic pathway via the astrocyte endfeet, a connection to the vascular system, allowing transport and clearance of metabolites (Bushong *et al.*, 2004, Perez-Alvarez *et al.*, 2014, Nedergaard *et al.*, 2002, Iadecola and Nedergaard, 2007); astrocyte endfeet are an integral part of the blood brain barrier (BBB). On the whole, astrocytes are essential for the proper functioning of neurones, are fundamental to memory formation and are crucial components in the adaptive plasticity of the CNS (Verkhratsky and Nedergaard, 2018).

1.5.1 Astrocyte morphology

As the name suggests, astrocyte morphology is roughly stellate, typically consisting of a cell body with numerous, often branching, processes. As recognised by Ramón y Cajal over 100 years ago, astroglial morphologies are highly varied (Garcia-Lopez *et al.*, 2010). These morphologies roughly correlate with neuroanatomical location and specific functions (Parpura *et al.*, 2012, Zorec *et al.*, 2015). Astrocytes can be generally categorised into the protoplasmic of the grey matter (Figure 1.3, A), which possess thicker, defined processes splitting into finer branches; and fibrous astrocytes of the white matter (Figure 1.3, B), morphologically differing by copious fibrous processes (Rodriguez *et al.*, 2009, Sofroniew and Vinters, 2010). Additionally, several subtypes of the above have been identified, including interlaminar astrocytes (Colombo and Reisin, 2004), varicose projection astroglia (Oberheim *et al.*, 2009), Bergmann glia and Müller glia (Eroglu and Barres, 2010). It is generally accepted that further subpopulations of astrocytes are yet to be defined and likely play diverse roles in health and disease (Miller, 2018).
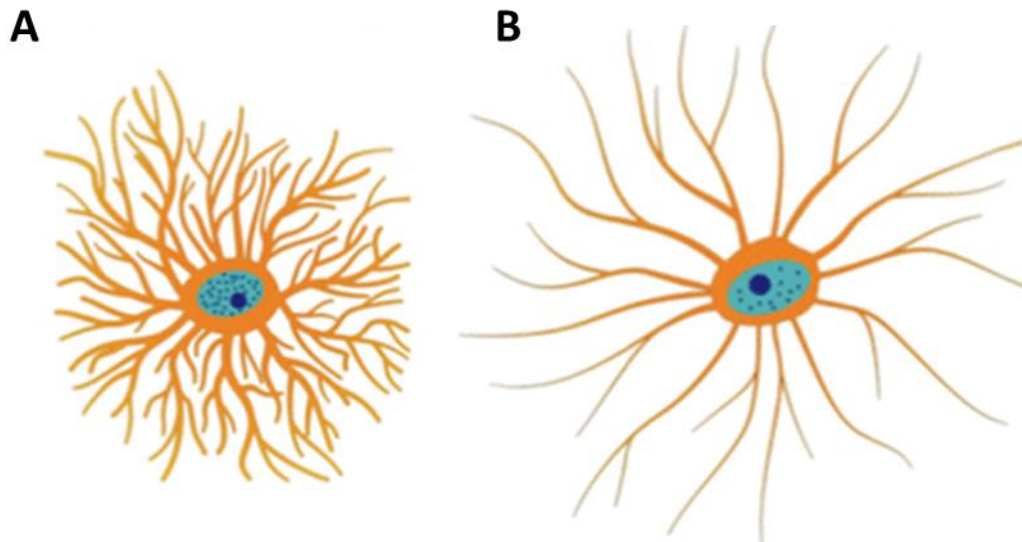
Figure 1.2 Diagram showing gross morphologies of protoplasmic (A) and fibrous (B) astrocytes

(Adapted from Carson et al., 2018)

1.5.2 Astrocyte function

The unique morphology of astrocytes is integral to abundant functions in the central nervous system (CNS). Numerous processes allow them to form gap junctions with other astrocytes and connect to the vascular system via endfeet (Bushong *et al.*, 2004, Perez-Alvarez *et al.*, 2014, Nedergaard *et al.*, 2002, Iadecola and Nedergaard, 2007), permitting transport, clearance and release of ions, hormones, neuromodulators, metabolites and neurotransmitters, such as GABA, glutamate and D-serine (Cheung *et al.*, 2015, Martineau *et al.*, 2014, Parpura *et al.*, 2012). This exchange, release and uptake of molecules is regulated via numerous transporters and by exocytosis (Parpura *et al.*, 2012, Lalo *et al.*, 2011, Walz, 2000). Importantly, astroglia have been shown to modulate synaptic function and plasticity by stimulating synaptogenesis and altering the structural characteristics of dendritic spines, including the stabilisation of individual dendritic protrusions and subsequent maturation into spines (Fields *et al.*, 2015, Nishida and

Okabe, 2007). The above is dependent on the ability of astrocyte processes to directly contact synapses, coupling morphology to function (Hama *et al.*, 2004). Hence, astrocyte processes are structurally interwoven with the pre- and post-synaptic membranes, forming a functional unit known as the tripartite synapse, Figure 1.3 (Perea *et al.*, 2009).
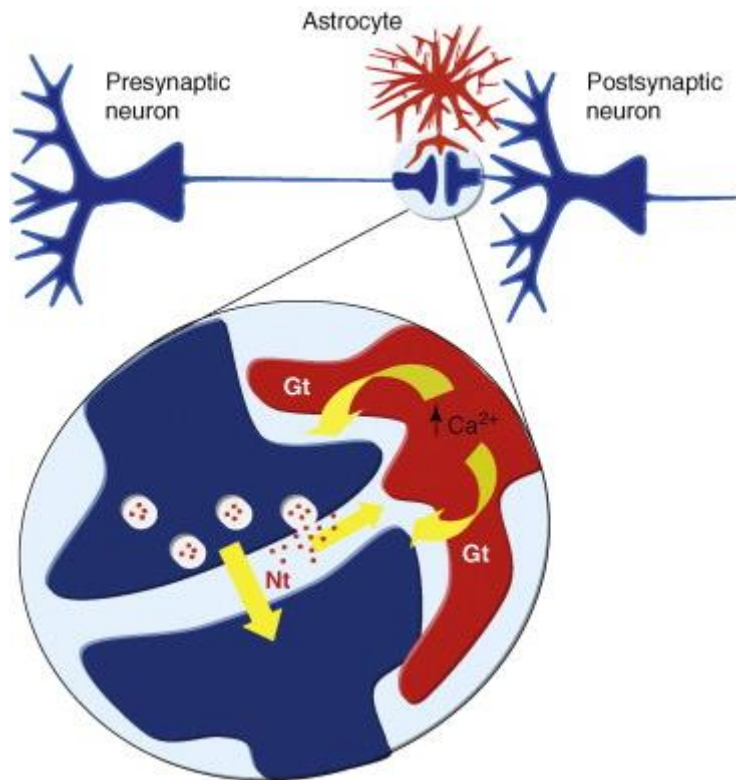
Figure 1.3 Scheme of the tripartite synapse

Figure representing the transfer of information between neuronal elements and astrocyte at the tripartite synapse. (Perea et al., 2009)

Despite some original scepticism within the research community, numerous studies have now shown that astrocytes actively influence synaptic activity (Baldwin and Eroglu, 2018, Santello *et al.*, 2019, Perez-Alvarez *et al.*, 2014, Zorec *et al.*, 2015). Astrocytes support and maintain the synaptic plasticity required for learning and memory formation

(Zovkic *et al.*, 2013, Alberini *et al.*, 2018). To fulfil synaptic requirements, astrocytes exhibit enormous structural plasticity, allowing these cells to remodel processes (Perez-Alvarez *et al.*, 2014). Such structural plasticity requires intracellular signalling inducing extensive cytoskeletal rearrangement (Bernardinelli *et al.*, 2014, Heller and Rusakov, 2015).

1.5.3 Astrocytes in Alzheimer's disease

Although astrocyte pathologies have long been ignored, aberrant astrocyte morphology and function have been reported for several neurological disorders, such as Amyotrophic Lateral Sclerosis, Parkinson's disease and AD (Robinson *et al.*, 2016, Pehar *et al.*, 2017, Kohutnicka *et al.*, 1998, Verkhratsky *et al.*, 2014). Neurons are more susceptible to injury and rely on astroglial protection (Verkhratsky and Nedergaard, 2018), highlighting the importance of astrocytes in neurological disorders. As with healthy astrocytes, astrogliopathologies are equally as hetereogeneous and complex and astrocytes contribute to neurological diseases in several different ways.

Pathological changes of astrocytes include remodelling, atrophy and hypertrophy (Verkhratsky *et al*., 2017). Hypertrophic astrocytes are characterised by enlarged somata and thicker membrane processes, which coincide with an upregulation of GFAP and vimentin (Pekny and Pekna, 2014, Zhang *et al.,* 2017). Hypertrophic astrocytes are inherent to reactive astrogliosis and a direct consequence of brain injury (Schiweck *et al.,* 2018). Astrogliosis is scar forming defence mechanism to confine the affected area, increase neuroprotection and aid lesion regeneration (Pekny *et al.,* 2016). Inhibition of pathways, triggering astrogliosis, such as the Signal transducer and activator of transcription 3 (STAT3) pathway, including downstream pro-inflammatory messengers such as interleukin 6 (IL6) or Leukaemia inhibitory factor (LIF), has been shown to result

in larger lesions (Herman *et al.,* 2008, Sriram *et al*., 2004), indicating a neuroprotective role for astrogliosis. But reactive astrocytes have also been shown to lead to neurotoxicity after prolonged damage (Pekny and Pekna, 2014) as they show varying characteristics in different disorders (Matias *et al.,* 2019). In neurodegenerative disorders, they are induced by microglia (Liddelow *et al.,* 2017), suggesting that reactive/hypertrophic astrocytes are not a single manifestation, but rather a group of manifestations with differing roles, dependent on the cause of activation.

In AD, hypertrophic astrocytes have been found in *in vitro* studies, human post-mortem brain samples and in animal models, such as the triple transgenic mouse model of AD (3xTg-AD), which contains three mutations associated with familial Alzheimer's disease (Olabarria *et al.*, 2010, Verkhratsky *et al.*, 2016, Vijayan *et al.*, 1991, Perez-Nievas and Serrano-Pozo, 2018). In AD, hypertrophy/reactivity of astrocytes, believed to be induced by activated microglia in response to the presence of amyloid β plaques (Abramov *et al.*, 2003, Grolla *et al*., 2013). It is unclear how these astrocytes contribute to synaptic loss (Lidelow *et al.,* 2017) but disruption of astrocyte calcium and glutamate signalling by amyloid plaques may play a role (Vincent *et al.*, 2010). A similar mechanism of reactive astrocytes is also indicated in Parkinson's disease, where accumulation of α-synuclein disrupts astrocyte glutamate transport (Gu *et al.,* 2010) and Amyotrophic Lateral Syndrome (ALS), where aberrant glutamate signalling leads to cell death (Martorana *et al.,* 2012). Astrogliosis being a robust hallmark of several neurodegenerative disorders, highly hypertrophic astrocytes manifest during the later, symptomatic stages of AD (Olabarria *et al.*, 2010, Rodriguez-Arellano *et al.*, 2016, Vijayan *et al.*, 1991, Heneka *et al.*, 2015).

Recent studies focus on the presence of atrophic astrocytes in AD, as these have been shown to accumulate in amyloid plaques-free areas and prior to neurodegeneration

(Kulijewicz-Nawrot *et al.*, 2012, Olabarria *et al.*, 2010, Yeh *et al.*, 2011) but have also been shown to be induced by intracerebral injection with Aβ oligomers in mice (Diniz *et al.,* 2017). Astrocyte atrophy manifests during the early stages of AD, as found in the 3xTg-AD mouse model, PDAPP-J20 transgenic mice (Pomilio *et al.*, 2016, Kulijewicz-Nawrot *et al.*, 2012, Olabarria *et al.*, 2010, Yeh *et al.*, 2011). Most recently, AD-associated astrocyte atrophy has been demonstrated in human induced pluripotent stem cell (iPSC)-derived astrocytes from both EOAD and LOAD patients (Jones *et al.*, 2017), which revealed the same phenotypic changes in both forms of the disease. Atrophic astrocytes are characterised by reduced somata volumes and process shrinkage (Verkhratsky *et al.*, 2010). What exactly leads to this aberrant astrocyte morphology remains unknown. As atrophic astrocytes present with a decreased level of glial fibrillary acidic protein (GFAP), as well as other cytoskeletal proteins (Jones *et al.*, 2017, Olabarria *et al.*, 2010, Rodriguez-Arellano *et al.*, 2016), mechanisms involved in cytoskeletal structure and motility may be affected in AD. It remains unknown if atrophic astrocytes become hypertrophic during later stages of the disease, if either are brain region dependent or whether there is a relationship between hypertrophic and atrophic astrocytes at all; hypertrophic and atrophic astrocytes may well be completely independent manifestations in the AD brain. It could be hypothesised, that atrophic astrocytes become reactive/hypertrophic due to β-amyloid plaques, as atrophic cells lose functions and may thus be unable to deal with the plaque burden. Furthermore, the loss of membrane processes, as described by Jones *et al.* (2017) would suggest that these astrocytes are unable to retain contact with synapses, leading to loss of homeostasis and ultimately loss of these synapses. However, this remains speculative and requires more research as no study to date has revealed mechanisms leading to astrocyte atrophy or determined functional consequences.

As proper morphology is vital to astrocyte function, astrocyte dystrophy coincides with aberrant cell function. A study of AD animal models has identified dynamics of astroglial functional marker profiles during different stages of AD (3, 9, 18 and 24 months disease development). This study employed assessment of GFAP (intermediate filament, primarily expressed in astrocytes), glutamine synthetase (enzyme responsible for metabolic regulation of glutamate) and S100 calcium-binding protein B (s100β), in atrophic astrocytes, which were found to be distinctively expressed during different stages of the disease (Rodriguez *et al.*, 2014). This appeared to be region-dependent; as atrophy appeared first (at 1 month of age) in the entorhinal cortex, around 6 months of age in the prefrontal cortex and ~12 months of age in the hippocampus, implicating how astrocyte morphology and function changes during disease development. Furthermore, a recent study by Jones *et al.* (2017), also established a change of key markers in iPSC derived astrocytes from AD patients, detecting decreased GFAP, glutamate transporters and GS in the iPSC astrocytes. Altered expression of key markers in AD astrocytes implicate aberrant function, which is particularly interesting as the iPSC astrocytes were investigated in an autonomous culture, hence free of any environmental influences, such as dysfunctional neurons or aberrant proteins. As these astrocytes showed aberrant morphology, a change in cytoskeletal proteins, such as GFAP, is a likely consequence. The decrease in glutamate transporters and GS indicates that these cells may have lost their ability to maintain glutamate homeostasis, which could lead to neurotoxicity and subsequently loss of synapses.

A known altered function in astrocytes is abnormal calcium signalling (Abramov *et al.*, 2003, Grolla *et al.*, 2013, Rodriguez-Arellano *et al.*, 2016). Conflicting studies argue that abnormal Aβ is the cause of aberrant calcium signalling in astroglia (Alberdi *et al.*, 2013, Abramov *et al.*, 2003, González-Reyes *et al.*, 2017), yet others report no effect (Casley *et*

al., 2009, Toivari *et al.*, 2011). To date, nothing is known about the cause of aberrant calcium signalling in atrophic astrocytes, found during early stages of AD development. The aforementioned iPSC study also found that the calcium binding protein100β was not only reduced, but mislocated to the nucleus. Why or how such mislocation occurs and whether it is cause or effect of aberrant calcium signalling, remains to be fully elucidated and highlights how much about AD aetiology is yet to be discovered. The findings of Jones *et al*. (2017) provide a new role of astrocytes in AD. Identifying the underlying mechanisms leading to this manifestation could lead to the discovery of new therapeutic targets in the early stages of AD, prior to cognitive decline. This thesis proposes a possible mechanism leading to atrophic astrocytes.

1.6   Aims and objectives

This thesis aims to explore if altered expression of the Cas-proteins leads to AD-associated aberrant morphology and function of astrocytes, predicated on a number of lines of evidence:

- GWAS has identified both NEDD9 and CASS4 as risk factors for AD.

- Although less frequent than other risk factors, NEDD9 and CASS4 are the only LOAD risk factors involved in cytoskeletal arrangement and thus morphology.

- CASS4 and NEDD9 have both been shown to have roles in the control of cellular morphology and during preliminary experiments, it was found overexpression of both NEDD9 and CASS4 induced morphological changes in epithelial cells, including the generation of cellular processes atypical for this cell type (Ulzheimer and Jones, 2016; unpublished data), further confirming the impact of

Cas-protein expression on morphological changes and hence a possible role in aberrant astrocyte morphology in AD.

- Astrocytic atrophy and process loss are early factors of AD pathology, exhibiting reduced cell size and loss of processes. This likely impairs the ability to support neurones and maintain synapses. The cause is unknown.

- NEDD9 knockout mice display extensive hippocampal dendritic spine loss, suggesting that downregulation of the Cas-protein may also cause atrophy in astrocytes and hence play a part in AD.

Specific objectives

The overarching aim of this thesis is to find a therapeutic way of reverting atrophic astrocytes to a healthy phenotype. In order to achieve this, first, the unknown mechanisms leading to atrophy must be unearthed.

Based on the above, the specific objectives of this thesis are as follows:

1. To test if NEDD9 and CASS4 are expressed in normal human cortical astrocytes, glial cell lines using immunofluorescence and western blotting. As NEDD9 and CASS4 expression has not been tested in astrocytes to date, this thesis aims to establish robust expression of the proteins in the glial cells.

2. To establish expression of NEDD9 and CASS4 in the adult brain. Although the Cas-proteins have been identified as LOAD risk genes, which signifies expression in the adult brain, previous studies had recorded low or no expression in the adult brain. As primary human astrocytes are foetal and human brain tissue was not

available for this thesis, expression of NEDD9 and CASS4 will be tested in adult mouse brain tissue to further validate this model.

3. Construct overexpression and knock-down *in vitro* models of both NEDD9 and CASS4 in normal human astrocytes via transient transfection of CMV-driven plasmids for overexpression or siRNA-encoding plasmids for knock-down of the genes. Overexpression and knock-down will be validated via immunocytochemistry (measuring fluorescence intensity) and western blotting, followed by densitometry analysis. These models will be the foundation for the investigation into the effect of altered expression on astrocyte morphology and function.

4. Investigate if altered expression of NEDD9 or CASS4 affects astrocyte morphology. This will be assessed via visual analysis (deconvolution microscopy) categorising of cell morphology to evaluate the distribution of morphologies under different transfection conditions. Additionally, 3D isoSurface renders of confocal Z-stacks will be constructed for morphometric quantitative analysis. This will establish how overexpression or downregulation of the Cas-proteins will affect astrocyte morphology and if these changes are implicated in LOAD pathology.

5. Investigate whether altered expression of NEDD9 or CASS4 might affect astrocyte function. This will be assessed by immunostaining for astrocyte functional markers (GFAP, s100B, EAAT2, Actin, Tubulin), followed by comparison of fluorescence intensity under different transfection conditions and visual inspection of marker subcellular localisation. This will be the first step in functional assessment of the NEDD9/CASS4 overexpression and knockdown

models and give an indication of how the Cas-proteins may be involved altered

astrocyte function in LOAD.

Chapter 2

Materials and Methods

2 Chapter 2 – Materials and Method

2.1 Materials

Unless otherwise stated, all laboratory reagents were purchased from Fisher Scientific (Loughborough, UK). All solutions were made up with de-ionised water (dH$_2$O).

2.1.1 Plasmids

The pcEGFP-C1 expression vector was obtained from Clontech laboratories (Saint-Germain-en-Laye, France). NEDD9 Lentiviral Vector (pLenti-GIII-CMV-GFP-2A-Puro), CASS4 Lentiviral Vector (pLenti-GIII-CMV-GFP-2A-Puro), CASS4 set siRNA/shRNA/RNAi Lentivector, NEDD9 set siRNA/shRNA/RNAi Lentivector, Scrambled siRNA control vector and blank control vector were sourced from Applied Biological Materials Inc (Richmond, BC, Canada). Descriptions of the gene of interest encoded in each plasmid, tags and abbreviated names used throughout this thesis may be found in Table 2.1. A generic plasmid map for the pLenti-GIII-CMV-GFP-2A-Puro lentiviral expression vector backbone is outlined in Figure 2.1.

Table 2.1 Plasmids

Official name	Encoded Gene	Description	Tag	Abbreviation
pEGFP-C1	EGFP	Induce expression of EGFP via CMV promoter	EGFP (N-terminal)	GFP plasmid
CASS4 Lentiviral Vector (Human) (CMV) (pLenti-GIII-CMV-GFP-2A-Puro)	CASS4	Induce overexpression of CASS4 via CMV promoter	CopGFP	CASS4 LV-CMV
NEDD9 Lentiviral Vector (Human) (CMV) (pLenti-GIII-CMV-GFP-2A-Puro)	NEDD9	Induce overexpression of NEDD9 via CMV promoter	CopGFP	NEDD9 LV-CMV
Blank pLenti-GIII-CMV-GFP-2A-Puro	Empty	Blank vector control. Induce expression of CopGFP only via CMV promoter	CopGFP	Blank vector
CASS4-set siRNA/shRNA/RNAi Lentivector (Human)	siRNA against CASS4	Knock down of CASS4 expression	CopGFP	CASS4 siRNA
NEDD9-set siRNA/shRNA/RNAi Lentivector (Human)	siRNA against NEDD9	Knock down of NEDD9 expression	CopGFP	NEDD9 siRNA
Scrambled siRNA GFP Lentivirus	Scrambled siRNA	Knock down control	CopGFP	Scramble
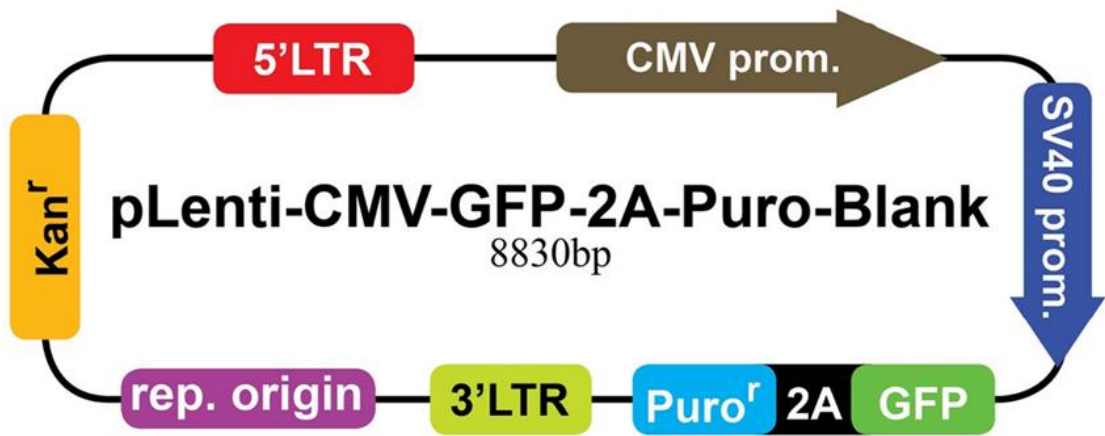
Figure 2.1 pLenti-CMV-GFP-2A-Puro-Blank plasmid map

Vector map (Applied Biological Materials Inc); www.abmgood.com

2.1.2 Cell culture reagents

The SVG p12 human foetal astrocyte cell line and the HeLa human epithelial cervical adenocarcinoma cell line were obtained from ATCC (Manassas, USA), while the 1321N1 human astrocytoma cell line was obtained from European Collection of Authenticated Cell Cultures (Porton Down, UK). Normal human astrocytes (NHA) cells from three separate male donors were purchased from LONZA (Slough, UK).

Media, cell culture reagents and supplements for cell lines were purchased from Fisher Scientific (Loughborough, UK). Media for primary cells (NHA) were purchased from Fisher Scientific (Loughborough, UK), while cell culture reagents and supplements for NHA culture (trypsin EDTA and trypsin neutralising solution) were purchased from LONZA (Slough, UK).

Phosphate buffered saline (PBS) was made with 10 mM phosphate, 137 mM NaCl, 2.7 mM KCl, the pH was adjusted to 7.4.

2.1.3 SDS-PAGE and Western blotting buffers

RIPA buffer was prepared containing 50 mM Tris-HCl (pH 8.0), 150 mM NaCl, 0.5 % (w/v) sodiumdeoxycholate and 1 % (v/v) Triton X-100. Prior to use, Halt™ Protease Inhibitor Cocktail was added.

Laemmli buffer was prepared containing 125 mM Tris-HCl, 4 % (v/v) SDS, 10 % (v/v) mercaptoethanol, 20 % (v/v) Glycerol and 0.004 % (w/v) bromophenol blue. The pH was adjusted to 6.8.

SDS-PAGE running buffer was prepared containg 25 mM Tris base, 190 mM glycine and 0.1 % (v/v) sodium dodecyl sulphate (SDS), aiming for a pH of 8.3.

Western blot transfer buffer was prepared containing 2.5 mM Tris base and 19 mM glycine. Prior to use 20 % (v/v) methanol was added to the buffer.

TBS-T was prepared containing 20 mM Tris-HCl pH 7.5, 150 mM NaCl and 0.1 % (v/v) Tween®.

Blocking buffer was made fresh with TBS-T, containing 5 % (w/v) non-fat dry milk powder.

2.1.4 Antibodies

Primary and secondary antibodies used for immunocytochemistry (ICC) or Western blot (WB) are listed in Table 2.2, together with working dilution factors and sources.

Table 2.2 Primary and scondary antibodies

Target	Species	Isotype	Clone	Dilution	Source
CASS4	Rabbit	IgG	mono	1:100 (ICC), 1:1000 (WB)	Abcam, Cambridge, UK
NEDD9	Mouse	IgG1	mono	1:100 (ICC), 1:1000 (WB)	Abcam, Cambridge, UK
GFAP	Rabbit	IgG	poly	1:250 (ICC), 1:5000 (WB)	Sigma Aldrich, Irvine, UK
β actin	Mouse	IgG1	mono	1:250 (ICC), 1:5000 (WB)	Abcam, Cambridge, UK
α tubulin	Rabbit	IgG	mono	1:250 (ICC), 1:5000 (WB)	Abcam, Cambridge, UK
EAAT1	Rabbit	IgG	Poly	1:250 (ICC), 1:5000 (WB)	Abcam, Cambridge, UK
S100B	Rabbit	IgG	Mono	1:250 (ICC), 1:5000 (WB)	Abcam, Cambridge, UK
Alexa Fluor 555	Goat	IgG	_	1:500 (ICC)	Abcam, Cambridge, UK
Alexa Fluor 555	Goat	IgG	_	1:500 (ICC)	Abcam, Cambridge, UK

Anti-Mouse IgG H&L (HRP)	Rabbit	IgG	Poly	1:5000 (WB)	Abcam, Cambridge, UK
Anti-Mouse IgG H&L (HRP)	Goat	IgG	Poly	1:5000 (WB)	Abcam, Cambridge, UK

2.2 Molecular Biology

2.2.1 Bacterial work

Aseptic technique was adhered to at all times when working with bacteria and when preparing any reagents or growth media for use with bacteria.

2.2.2 Lysogeny broth

Lysogeny broth (LB) was prepared by adding Miller's LB base powder to de-ionised water at a final concentration of 20 g/L and autoclaved. The sterile broth was then stored in sealed bottles at room temperature. Antibiotics were added to the broth immediately prior to use.

2.2.3 Agar plates

LB agar plates were prepared as follows; 32 g/L of LB agar powder was added to de-ionised water and autoclaved. When the agar solution was hand-hot, antibiotics were added and the mixed solution poured into 10cm petri dishes and allowed to set. After

setting, the agar plates were dried in a 37 °C oven and stored upside-down at 4 °C until use.

2.2.4 Super optimal broth with catabolite repression

Super optimal broth with catabolite repression (SOC) consisted of LB broth supplemented with 2.5 mM KCl, 10 mM MgCl2.6H2O and 20 mM glucose. Supplements were filtered with 0.22 µm filter into autoclaved LB broth to avoid glucose burning.

2.2.5 Antibiotics

Antibiotics were used where appropriate to select for transformed bacteria. All constructs used in this thesis contained kanamycin resistance genes. Hence, kanamycin sulphate (Sigma Aldrich, Gilingham, UK) was added to growth media where required at a concentration of 50 µg/ml.

2.2.6 Bacterial transformations

Plasmids were amplified by transformation of STBL3 competent *E.coli* cells, obtained from Thermo Fisher, Altrincham, UK. Competent *E.coli* (50µl) were thawed on ice and 100 ng of plasmid DNA was gently added. Following gentle swirling, the mixture incubated on ice for 30 minutes. The mixture was then heat-shocked for exactly two minutes at 42 °C before being placed on ice for a further two minutes to restore the cell membrane. 250 µl of warm SOC medium was added and the transformation mixture incubated at 37 °C, shaking at 225rpm for a minimum of one hour for recovery. 50-100 µl of transformed cells were spread on agar plates, containing 50 µg/ml kanamycin. Plates were sealed with para-film and incubated upside-down overnight at 37 °C.

2.2.7 Plasmid purification

In preparation for plasmid maxi-preps, single bacterial colonies were picked from fresh agar plates and added to 200 ml LB broth, containing 50µg/ml kanamycin. Each broth

was incubated at 37°C in a shaker (200-250rpm) for 24 hours. Plasmids were extracted from these overnight cultures using Hi-speed plasmid maxiprep kits (Qiagen, Crawley, UK) as per the manufacturer's instructions. Such preparations provided, typically, 900 µl of plasmid DNA solution at a concentration of 150-1000 ng/µl.

2.2.8 Measuring DNA concentrations

The concentration of purified DNA was determined using a NanoDrop ND-1000 spectrophotometer (Labtech International Ltd., Ringmer, UK). Absorbance was measured at 260nm (A260) and concentration was estimated based upon an A260 of 1.0 being equivalent to 50 µg/ml double-stranded DNA. A260/280 ratios were also calculated to determine DNA purity, with ratios of >1.8 being deemed acceptable for transfections.

2.3 Mammalian cell culture

Expression of NEDD9 and CASS4 has not been confirmed in astrocytes. To establish which cell line expresses the proteins and would be best suited as a model for this thesis, several astrocyte cell lines were used. Expression of the Cas-proteins had been confirmed in cervical cancer, HeLa cells were thus used as positive control.

2.3.1 Cell culture

The SVGp12 (human foetal astrocytes) and HeLa (human epithelial cervical adenocarcinoma) cell lines were maintained in Eagle's minimal essential medium, supplemented with 10 % (v/v) Foetal Bovine Serum (FBS), 2 mM L-glutamine, 1 % (v/v) non-essential amino acids (NEAA), 1 mM sodium pyruvate and 1 % (v/v) penicillin/streptomycin. 1321N1 cells were maintained in Dulbecco's Modified Eagle's Medium, plus 10 % (v/v) FBS, 2 mM L-glutamine and 1 % (v/v) penicillin/streptomycin. All cell lines were incubated in a humidified incubator at 37 °C with 5 % CO_2. Cells were grown in tissue culture-treated vented T75 culture flasks (ThermoFisher, Altrincham,

UK) and passaged at 80 % confluency (approximately twice weekly). Cells were rinsed with PBS to remove excess medium before the addition of 2 ml 1 % (v/v) trypsin in PBS. The flask was returned to the incubator for sufficient time for cells to begin to detach from the flasks (as determined by viewing down a tissue culture microscope). Trypsin activity was immediately quenched by the addition of 20 ml fresh complete culture medium. The cell/medium mix was centrifuged at 800 xg for 5 minutes to gently pellet cells. The supernatant was carefully discarded and the pellet gently re-suspended in fresh warm culture medium, prior to re-seeding into T75 flasks at a cell-appropriate density. Typically, 1:4 to 1:6 seeding ratios were appropriate for all cell lines to reach 80 % confluency in 3-4 days. Cell lines were only utilised up to a maximum number of 20 passages.

2.3.2 Primary cell culture

Normal (cortical) human astrocytes, obtained from LONZA (Slough, UK), were maintained in Dulbecco's Modified Eagle Medium/Nutrient Mixture F-12 (1:1), supplemented with 10 % (v/v) FBS and 2 mM L-glutamine. Culture medium was exchanged every other day and the volume increased as cells became more confluent. Cells were initially resurrected into T25 flasks until good growth was established, and thereafter grown in T75 flasks. Flasks were incubated with 5% CO_2 in a humidified incubator at 37 °C and passaged when a confluency of 80 % was reached – typically once every two weeks. Cells were detached from flasks using 0.25 % (w/v) trypsin and 1 mM EDTA in Hank's buffered saline solution, quenched with trypsin neutralising solution and centrifuged at 800 xg for 4 minutes. Supernatants were discarded and cells gently re-suspended in fresh warm culture medium, counted and reseeded in T75 flasks at a seeding density of 5000 cells/cm2. Cell lines were only utilised up to a maximum number of 5 passages.

2.3.3 Transfections and puromycin selection

Prior to transfection, cells were seeded directly onto sterile No. 1.5 glass cover slips (Scientific Laboratory Supplies Limited, Nottingham, UK) in 24-well tissue culture plates (Thermo Fisher, Altrincham, UK) and incubated at 37 °C for a minimum of 24 hours, until a confluency of 60-70 % was reached. Culture medium was exchanged on the morning of transfection. Transfection was achieved using the Lipofectamine™ 3000 Transfection Reagent (Thermo Fisher, Altrincham, UK) for all plasmids at optimised concentrations, based on manufacturer's guidelines. Culture medium was exchanged 6 hours after transfection to avoid DNA-reagent complex-induced toxicity. pEGFP-C1, blank vector or scramble vector were used as positive transfection controls in all cases. Negative controls included non-transfected and Lipofectamine-only (no DNA) cells. Population enrichment for Western blotting was achieved by adding 5µg/ml puromycin to the cell growth medium 24 hours after transfection. The optimal concentration for puromycin selection was established with a puromycin kill curve experiment, whereby varying concentrations of puromycin (1-5µg/ml) were added to cells, followed by cell counts at 24, 48 and 72 hours to establish cell viability. Knock-down was achieved 48 hours post transfection, but cells would detach by 72 hours; hence the ideal concentration would require sufficient enrichment of transfected cell populations sufficiently, 24 hours after supplementing medium with puromycin (48 hours post transfection). Non-transfected cell numbers were sufficiently and consistently reduced with 5µg/ml puromycin after 24 hours, to validate knock-down via Western blotting.

Transfection efficiency was established by counting GFP+ cells in >10 random fields of view in comparison to total cell numbers (DAPI channel), enabling calculation of

transfection efficiency percentage. This experiment was repeated with cells from three donors with three repeats within each experiment.

2.4 Fixation and Immunocytochemistry

Mammalian cells grown on coverslips were washed twice in PBS prior to fixation with 4 % (v/v) formaldehyde in PBS for 10 minutes. Cells were then treated with 0.1 M glycine in PBS to quench formaldehyde cross-linking and permeabilised with 0.1% (v/v) Triton X-100 in PBS. Cells were blocked for 1 hour at 4 °C with 1 % (w/v) bovine serum albumin diluted in PBS ("blocking solution") to prevent non-specific antibody binding. All antibodies were diluted in blocking solution. Primary antibodies were either applied for 1 hour at room temperature or incubated at 4˚C overnight (for anti-NEDD9 and anti-CASS4), as appropriate. In either case, coverslips were placed cell side-down onto a 50 µl drop of diluted antibody placed on parafilm in a home-made humidity chamber. Subsequently coverslips were washed in excess PBS and a mixed solution of the appropriate fluorophone-conjugated secondary antibody diluted in PBS also containing 0.1 µg/ml 4',6-diamidino-2-phenylindole (DAPI) was applied and incubated for 30 minutes at room temperature in the dark. Immunostained cells were mounted onto glass microscope slides with ProLong Diamond mountant (Thermo Fisher, Altrincham, UK) and cured overnight at room temperature prior to being sealed with nail varnish.

2.5 Cell fixation for flow cytometry

Cells were fixed in solution with 4% (v/v) formaldehyde in PBS as described above. Cells were centrifuged at 800 xg for 5 minutes in between each step. Cell pellet was resuspended in primary antibody diluted 1 % (w/v) bovine serum albumin (in PBS) and incubated at 4˚C overnight. Cells were washed with PBS and centrifuged at 800 xg for 5 minutes, followed by incubation with a secondary antibody, diluted in 1 % (w/v) bovine

serum albumin (in PBS), for one hour at room temperature. Cells were washed and centrifuged once more and stored in PBS at 4˚C until use (maximum of 24 hours).

2.6   Mouse brain tissue

Despite being identified as LOAD 'risk genes', NEDD9 and CASS4 expression had previously been questioned in the adult brain. Wild type adult mouse brain tissue was used to confirm NEDD9 and CASS4 expression in the adult brain, as human brain tissue was unavailable for this thesis.

All mouse brain tissues were obtained for secondary use from Dr Donna Daly (University of Central Lancashire) and in accordance with local ethical approvals. Male C57BL/6 wildtype mice were purchased from Charles River (Harlow, UK) and sacrificed aged 24 weeks under Schedule 1 of the Animals (Scientific Procedures) Act 1986. Mouse brain tissues were excised and entorhinal cortices were flash frozen on dry ice by Mr Atte Räsänen (University of Central Lancashire). Brain tissue was lysed with CelLytic M (Sigma Aldrich, Gilingham, UK) according to manufacturer's guidelines and stored at -20 °C until use.

2.7   Fluorescence microscopy and flow cytometry

2.7.1   Deconvolution microscopy

Initial visualisation of immunofluorescently stained cells, morphological binning (see morphological analysis, Table 2.3) and transfection efficiency calculations were undertaken using a Zeiss cell observer Axio Z1 system, equipped with a colibri LED light source (25% intensity), AxioCam and ZEN software (Carl Zeiss, Cambridge, UK). Cells were visualised using 20x PL Apo (0.8 NA), 40x LD Plan-Neofluar (0.6 NA) and 63x PL Apo (1.4 NA) oil objectives and GFP/dsRed/DAPI filter sets. All images were taken with

the same exposure time (DAPI: 63 msec; GFP: 400 msec; dsRED: 800 msec). Deconvolution of images was carried out using the constrained iterative method with a maximum of 10 iterations. Total and GFP+ cells were counted from a minimum of 5 fields of view at 20x magnification per coverslip to estimate mean transfection efficiencies.

2.7.2 Confocal microscopy

Individual cell images for later morphometric analysis were collected on a Leica TCS SP8 AOBS inverted confocal microscope using a 100x Plan Fluotar (1.40 NA) objective and Hybrid photon detectors. Images were collected using the following detection mirror settings; DAPI 400-460 nm; Alexa Fluor 488 480-550 nm; Alexa Fluor 555, 555-590 nm using 488nm (5 % power), 594nm (10 % power) and 633 nm (10% power) laser lines respectively. Image acquisition confocal settings were identical for all experiments, as follows; pinhole - 1 airy unit, scan speed – 600 Hz unidirectional scan, confocal zoom – 0.75x, and format - 1024 x 1024 pixels. Z stacks were acquired using the Leica Application Suite X to determine the optimal number of slices per cell for offline 3D reconstruction. The top and bottom of each stack was carefully set to ensure none of the cell was lost, which would negatively influence later morphometric analyses.

2.7.3 Flow cytometry

Fixed and stained cells in suspension (PBS) were analysed with the Amnis ® ImageStream[x] Mk2. Cells were detected using lasers at 488nm (GFP, green) and 561nm (Alexa Fluor 555, red). This method was unsuccessful.

2.8 Image Processing

2.8.1 Fluorescence intensity analysis

Relative expression levels of individual proteins were analysed semi-quantitatively through calculation of the relative fluorescence density of immunofluorescently stained cells using FIJI ImageJ (Schindelin *et al.*, 2012, Rueden *et al.*, 2017). Fluorescence density was measured from at least ten cells (selected at random in the DAPI channel) from a minimum of three separate experiments. Individual cells were selected using the freehand selection tool to draw around the entire cell. The measure tool was then used to calculate cell area and integrated pixel density (conceptually equivalent to 'total fluorescence') per selected cell. Background fluorescence was calculated from a minimum of five fields of view from unstained control cell coverslips. Fluorescence intensity was corrected for background levels as follows:

Corrected integrated density = measured integrated density – (area of selected cell x mean background fluorescence).

2.8.2 Morphological analysis

Morphological analysis of transfected normal human astrocytes was performed by visually binning observed cells into four categories: fibroblast-like cells; polarised cells; arborised cells; and atrophic cells. Each category was defined as outlined in Table 2.3.

Table 2.3 Astrocyte morphology types

Morphological type	Characteristics
Fibroblast-like	Flattened, process-devoid, oblong to triangular shape
Polarised	Elongated, polarised apical domains, process-devoid
Arborised	Process bearing, > three branching processes
Atrophic	Process-devoid or elongated with soma width $< 20\mu m$

Binning was carried out in a blinded manner. Microscope slide annotations (indicating transfection conditions) were obscured by an independent third party prior to visualisation and binning.

2.8.3 Morphometric quantification

Confocal z stacks of individual cells were assessed with IMARIS 9.1 (Bitplane AG, Zurich, Switzerland) as described by Jones *et al.* (2017). 3D isosurface renders were created based on the extent of GFP within the cell (to reveal the entire cell morphology) or immunofluorescent staining of GFAP (to reveal the GFAP cytoskeleton morphology, as per Olabarria *et al.*, 2010 and related methods). The edges of the fluorescence signal were carefully demarcated to include the entire cell and voxels were removed. These 3D renders then allowed the calculation of morphometric measurements including surface area, volume, axis lengths and sphericity. Analysis were carried out on CASS4 and NEDD9 overexpression and knock-down models of normal human astrocytes together

with controls, for comparison. A minimum of 10 cells were analysed per experiment with three individual experiments carried out for each of the three NHA donors per transfection condition.

2.9 Protein Biochemistry

2.9.1 Whole cell lysate preparation

Cells were detached with trypsin (as for the start of the cell culture protocol, section 2.3) and pelleted at 800 xg for 5 minutes, washed with cold PBS and pelleted 14,000 xg for 1 minute. The pellet was placed on ice and resuspended in cold RIPA buffer supplemented with EDTA-free Halt™ Protease and Phosphatase Inhibitor Cocktail (Thermo Fisher, Altrincham, UK). The cell suspension was kept on ice for 30 minutes whilst being vortexed every 5 minutes to allow for lysis. Lysates were spun in a pre-cooled (4˚C) centrifuge at 16,000 xg for 20 minutes to remove unlysed cells and large membrane fragments. Protein-containing supernatants were collected and stored at -20 °C. Protein content was measures just prior to use with Pierce BCA Protein Assay Kit.

2.9.2 SDS-PAGE

Sodium dodecyl sulphate polyacrylamide gel electrophoresis (SDS-PAGE) was performed using the Bio-Rad Mini-PROTEAN® vertical electrophoresis system and PowerPac Basic power supply with pre-cast 10 % mini-PROTEAN® TGX acrylamide gels (Bio-Rad, Watford, UK). Whole cell lysates were mixed with 2x Laemmli loading buffer (1:1, v/v) and boiled to 95 °C for 5 minutes prior to loading. 5-20 µg of lysate were loaded per well. Running buffer (25mM Tris, 190mM glycine, 0.1% SDS) was added to the gel tank and the apparatus checked for leaks. Gels were run at 50 V for 5 minutes to

allow the proteins to pass the stacking gel, followed by a constant of 100 V for 80 minutes to achieve protein separation.

2.9.3 Western blotting

Transfer of resolved proteins to nitrocellulose was achieved at 300 mA for 80 minutes in transfer buffer using the Bio-Rad Mini Trans-Blot® Module. Membranes were subsequently treated with blocking buffer (5 % milk in TBS-T) for 1 hour at RT and then incubated with appropriate primary antibody diluted as per Table 2.2 in blocking buffer overnight at 4°C. After three 10 minute washes TBS-T, primary antibodies were detected using species-matched horseradish peroxidase (HRP)-conjugated secondary antibodies, diluted 1:5000 in blocking buffer, for one hour at room temperature. The immunoblot membranes were then washed extensively with TBS-T. Blots were developed using the SuperSignal™ West Pico PLUS Chemiluminescent ECL kit (Thermo Scientific, Loughborough, UK). The membrane was imaged with a Bio-Rad ChemiDoc XRS+, equipped with Image Lab™ Software. Membranes were stripped with a mild stripping buffer (0.2 M glycine, 3.5 mM SDS, 0.1% (v/v) Tween, pH 2.2), re-blocked in 5% milk/TBS-T and re-probed for β-actin as a loading control.

2.9.4 Densitometric analysis

Densitometric analysis of Western blots was performed with FIJI ImageJ. Images were converted to 8-bit grey scale prior to measuring relative band intensities. Relative densities of target proteins were calculated by dividing measured intensities by intensity of the β actin loading control.

2.10 Statistical analysis

Statistical analyses were performed using IBM SPSS 22 (IBM Corporation, Armonk, USA). Data are presented as mean ± SEM unless otherwise stated. SEM is preferred over

SD when comparing populations (Altman and Bland, 2005). A p-value of ≤ 0.05 was considered significant throughout this thesis. All data sets were tested for normality using the Shapiro-Wilks test prior to selection of the appropriate statistical test.

2.10.1 Comparison of fluorescence intensities

Comparison of integrated fluorescence densities between overexpression and blank-transfected cells or knock-down vs scramble cells was carried out via independent sample Student's t-tests.

2.10.2 Comparison of morphometric measurements

Comparison between groups was carried out by either Kruskal-Wallis, followed by pairwise comparison via Dunn-Bonferroni method (where data were found to be non-parametric) or one-way ANOVA (for parametric data), followed by Tukey-HSD (equal variance) or Games-Howell (non-equal variance) post hoc to identify significant differences. The Levene's F test was used for testing homogeneity of variance between groups.

2.10.3 Comparison of density measurements

Comparison of normalised values (density) of Western blot bands from overexpression and knock-down experiments was carried out via independent sample Student's t-tests.

Chapter 3

Endogenous expression of NEDD9 and CASS4

3 Chapter 3 – RESULTS: Endogenous expression of CASS4 and NEDD9

3.1 Background

While endogenous expression of CASS4 and NEDD9 in adult human astrocytes is predicted by several studies, confirmation of Cas-protein expression is lacking in the literature. As outlined in the introduction to this thesis, no studies have confirmed expression in astrocytes to date and expression in the adult brain varies between studies (Law *et al.*, 1998). Hence, at the outset of this thesis it was necessary to undertake experiments to detect CASS4 and NEDD9 via western blot and immunocytochemistry in glial cell lines, primary human astrocytes to determine which cell line is most suited for further investigations. Additionally, NEDD9 and CASS4 expression was tested in adult mouse brain tissues to validate expression in the adult brain, as this has previously been challenged. Ideally, human brain tissue should be tested, but was not available for this thesis.

3.1.1 NEDD9 expression

The majority of published studies related to NEDD9 have focused on its role as a promoter of metastasis in cancer (Beck *et al.*, 2014, Shagisultanova *et al.*, 2015). As such, the expression of NEDD9 has been demonstrated in numerous cancers including leukaemia, lymphoma, breast cancer, lung cancer, and brain tumours including glioblastoma and neuroblastoma (Shagisultanova *et al.*, 2015, Jurcic *et al.*, 2019, Gabbasov *et al.*, 2018, Xu *et al.*, 2019). These studies have revealed that NEDD9 has influences in both cancer initiation and progression, implicating a correlation between

NEDD9 expression and cellular changes (Izumchenko *et al.*, 2009, Li *et al.*, 2011, Deng *et al.*, 2013, Wang *et al.*, 2017). Given the robust expression of NEDD9 in most cancers, it is unsurprising that it has been detected in many cancer cell lines, including HeLa cells (Sima *et al.*, 2013), offering another means for experimentation which was exploited within this thesis.

Unlike its paralogue CASS4, much more is known about NEDD9 expression and the protein is abundant in many tissues (Fashena *et al.*, 2002, Minegishi *et al.*, 1996), including the brain, where it has been shown to regulate neural crest cell migration during embryogenesis, a process vital for proper brain development (Aquino *et al.*, 2008).

NEDD9 is believed to be highly expressed during development but has been suggested to be downregulated in the adult brain (Kumar *et al.*, 1992, Law *et al.*, 1996); hence its name 'neurally-expressed, developmentally-downregulated 9'. These findings, however, are based only on mRNA expression rather than actual protein expression. It is known that cellular protein levels can differ markedly from transcript levels (Liu *et al.*, 2016). This is attributed to a number of factors including the predominant control of protein expression at the level of translation and highly variable protein half-lives (Schwanhausser *et al.*, 2011). Accordingly, Li *et al.*, 2008, determined significant NEDD9 expression in adult human brain tissue via immunohistochemistry, although they did not explore expression in glia.

3.1.2 CASS4 expression

CASS4 is the most recent addition to the Cas-proteins family, hence relatively little is known about its canonical functions or tissue expression (Singh *et al.*, 2008). CASS4 shares much structural homology with NEDD9 and other members of the Cas-proteins

family (Beck *et al.*, 2014). While its exact functions or expression patterns remain largely unknown, its activity is believed to be dependent on the presence of other Cas-protein (Deneka *et al.*, 2015), suggesting expression in similar tissues.

During the initial identification of CASS4, RT-PCR revealed high expression of mRNA in the spleen and lungs as well as in leukaemia and ovarian cancer (Singh *et al.*, 2008). CASS4 transcripts have since been detected in a number of other tissues, including the cerebral cortex and hippocampus; albeit at rather low levels (Kim *et al.*, 2014). As discussed above, although a correlation between mRNA levels and protein expression is often assumed, mechanisms involved in translation are complex; hence cellular protein levels are difficult to predict from mRNA transcript levels (Greenbaum *et al.*, 2003, Liu *et al.*, 2016).

3.2   Results

3.2.1   Basal expression of CASS4 & NEDD9 in cell lines

3.2.2   HeLa - cervical cancer cell line

Given the reported expression of both CASS4 and NEDD9 in a number of cancers, including gliomas, initial confirmation of expression was undertaken in the astroglial cell line 1321N1 (human stage 2 astrocytoma). The SVG p12 human foetal astrocyte cell line, which is also an astroglial cell line, was tested alongside. The HeLa (human epithelial cervical adenocarcinoma) has previously been shown to express NEDD9 (Sima *et al.*, 2013) and hence was employed as both a positive control and as a non-glial control cell line.

Western blotting (WB) of HeLa lysates using an anti-NEDD9 antibody revealed two bands at 65 kDa and 55 kDa (Figure 3.1, A). Protein loads between 5 and 20 µg were

trialled, with both bands being visible at all loads, suggesting a robust expression of NEDD9 in HeLa cells, as expected. Both visible bands correlate with known isoforms of NEDD9, which are cleaved from the full length protein (93 kDa) (Deneka *et al.*, 2015, Law *et al.*, 1998). Full-length NEDD9 is known to undergo post-translational modifications, particularly phosphorylation, leading to two species of 105 kDa and 115 kDa; however, these two bands were not seen in HeLa cell lysates.
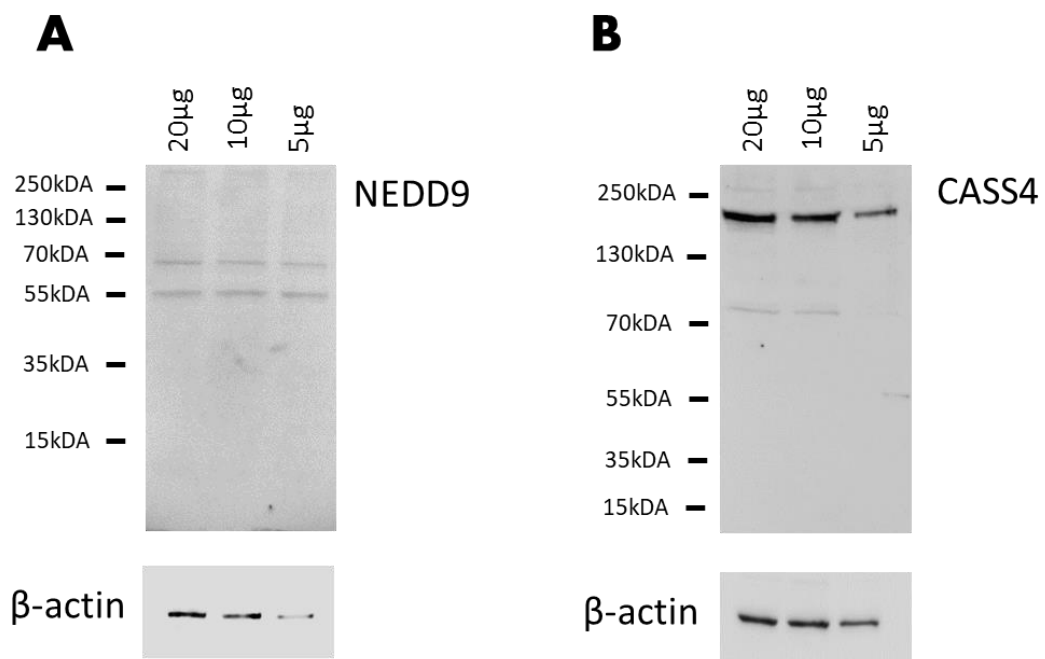
Figure 3.1 Western blotting of HeLa whole-cell lysates confirms expression of both NEDD9 and CASS4

Following separation by SDS-PAGE and blotting, two bands for were apparent using antibodies against NEDD9 (55 kDa, 65 kDa) (A) and two bands using anti-CASS4 antibodies (76 kDa, 230 kDa) (B), confirming expression of both proteins in this cell type. Actin used as loading control. N=3.

Western blotting for CASS4 at revealed two bands at 230 kDa and 76 kDa in the HeLa cell lysates (Figure 3.1, B). 76 kDa coincides with the size of a known isoform of CASS4

(isoform 2). 230 kDa does not correlate with any known CASS4 isoform and may be the result of dimerisation and/or post translational modifications, such as glycosylation or phosphorylation. Bands were not seen at 87 kDa or 38 kDa, which are other known isoforms of CASS4. As with NEDD9, bands were visible at protein loads as low as 5-10 µg, suggesting a robust expression of CASS4 in HeLa cells. This is in keeping with the prediction that CASS4 expression follows that of its paralogue, NEDD9.

To further validate the expression of NEDD9 in HeLa cells, immunofluorescence staining was undertaken with the same NEDD9 primary antibody together with an Alexa Fluor 555 secondary antibody (Figure 3.2). Fluorescence imaging revealed fluorescence in all cells, indicating the expression of NEDD9. The pattern of fluorescence was slightly punctate and extended throughout the entire cell, consistent with expected cytosolic localisation of NEDD9. Omission of the primary antibody revealed no fluorescence, confirming that the staining observed was due to the specificity of the primary antibody.
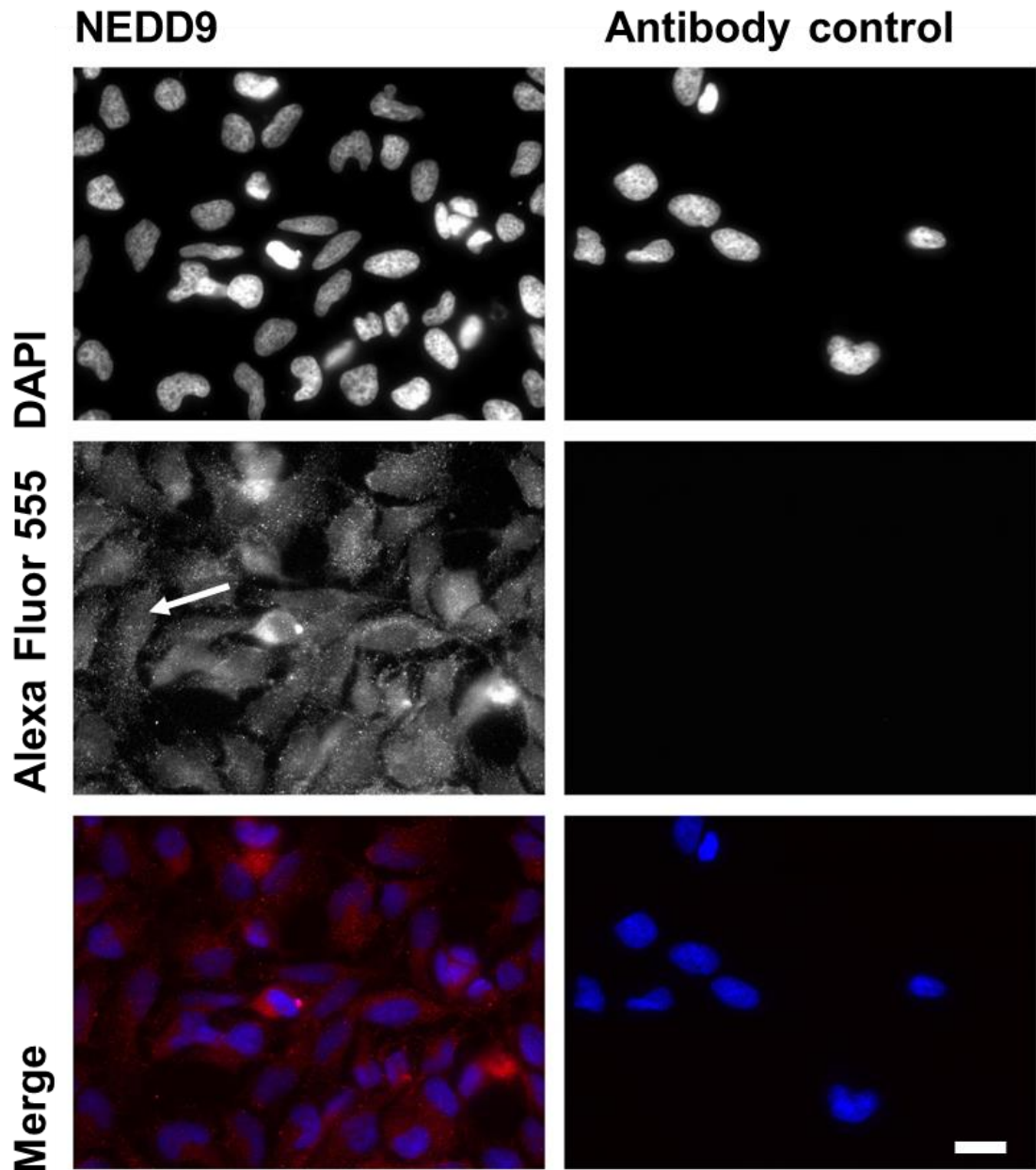
Figure 3.2 Immunofluorescence staining of HeLa cervical cancer cells reveals NEDD9 expression.

HeLa cells were stained using a primary antibody against NEDD9 followed by an Alexa Fluor 555 secondary antibody, revealing a slightly punctate pattern of staining throughout the cell (Left). Secondary antibody (only) used as control (Right). N=3. Scale bar = 20μm.

The expression of CASS4 was also established via immunofluorescence staining using the same antibody as for the Western blot, followed by an Alexa Fluor 555 secondary antibody (Figure 3.3). As expected, based upon the Western blot, fluorescence imaging revealed CASS4 expression within the HeLa cells. This followed a similar pattern to NEDD9, with the addition of some small cellular inclusions, which may possibly be related to the unknown higher molecular weight species (230 kDa) seen on the blot (Figure 3.1, B).
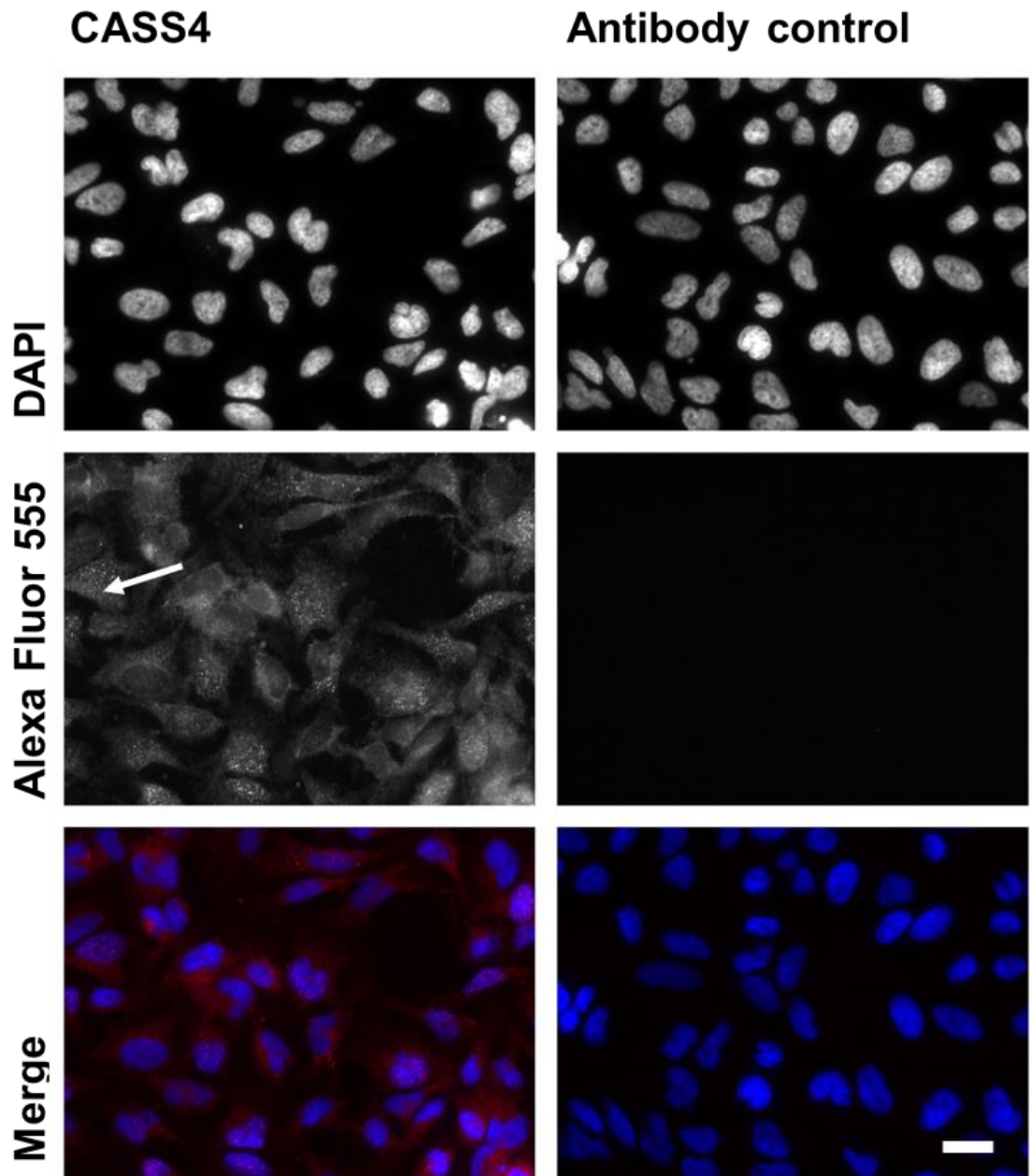
Figure 3.3 Immunofluorescence of fixed HeLa cervical cancer cells validates CASS4 expression.

Fixed HeLa cells were stained using an anti-CASS4 primary antibody followed by Alexa Fluor 555 secondary revealing a punctate pattern of staining throughout the cell with small intracellular inclusions (Left). Secondary antibody (only) used as control (Right). N=3. Scale bar = 20μm.

3.2.3 1321N1 – astrocytoma cell line

Western blotting of 1321N1 whole-cell lysates and probing for CASS4 and NEDD9 revealed that both Cas-proteins are expressed in 1321N1 cells (Figure 3.4). In the case of NEDD9 (Figure 3.4, A), two bands were clearly visible corresponding with the known cleaved isoforms at 55 kDa and 65 kDa. Neither the full-length protein (93 kDa) nor its phosphorylated forms (105 kDa and 115 kDa) were seen in the 1321N1 lysates. This is in keeping with the result obtained for the HeLa cell line. Blotting for CASS4 revealed the 76 kDa isoform 2 and the unexplained heavy band of 230 kDa, again echoing the results from the HeLa cells. These bands were visible with as little as 5 µg protein load, suggesting a robust expression of CASS4 in this astrocytoma cell line.
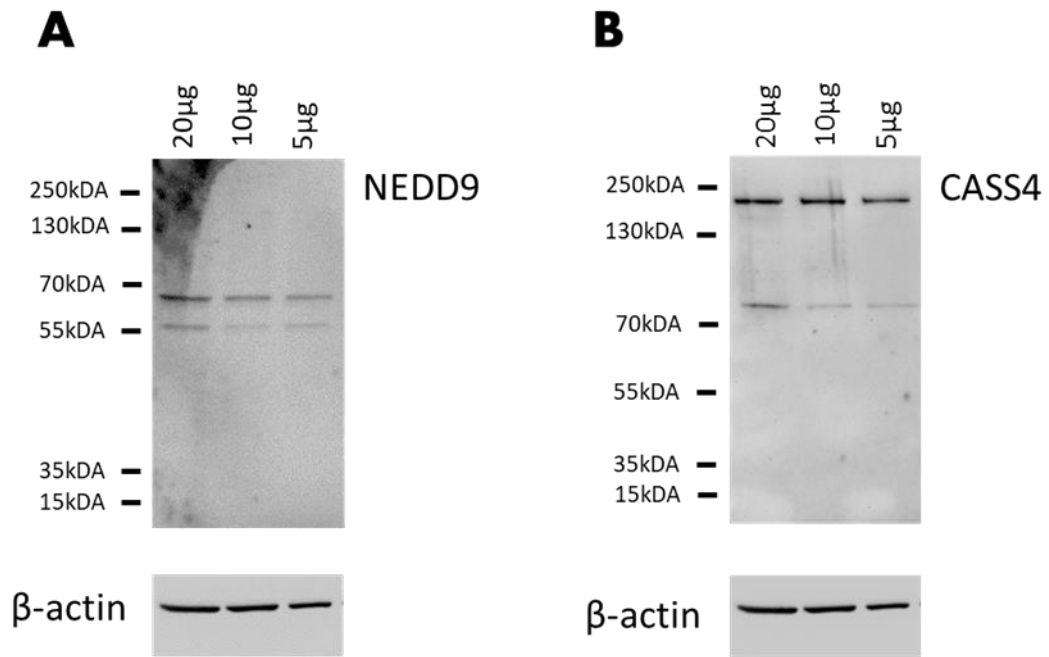
Figure 3.4 Western blotting of 1321N1 human astrocytoma whole-cell lysates confirms expression of both NEDD9 and CASS4.

Following separation by SDS-PAGE and blotting, two bands for were apparent using antibodies against NEDD9 (55 kDa, 65 kDa) (A) and two bands using anti-CASS4 antibodies (76 kDa, 230 kDa) (B), confirming expression of both proteins in this cell type. Actin used as loading control. N=3.

To further validate NEDD9 expression in the 1321N1 cell line, immunofluorescence staining was undertaken (Figure 3.5). This revealed the same slightly punctate pattern of NEDD9 staining throughout the entire cell as was seen in HeLa cells, consistent with expected cytosolic localisation. Omission of the primary antibody revealed no fluorescence, confirming that the staining observed was due to the specificity of the primary antibody.
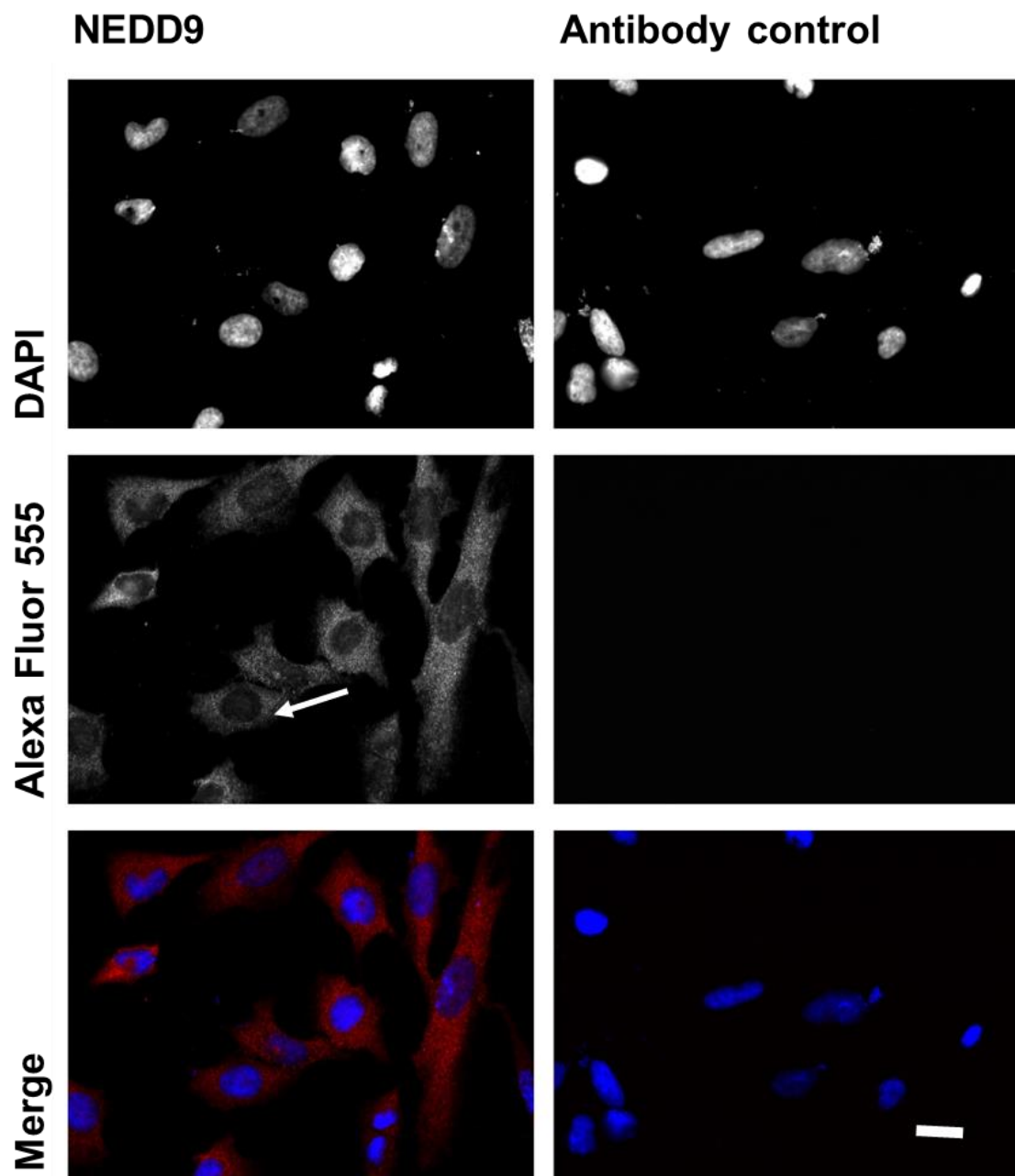
Figure 3.5 Immunofluorescence staining of 1321N1 human astrocytoma cells validates NEDD9 expression.

Fixed 1321N1 cells were stained for NEDD9 followed by Alexa Fluor 555 secondary antibody revealing a slightly punctate pattern of staining throughout the cell (Left). Secondary antibody (only) used as control (Right). N=3. Scale bar = 20µm.

Immunofluorescence staining using the CASS4 antibody followed by an Alexa Fluor 555 secondary antibody was also used to validate the expression of CASS4 in the 1321N1 cells (Figure 3.6). A slightly punctate pattern of staining was evident in all cells. Many cells also exhibited small cellular CASS4+ inclusions towards the centre of the cell. Omission of the primary antibody revealed no fluorescence.
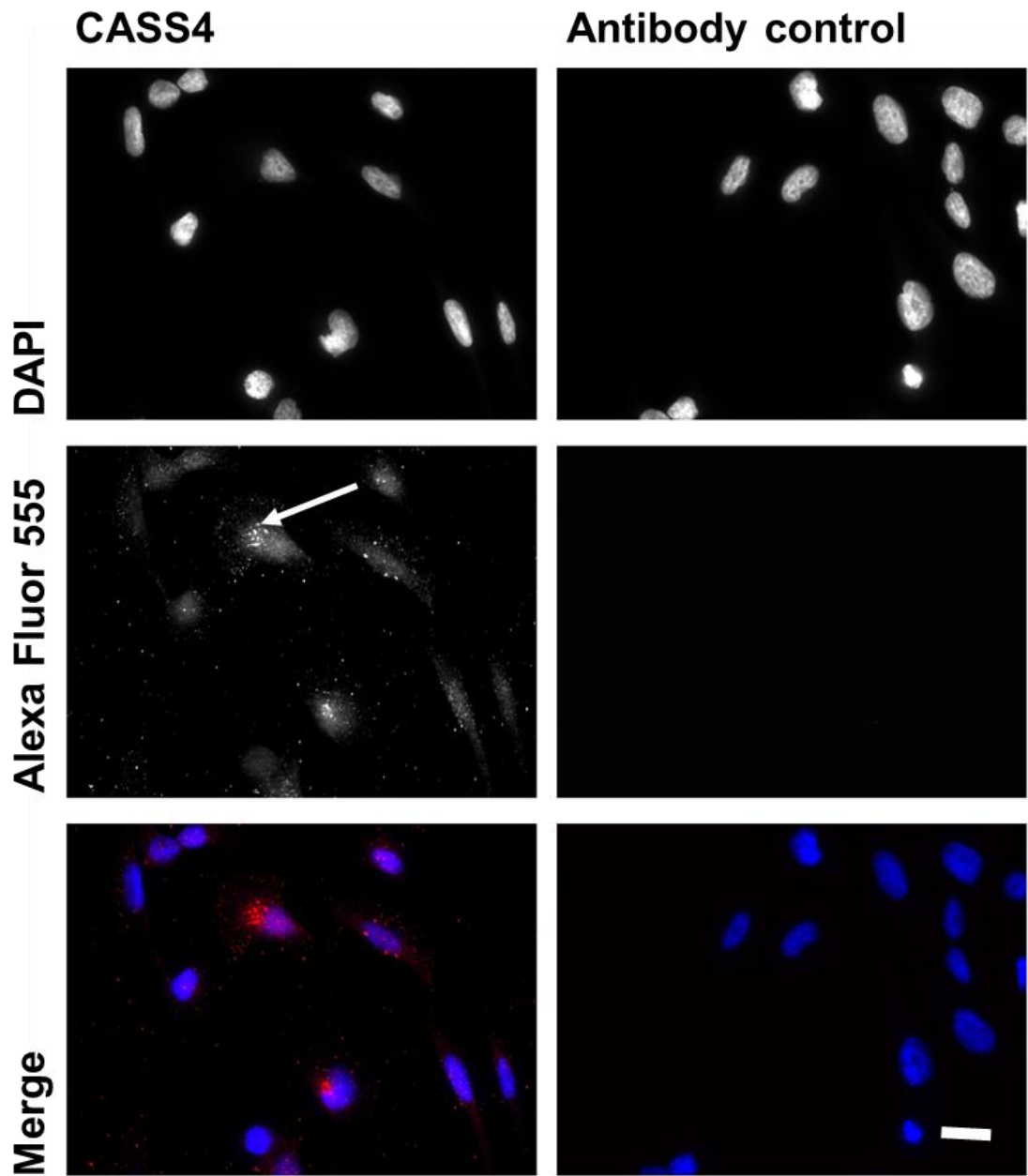
Figure 3.6 Immunofluorescence image of 1321N1 cells, showing CASS4 expression.

1321N1 cells were stained using an anti-CASS4 antibody, followed by Alexa Fluor 555 secondary antibody revealing a slightly punctate pattern of staining throughout the cell (Left). Secondary antibody (only) used as control (Right). N=3. Scale bar = 20μm.

3.2.4 SVG p12 – Human foetal glial cell line

Western blotting of SVG p12 lysates using the NEDD9 antibody revealed two bands at 65 kDa and 55 kDa (Figure 3.7, A), correlating to the known isoforms seen in HeLa and 1321N1 cell lysates. These bands were clearly visible at loads as low as 5 µg. Again, full-length (93 kDa) and phosphorylated forms (105 kDa and 115 kDa) of NEDD9 were absent in the SVG p12 lysates.
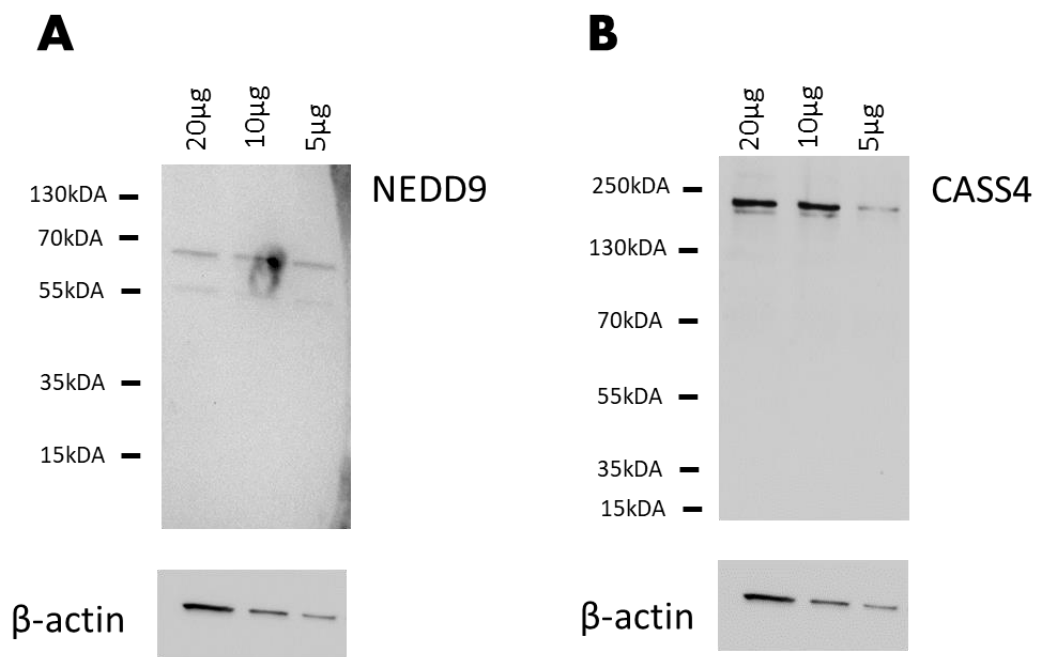
Figure 3.7 Western blotting of SVGp12 lysates, using antibodies to NEDD9 and CASS4.

Following separation by SDS-PAGE and blotting, two bands for were apparent using antibodies against NEDD9 (55 kDa, 65 kDa) (A) and two bands using anti-CASS4 antibodies (76 kDa, 230 kDa) (B), confirming expression of both proteins in this cell type. Actin used as loading control. N=3.

Blotting for CASS4 revealed a large sized doublet at around 230 kDa (Figure 3.7, B), which was not seen in any of the cancer cell lines. The lower molecular weight isoform 2 band (76 kDa) seen in both HeLa and 1321N1 lysates was absent in this human foetal astrocyte cell line. These findings suggest some cell-type specific isoform expression.

To further validate the expression of NEDD9 in the foetal astrocyte cell line SVGp12, immunofluorescence staining with the same NEDD9 antibody was undertaken (Figure 3.8). This revealed a slightly punctate pattern of NEDD9 staining throughout the entire cell, consistent with the cytosolic localisation seen in the other cell lines. Omission of the primary antibody revealed no fluorescence, confirming that the staining observed was due to the specificity of the primary antibody.
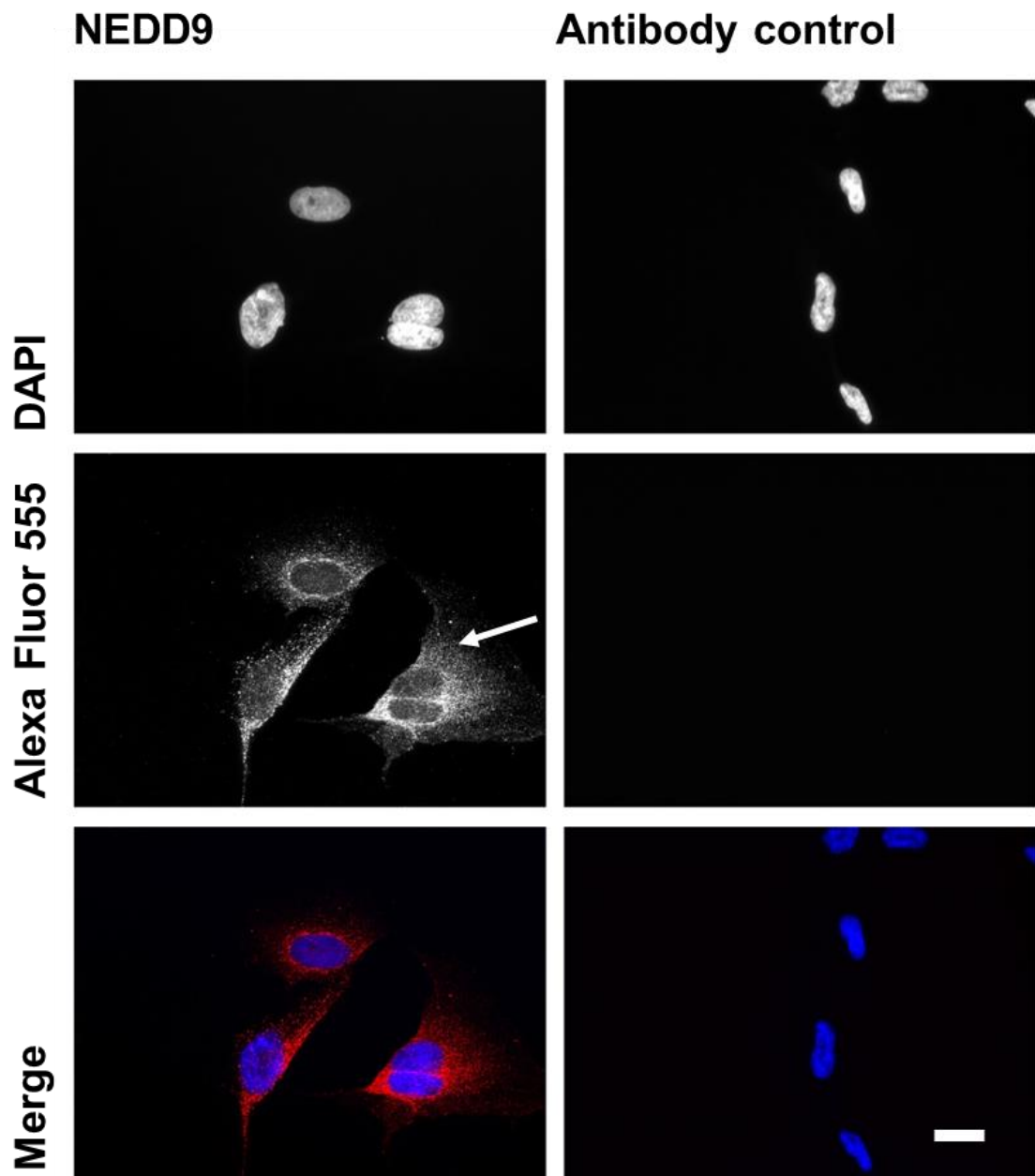
Figure 3.8 Immunofluorescence staining of SVG p12 cells reveals NEDD9 expression.

SVG p12 cells were fixed and stained with an anti-NEDD9 primary antibody, followed by an Alexa Fluor 555 secondary antibody, revealing a slightly punctate pattern of staining throughout the cell (Left, arrow). Secondary antibody (only) used as control (Right). N=3. Scale bar = 20μm.

CASS4 expression in SVG p12 cells could also be validated using immunofluorescence staining of fixed cells (Figure 3.9). As seen in other cell lines, CASS4 revealed a similar punctuate pattern of staining as for NEDD9 with the addition of a number of small cellular inclusions, towards the centre of the cells. A negative control by omission of the primary antibody exhibited no fluorescence.
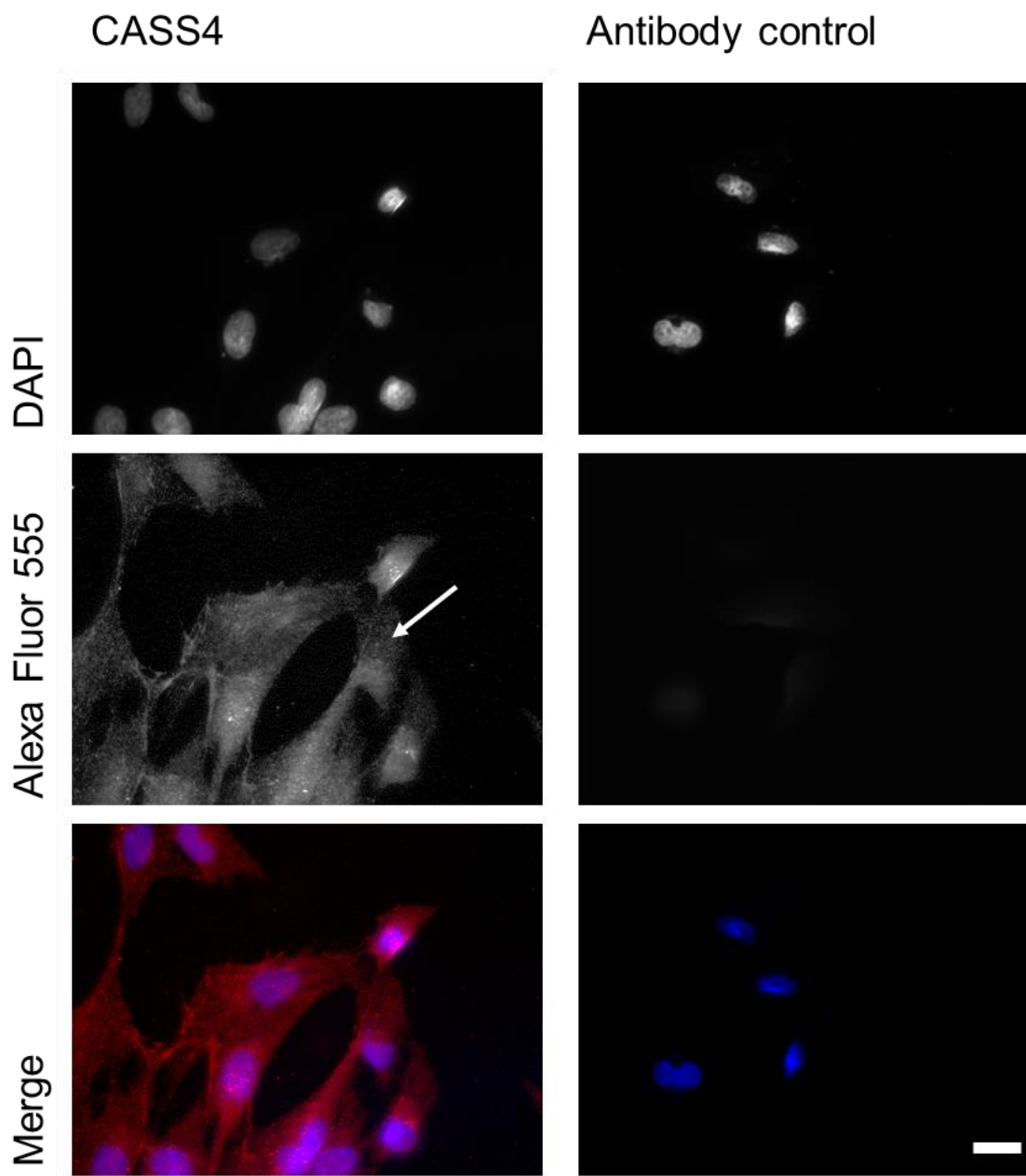
Figure 3.9 Immunofluorescence staining of SVG p12 human foetal glial cells confirms CASS4 expression.

Fixed SVG p12 cells were immunofluorescently stained using an anti-CASS4 antibody, followed by Alexa Fluor 555 secondary antibody, revealing a slightly punctate pattern of staining throughout the cell (Left). Secondary antibody (only) used as control (Right). N=3. Scale bar = 20μm.

3.2.5 Basal expression in primary human astrocytes

Although expression of the Cas-protein was confirmed in the astroglial cell lines SVGp12 and 1321N1, expression profiles often differ markedly between cell lines and primary cells (Pan *et al.*, 2009). NEDD9 and CASS4 expression was thus next examined in primary human cortical astrocytes (NHA). Expression of the Cas-protein was determined in NHAs from three separate male donors; representative results are shown.

Western blotting of NHA whole-cell lysates for NEDD9 revealed three bands at 65 kDa, 105 kDa and 115kDa, all correlating with known isoforms (Law *et al.,* 1998) (Figure 3.10, A). The 65 kDa band was rather faint and only visible at a high protein load of 20 µg. This band corresponds to the cleaved isoform which was previously found in the cell lines. The 55 kDa band seen in all the cell lines was absent from the NHA lysates. The 105 kDa band was most evident on the blot and, along with the fainter 115 kDa band, corresponds to phosphorylated forms of the full-length protein. These two bands were not seen in any of the cell lines. These results suggest that NEDD9 expression differs substantially in primary human astrocytes in comparison to the astroglial cell lines.
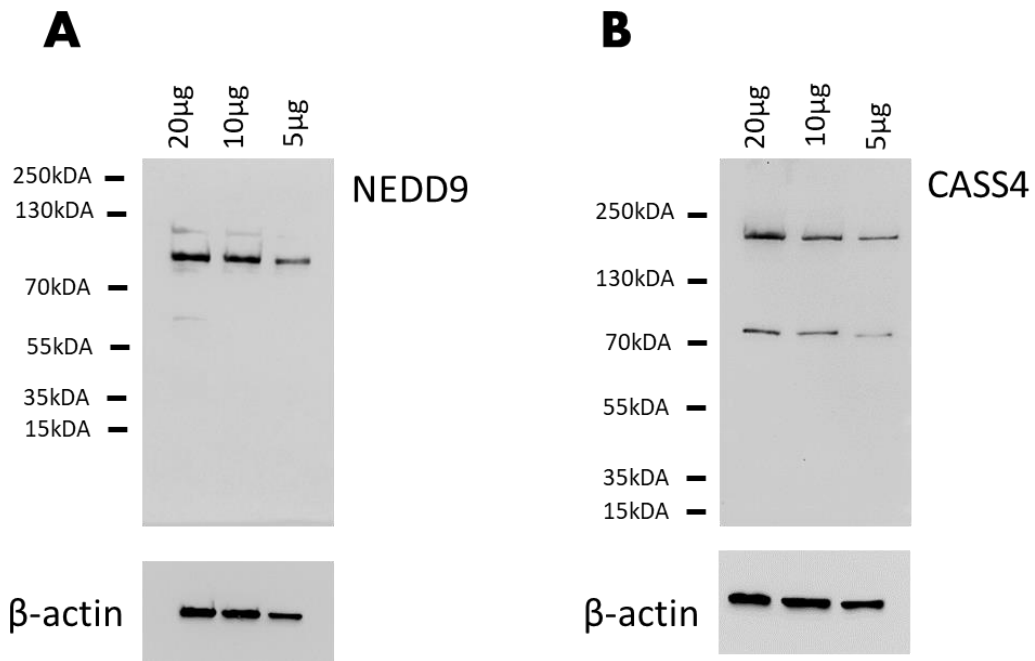
Figure 3.10 Western blotting of NHA lysates reveals expression of NEDD9 and CASS4.

Following separation by SDS-PAGE and blotting, three bands for were apparent using antibodies against NEDD9 (65 kDa, 105 kDa, 115 kDa) (A) and two bands using anti-CASS4 antibodies (76 kDa, 230 kDa) (B), confirming expression of both proteins in this cell type. Actin used as loading control. N=3.

Western blotting of NHA lysates for CASS4 revealed two bands of 76 kDa and 230 kDa (Figure 3.10, B), which had also been seen in the cell lines. As with the cell lines, protein loads between 5 and 20 µg were trialled, with both bands being visible in all cases, suggesting a robust expression of CASS4 in primary human astrocytes.

To further validate NEDD9 expression in primary human astrocytes, immunofluorescence staining was performed using the same antibody as for the Western blot (Figure 3.11). This revealed a slightly punctate pattern of NEDD9 staining which extended throughout the entire cell, consistent with expected cytosolic localisation. All cells observed exhibited NEDD9 staining. Omission of the primary antibody revealed no fluorescence, confirming the specificity of the primary antibody.
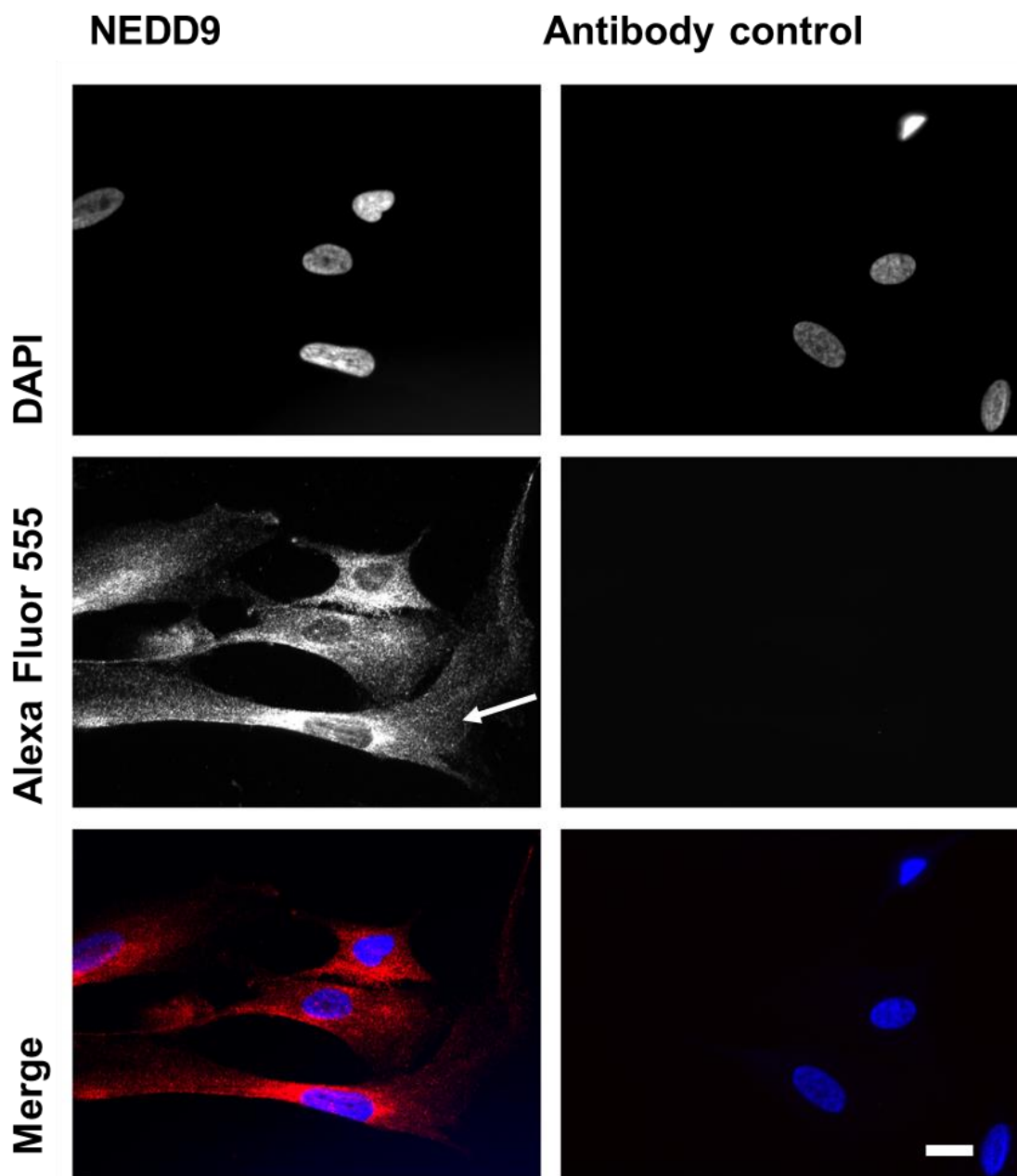
Figure 3.11 Immunofluorescence staining of primary human astrocytes (NHA) confirms NEDD9 expression.

Fixed NHA were stained using an anti-NEDD9 primary antibody, followed by Alexa Fluor 555 secondary antibody revealing a slightly punctate pattern of staining throughout the cell (Left). Secondary antibody (only) used as control (Right). N=3. Scale bar = 20μm.

Immunofluorescence staining of primary human astrocytes with CASS4 revealed a similar punctuate cytosolic pattern as for NEDD9, although somewhat fainter (Figure 3.12). The small cellular inclusions seen in the cell lines, were clearly visible in this cell type and appear more frequent than in the cell lines, suggesting that CASS4 localisation may differ in primary human astrocytes. Omission of the primary antibody revealed no fluorescence.
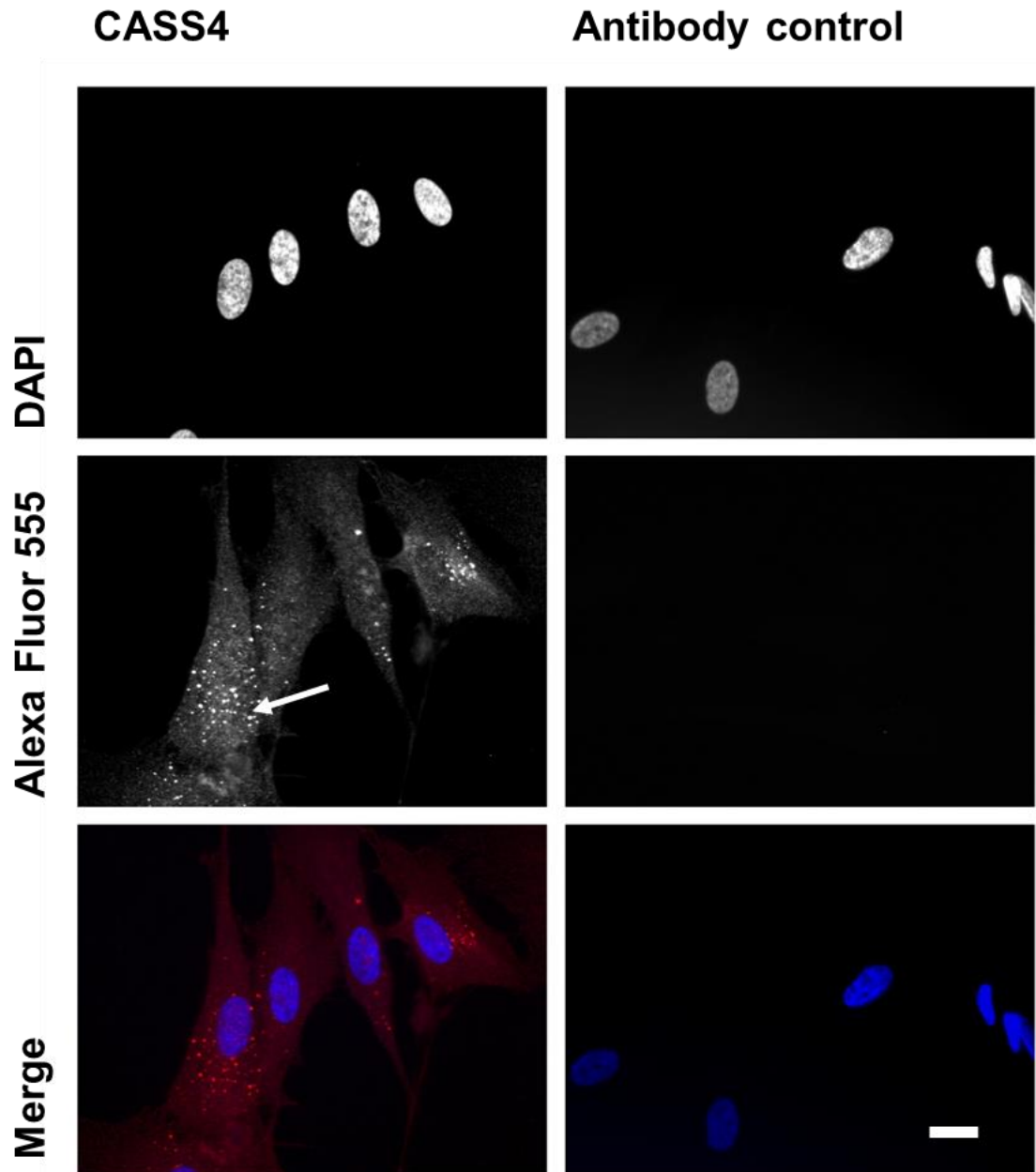
Figure 3.12 Immunofluorescence staining of primary human astrocytes (NHA) reveals expression of CASS4.

Fixed NHA were stained using a primary antibody for CASS4 followed by an Alexa Fluor 555 secondary antibody revealing a slightly punctate pattern of staining throughout the cell and numerous cellular inclusions (Left). Secondary antibody (only) used as control (Right). N=3. Scale bar = 20μm.

3.2.6 Basal expression in the adult mouse brain

Expression of CASS4 and NEDD9 was clearly evident in the cell lines tested and in normal human astrocytes. Notwithstanding, it could be argued that the cells types tested were of an 'immature' form. For example, cancer cells tend to revert back to stem-cell like states (Holmberg *et al.*, 2011, Hattermann *et al.*, 2016), and the NHAs utilised are derived from foetuses. Thus, to overcome the claims that NEDD9 (and by association, CASS4) is not expressed in the adult brain, it was necessary to test for expression in the adult brain.

As there were no human brain samples available to the project, expression of both CASS4 and NEDD9 was examined in adult mouse brain. Specifically, expression in the entorhinal cortex was tested as it is one of the primary regions which exhibits astrocytic atrophy in the 3xTg-AD mouse model (Yeh *et al.*, 2011).

Western blotting was carried out on pooled mouse entorhinal cortex lysates from three animals aged between three and four months. Staining of the blot with antibodies against NEDD9 revealed four bands at 19 kDa, 70 kDa, 105 kDa and 115 kDa (Figure 3.13, A). The two larger bands correlated with the phosphorylated forms of the full-length protein which were also found in the NHA lysates. The band at around 19 kDa likely corresponds to NEDD9 isoform 2. This band was not seen in any of the cell types. The final 70 kDa band had previously not been found in any of the cell lines or the primary human astrocytes but is likely a post-translationally modified version of the cleaved 65 kDa isoform.
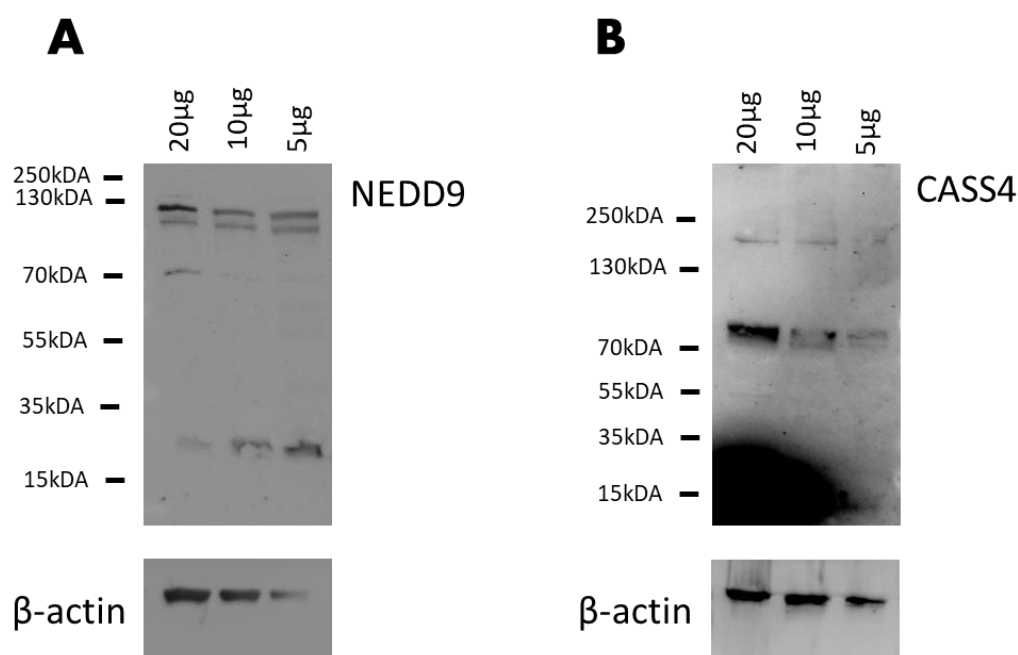
Figure 3.13 Western blotting of Mouse entorhinal cortex lysates reveals expression of various NEDD9 and CASS4 isoforms.

Following separation by SDS-PAGE and blotting, four bands were seen using antibodies against NEDD9 (19 kDa, 70 kDa, 105 kDa, 115 kDa) (A), and two bands using anti-CASS4 antibodies (76 kDa, 230 kDa) (B), confirming expression of both proteins in the adult mouse brain. Actin used as loading control. Pooled lysates from N=3 mice.

Western blotting of mouse entorhinal cortex lysates for CASS4 revealed a doublet at around 76 kDa and a single, fainter band at 230 kDa (Figure 3.13, B). While the unexplained 230 kDa band had been seen in all blots from the cell lines and human astrocytes, the usual single band at 76 kDa (corresponding to CASS4 isoform 2) was replaced by a doublet, potentially indicating some alteration of post-translational processing. As with cell lines and NHAs, protein loads between 5 and 20 µg total protein were trialled, with bands being visible in all cases, suggesting a robust expression of CASS4 in the entorhinal cortex of the adult mouse brain. Notably, the smaller isoform

(76 kDa) appears to be stronger expressed than the unexplained larger form (230 kDa), contrary to the findings in human cells, where the larger form appeared to be the more prominent.

3.3   Discussion

While NEDD9 and CASS4 have previously been reported to be expressed in many tissues (Deneka *et al.*, 2015), the evidence from the brain has been limited. NEDD9 was found to be expressed in neural progenitor cells in the mouse brain (Aquino *et al.*, 2008, Kumar *et al.*, 1992), but these and other earlier studies found that NEDD9 was absent or downregulated in the adult brain (Kumar *et al.*, 1992, Law *et al.*, 1996). CASS4 expression in the brain has also been dismissed as almost negligible (Kim *et al.*, 2014). Yet, these adult brain findings have been based on mRNA expression alone. The correlation between mRNA and protein expression is not straight forward and involves complex translational mechanisms, which are varied and hence difficult to predict (Greenbaum *et al.*, 2003, Liu *et al.*, 2016). Only one study to date found NEDD9 expression in human brain tissue (Li *et al.*, 2008) and no study has explored CASS4 expression in the human brain. Furthermore, expression of neither of the Cas-protein had not been confirmed in astrocytes.

Here it was found that both Cas-protein are expressed in cancer-derived cells (HeLa & 1321N1) as well as foetal human astrocytes (SVG p12), normal human astrocytes and the entorhinal cortex of the adult mouse brain. Basal expression was confirmed via immunocytochemistry and western blotting.

Western blotting for NEDD9, which has an actual molecular weight of 93 kDa, but exists as phosphorylated versions of 105kDa and 115kDa (Singh *et al*., 2007) revealed muliple bands of different weights. In addition to the full length versions, a band of 65 kDa, correlating with the size of a known isoform (Deneka *et al.*, 2015) and a 55kDa band, correlating with a splice variant (Law *et al.*, 2000) that was observed in all cell line lysates.

Blotting of NHA lysates also revealed the 55 kDa NEDD9 band, as well as two additional bands at around 105 kDa and 115k Da. The bands of 105 kDa and 115 kDa correspond to phosphorylated isoforms of the full-length protein, which had previously been identified (Law *et al.*, 1998, Bradshaw *et al.*, 2011). The 65 kDa isoform, however, was not present. This reveals key differences between the immortalised glial cell lines and the primary astrocytes. It is unclear why these differences, particularly between the immortalised cell lines and primary astrocytes, occur, but different NEDD9 splice variants might serve different roles within each cell type and might arise from cell type-specific post-translational modifications. This indicates that glial cell lines are likely not suitable for the investigation of the role of NEDD9 in astrocyte atrophy and that NHAs themselves are likely the best model for the investigation as primary cells are more likely to resemble cells *in vivo.*

Blotting of adult mouse entorhinal cortex lysates revealed the two phosphorylated forms (105 kDa and 115 kDa) of the full-length NEDD9 protein as was seen in the NHAs, as well as a band at 70 kDa, which is likely a phosphorylated version of the 65 kDa isoform (not present in the NHAs). Additionally, a 19 kDa band was found in the mouse lysate, which had not been found in any human cell types. This corresponds to the NEDD9 isoform 2 and as Cas-protein are known to undergo extensive phosphorylation (Singh *et al.*, 2007), this could lead to these heavier forms of the protein. The myriad of NEDD9

isoforms is regulated by cell cycle phases and influenced by integrin binding (Law *et al.*, 1998, Singh *et al.*, 2007). It is hence impossible to establish which forms may be expressed in a cell population or tissue at any given time. However, the varied expression of NEDD9 isoforms in different tissues, suggests that the protein expression is also tissue specific.

In the case of CASS4, two bands were consistently seen in all cell lines, NHAs and in mouse brain tissue. The first band of 76 kDa corresponds with a known isoform of the protein appeared as a single strong band in all cases, with the exception of the mouse brain tissue, where it appeared as a doublet. This might suggest that there is some additional modification in brain tissue, or it might be a form which is seen in non-astrocyte cell type, such as neurones, as whole tissue lysates were used. Determining astrocyte specific expression of CASS4 (or NEDD9) in the adult mouse brain would require immunohistochemistry. This would allow to use double staining, to identify astrocytes *in situ* and determine Cas-protein expression of this specific cell type in the adult mouse brain. Immunohistochemistry was not within the scope of this thesis but could be beneficial, particularly for human brain tissue, to further validate the Cas-protein expression in the future.

A second CASS4 band was observed at 230 kDa in all lysates. This does not correlate with any known isoform of CASS4, nor to the full-length protein (87 kDa). Given the very large molecular weight of this band, it is unlikely that this is due to phosphorylation or other post-translational modifications and is more likely a complex, although it did resist attempts to break up with harsher denaturing conditions. Intriguingly, this heavier CASS4 band has also been observed in the laboratories of Dr Mahendra Singh and Prof Erica Golemis (personal correspondence). One possibility is that the band might be a tightly-bound complex of CASS4 with an associated kinase such as Abelson murine

leukaemia (Abl) kinase (Witte *et al.*, 1980, Shagisultanova *et al.*, 2015), which would require further research.

Despite the fact that the large size of CASS4 remains unexplained and the expression of NEDD9 isoforms varies, these results nonetheless confirm:

a)   NEDD9 and CASS4 are expressed in cell lines of different tissue origin (cervical cancer, astrocytoma, foetal astrocytes)

b)   NEDD9 and CASS4 are expressed in primary cortical human astrocytes

c)   NEDD9 and CASS4 are expressed in the adult mouse brain (entorhinal cortex)

Although immortalised cell lines can often provide a good basis for an *in vitro* model, as they are robust, highly proliferative and easy to culture, they have been shown to differ genotypically and phenotypically from the tissue origin (Alge *et al.*, 2006, Pan *et al.*, 2009). Primary cells are only maintained in culture for a relatively short period of time, in order to retain native phenotype and are hence more reflective of an *in vivo* environment. While the CASS4 results were similar across all cells/tissues tested, the expression results from NEDD9 show marked differences in protein isoforms present in the cell lines compared to the primary astrocytes. Thus, the remainder of this thesis will utilise NHAs as a model for the investigation of the influence of the Cas-proteins in astrocyte morphology and function.

Chapter 4

Overexpression and knock-down models of NEDD9 & CASS4 in normal human astrocytes

4 Chapter 4 – RESULTS: Overexpression and knock-down models of NEDD9 & CASS4 in normal human astrocytes

4.1 Background

Several GWAS studies have found that several SNPs in the genes NEDD9 (Li *et al*., 2008) and CASS4 (Lambert *et al*., 2013), which encode the Cas-proteins NEDD9 and CASS4, are associated with a risk of developing AD. Follow-up studies tested the significance of these SNPs and found that NEDD9 SNP rs760678 showed the strongest association with LOAD development (Li *et al*., 2008, Fu *et al*., 2012, Xing *et al*., 2011). In 2013, Lambert *et al*. found that SNP rs7274581 of the CASS4 gene reached genome-wide significance. Two more susceptibility loci were since added to the list of CASS4 LOAD risk variants, rs16979934 (Wang *et al*., 2015) and rs6024870 (Rosenthal *et al*., 2014). The SNPs in both NEDD9 and CASS4 are not within exons, suggesting that the gene products are not affected; the proteins are not mutated and retain normal biological function. Instead, the SNPs are found in transcription factor (TF) binding sites (Chapuis *et al*., 2008, Rosenthal and Kamboh, 2014). Specifically, the rs760678 polymorphism of NEDD9 maps near a GATA1 transcription factor binding site (Li *et al*., 2008). SNPs in this region would be expected to lead to a decrease in expression if a transcription factor (TF) cannot bind or an increase if a TF repressor cannot bind (Beck *et al*., 2014, Gan *et al*., 2018, Kamanu *et al*., 2012, Tugrul *et al*., 2015). Based on this, both, overexpression and knock-down models of NEDD9 and CASS4 in primary human astrocytes were generated to investigate the effect of altered expression of the Cas-proteins on astrocytes.

Mammalian overexpression systems generally rely on the use of a plasmid expression vector containing the gene of interest (GOI); here, NEDD9 or CASS4, together with a strong promoter to drive expression. The expression vectors used in this thesis were based on a commercially-available pLenti-GIII-CMV-GFP-2A-Puro backbone which has several advantageous features: (1) A cytomegalovirus (CMV) promoter; a long-established method to drive robust expression of the GOI (Rotonardo *et al*., 1996); (2) An internal ribosomal entry site (IRES) to allow bicistronic expression of the GOI alongside a reporter gene (Mansouri *et al*., 2016, Kim *et al*., 2004); (3) a soluble green fluorescent protein (GFP) in the form of CopGFP (also known as ppluGFP2) (Shagin *et al*., 2004) to both signal which cells have taken up the vector and serve as a means to fluorescently visualise the cell; (4) a puromycin resistance gene, allowing selection of transfected cells where necessary; and, (5) lentiviral vector packaging signals to permit the plasmid to be used to create lentiviral vector particles for virus-mediated gene delivery, if necessary (Follenzi and Naldini, 2002).

Primary cells, particularly neural cells, are notoriously difficult to transfect (Gresch and Altrogge, 2012, Alabdullah *et al*., 2019). Viral delivery methods, such as lentiviral transduction, have shown to yield high efficiencies in primary cells and allow to produce stable transfection of the target gene (Jakobsson *et al*., 2006, Merienne *et al*., 2013, Fassler *et al*., 2013). This method is not without pitfalls, as it can introduce insertions and lead to inactivation of tumour suppressor genes (Bett *et al*., 1993, Shearer and Saunders, 2015). Furthermore, viral delivery systems are time consuming, require specific laboratory safety procedures and are subject to a limited cargo load (Mansouri *et al*., 2016). Hence, viral delivery methods should only be utilised where needed. On the contrary, while transient transfection methods, particularly lipid-mediated delivery, yield generally lower transfection efficiencies in primary cells, they do not require extensive

safety procedures, are less time consuming and easily reproducible (Shi *et al*., 2018, Alabdullah *et al*., 2019). Based on this, transient transfection via lipid-mediated delivery was initially trialled to achieve overexpression Cas-proteins.

A well-established method of depleting levels of a protein of interest in target cells is to utilise RNA-interference (RNAi). RNAi is a process in eukaryotes that regulates silencing of genes post transcription by utilising double stranded RNA (dsRNA). The dsRNA is then cleaved into a shorter, small interfering RNA (siRNA) by the RNase III endonuclease Dicer (Zhang *et al*., 2004). The dicer complex then aids the small siRNAs to bind to other proteins, including Ago-2, an argonaute protein which harbours a catalytic domain for cleavage of the RNA (Meister *et al*., 2004), to form a multiprotein complex, RISC. Through Ago-2 activity, the double stranded siRNA is unwound into single stranded RNA with a high binding affinity for the target gene mRNA. The RISC complex then targets the complementary mRNA and silences the gene by inducing cleavage and degradation of the transcript (mRNA) (Almeida and Allshire, 2005). This biological process can be 'hijacked' and used to silence genes of interest through the introduction of exogenous siRNAs. This can be achieved via direct transfection of cells with siRNA which produces transient gene silencing, or by transfection with a siRNA-encoding expression vector. Using a vector is superior in that it produces longer-lasting effects (since the siRNA will be produced for as long at the expression plasmid remains in the cell), and selection markers and fluorescent transporters can be inserted into the vector to co-express alongside the siRNA. Simultaneous transfection of several vectors which encode siRNAs complimentary to various target sequences within the same transcript are known to provide enhanced gene silencing (Parsons *et al*., 2009). SiRNA vectors built on the same pLenti-GIII-CMV-GFP-2A-Puro backbone as the overexpression vector were employed, whose GOI was either siRNA against NEDD9 or CASS4. In all cases, pools

of vectors encoding four siRNAs targeted against different regions of each Cas-protein transcript were transiently transfected into the NHAs using a lipofection method, as it has been shown to yield positive results in astrocytes (Ishii *et al*., 2017, Youn *et al*., 2015). Each siRNA was transfected at a relatively low level to minimise off-target effects.

4.2   Results

4.2.1   Cas-protein overexpression models

Overexpression of the Cas-proteins in NHAs *in vitro* was achieved via transiently transfecting CASS4 or NEDD9 encoding plasmids (pLenti-GIII-CMV-GFP-2A-Puro), which are driven by CMV promoters to induce overexpression of the Cas-proteins. An empty/blank pLenti-GIII-CMV-GFP-2A-Puro vector was transiently transfected into control NHAs. Biscistronic expression of GFP alongside the target gene which permitted confirmation of transfection as well as the visualisation of entire cells for subsequent morphometric analysis. Immunofluorescent staining with primary antibodies against CASS4 or NEDD9 followed by an Alexa Fluor 555 (red) secondary antibody permitted assessment of intracellular levels of the Cas-proteins. Cells were counted and assessed in 20 random fields of view at x40 magnification in three repeats of the experiment (N=3).

Overexpression model of NEDD9 in normal human astrocytes

Transfection of NHAs with Cas gene-containing LV-CMV vectors yielded comparable results as transfection with the GFP-only blank vector, in that GFP spread through the entire cell, permitting visualisation of cell morphologies. Transfection efficiencies also averaged 30-50% with no signs of toxicity. There is no standard for sufficient transfection efficiencies. Although on the lower end of the spectrum, the achieved 30-50% were sufficient to visualise cells via microscopy, as transfected cells are GFP positive and could thus be chosen for analysis. Transient transfection of the LV-CMV vectors for NEDD9 and CASS4 via lipid-mediated delivery was thus deemed suitable for undertaking the planned experiments for this thesis.

NHAs transfected with the NEDD9 LV-CMV overexpression vector or blank vector control were immunostained for NEDD9 (Figure 4.1). Fluorescence imaging revealed a slightly punctate staining pattern throughout the cytosol for NEDD9 in both transfection conditions, consistent with that observed in non-transfected cells (Chapter 3). An increase in NEDD9 fluorescence could be visually observed in the NHAs transfected with a NEDD9 overexpression vector in comparison to control cells (Figure 4.1).
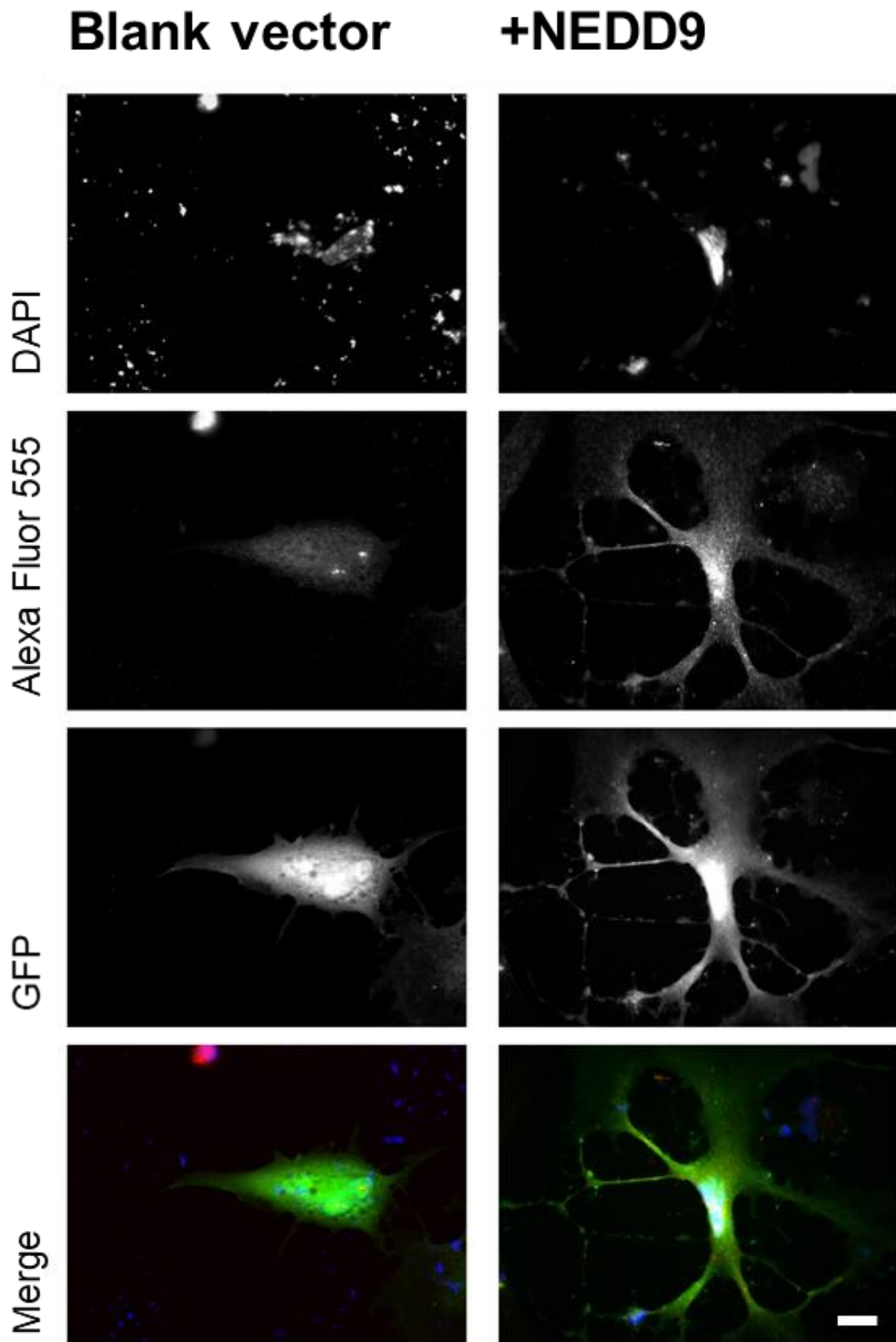
Figure 4.1 Fluorescence of NEDD9 is increased in NHAs transfected with the NEDD9 LV-CMV vector in comparison to the blank vector control.

Fixed NHA were stained using a primary antibody for NEDD9 followed by an Alexa Fluor 555 secondary antibody revealing increased NEDD9 fluorescence in the cells transfected with NEDD LV-CMV in comparison to the blank vector transfected control. N=3 (donors), three technical repeats. Scale bar = 20μm.

Fluorescence intensities (NEDD9) of NHAs transfected with NEDD9 LV-CMV and a blank vector control were measured and compared (Figure 4.2). An independent-samples t-test showed that there was a significant increase of fluorescence $t(4) = 12.485$, $P < 0.001$) between the cells, transfected with a blank vector control (M= 135.66, SD= 8.36) and the cells, transfected with NEDD9 LV-CMV (M= 471.67, SD= 45.85), indicating that transfection of NHAS with NEDD9 LV-CMV induces increased NEDD9 expression.
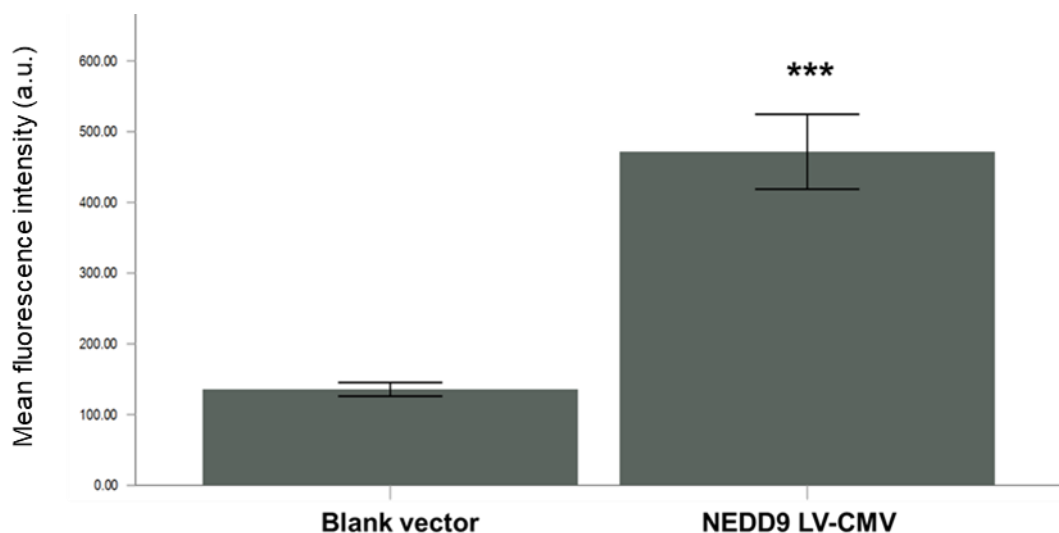
Figure 4.2 Transfection of NHAs with NEDD9 LV-CMV leads to increased fluorescence

*Fluorescent images of NHAs, transfected with either NEDD9 LV-CMV or a blank vector control were analysed with ImageJ. Measured fluorescence intensity was compared between the two groups, showing a significant increase in the NEDD9 LV-CMV cells. N=3, three technical repeats. Error bars ± 2 SEM. *** $p \le 0.001$*

To further validate the overexpression of NEDD9, Western blotting of whole-cell lysates from NHAs transfected with the NEDD9 LV-CMV or blank vector, was performed, followed by densitometric analysis with ImageJ. Relative density data were normalised to the β- actin loading control and statistically compared. All bands previously identified as endogenously expressed in NHAs (65, 105 and 115 kDa) were still evident in the NEDD9 LV-CMV transfected NHAs (Figure 4.3, A). All bands appeared to be enriched in the NEDD9 LV-CMV transfected cells compared to controls. This was particularly clear for the 115 kDa isoform band. Following normalisation, densitometric analysis of all bands together revealed a significant increase of NEDD9 expression is NHAs transfected with NEDD9 LV-CMV (M= 1.45, SD= 0.079) in comparison to the NHAs, transfected with the blank vector control (M= 0.58, SD= 0.02) (t(4)=18.16, $P<0.001$; Figure 4.3, B) suggesting that overexpression of NEDD9 was achieved.
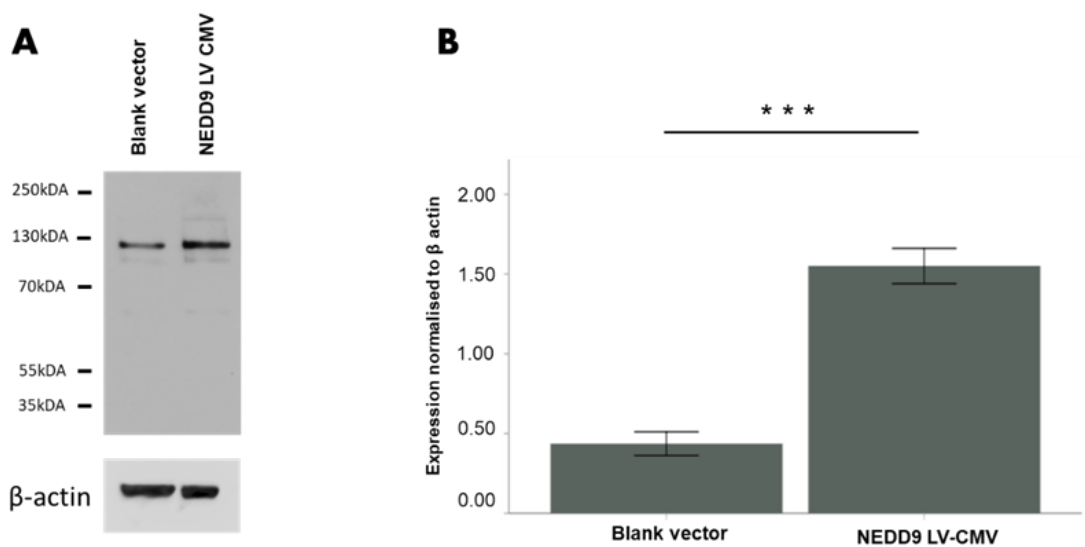
Figure 4.3 Overexpression of NEDD9 was achieved in normal human astrocytes

Western blotting of lysates from NHAs, transfected with NEDD9 LV-CMV show a visible stronger band at 115kDa comparison to lysates from cells transfected with a blank vector control; loading control: β actin (A) Densitometric analysis revealed a significant increase of density in the NEDD9 LV-CMV band in comparison to the control band (B). Error bars ± SEM. *** p≤ 0.001

Overexpression model of CASS4 in normal human astrocytes

NHAs transfected with the CASS4 LV-CMV overexpression vector or blank vector control were immunostained for CASS4 (Figure 4.3). Fluorescence imaging revealed a staining pattern throughout the cytoplasm for CASS4 in both transfection conditions, consistent with that observed in non-transfected cells (Chapter 3). A clear increase in CASS4 fluorescence was observed in the NHAs transfected with a CASS4 overexpression vector in comparison to control cells (Figure 4.4).
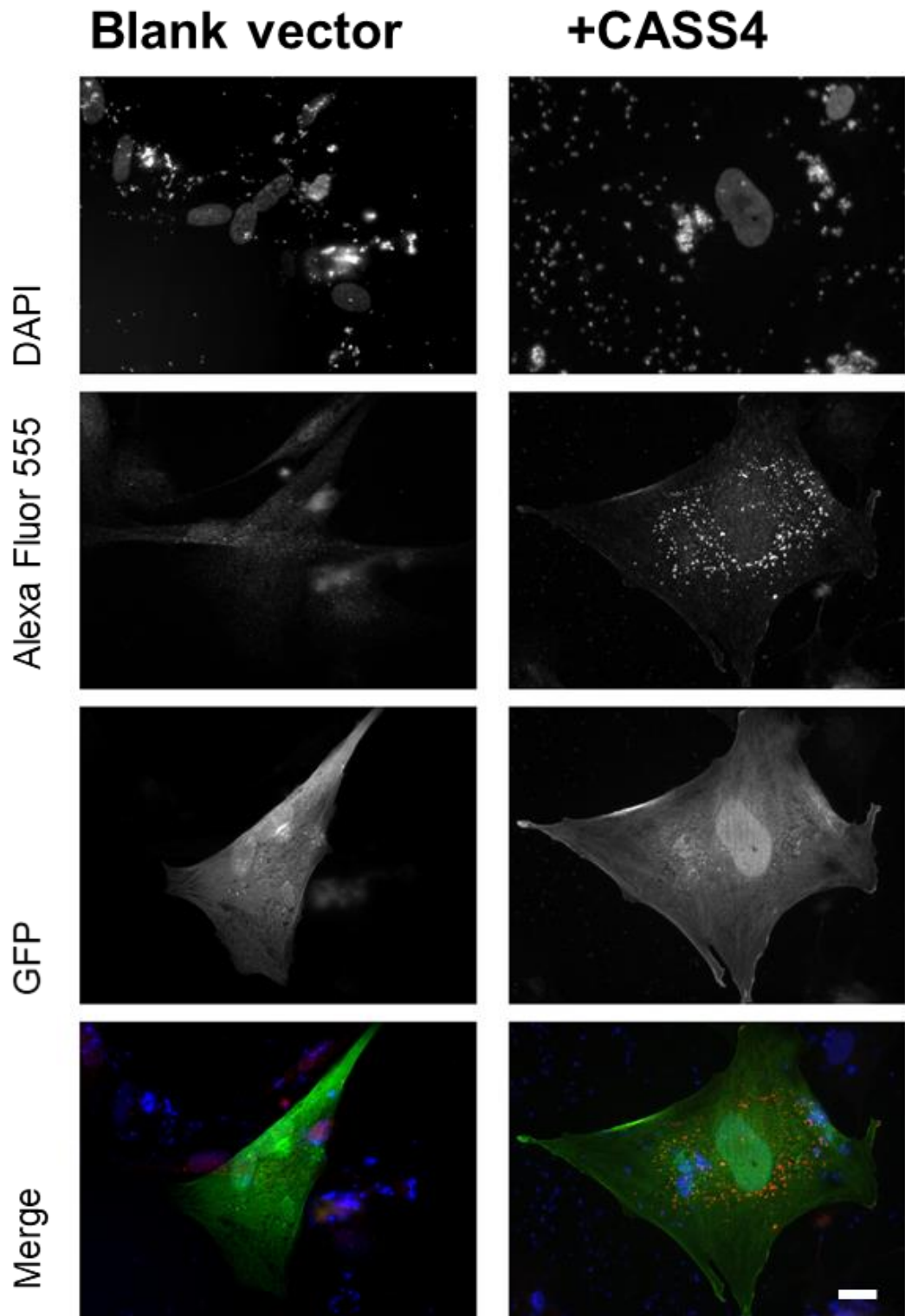
Figure 4.4 Fluorescence of CASS4 is increased in NHAs transfected with the CASS4 LV-CMV vector in comparison to the blank vector control.

Fixed NHA were stained using a primary antibody for CASS4 followed by an Alexa Fluor 555 secondary antibody revealing increased CASS4 fluorescence in the cells transfected with CASS4 LV-CMV in comparison to the blank vector transfected control. N=3, three technical repeats. Scale bar = 20μm.

Image analysis, measuring integrated density of cells in both transfection conditions revealed a rise in fluorescence for NHAs, transfected with CASS4 LV-CMV. When compared to blank vector transfected control cells, CASS4 LV-CMV transfected cells showed a significantly higher amount of CASS4 fluorescence intensity (Figure 4.5). Independent-sample t-Test; CASS4 LV-CMV cells (M= 529.17, SD= 27.83) versus blank vector transfected control (M= 135.66, SD= 8.36); t(4)= 23.542, *P*= <0.001, suggesting that transfection of NHAs with CASS4 LV-CMV induces increased expression of CASS4.
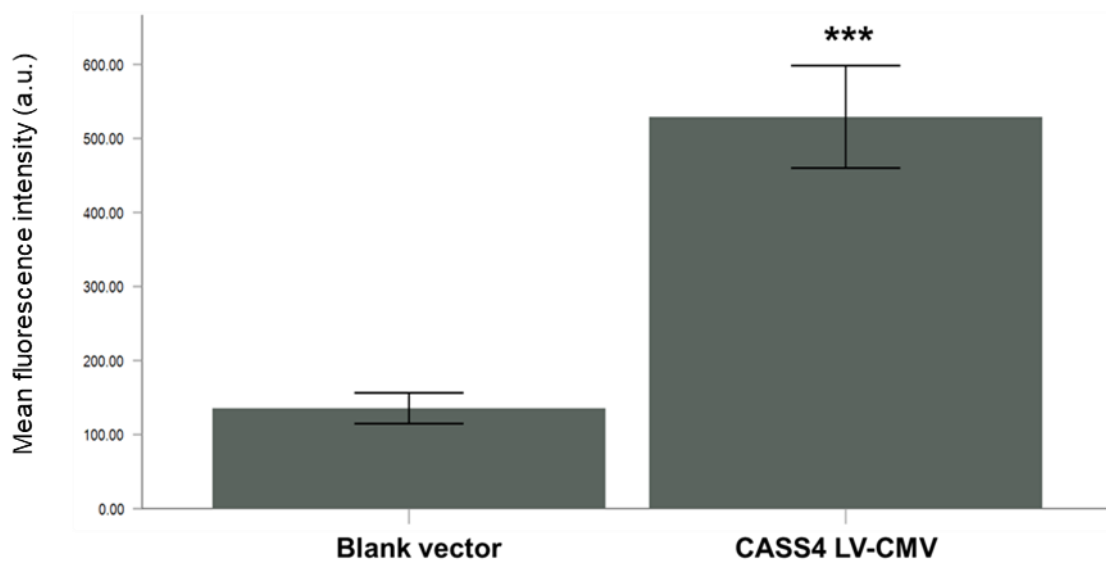
Figure 4.5 Transfection of NHAs with CASS4 LV-CMV leads to increased fluorescence

Fluorescent images of NHAs, transfected with either CASS4 LV-CMV or a blank vector control were analysed with ImageJ. Measured fluorescence intensity was compared between the two groups, showing a significant increase in the CASS4 LV-CMV cells. N=3, three technical repeats. Error bars ±2 SEM. *** p≤ 0.001

To further validate the overexpression of CASS4, Western blotting of whole-cell lysates from NHAs transfected with the CASS4 LV CMV or blank vector was performed, followed by densitometry analysis with ImageJ. Relative density data were normalised to the loading control (β-actin) and compared. Both bands previously identified as endogenously expressed (76 and 230 kDa), but only the 230kDa was seen to become thickened in the CASS4 LV-CMV transfected cells (Figure 4.6, A). Densitometry analysis of all bands revealed a significant increase of expression of CASS4 for NHAs transfected with CASS4 LV-CMV (M= 1.49, SD= 0.49) compared to NHAs transfected with the blank vector control (M= 0.46, SD= 0.11) (t(4)=14.59, $P<0.001$; Figure 4.6, B), suggesting that overexpression of CASS4 in primary astrocytes was achieved and confirming the immunofluorescence analysis results.
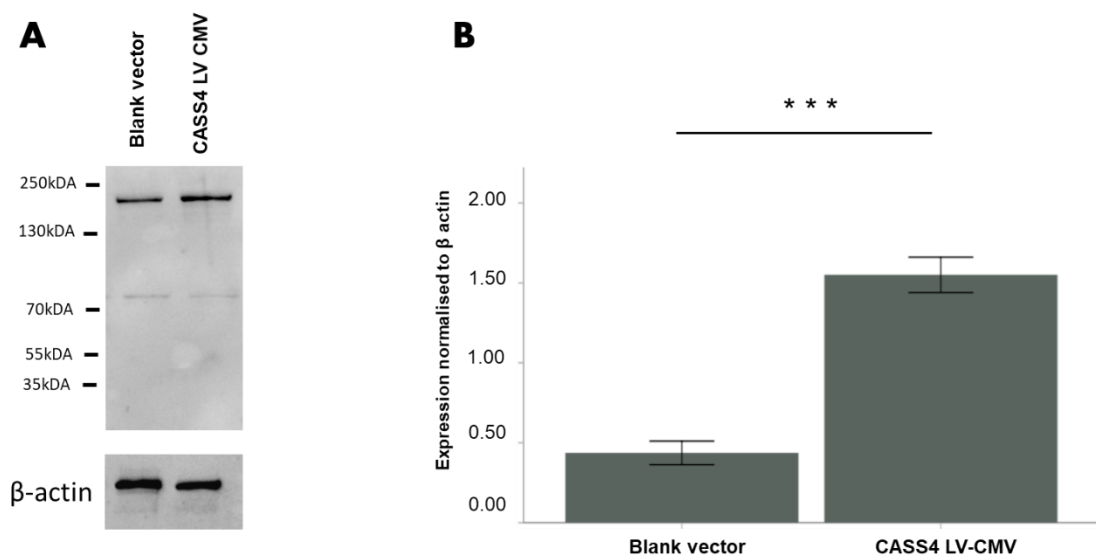
Figure 4.6 Overexpression of CASS4 was achieved in normal human astrocytes

Western blotting of lysates from NHAs, transfected with CASS4 LV-CMV show a visible stronger band at 115kDa comparison to lysates from cells transfected with a blank vector control; loading control: β actin (A) Densitometric analysis revealed a significant increase of density in the CASS4 LV-CMV band in comparison to the control band (B). Error bars ± SE. *** p≤ 0.001

4.2.2   Cas-protein knock-down models

Depletion of Cas-protein expression was achieved by transiently transfecting a set of four piLenti-siRNA-GFP vectors encoding siRNAs targeted to NEDD9 or CASS4 transcripts. The siRNA vectors were bicistronic; expressing GFP alongside the siRNA to allow for visualisation of the entire cell. A vector encoding a scramble siRNA designed not to target any cellular transcript was used as a control. Cells were immunofluorescently stained for CASS4 and NEDD9 to assess whether knock down of CASS4 or NEDD9 had been achieved. Cells were counted and assessed in 20 random fields of view at x40 magnification in three repeats of the experiment (N=3). Image analysis with ImageJ was performed to measure fluorescence intensity and compare the NEDD9 and CASS4 KD cells to cells, transfected with a scramble control.

Knock-down model of NEDD9

Transient transfection of NHAs with a NEDD9 siRNA-encoding plasmids induced no change in the subcellular distribution of NEDD9 (Figure 4.7). A reduction in NEDD9 fluorescence intensity in comparison to the control cells transfected with a scramble control, suggesting a downregulation of NEDD9 expression. Of further note was that by 48 hours of transfection cells transfected with NEDD9 siRNA had begun to detach from the cultureware, limiting the ability to maintain them in culture for any prolonged period of time.
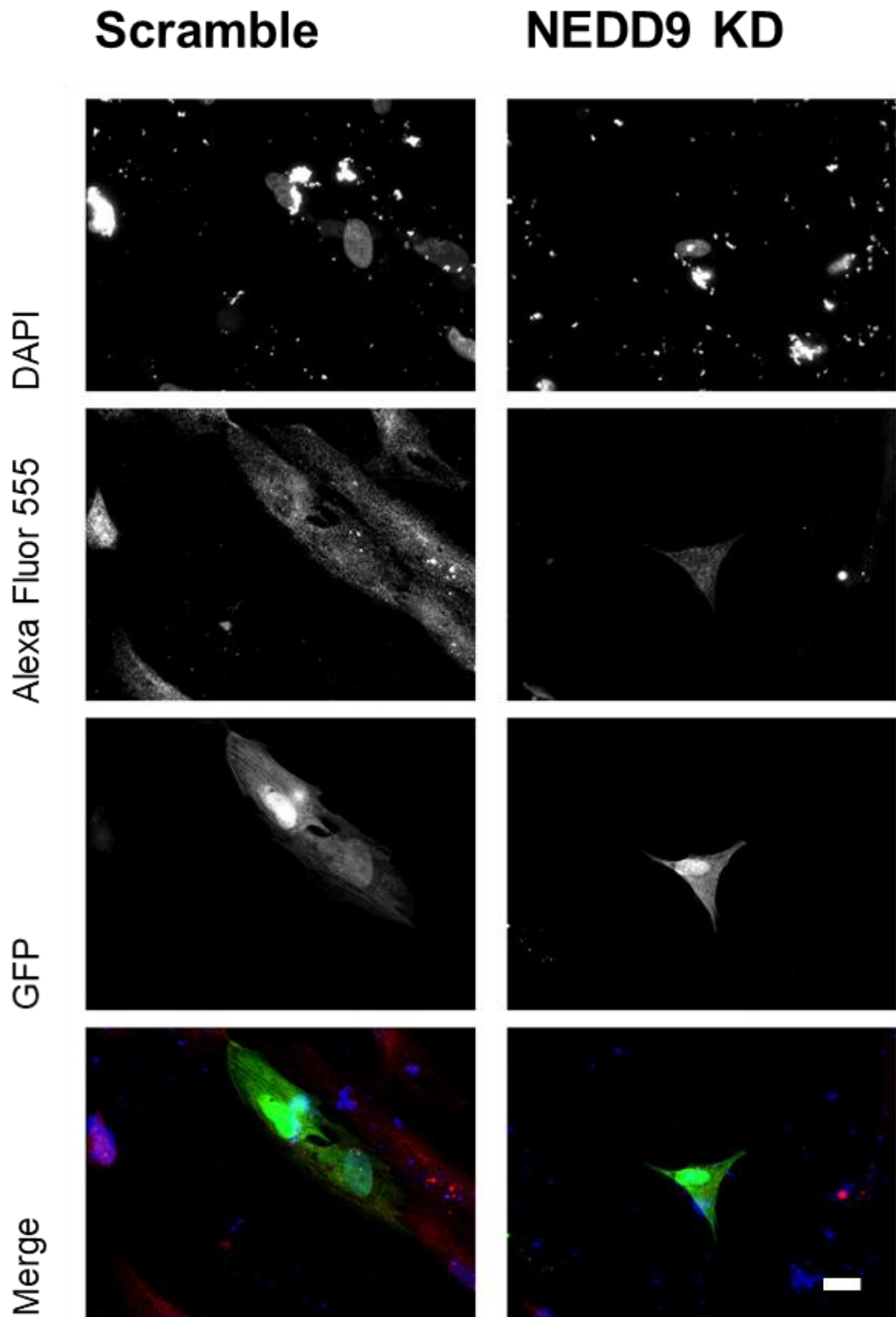
Figure 4.7 Fluorescence of NEDD9 is reduced in NHAs transfected with the NEDD9 siRNA in comparison to the scramble control.

Fixed NHA were stained using a primary antibody for NEDD9 followed by an Alexa Fluor 555 secondary antibody revealing reduced NEDD9 fluorescence in the cells transfected with NEDD siRNA in comparison to the scramble transfected control. N=3, three technical repeats. Scale bar = 20μm.

Comparing integrated density measurements of NEDD9 immunofluorescence in NHAs

transfected with NEDD9 siRNA or a scramble control revealed a significant reduction of

NEDD9 fluorescence intensity in the NEDD9 siRNA transfected cells (M=27.38,

SD=1.87) in comparison to the scramble control (M=124.74 , SD=5.23) (t(4)= 30.338,

$P< 0.001$; Figure 4.8), indicating that transfection with a set of NEDD9 siRNA encoding

vectors induced a reduction of NEDD9 expression.
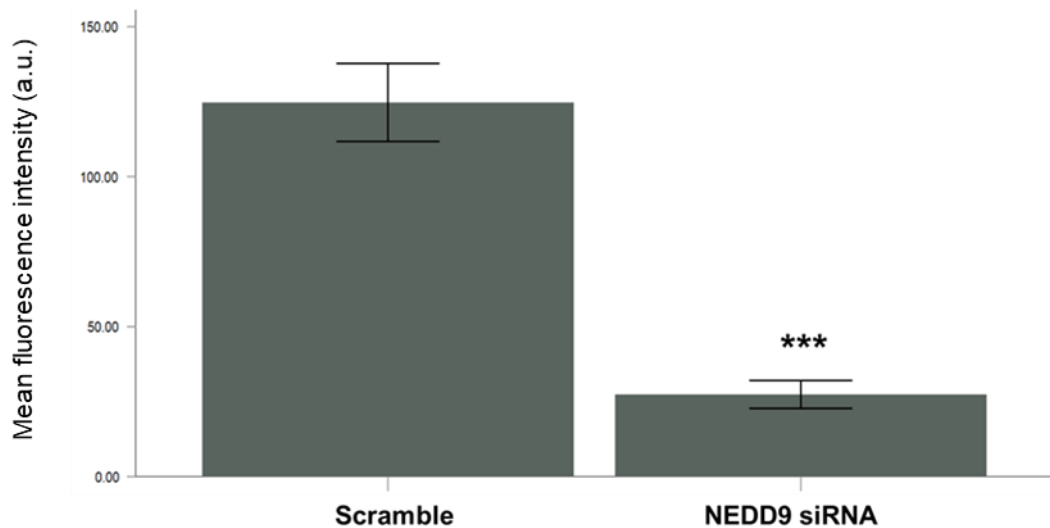
Figure 4.8 Transfection of NHAs with NEDD9 siRNA leads to reduction of fluorescence

> *Fluorescent images of NHAs, transfected with either NEDD9 siRNA or a scramble control were analysed with ImageJ. Measured fluorescence intensity was compared between the two groups, showing a significant decrease in the NEDD9 siRNA cells. N=3, three technical repeats. Error bars ± 2 SEM. *** p≤ 0.001*

To further validate these findings, Western blotting of lysates from NHAs, transfected

with NEDD9 siRNA encoding vectors or a scramble control and enriched via puromycin

selection, were performed, followed by densitometric analysis. Initially, the transfection

efficiency achieved by transient transfection proved problematic as endogenous Cas-protein expression in un-transfected cells masked the knock-down, since WB is not sensitive enough to pick up modest changes in expression levels. In order to achieve unambiguous results, enrichment of transfected (i.e. knocked-down) cells via puromycin selection was performed. Cells were exposed to medium, supplemented with puromycin for 24 hours to reduce the number of non-transfected cells, which caused an adequate reduction of non-transfected cells to detect the knock-down. To establish the optimal concentration of puromycin to select transfected cells, a dose response experiment (puromycin kill curve) was conducted (Figure 4.9).

NHA growth curve in presence of puromycin
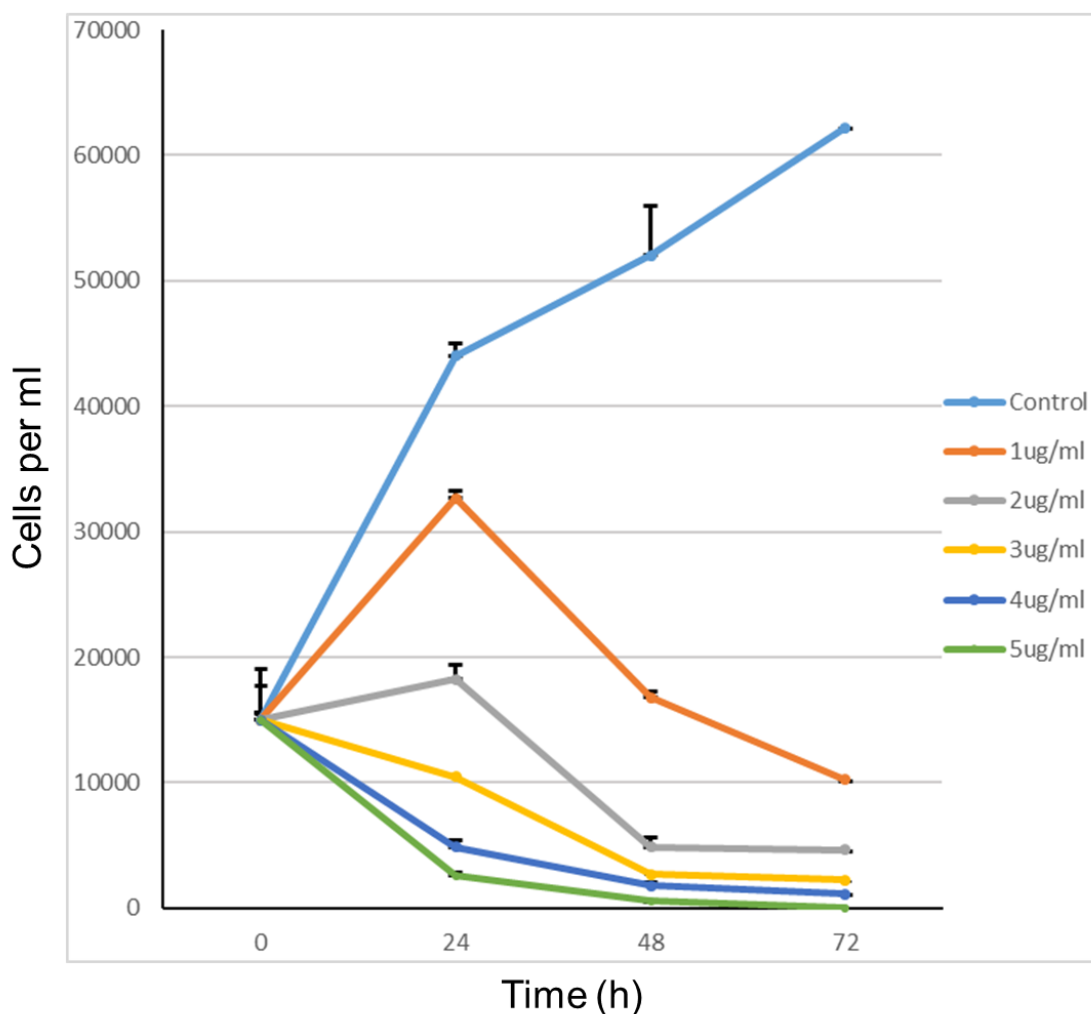
Figure 4.9 Growth curve for NHA in presence of increasing concentrations of puromycin

Increasing concentrations of puromycin (0-5µg/ml) were added to cell medium. Cells were counted at 24, 48 and 72 hours. N=3, three technical repeats. Error bars= SEM

All concentrations of puromycin tested were effective in reducing the growth of NHAs in culture in a dose-dependent manner. Both 4 µg/ml and 5 µg/ml had all but killed all NHAs within 48 hours. As outlined above, by 48 hours NEDD9 siRNA transfected NHAs had started to detach from the growth surface and hence could not be grown for this period. Hence a concentration of 5 µg/ml was chosen, as this induced an adequate effect after only 24 hours, reducing non-transfected cells sufficiently to conduct WB.

Western blotting of lysates from NHAs transfected with a scramble control showed two bands for NEDD9 (115 kDa and 105 kDa); both bands are visibly fainter in the NEDD9 siRNA lysates. The NHA NEDD9 siRNA lysates unusually revealed the known isoform of 65kDa, which was absent in the control (Figure 4.10, A) and only faintly visible in the endogenous expression experiments (Chapter 3). Densitometric analysis of the combined bands in the blots showed a significant decrease of expression between in the NEDD9 siRNA NHAs (M= 0.47, SD= 0.545) compared to the scramble control (M= 2.51, SD= 0.103) (t(4)= 3.404, P= 0.027; Figure 4.10, B), suggesting that a NEDD9 knock-down was achieved in normal human astrocytes. The large error bars of the scramble densitometric data reflects the variation of Cas-protein expression in the NHA control cell population.
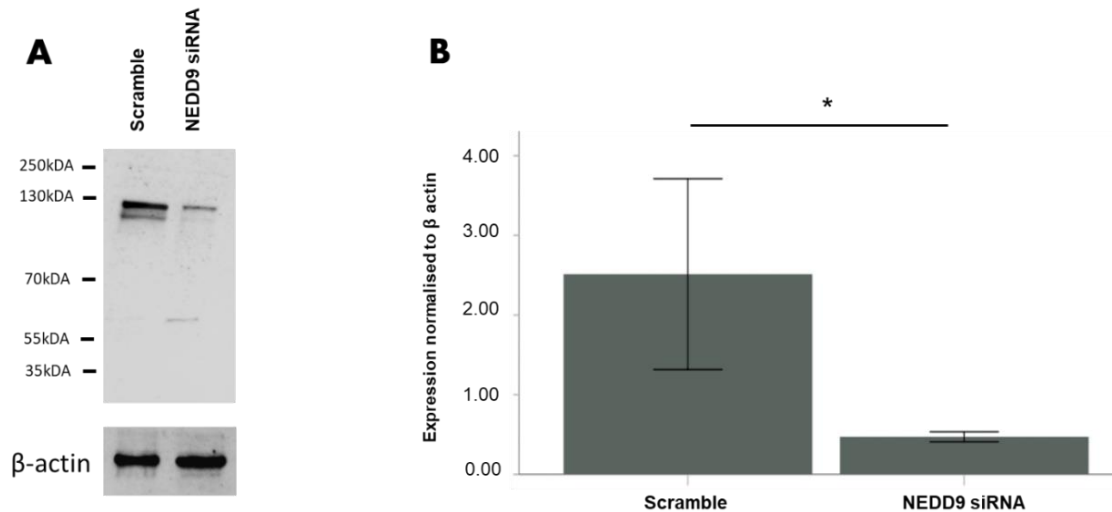
Figure 4.10 Knock-down of NEDD9 was achieved in normal human astrocytes

> *WB of lysates from NHAs, transfected with NEDD9 siRNA show a visibly lighter band at 115kDa comparison to lysates from cells transfected with a scramble control which also showed the 105kDa isoform; loading control: β actin (A) Densitometric analysis revealed a significant decrease of density in the NEDD9 siRNA band in comparison to the control band (B). Error bars ± 2 SEM. * p≤ 0.05*

Knock-down-model of CASS4

Transient transfection of NHAs with a CASS4 siRNA-encoding plasmids induced no change in the subcellular distribution of CASS4 (Figure 4.11). A decrease in CASS4 fluorescence intensity in comparison to the control cells transfected with a scramble control, suggesting a downregulation of CASS4 expression. Of further note, as was the case in the NEDD9 knock-down cells, by 48 hours of CASS4 siRNA transfection, cells had begun to detach from the growth surface, limiting the ability to maintain them in culture for any prolonged period of time.
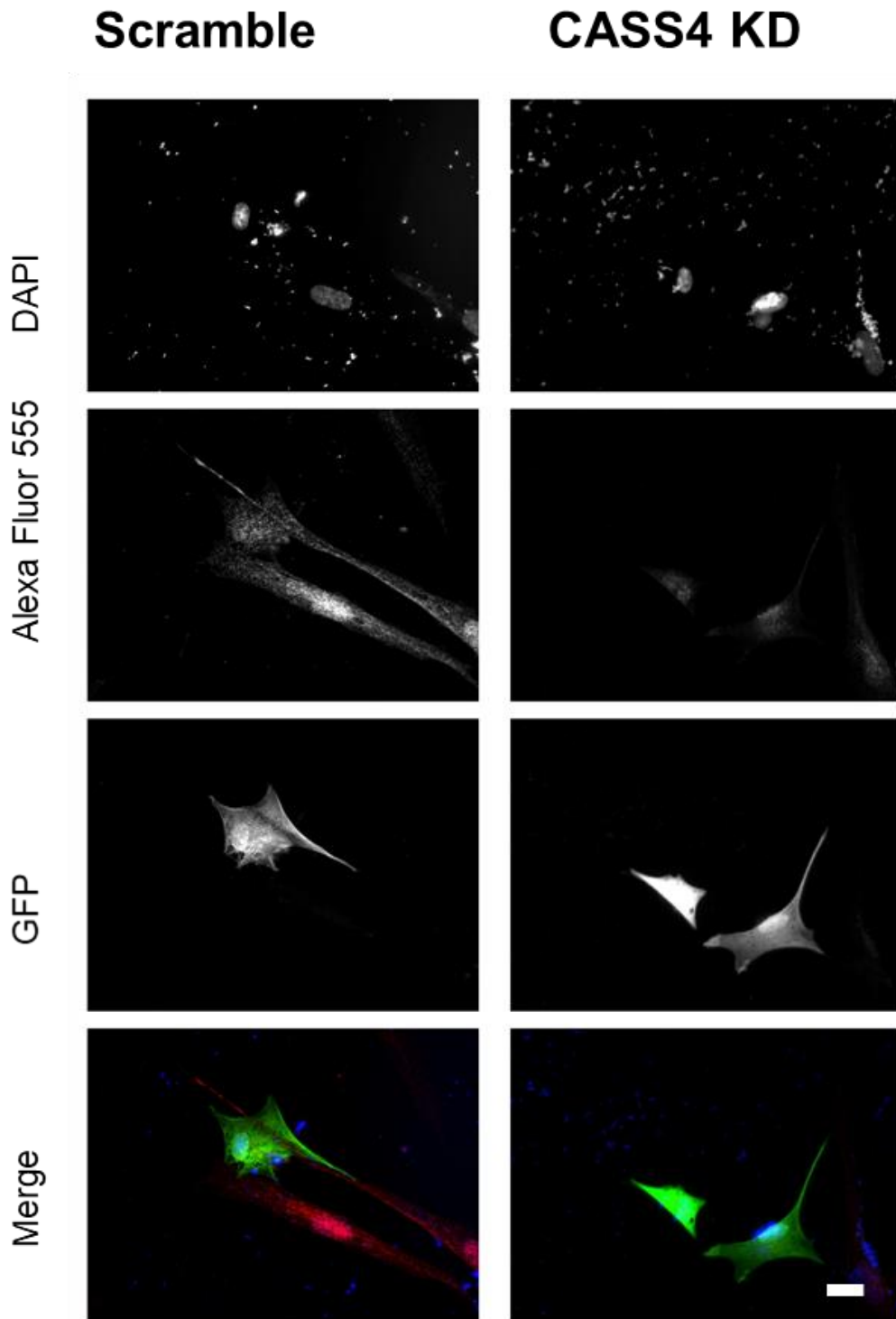
Figure 4.11 Fluorescence of CASS4 is reduced in NHAs transfected with the CASS4 siRNA vectors in comparison to the scramble control.

Fixed NHA were stained using a primary antibody for CASS4 followed by an Alexa Fluor 555 secondary antibody (red) revealing decreased CASS4 fluorescence in the cells transfected with CASS4 siRNA in comparison to the scramble transfected control. Transfected GFP+ cells, green. N=3, three technical repeats. Scale bar = 20μm.

Comparing measurements of CASS4 fluorescence in NHAs transfected with either

CASS4 siRNA encoding vectors or a scramble control, revealed a significant reduction

of CASS4 fluorescence intensity in the CASS4 siRNA transfected cells (M=26.60,

SD=0.92) in comparison to the scramble control (M=124.74, SD=5.23); t(4)= 31.987,

P<0.001;Figure 4.12), indicating that transfection with a set of CASS4 siRNA encoding

vectors induced a reduction of CASS4 expression.
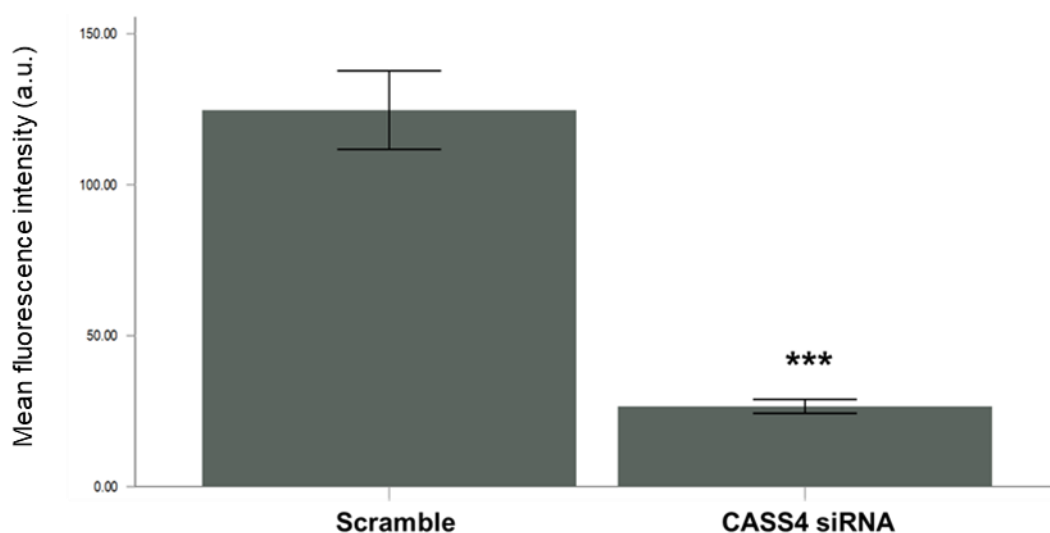
***Figure 4.12 Transfection of NHAs with CASS4 siRNA leads to a reduction of fluorescence***

Fluorescent images of NHAs, transfected with either CASS4 siRNA or a scramble control were analysed with ImageJ. Measured fluorescence intensity was compared between the two groups, showing a significant decrease in the CASS4 siRNA cells. N=3, technical repeats. Error bars ± SEM. *** p≤ 0.001

To further validate these findings, WB of lysates from NHAs, transfected with CASS4

siRNA encoding vectors or a scramble control and enriched via puromycin selection,

were performed, followed by densitometric analysis. Western blotting of the scramble control revealed two bands for CASS4 (230 kDa and 76 kDa; Figure 4.13, A), as was seen in the endogenous expression chapters (Chapter 3). The same bands were also in the lysates from NHAs transfected with CASS4 siRNA, although they were fainter than in the control. Comparison of density revealed a significant reduction between the scramble control (M= 1.19, SD= 0.045) and the CASS4 knock-down cells (M= 0.76, SD= 0.036) (t(4)= 12.553, $P<$ 0.001; Figure 4.13, B) indicating that a CASS4 knock-down was successfully achieved.
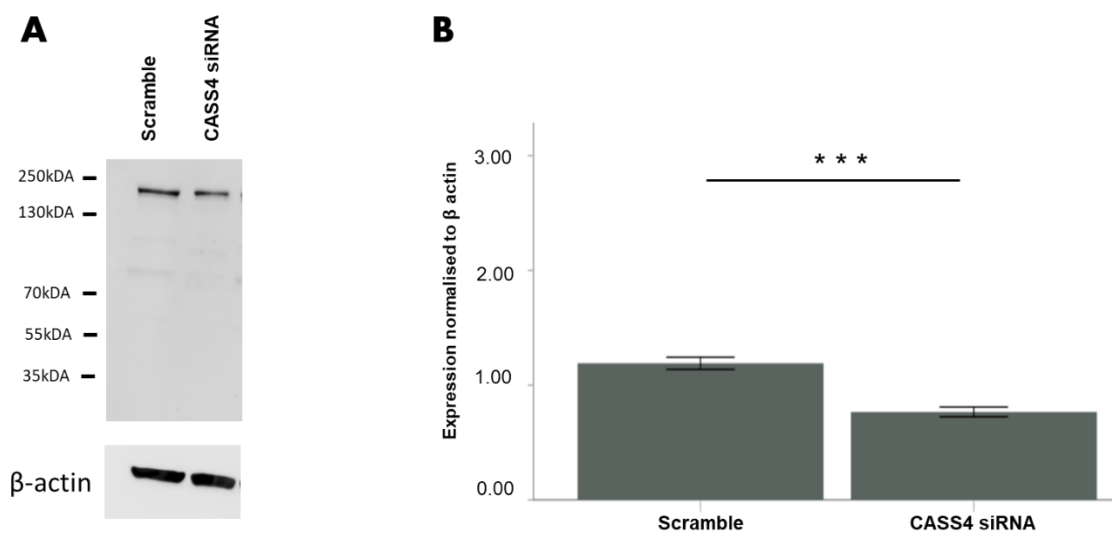
Figure 4.13 Knock-down of CASS4 was achieved in normal human astrocytes

WB of lysates from NHAs, transfected with CASS4 siRNA show a visibly lighter band at 230kDa comparison to lysates from cells transfected with a scramble control; loading control: β actin (A) Densitometric analysis revealed a significant decrease of density in the CASS4 siRNA band in comparison to the control band (B). Error bars ± 2 SEM. *** p≤ 0.001

4.3 Discussion

The main aim of this thesis was to investigate the effect of altered NEDD9 or CASS4 expression on astrocyte morphology and function *in vitro*. In order to undertake such assessments, NEDD9 and CASS4 overexpression and knock-down models in normal human astrocytes were designed. As outlined in the introduction to this chapter, primary cells are difficult to transfect (Alabdullah *et al*., 2019, Gresch and Altrogge, 2012) but based on the findings of the previous chapter, primary human astrocytes delivered the only viable model for this investigation.

Transient lipid-mediated transfection yielded sufficient transfection efficiencies to validate both overexpression and knock-down via immunocytochemistry, as transfected cells express GFP and could hence be visualised and selected for analysis, even with low transfection efficiencies. This revealed a significant increase of NEDD9 or CASS4 expression in the cells transfected with the LV-CMV overexpression vectors and a significant reduction of expression in the cells transfected with the siRNA-encoding vectors. As the measurement of immunofluorescence is only a semi-quantitative measure for protein expression, confirmation of overexpression and knock-down was also conducted via Western blotting. Here the relatively low transfection efficiency (30%) led to complications. With non-transfected cells forming the majority of the NHA population used for producing lysates, WB was not initially able to reveal modest changes in overall expression levels (i.e. the endogenous expression of the Cas-proteins in the non-transfected cells masked the knock-down). Puromycin selection for 24 hours was sufficient to reduce the number of non-transfected cells low enough to detect the knock-down. Densitometric analysis of the blots revealed significant reductions in Cas-protein expression in the transfected cells in comparison to the control cells transfected with scramble RNA.

Validation of overexpression and knock-down via immunocytochemistry is a relatively simple and fast way to get an indication of expression changes and is often paired with Western blotting, which is a standard and commonly used method to validate overexpression or knock-down (Erustes *et al*., 2018, Kikuno *et al*., 2007, LaRocca *et al*., 2019, Liu *et al*., 2009). Both immunocytochemistry and WB delivered agreeing results here, with a knockdown of 48% for CASS4 and 88% for NEDD9. Transient knockdown at the protein level is highly variable, depending on the affinity of siRNA to the target sequence and protein turnover times but should be sufficient to explore the consequences, such as morphological and functional changes (Mocellin and Provenzano, 2004, Abel and Redersdorff, 2015). Knockdown efficiencies can thus vary greatly and reach from 20-90% (Pachernegg *et al.,* 2018, Burnell *et al*., 2018, Wu *et al*, 2004), placing the knockdown efficiencies of this thesis within the acceptable spectrum. Comparison of expression in transfected cells versus non-transfected cells was not undertaken. Although this would be of interest, the blank vector and scramble controls deliver a better base line for comparison, as these cells were treated with the same reagents under the same conditions as the overexpression and knockdown cells.

Overexpression and knock-down are also routinely validated using qRT-PCR (Sato *et al*., 2018, Zhao *et al*., 2018), which could add to the validation of the NHA models. However, as outlined in the introduction to the previous chapter, this method cannot predict actual protein expression (Greenbaum *et al*., 2003, Liu *et al*., 2016) due to control of protein expression at the level of translation and highly variable protein half-lives (Schwanhausser *et al*., 2011). Moreover, since qRT-PCR-based methods have previously concluded that NEDD9 is absent from the adult brain, a result contradicted by the

endogenous expression experiments presented in Chapter 3, this method was not considered to be suitable for the purpose of this project.

The combined results of this chapter confirm that:

a) Overexpression of both NEDD9 and CASS4 was achieved in primary human astrocytes *in vitro* via transient transfection cells with CMV promoter driven vectors.

b) Knock-down of both NEDD9 and CASS4 was achieved via transient transfection of NHAs *in vitro* with a set of four siRNA encoding bicistronic vectors.

c) Overexpression and KD models of NEDD9 and CASS4 in human astrocytes were successfully created and could be used as a model to investigate Cas-protein effects on astrocyte morphology and function.

Chapter 5

Morphological analyses

5 Chapter 5 – RESULTS: Morphological analyses

5.1 Background

As outlined earlier, astrocytes are the most abundant and heterogeneous cells in the human brain. Astrocyte morphogenesis and the development from radial glial precursor cells to complex mature astrocytes remains incompletely understood (Zhou *et al*., 2019) but requires extensive cytoskeletal remodelling (Schiweck *et al.,* 2018). Most of what is known is based on animal models, which delivers another challenge as human astrocytes differ greatly to rodent or murine astrocytes (Oberheim *et al*., 2009, Verkhatsky *et al.,* 2019). The unique astrocyte morphology is integral to copious functions in the central nervous system (CNS). Owing to this exceptional morphology, it is speculated that a single astrocyte may contact over 2 million synapses (Oberheim *et al.*, 2009). Moreover, each astrocyte forms many gap junctions with other astrocytes to form functional syncytia, able to integrate and carry information from synapse to synapse outside of the neurone (Mohamet *et al.*, 2018). As part of the tripartite synapse, astrocytes support and maintain synaptic plasticity, required for learning and memory formation (Zovkic *et al.*, 2013, Zorec *et al.*, 2015). To fulfil synaptic requirements, astrocytes exhibit enormous structural plasticity, allowing these cells to remodel cell processes rapidly (Perez-Alvarez *et al.*, 2014). Such structural plasticity requires extensive intracellular signalling inducing cytoskeletal rearrangement (Heller and Rusakov, 2015, Schiweck et al., 2018a); a process, as mentioned in the previous chapter, which involves scaffolding proteins such as NEDD9 and CASS4.

Given the above, it is not surprising that aberrant astrocyte morphologies have been linked to several neurological pathologies, including Amyotrophic Lateral Sclerosis, Parkinson's disease and AD (Kohutnicka *et al.*, 1998, Verkhratsky *et al.*, 2014, Yamanaka and Komine, 2018). Aberrant astrocyte morphology will inevitably have functional consequences as aberrant cells are likely unable to maintain homeostasis of neurotransmitters, amyloid clearance and lose control of neuronal synaptic transmission, leading to neurotoxicity and hence synaptic loss (Hefendehl *et al.*, 2016, Woltjer *et al.,* 2010).

Two morphological phenomena of astrocytes are present in the AD brain: reactive/hypertrophic astrocytes and atrophic astrocytes (Olabarria *et al.*, 2010). Hypertrophic astrocytes are characterised by enlarged somata and thicker membrane processes and have been found in *in vitro* studies, animal models (e.g. 3xTg-AD) and post-mortem brain samples of AD patients (Olabarria *et al.*, 2010, Verkhratsky *et al.*, 2016, Vijayan *et al.*, 1991). Astrocytes become activated/hypertrophic as a result to injury, which can be in form of a traumatic brain injury (Robinson *et al.,* 2016), oxidative stress and inflammation (Gonzales-Reyes *et al.,* 2017). The exact mechanisms remain largely unknown, but Notch signalling, the NF-κB (nuclear factor kappa-light-chain-enhancer of activated B cells) pathway and MAPK (mitogen-activated protein kinase) activation are likely to play a role (Acaz-Fonseca *et al.,* 2019). In AD reactivity/hypertrophy is believed to be induced by the presence of Aβ plaques (Abramov *et al.*, 2003, Grolla *et al.*, 2013), but has been shown to have a neurotoxic as well as a neuroprotective role (Liddelow et al., 2017). Hypertrophic astrocytes are evident only in the later stages of AD (Olabarria *et al.*, 2010, Rodriguez-Arellano *et al.*, 2016, Sofroniew and Vinters, 2010).

More recent studies focus on the presence of atrophic astrocytes in AD. These precede amyloid plaques and neurodegeneration, manifesting during the early stages of AD, as found in the 3xTg-AD mouse model and iPSC-derived astrocytes from AD patients (Jones *et al.*, 2017, Verkhratsky *et al.*, 2016, Yeh *et al.*, 2011).

Atrophic astrocytes are characterised by somata and process shrinkage. IPSC studies have revealed that these are cell autonomous effects, but what exactly leads to this aberrant astrocyte morphology remains unknown (Jones *et al.*, 2017). As atrophic astrocytes present with a decreased level of glial fibrillary acidic protein (GFAP), as well as other cytoskeletal proteins (Olabarria *et al.*, 2010, Rodriguez-Arellano *et al.*, 2016), mechanisms involved in cytoskeletal structure and motility may be affected in AD.

As mentioned above, NEDD9 and CASS4 have been implicated in such pathways. Appropriate microtubule assembly is essential to maintain structural plasticity. NEDD9 interacts with AURKA responsible for microtubule assembly and mitotic spindle organisation (Nikonova *et al.*, 2013, Pugacheva and Golemis, 2005). Further, studies have shown how overexpression of NEDD9 promotes process formation in epithelial derived cancer cells (Bargon *et al.*, 2005) and, during preliminary experiments, we found overexpression of both NEDD9 and CASS4 induced morphological changes in epithelial cells, generating processes atypical for this cell type (Ulzheimer & Jones, 2016; unpublished data).

Only one study to date has investigated the effect of NEDD9 on brain function; finding that *NEDD9* knock-out mice suffer extensive dendritic spine loss in the dentate gyrus and CA1 regions of the hippocampus (Knutson *et al.*, 2016). Consequently, these *NEDD9* null mice displayed deficits in learning and memory via the Morris water maze test. Unfortunately, astroglial function was not directly assessed in this study. However, it is clear that a *NEDD9* knock out alters synaptic integrity; a process heavily shaped by

astrocytes. Altered expression of *NEDD9* or its paralogue *CASS4* are likely to induce morphological changes in astrocytes and based on the evidence above, could be involved in aberrant astrocyte morphology in AD, identifying a new mechanism of morphological control in these cells. Identifying pathways, leading to aberrant astrocyte morphology, could lead to the identification of new therapeutic targets.

5.2   Heterogeneous morphology of astrocytes *in vitro*

Astrocytes are known to be highly heterogeneous *in vivo* (Miller, 2018, Matyash and Kettenmann, 2010, Olude *et al.*, 2015), but it is unknown if the normal human astrocytes exhibit the same heterogeneity in a 2D culture. To test the morphological characteristics *in vitro*, normal human astrocytes were transiently transfected with pEGFP-C1 (a vector expressing only EGFP) to permit visualisation of the full extent of the cell. Untransfected cells are difficult to assess, as no stain allows visualisation of entire cell morphology comparable to GFP. Brightfield microscopy or a cell membrane stain could be used, to visualise untransfected cells, but such methods are not suitable for morphometric quantification and hence unsuitable for this thesis.

The gross morphology of fixed primary human astrocytes was assessed in 20 random fields of view each from three separate donor pools. As expected, EGFP filled the entire cell, including all processes and soma (Figure 5.1). Four distinct morphologies were evident, and cells were thus binned into four categories: fibroblast-like (A - large $>20\,\mu$m, process-devoid), polarised (B - exhibiting a single, usually thick, process), arborised (C - consisting of a small soma with multiple ramified processes), and atrophic (D - process-devoid with reduced soma width, $<10\,\mu$m).
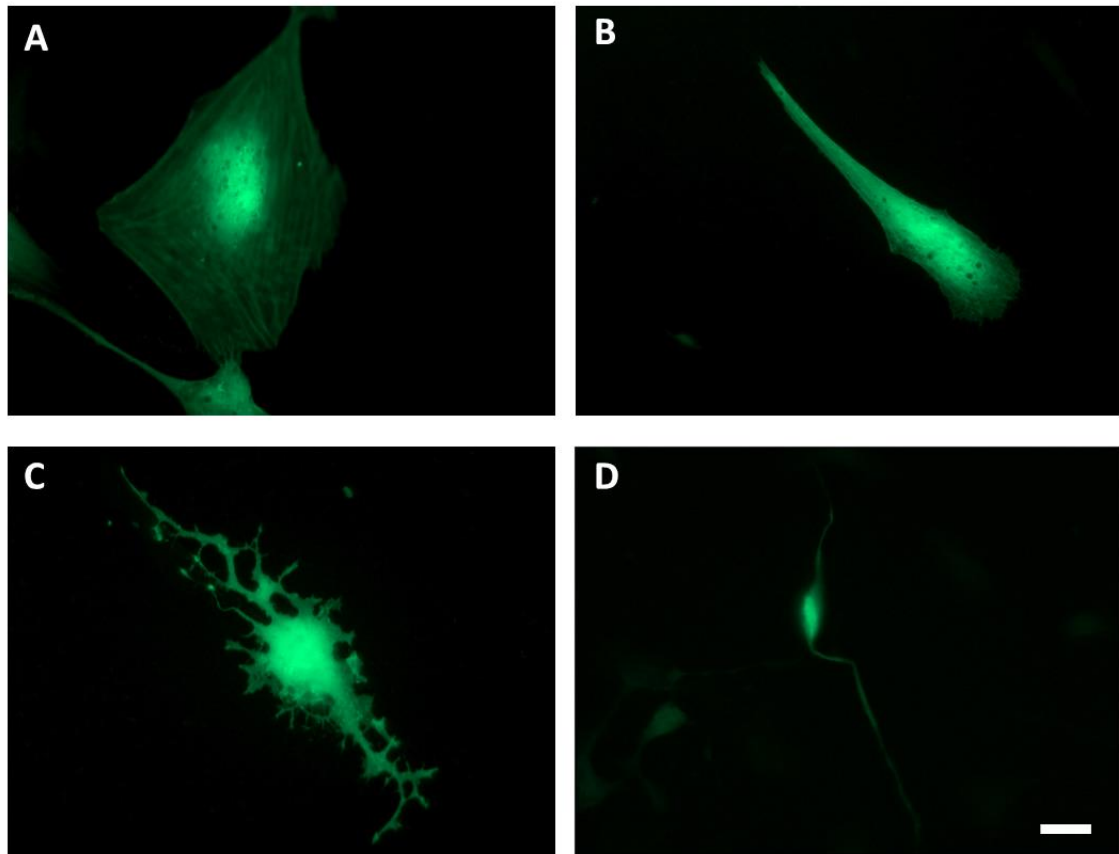
Figure 5.1 NHAs transfected with pEGFP-C1 exhibit four distinct morphological types.

Representative images of Fibroblast-like, process devoid cells (A), polarised, asymmetric cells (B), arborised cells (C) and atrophic cells with reduced soma width (D). Scale bar = 20µm

The populations of astrocytes transfected with pEGFP-C1 revealed an uneven distribution of morphologies, whereby most cells exhibited fibroblast-like morphology 37.7±0.9 % or polarised morphology 36.7±1.2 %. Fewer arborised cells 18.0±0.8 % were seen, and only a small number of cells with an atrophic morphology 7.5±1.1 % could be observed in this cell population (Figure 5.1), indicating that, although some heterogeneity exists, healthy, untreated human astrocytes *in vitro* display primarily fibroblast-like and polarised morphologies.
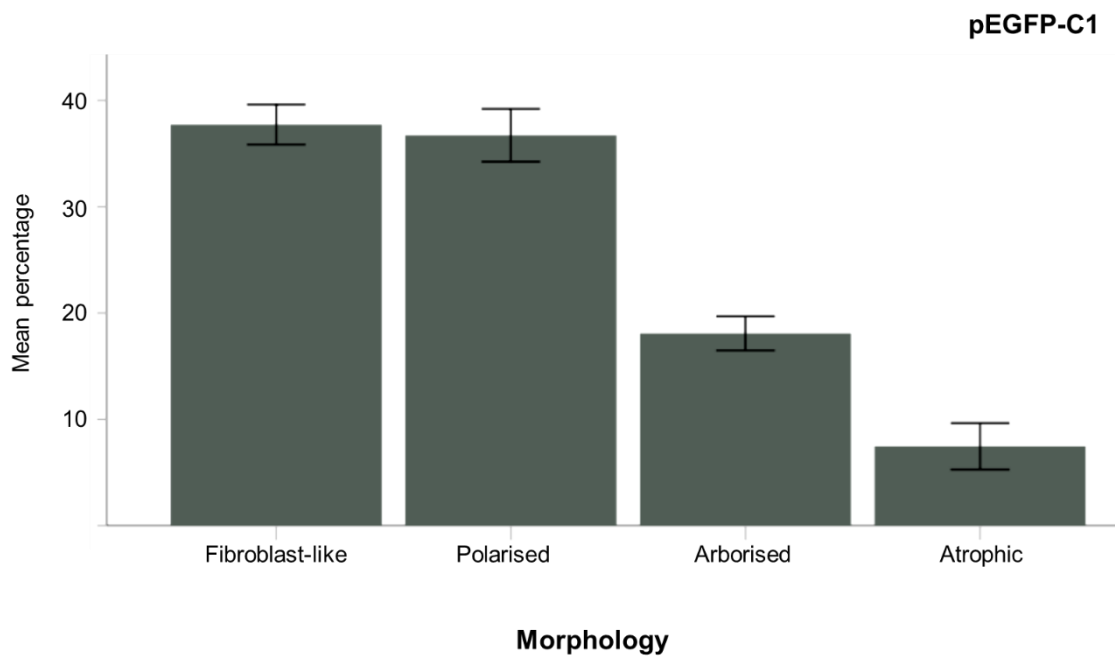
Figure 5.2 NHA distribution of morphologies in vitro

Astrocytes in vitro display mainly fibroblast-like 37.7±0.9 % and polarised 36.7±1.4 % morphologies. Arborised cells made up 18.0±0.8 % and few atrophic cells 7.5±1.1 % were found in NHAs transfected with a GFP expressing plasmid (control group), N=3, three repeats per N. Error bars ± SEM.

The visual binning of NHAs into morphological groups reveals that these cells exhibit heterogeneity *in vitro*. Although most cells displayed a fibroblast-like morphology, as can be expected in 2D cultures, almost as many cells revealed a polarised shape and just over a quarter of cells exhibiting different morphologies, showing how diverse astrocytes are, even grown in culture.

5.3 Overexpression of the Cas-proteins in normal human astrocytes

5.3.1 Morphological distribution in NEDD9 and CASS4 overexpression models

To determine the effect of overexpressing the Cas-proteins on primary human astrocyte morphology, fixed primary astrocytes, which had been transfected with NEDD9 LV-CMV, CASS4 LV-CMV or the blank GFP-only vector were visually binned into the previously established morphological categories. Importantly, the LV-CMV expression vectors bicistronically co-express a GFP (CopGFP2) alongside either NEDD9 or CASS4 to permit both the identification of transfected cells and the visualisation of the entire cell. The gross morphology of fixed primary human astrocytes was assessed in 20 random fields of view each from three separate donor pools for each of the transfection conditions. Analysis was undertaken in a blinded manner (a third party obscuring all slide labels) to avoid any bias.

The control group (Blank GFP-only LV vector) exhibited each of the four morphologies identified with the pEGFP-C1-transfected cells. Again, the distribution of morphologies was uneven and was indistinguishable to that seen with pEGFP-C1 (Figure 5.2), suggesting that the CopGFP2-expressing vector did not cause any morphological changes to the NHAs compared to the more widely utilised pEGPF-C1. Specifically, the blank vector transfected cells comprised predominantly fibroblast-like (37.7±0.4 %) (Figure 5.3) and polarised cell (34.3± 1.5 %) morphologies, with significantly fewer arborised (19.3 ±1.5 %) and atrophic (9.3 ±0.6 %) cells (Kruskal-Wallis; H(3)= 88.021, $P<0.001$; Dunn-Bonferroni pairwise comparisons; fibroblast vs arborised or atrophic, $P<0.001$; polarised polarised vs arborised or atrophic, $P< 0.001$). It was vital to establish the statistical significance between the morphology groups within the control cell population in order to compare these findings with the data of NEDD9 or CASS4 overexpressing or

depleted cell populations. This allows a comparison of morphology distributions within and across populations and whether the differences are statistically significant.
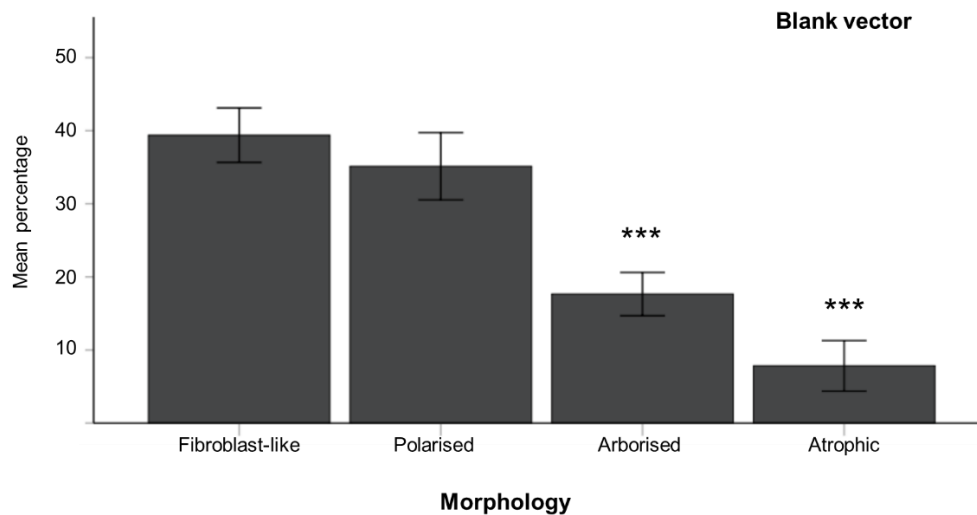
Figure 5.3 Distribution of morphologies in the blank vector control group

Visual binning into morphological categories and comparison of the distribution revealed that populations of NHAs, transfected with a blank vector display significantly fewer arborised and atrophic cells than fibroblast-like and polarised cells. N=3 donors, three repeats per N. Error bars ± SEM. *** p≤ 0.001.

As with the blank GFP-only transfected cells, the CopGFP2 expressed alongside either NEDD9 or CASS4 from the LV-CMV expression vectors filled the entire cell and permitted visualisation of all processes (e.g. Figure 5.1).

Cells overexpressing NEDD9 retained heterogeneity of morphology, exhibiting all four morphological classifications (Figure 5.4). Similar to control cells, the distribution of these morphologies was not even (Kruskal-Wallis; $H(3)=35.7$, $P<0.001$), however the NEDD9 overexpressing NHAs were predominantly arborised (36.1±1.3 %), with a significantly greater proportion compared to fibroblast-like (19.9±1.0 %) cells (Dunn-

Bonferroni pairwise comparison, $P= 0.005$). There were also significantly fewer atrophic cells (7.3 ± 1.3 %) than any other morphological type (Dunn-Bonferroni pairwise comparison, $P<0.001$, all other morphology groups).
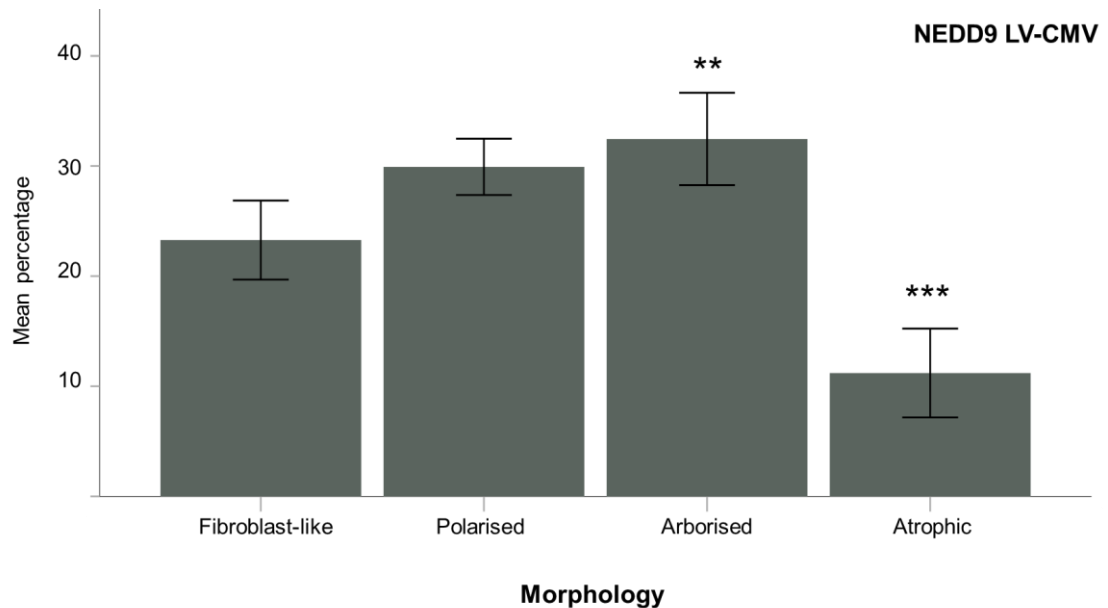
Figure 5.4 Distribution of morphologies in NHAs overexpressing NEDD9

*Visual binning into morphological categories and comparison of the distribution revealed that populations of NHAs, overexpressing NEDD9 display significantly fewer fibroblast-like cells and significantly more arborised cell.s N=3 donors, three repeats per N. Error bars ± SEM. ** p ≤ 0.01, *** p ≤ 0.001.*

Astrocytes overexpressing CASS4 also retained a heterogenous set of morphologies (Figure 5.5; Kruskal-Wallis; H(3)=48.485, $P< 0.001$). Crucially, this distribution of morphologies was distinct to that of the blank control cells; but very similar to the NEDD9 overexpressing cells. Again, like the NEDD9 overexpressing cells, CASS4

overexpression induced a predominantly arborised morphology (Figure 5.5), with a significantly greater proportion of these cells compared to fibroblast-like cells (Dunn-Bonferroni pairwise comparison, $P < 0.001$). Conversely, there was a significantly reduced number of atrophic cells compared to all other morphological categories (Dunn-Bonferroni pairwise comparison, $P < 0.001$).
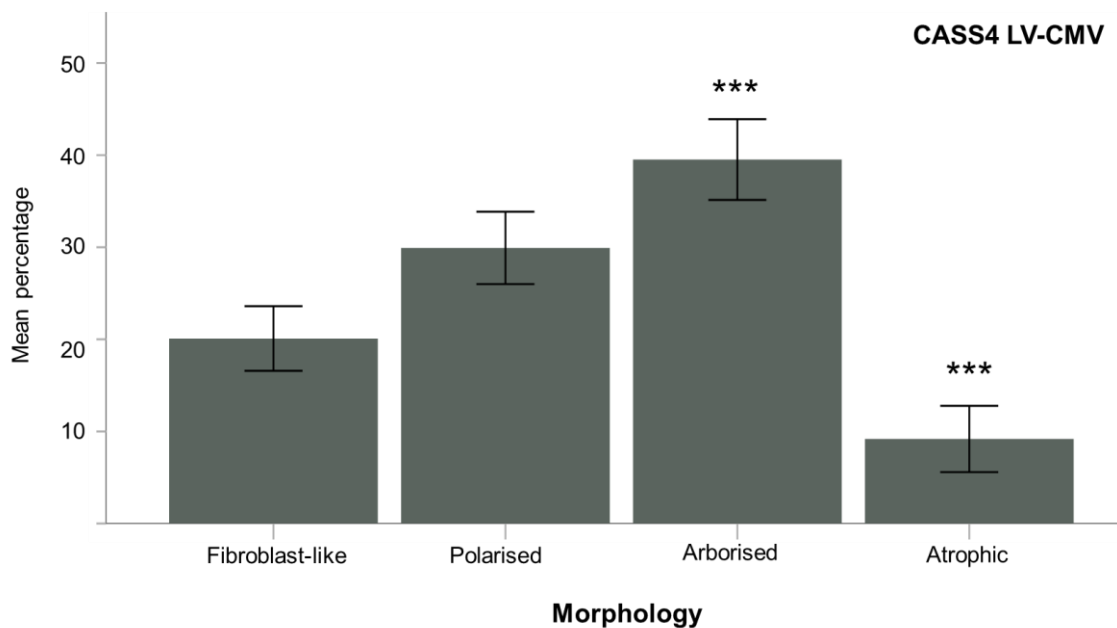
Figure 5.5 Distribution of morphologies in NHAs overexpressing CASS4

Visual binning into morphology categories and comparison of the distribution revealed that populations of NHAs, overexpressing CASS4 display significantly less fibroblast-like cells and significantly more arborised cells. N=3, with three repeats per N. Error bars ± SEM. *** p≤ 0.001

The above data suggested that NEDD9- and CASS4-overexpressing cells exhibited patterns of morphologies which were similar to one another and clearly distinct from control cells. To investigate, the relative proportions of each morphological type were compared across each of the transfection groups (Figure 5.6).

It was found that the distribution differed between the groups (ANOVA; $F_{(2,6)}= 134.945$, $P< 0.001$), suggesting that CASS4 and NEDD9 expression plays a role in astrocyte morphology. The control blank vector group comprised a significantly greater number of fibroblast-like cells than the cells overexpressing either CASS4 or NEDD9 (Tukey *post hoc*, $P <0.001$, for both). No significant difference in the distribution of polarised or atrophic cells was seen across the transfection groups (Tukey *post hoc*, $P= NS$, for all comparisons). NEDD9 and CASS4 overexpression did induce a significant increase in the proportions of arborised NHA cells in comparison to the control group (Tukey *post hoc*, $P= 0.015$ and $P= 0.045$, respectively), suggesting that overexpression of the Cas-protein is capable of promoting process formation in astrocytes *in vitro*.

.
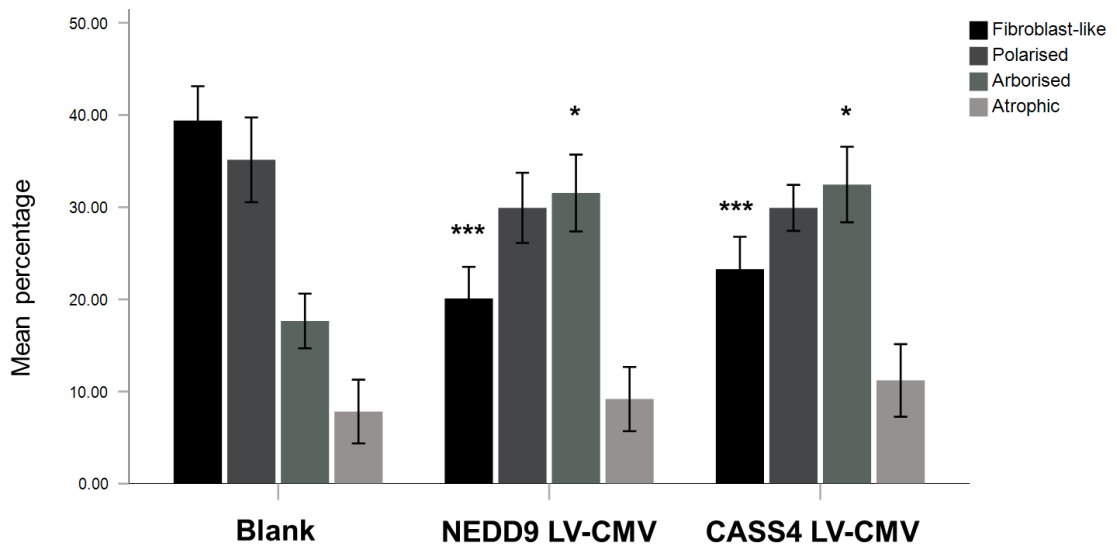
Figure 5.6 Distribution of morphologies of cells overexpressing NEDD9 or CASS4 differs significantly from the blank vector control population.

Distribution of morphologies was compared across groups, showing a decreased number of fibroblast-like and polarised cells and an increase of arborised cells in populations overexpressing NEDD9 or CASS4 compared to the blank vector transfected control population. Error bars ± SEM. *p≤ 0.05; ***p≤ 0.001

129

5.3.2 Morphometric analysis of NEDD9 & CASS4 overexpression models

Although bias was avoided by numbering slides whilst assessing the distribution of morphologies under different transfection conditions, this method of morphological assessment remains somewhat subjective and is only semi-quantitative. To quantify any morphological changes induced by the overexpression of NEDD9 or CASS4, overexpressing NHAs and control cells were imaged using confocal microscopy to generate 3D images suitable for morphometric analyses. In all cases, z-stacks of entire cells were collected from a minimum of 20 cells from each of three separate donor NHA pools. This permitted the creation of 3D isosurface renders, which could be analysed for morphometric characteristics.

Initial visualisation of 3D isosurface renders of cells overexpressing NEDD9 or CASS4 appeared markedly larger in comparison to the blank vector transfected control, although the tendency towards arborisation was not as readily apparent (Figure 5.7).
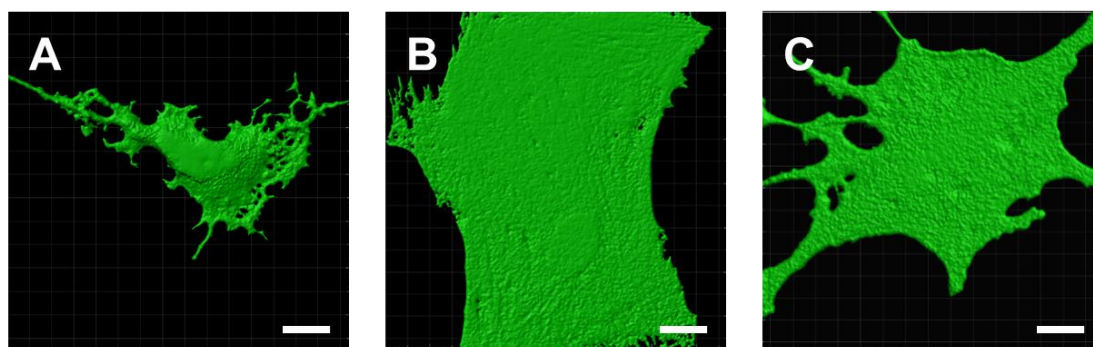
Figure 5.7 Overexpression of NEDD9 or CASS4 induces larger cells sizes compared to controls

Representative 3D isosurface renders of transfected NHAs expressing GFP permitted visualisation of the entire cell. Optical z-stacks were compared to 3D vectors and revealed an increase in size of NHAs overexpressing NEDD9 (B) or CASS4 (C) in comparison to the blank vector control (A). Scale bar = 20μm.

Morphometric analysis of 3D isosurface renders from normal human astrocytes, overexpressing NEDD9 revealed a significant increase in both cell surface area (ANOVA, $F_{(2,6)}$= 14.041, P= 0.005) and a Tukey *post hoc* test revealed that cell surface area of cells overexpressing NEDD9 (13740.66±1077.79 μ^2) was significantly larger (P= 0.008) than the blank vector transfected control (5817.56±472.61 µ2). There was also a significant difference of volume (ANOVA, $F_{(2,6)}$= 10.097, P= 0.12) and a Tukey *post hoc* test revealed that cell volume of cells overexpressing NEDD9 (17356.31±1392.75 μ^3) was also significantly increased (P= 0.01) versus blank vector transfected control NHAs (8027.5±1674.8 μ^3), (Figure 5.10). The same was found for CASS4 overexpressing cells, which also showed significant increases in both cell surface area (13549.4±1725.9 μ^2) and volume (13543.4±1338.3 μ^3) versus blank vector transfected control NHAs (5817.5±472.6 µ2 and 8027.5±1674.8 μ^3, respectively) (Figure 5.10; P= 0.009 and P= 0.029). Taken together this finding suggests that both Cas-proteins are able to influence astrocyte morphology when overexpressed.

A comparison of cell surface area to volume (SA:V) ratio revealed no significant changes between cells overexpressing either of the Cas-protein in comparison to the blank vector transfected controls (Figure 5.8, C), suggesting that surface area and volume increase in relation; overexpression of CASS4 and NEDD9 produces proportionately larger cells.

A
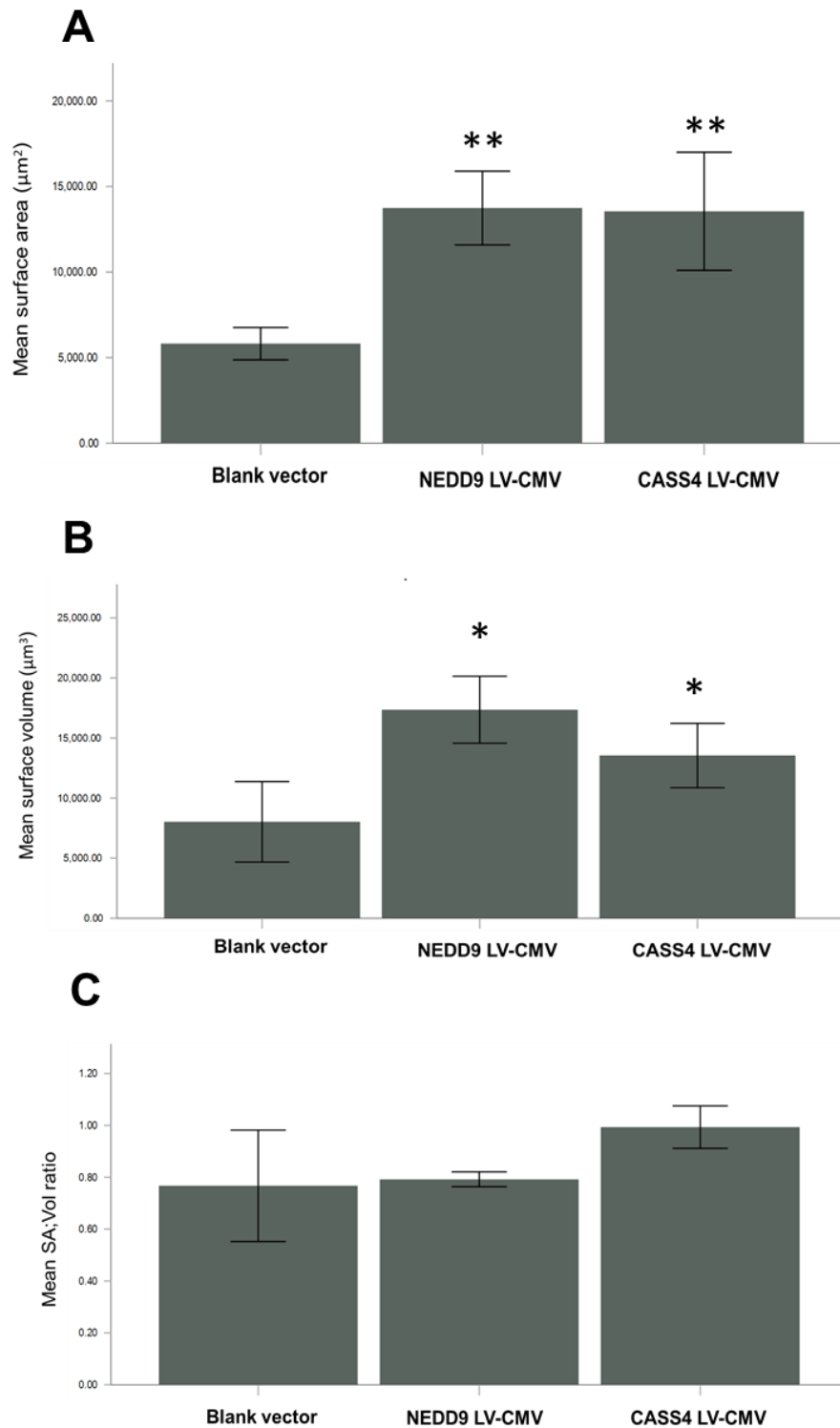
Figure 5.8 Overexpression of NEDD9 or CASS4 increases cell surface are and volume

Morphometric analyses of 3D isosurface renders of NEDD9 or CASS4 overexpressing NHAs showed that cell surface area and volume are significantly increased in the NHAs overexpressing either of the Cas-protein in comparison to control NHAs. Surface to volume ratio remained the same across all transfection groups. N=3 donors, two technical repeats. Error bars ± SEM. *p≤ 0.05; ** p≤ 0.01.

5.4 Knock-down model

5.4.1 Morphology distribution in NEDD9 & CASS4 knock-down models

To determine the effect of NEDD9 or CASS4 knock-down on primary human astrocyte morphology, fixed primary astrocytes (N=3) were assessed in >20 random fields of view. Prior to analysis, transfection conditions were obscured by randomly numbering all slides to avoid any bias. The distribution of morphologies within groups of transfection conditions a) Scramble RNA, b) NEDD9 siRNA, c) CASS4 siRNA was assessed and compared to determine the how knock-down of the Cas-proteins affects astrocyte morphology *in vitro*.

The control group (scramble) presented with a heterogeneous distribution (Figure 5.9) of morphologies but presenting with a large number of fibroblast-like (34.2±1.9 %) and polarised cells (39.7±0.8 %) and significantly less arborised (16.9±2.2 %) and atrophic cells (9.1±0.6 %) (Kruskal-Wallis; $H(3)= 44.985$, $P<0.001$), reflecting the discrepancies between fibroblast-like and arborised or atrophic cells (Dunn-Bonferroni pairwise comparison, $P= 0.022$, $P= 0.003$; respectively). As well as significantly less arborised and atrophic cells in comparison to polarised cells (Dunn-Bonferroni pairwise comparison, $P< 0.001$; both), reflecting the distribution of morphologies in the blank vector control group in the overexpression experiment.
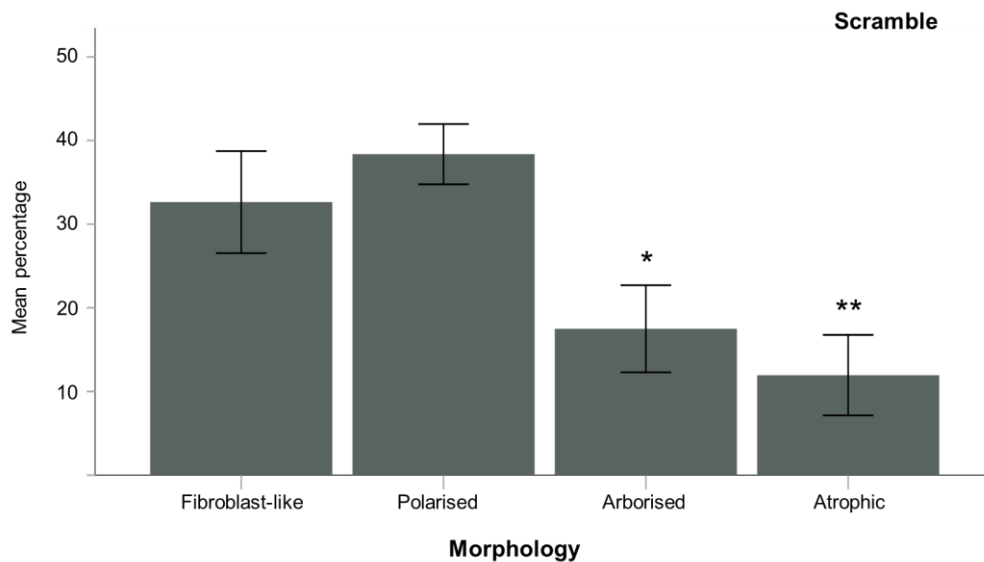
Figure 5.9 Distribution of NHA morphologies in the scramble control group

Visual binning into morphology categories and comparison of the distribution revealed that populations of NHAs, transfected with a scramble control display significantly less arborised and atrophic cells than fibroblast-like and polarised cells. N=3 donors, two technical repeats. Error bars ± SEM. *p≤ 0.05; ** p≤ 0.01.

NEDD9 knock-down NHAs presented with a distribution of morphologies distinctly different from the scramble control group (Figure 5.10). Although all four morphologies were still evident (Kruskal-Wallis; H(3)= 9.801, *P*= 0.02), the atrophic morphological phenotype predominated. A significant increase of atrophic cells (39.1±0.7 %) could be found in comparison to fibroblast-like (15.8±1.6 %) or arborised cells (18.8±0.8 %). (Dunn-Bonferroni pairwise comparison, *P*= 0.002 and *P*< 0.001, respectively). These data suggest that knock-down of NEDD9 promotes atrophic morphologies in astrocytes.

KD NEDD9
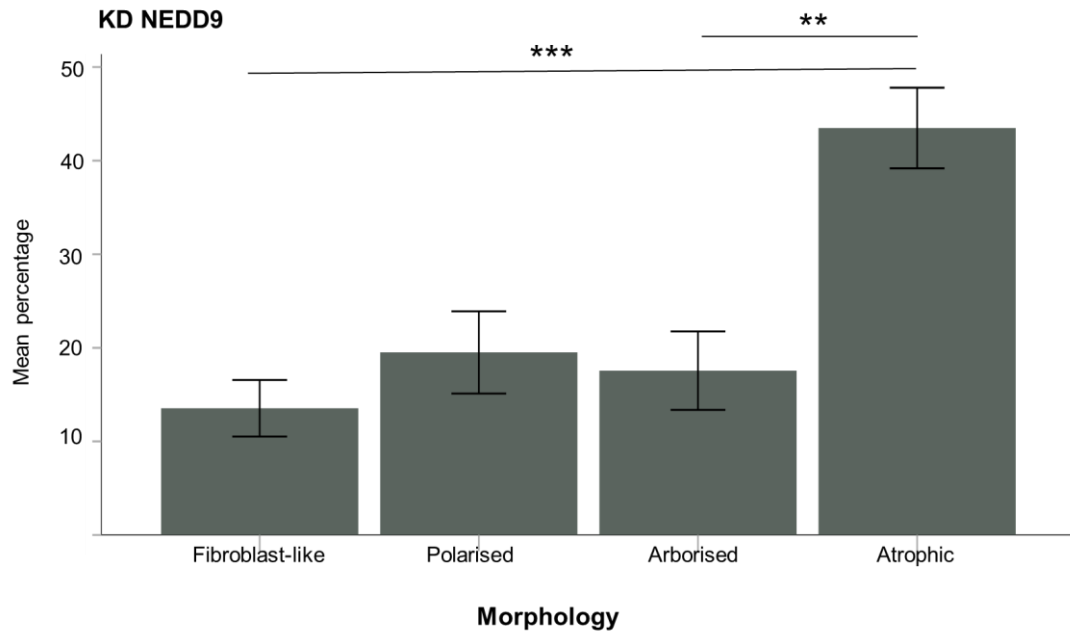
Figure 5.10 NEDD9 knock-down leads to a significant increase of atrophic cells

*Visual binning into morphology categories and comparison of the distribution revealed that populations of NHAs, depleted of NEDD9 display significantly more atrophic cells and significantly less of any other morphology type. N=3 donors, two technical repeats. Error bars ± 2 SE. ** p≤ 0.01; *** p≤ 0.001*

CASS4 knock-down NHAs demonstrated a similar distribution as for NEDD9 knock-down; specifically a robust shift towards atrophic morphologies (Figure 5.11). Comparison of morphologies across the CASS4 knock-down group were revealed a significantly uneven distribution (Kruskal-Wallis; $H(3) = 48.2$, $P < 0.001$), indicating that morphological heterogeneity persisted. A significantly increased number of atrophic cells (39.7 ± 1.1 %) was found in comparison to the other morphology types of fibroblast-like (18.5 ± 0.7 %), polarised (24.7 ± 1.2 %) and arborised (17.0 ± 1.0 %) (Dunn-Bonferroni pairwise comparison, $P < 0.001$; for all), suggesting that CASS4 depletion promotes an atrophic morphology of astrocytes, similar to its paralogue NEDD9.

KD CASS4
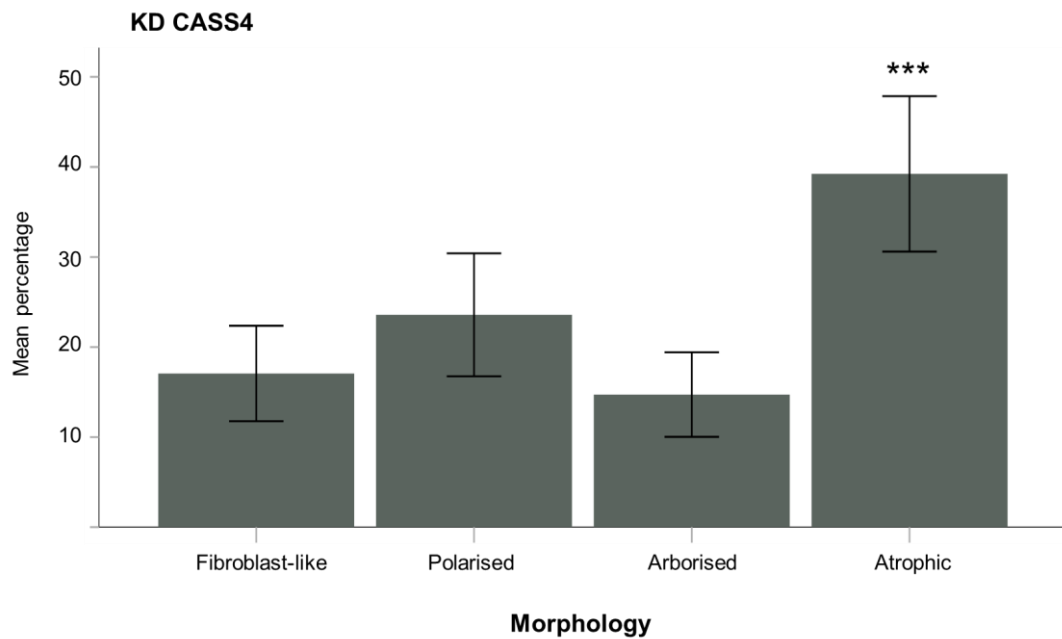
Figure 5.11 CASS4 knock-down leads to a significant increase of atrophic cells

> *Visual binning into morphological categories and comparison of relative proportions revealed that populations of NHAs depleted of CASS4 display significantly more atrophic phenotypes and significantly fewer of any other morphology type. N=3 donors, two technical repeats. Error bars ± SEM. *** p≤ 0.001*

As was seen with the overexpression studies, these data suggested that knock-down of NEDD9 and CASS4 in NHAs induce similar morphological changes (i.e. a shift towards the atrophic cellular phenotype), which are markedly distinct from scramble cells. To investigate, the relative proportions of each morphological type were compared across each of the transfection groups (Figure 5.12; ANOVA; $F_{(2,6)}= 55.732$, $P< 0.001$).

The number of fibroblast-like cells was significantly reduced upon knock-down of either NEDD9 or CASS4 compared to scramble controls (Tukey *post* hoc, $P< 0.001$ for both). A similar pattern was seen for polarised cells, the proportions of which were significantly decreased in either Cas-protein knock-down versus the scramble control (Tukey *post hoc*, $P< 0.001$ for both). This indicated that depletion of the Cas-proteins drives reduction of the two dominant NHA morphologies, fibroblast-like and polarised, found predominantly

in control NHA groups. No significant difference of distribution of arborised cells was found across the groups. As anticipated, a significant difference was found in the distribution of atrophic cells, which had been near absent in the control NHAs, but predominated in either NEDD9 or CASS4 knock-down cells (Tukey *post hoc*, $P< 0.001$ for both). Taken together these data suggest that depletion of either Cas-proteins leads to a rise of atrophic astrocyte profiles.
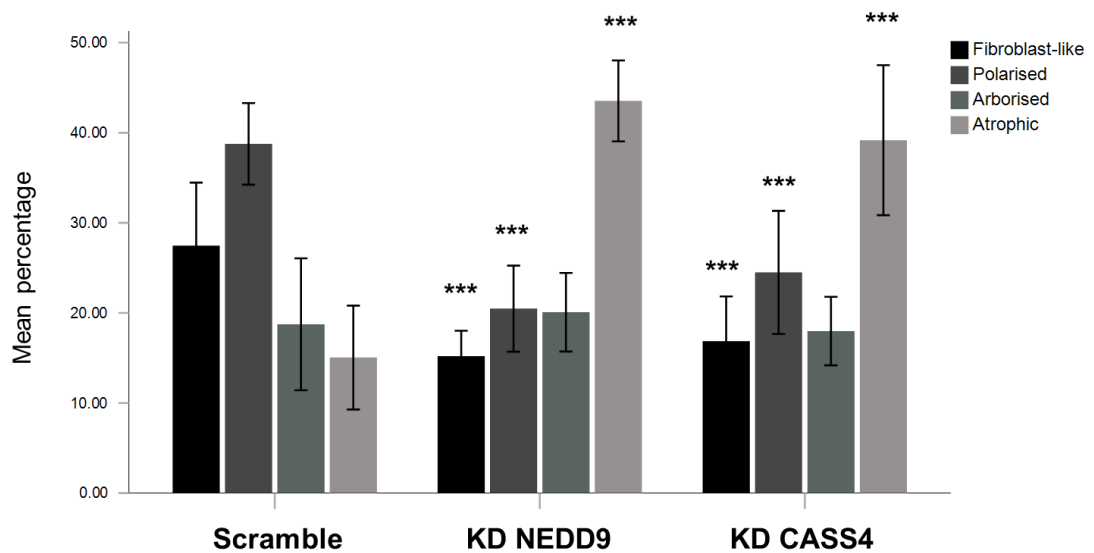
Figure 5.12 Distribution of morphologies of cells depleted of NEDD9 or CASS4 differs significantly from the control population.

The distribution of morphologies was compared across groups, showing a significant increase of atrophic cells in the populations depleted of NEDD9 or CASS4 in comparison to the scramble transfected control population. Error bars ± SEM. *** p≤ 0.001

5.4.2 Morphometric analysis of NEDD9 & CASS4 knock-down model

As outlined in the previous section, it is impossible to completely avoid any bias when assessing morphologies via visual binning; the method only delivers semi-quantitative results. To quantify any morphological changes, induced by the knock-down of NEDD9 or CASS4, Z-stack images of cells (>10 fields of view, N=3) were taken. This permitted the creation of 3D isosurface renders, which could be analysed for morphometric characteristics.

Observations of NEDD9 and CASS4 KD cells revealed a great amount of small atrophic cells, as found in the previous experiment of binning cells based on morphology. NHAs, depleted of NEDD9 or CASS4 appeared process-devoid and atrophic in comparison to the scramble control cells (Figure 5.13).
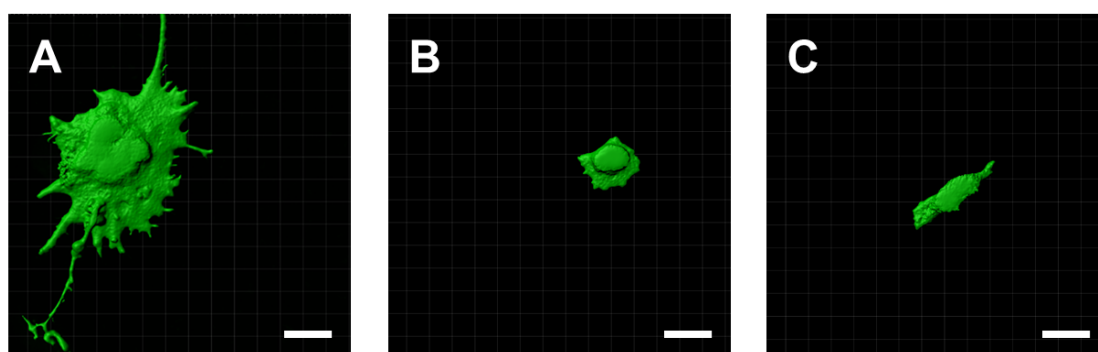
Figure 5.13 Knock-down of NEDD9 or CASS4 induces small, process-devoid cells compared to scramble controls

Representative 3D isosurface renders of optical stacks reveal a decrease in surface area and volume in NHAs depleted of NEDD9 (B) or CASS4 (C) in comparison to the scramble control (A). Scale bar = 20μm

Morphometric analysis revealed a difference of cell surface area and cell volume between groups (ANOVA, $F_{(2,6)}= 12.8$, $P= 0.007$). Although there was a tendency towards a reduction in cell surface area (40.68 ± 849.34 μ^2) and volume (5247.41 ± 1027.60 μ^3) in NHAs depleted for NEDD9 compared to the scramble control (6961.49 ± 12.41 μ^2 and 8344.13 ± 43.44 μ^3, respectively), these reductions did not reach statistical significance (Games-Howell *post hoc*, $P= 0.136$ and $P= 0.167$, respectively). On the other hand, analysis of NHAs with a CASS4 knock-down did reveal significant decreases in cell surface area (3761.99 ± 93.87 μ^2; $P=0.001$) and cell volume ($4893.0.1\pm129.93$ μ^3; $P=0.001$) in comparison to cells transfected with a scramble control. Although no significant difference was found between KD CASS4 astrocytes and KD NEDD9 astrocytes in cell surface area ($P= 0.901$) or cell volume ($P= 0.909$), this suggests that depletion of CASS4 is capable of inducing morphological changes in astrocytes and may do so a greater extent than NEDD9 depletion.

A comparison of surface to volume ratio revealed no significant differences between the Cas-proteins knock-downs and the scramble control, suggesting a proportionate relationship between cell surface and cell volume. This might suggest that depletion of CASS4, and to some degree NEDD9, leads to proportionately smaller cells.
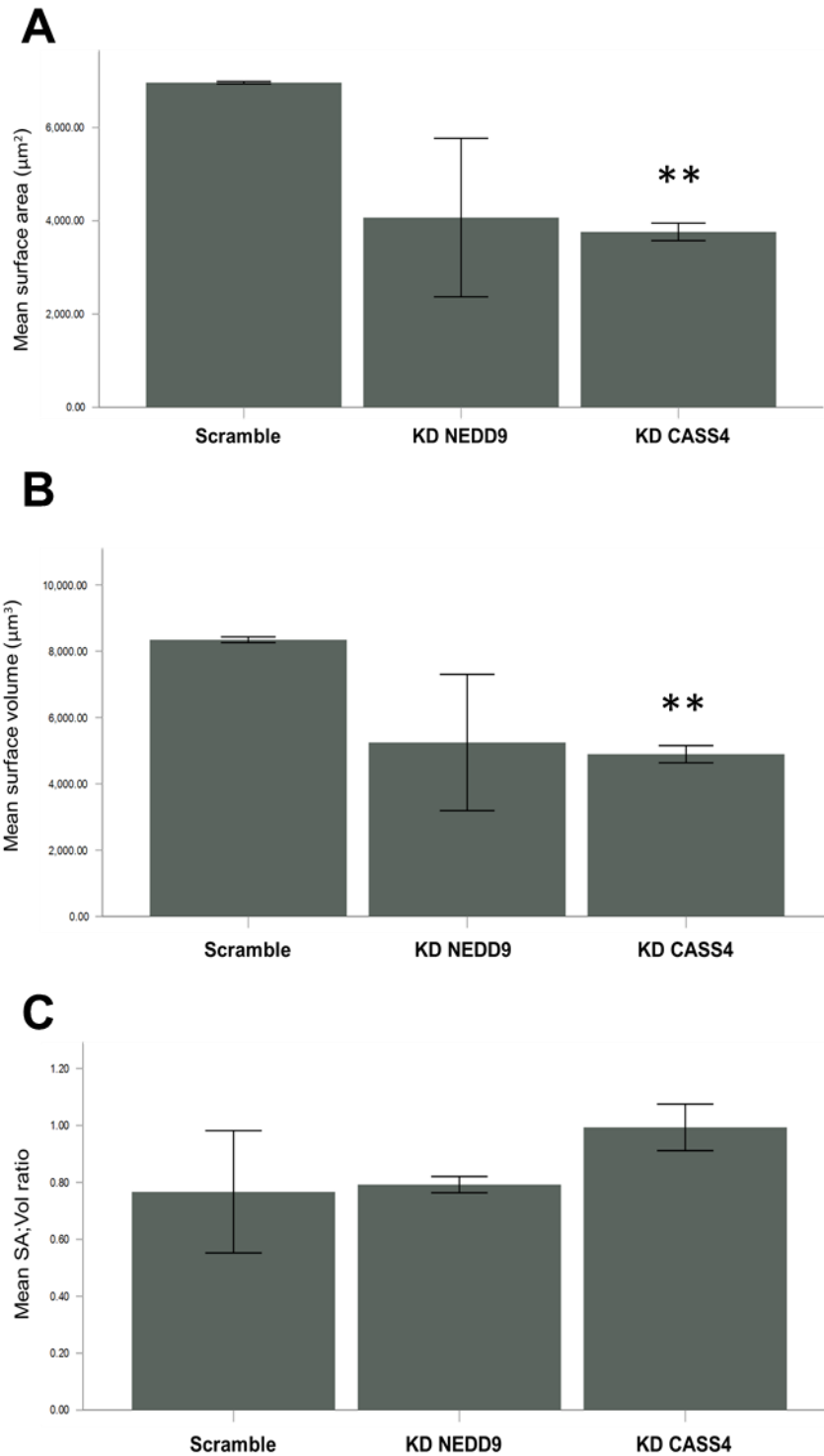
Figure 5.14 Knock-down of NEDD9 or CASS4 reduces cell surface are and volume

Morphometric analyses of 3D isosurface renders showed an increase of small, process-devoid cells in the KD models in comparison to the control population. Cell surface area and volume are significantly decreased in the NHAs depleted of the Cas-protein in comparison to the control. Surface to volume ratio remained the same across populations. N=3 donors, two technical repeats. Error bars ± 2 SEM. ** $p \leq 0.01$

5.5 Discussion

Previous studies have shown that altered expression of NEDD9 and CASS4 affect essential cellular mechanisms, including cell growth, migration and adhesion (Beck *et al.*, 2014, Singh *et al.*, 2008, Tikhmyanova *et al.*, 2010). Upregulation of the Cas-protein have been shown to promote migration, metastasis and invasion in numerous cancers (Zhou *et al.*, 2017, Li *et al.*, 2016, Wang *et al.*, 2017), including epithelial to mesenchymal transition in mammary epithelial cells (Kong *et al.*, 2011). All of these cellular processes exploit the Cas-protein abilities to induce changes in cellular morphology.

Here it was found that overexpression of either NEDD9 or CASS4 is capable of directing astrocyte morphology, a phenomenon not previously demonstrated, implicating a new role for the Cas-proteins in the regulation of astrocyte morphology. This indicates, that the proteins may play a role in astrocyte dystrophy in AD and could unearth mechanisms, which could be exploited as therapeutic targets.

Initially, the changes found between NEDD9 and CASS4 overexpression promoted a shift towards an arborised cell phenotype and a decrease in fibroblast-like cells. This is in keeping with previous findings that upregulation of NEDD9 promotes process formation in epithelial cancer cells (Bargon *et al.*, 2005), albeit under different conditions (in presence of Rho inhibitor) and in non-glial cells. Although the findings of this work suggest overexpression of the Cas-proteins promotes process formation in astrocytes and thus increasing the arborised cell types, the method of visually assessing cell morphology is limited by subjectively categorising cell morphologies.

On the contrary, the morphometric quantitative analysis revealed that overexpression of both, NEDD9 and CASS4 leads to generally larger cells, based on the measurements of

volume and cell surface. Yet no significant difference in surface to volume ratio was found, which indicates that the morphology is not necessarily more complex in the overexpressing cells, compared to the control group; a small soma with several processes would lead to a higher surface to volume ratio in comparison to cells of a less complex nature as fibroblast-like cells. As mentioned earlier, the initial assessment of morphologies revealed that overexpression of the Cas-proteins promoted process formation, leading to an increase of arborised cells in these populations, yet the surface to volume ratio comparison does not reflect these results. This may be as a result of some overlapping between the morphology categories or due to cells appearing more/less complex in 2D images than the actual 3D shape; isosurface renders used for morphometric analysis reflect the actual cell shape to a greater degree. On the contrary, software to create isosurface renders of cells may be unable to detect finer processes, which can be detected by the human eye. Both methods were used to gain a broader perspective on the morphological changes induced by NEDD9 and CASS4. To answer the question whether the Cas-proteins induce process formation, a third method, a modified method (ImageJ) of Scholl analysis was trialled. Scholl analysis is a quantitative method, which was originally used to assess neuron morphology, measuring dendritic processes and the number and size of branching processes to assess arborisation (Longair *et al*., 2011, Sholl, 1953). This method proved to be unsuitable for the assessment of astrocytic processes in 2D culture. Although a modified Sholl method has recently been applied to astrocytes, this was in whole tissue sections; where astrocytes exhibit native 3D conformations that include much finer processes emanating in all dimensions (Tavares *et al*., 2017).

Morphological analyses of the NEDD9/CASS4 knock-down model also confirmed that altered expression of the Cas-protein induces changes in astrocyte morphology. The results show that depletion of either of the proteins promotes atrophic cellular phenotypes. Morphometric quantitative analysis reflected these results, although depletion of CASS4 had a greater effect. In either case there was a tendency for the morphological heterogeneity of the cell population to be reduced in comparison to the control population. It had previously been shown that depletion of NEDD9 induces cell rounding in mouse embryo fibroblasts (Zhong *et al.*, 2012) and is capable of inducing dendritic spine loss of hippocampal neurons in mice (Knutson *et al.*, 2016).

These studies indicate that depletion of NEDD9 can inhibit the formation or maintenance of membrane protrusions, such as processes, as seen here. Intriguingly, these atrophic cells mimic the atrophic phenotype of astrocytes found in AD models of astrocytes (Jones *et al.*, 2017, Verkhratsky *et al.*, 2016, Yeh *et al.*, 2011). 3D isosurface renders of NHAs, depleted of NEDD9 and CASS4 (representative exemplar shown, Figure 5.15) display the same aberrant morphology as iPSC derived astrocytes of patients, carrying either EOAD (*PSEN1 M146L*) or LOAD (*ApoE4$^{+/+}$*) mutations (Figure 5.15).
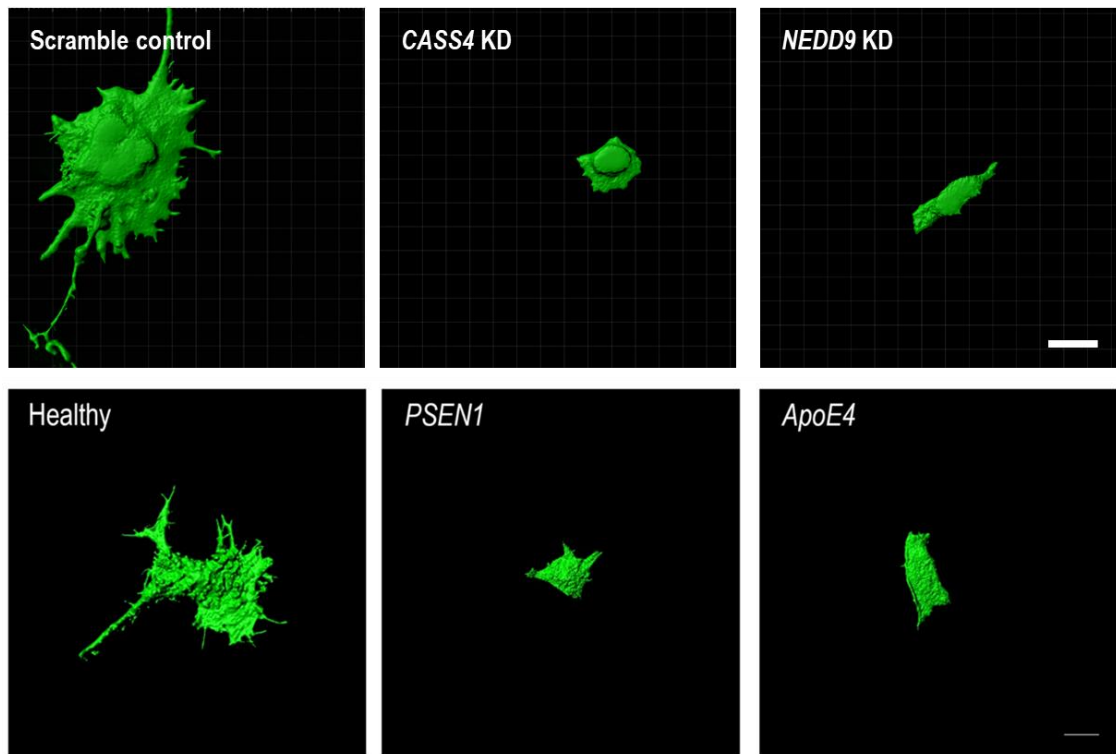
Figure 5.15 *NHAs depleted of NEDD9 or CASS4 mimic atrophic phenotype of astrocytes found in AD models of astrocytes*

Exemplar 3D isosurface renders constructed from serial confocal z-stacks of NHAs depleted of NEDD9 or CASS4 (top) display the same aberrant morphology found by Jones et al., 2017 in iPSC derived astrocytes of PSEN1 M146L LOAD and ApoE4+/+ EOAD patients (bottom). Scale bar (top) = 20μm; Scale bar (bottom) = 10μm.

The NHAs, depleted of NEDD9 or CASS4 display a morphology almost indistinguishable from the iPSPC derived astrocytes. Both are characterised by soma shrinkage and complete loss of cellular processes.

The iSPC model Jones *et al.* (2017) employed, originates from patients with mutations known to cause AD. Yet it is unclear how and if these mutations lead directly to this (atrophic) phenotype. In LOAD, only around 50% of patients are homozygous for the APOE ε4 allele (Huang *et al.*, 2004), so it is unclear whether astrocyte atrophy would be present in patients with LOAD who do not carry the gene. Testing this, is currently not

possible due to atrophy manifesting prior to symptoms; brain samples from deceased patients and hence late stage disease development would not display this astrocyte phenotype. Although an *in vivo* model of NEDD9-/- or CASS4 -/- may deliver some vital clues, as knock-down of the proteins alone caused clear phenotypical changes in this model. Furthermore, testing the expression levels of NEDD9 and CASS4 in iPSC derived astrocytes, originating from AD patients could indicate whether the Cas-proteins play an additional role.

Although it remains unknown how exactly altered expression of NEDD9 and CASS4 induces changes in astrocyte morphology, these results show that:

a) Both NEDD9 and CASS4 direct astrocyte morphology *in vitro*

b) Overexpression of the Cas-proteins leads to larger, possibly more arborsied cells

c) Depletion of CASS4 leads to atrophic astrocyte morphology (and NEDD9 depleted astrocytes tend towards being atrophic)

Chapter 6

Analyses of functional markers

6 Chapter 6 – RESULTS: Analysis of astrocyte functional markers

6.1 Background

Astrocyte morphology and function are inexorably connected. As proper morphology is vital to astrocyte function, astrocyte dystrophy coincides with aberrant cell function (Dossi *et al.*, 2018, Matias *et al.*, 2019, Zhou *et al.*, 2019). In order to indicate altered astrocytic function, several functional markers may be assayed, such as glial fibrillary acidic protein (GFAP), s100 calcium-binding protein B (S100B) and transporters such as the excitatory amino acid transporter 2 (EAAT2). An increase of s100B could initiate proliferation and inflammatory responses, similar to GFAP, but has also been shown to induce apoptosis in other cell types (Xia *et al.,* 2018). A downregulation of s100B has been indicated in a reduced inflammatory response (Ohtaki *et al*., 2007), suggesting that a decrease of s100B in astrocytes may hamper the neuroprotective role of astrocytes to brain insults, such as amyloid plaques or NFTs. Downregulation of the glutamate transporter EAAT2, which is responsible for removing excess glutamate from the synaptic cleft, would lead to a glutamate 'overspill', inducing neurotoxicity and thereby synaptic loss.

To investigate the astrocyte function in the model of this thesis, functional tests would be required, but were not within the scope of this thesis. Furthermore, as it is not known which functions may be affected, assessing the expression and localization of key markers could identify which functional tests should be undertaken in follow-up experiments. An

increase of functional markers, such as GFAP is a feature of reactive/hypertrophic astrocytes, which are a typical manifestation in neurodegenerative diseases such as AD.

GFAP is an intermediate filament and expressed almost exclusively in astrocytes (Brenner, 1994, Hol and Pekny, 2015, Sofroniew and Vinters, 2010). This protein is widely established as the typical marker for astroglia (Janke *et al.*, 2001, Moon *et al.*, 2011, Schitine *et al.*, 2015). Changes in the expression of GFAP have been linked to numerous neurological disorders such as schizophrenia, (Johnston-Wilson *et al.*, 2000), Parkinson's disease (Tong *et al.*, 2015), amyotrophic lateral sclerosis (Benninger *et al.*, 2016). Upregulation of GFAP is a typical hallmark of astrogliosis (Yang and Wang, 2015, Wakasa *et al.*, 2009), an ill-defined yet ubiquitous context-dependent defensive process in which astrocytes adopt a so-called 'reactive' phenotype that includes hypertrophic cellular re-modelling and altered gene expression, outlined in the previous chapter (Liddelow *et al.*, 2017, Pekny and Pekna, 2004). This astrocyte response is established with the later, symptomatic stages of AD (Osborn *et al.*, 2016, Colangelo *et al.*, 2014).

Although found in some other cells, S100B is primarily produced in astrocytes in the CNS (Donato *et al.*, 2013, Yardan *et al.*, 2011). Not all functions of S100B are known, but it is believed to be involved in cell proliferation, migration and differentiation, and as an inhibitor of apoptosis (Brozzi *et al.*, 2009, Lin *et al.*, 2010, Raponi *et al.*, 2007). In astrocytes, it has been shown to stimulate proliferation and inflammatory responses when overexpressed (Van Eldik and Wainwright, 2003) and altered expression has been implicated in several inflammatory and psychiatric diseases neurodegenerative disorders (Sathe *et al.*, 2012, Yardan *et al.*, 2011).

Glutamate is the principle excitatory neurotransmitter of the brain. Astrocytes play a crucial role in the production of glutamate; supplying neurones with the precursor glutamine via the glutamate-glutamine shuttle (Hertz, 2013). Moreover, astrocytes

rapidly scavenge glutamate from the synaptic cleft via several specific transporters, protecting neurons from excitotoxicity. EAAT2 is specifically expressed on astrocytic processes which ensheath synapses (Holmseth *et al.*, 2009) and is responsible for around 90% of glutamate uptake from the synaptic cleft (Kim *et al.*, 2011, Nedergaard *et al.*, 2002), meaning altered expression of this transporter will inevitably therefore lead to unbalancing glutamate homeostasis in the brain. Indeed, altered expression has been linked to several diseases, such as amyotrophic lateral sclerosis (Rattray and Bendotti, 2006), Huntington's disease (Arzberger *et al.*, 1997) and AD (Garcia-Esparcia *et al.*, 2018). It is hence of interest to establish if altered expression of NEDD9 or CASS4 and the corresponding morphological changes lead to a change of EAAT2 expression.

Altered expression of a wide array of functional astrocyte markers have been suggested to play a role in AD. Studies of AD murine models has identified variously changing astroglial profiles during different stages of AD (3, 9, 18 and 24 months disease development). Yeh *et al* (2011) reported alterations in GFAP, glutamine synthetase (GS) and S100B expression in 3xTg-AD mice, implicating astrocyte functional changes in AD. Furthermore, a recent study by Jones *et al.* (2017) established a change in key markers of induced pluripotent stem cell (iPSC)-derived astrocytes from AD patients, detecting decreased GFAP, excitatory amino acid transporter-1 (EAAT1) and GS compared to controls. Altered expression of key markers in AD astrocytes imply aberrant function, which is particularly interesting as the iPSC astrocytes were investigated in an autonomous culture, hence free of any environmental influences, such as dysfunctional neurons or aberrant proteins. The mechanisms underlying such changes are as-yet unexplored. Given that altered expression of NEDD9 and CASS4 are sufficient to recapitulate some of the aberrant morphological changes associated with AD, experiments were undertaken to establish whether the Cas-proteins were capable of

influencing established markers of aberrant function (namely GFAP, S100B and EAAT 2) also.

In addition to GFAP, S100B and EAAT 2, the expression of cytoskeletal proteins β-actin and α-tubulin was assessed. As outlined in the previous chapter, Cas-proteins are known to play a role in cytoskeletal arrangement. NEDD9 activates AURKA, which leads to microtubule assembly and mitotic spindle arrangement (Pugacheva *et al.*, 2007) and depletion of NEDD9 has been shown to downregulate AURKA, hence leading to destabilisation of the cytoskeleton (Ice *et al.*, 2013). Furthermore, NEDD9 regulates remodelling of microtubules neurite extension via AURKA activation, (Mori *et al.*, 2009, Pugacheva and Golemis, 2005), whereby depletion of NEDD9, demonstrated in a murine knockout study, causes dendritic spine loss (Knutson *et al.*, 2016). Also unknown to date, CASS4 is a paralogue of NEDD9 and is likely to have similar functions in the regulation of the cytoskeleton.

Actin filaments and microtubules are considered the master regulators of cell morphogenesis (Bouchet and Akhmanova, 2017). The actin cytoskeleton, composed of various distinct arrays of branched actin filaments, is considered the primary driver of cellular morphology. Growth of these filaments beneath the plasma membrane exerts a physical force which drives the production of protrusions, such as lamellipodia (Pollard and Borisy, 2003). Microtubules are rigid, hollow tubes composed of α- and β-tubulin heterodimers. The integrity of the microtubule network is considered secondary to that of actin; coordinating actin filament assembly, especially during cell migration (Etienne-Manneville, 2013). Interestingly, however, in some cell types, including human glioblastoma cells, cell motility occurs independently of actin, with the microtubule network playing the dominant role (Panopoulos *et al.*, 2011). Moreover, microtubules have specifically been shown to be responsible for generating membrane protrusions in

primary rodent astrocytes (Ellenbroek *et al*., 2012, Etienne-Manneville and Hall, 2001) although the exact mechanisms underlying astrocyte protrusion formation remain unexplored.

The involvement of NEDD9 in cytoskeletal arrangement and the morphological changes in both, the overexpression and KD model are likely to influence cytoskeletal structure in astrocytes. The effect on the cytoskeleton and its major components, tubulin and actin, has not been investigated to date. Astrocyte dystrophy is likely linked to cytoskeletal arrangement. Unearthing mechanisms, leading to astrocyte atrophy in AD, could aid the hunt for new and much needed therapeutic targets in AD.

6.2 Results

To assess the expression of astroglial functional markers, NHAs overexpressing either NEDD9 or CASS4, and NHAs depleted of NEDD9 or CASS4 were fixed and immuno-stained with target-specific primary antibodies (against GFAP, S100B, EAAT1, EAAT2 and GS) together with an Alexa Fluor 555 secondary antibody. Omission of the primary antibody was used as control to confirm the specificity of the primary antibody. As outlined in chapter four, co-expression of GFP permitted the identification of transfected cells. Transfected cells were imaged at x40 magnification in >10 random fields of view per experiment, for a total of three experiments each for three separate donor pools. Fluorescence intensity measurements of each marker were calculated using FIJI ImageJ.

Despite adherence to published protocols (e.g. Jones *et al.*, 2017) and subsequent attempts at optimisation; immunofluorescent staining for EAAT1 and GS was ultimately

unsuccessful. Limitations in the availability of the primary NHAs meant that further attempts at optimising the staining protocol were not possible.

6.2.1 Glial fibrillary acidic protein

Immunocytochemical staining of NHAs with anti-GFAP revealed a pattern of fluorescence which localised to filamentous structures throughout the entire cell, consistent with its expected localisation to intermediate filaments. No difference of GFAP localisation could be detected in NHAs overexpressing NEDD9 or CASS4 compared to the blank vector control group (Figure 6.1).
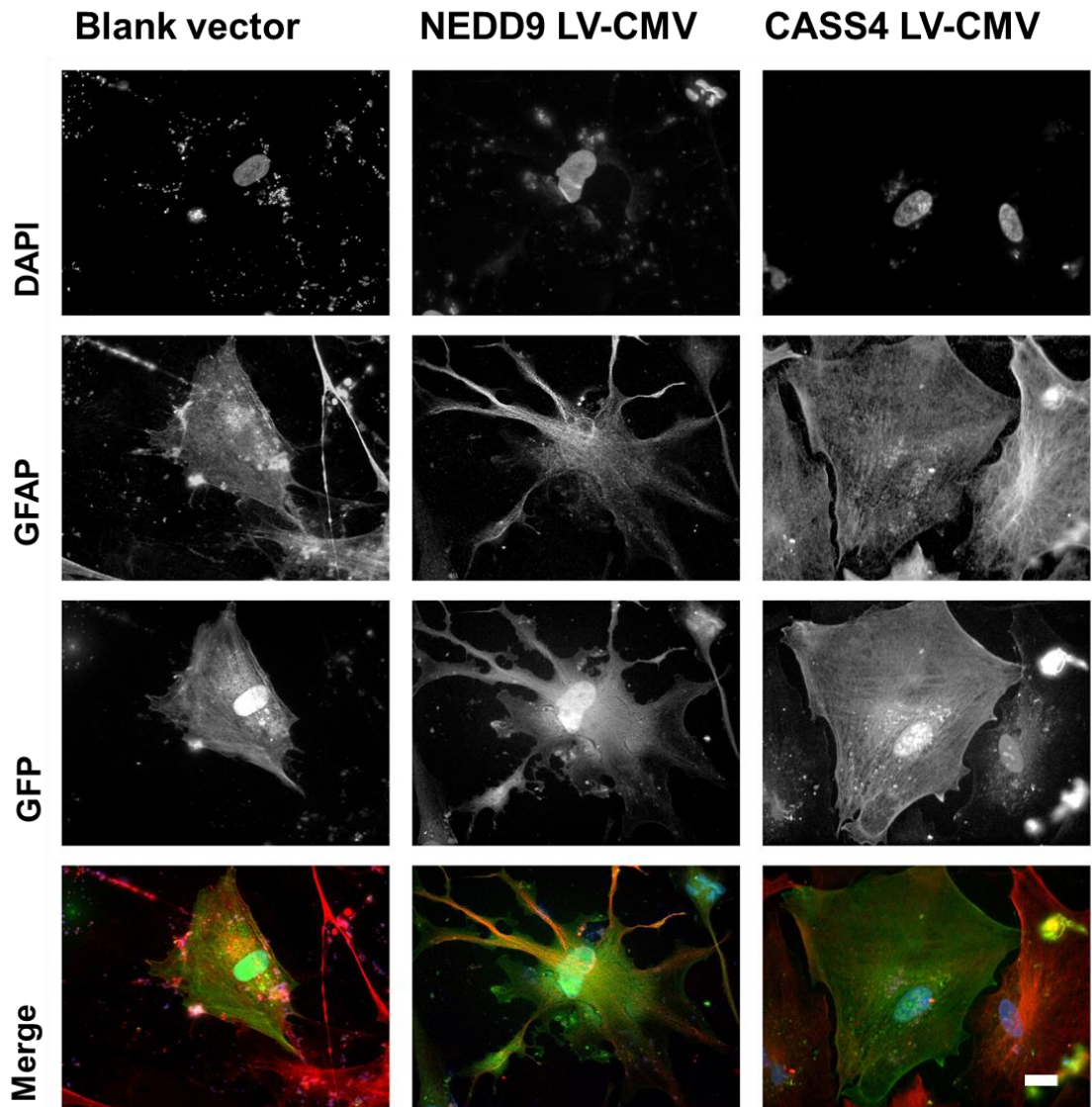
Figure 6.1 Overexpression of NEDD9 or CASS4 has no effect on GFAP fluorescence or localisation

Fixed NHAs were stained using an anti-GFAP primary antibody, followed by Alexa Fluor 555 secondary antibody (red) revealing slightly striated staining throughout the cell consistent with localisation to intermediate filaments. No alteration in staining was evident in cells overexpressing NEDD9 or CASS4 compared to blank vector controls. GFP+ transfected cells, green. N=3 donors. Scale bar = 20µm.

GFAP fluorescence intensities were calculated and compared between the blank control cells (1073.83±43.14 a.u.) and cells overexpressing NEDD9 (993.72±24.61 a.u.) or CASS4 (988.56±9.31 a.u.) (Figure 6.2). No significant difference of fluorescence

intensity was found (ANOVA, $F_{(2,6)}$= 2.685, P= 0.147), suggesting that overexpression of the Cas-proteins does not influence GFAP expression in these astrocytes.
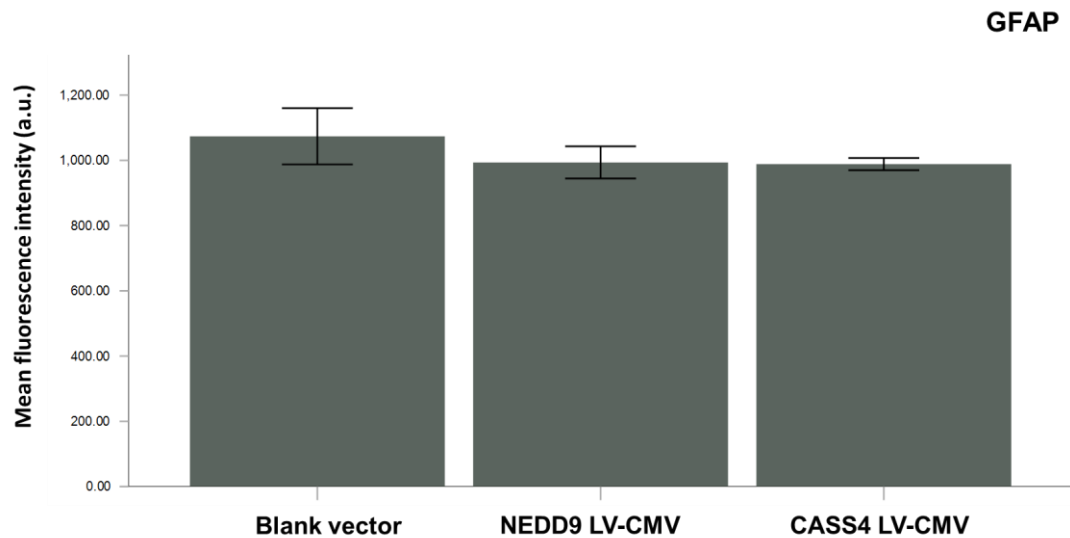
GFAP

Figure 6.2 Overexpression of NEDD9 or CASS4 has no effect on GFAP expression

Mean fluorescence intensity of GFAP staining in NEDD9 or CASS4 overexpressing NHAs in comparison to the blank vector control. Error bars ± SEM. N=3 donors. P=NS.

As discussed in Chapter 5, NHAs depleted of NEDD9 or CASS4 exhibit reduced size, complicating comparison of the pattern of GFAP staining in comparison to scramble siRNA transfected controls. Nonetheless, a faint filamentous pattern of staining could be seen in those cells which had some form of process (e.g. polarised cells), (Figure 6.3).
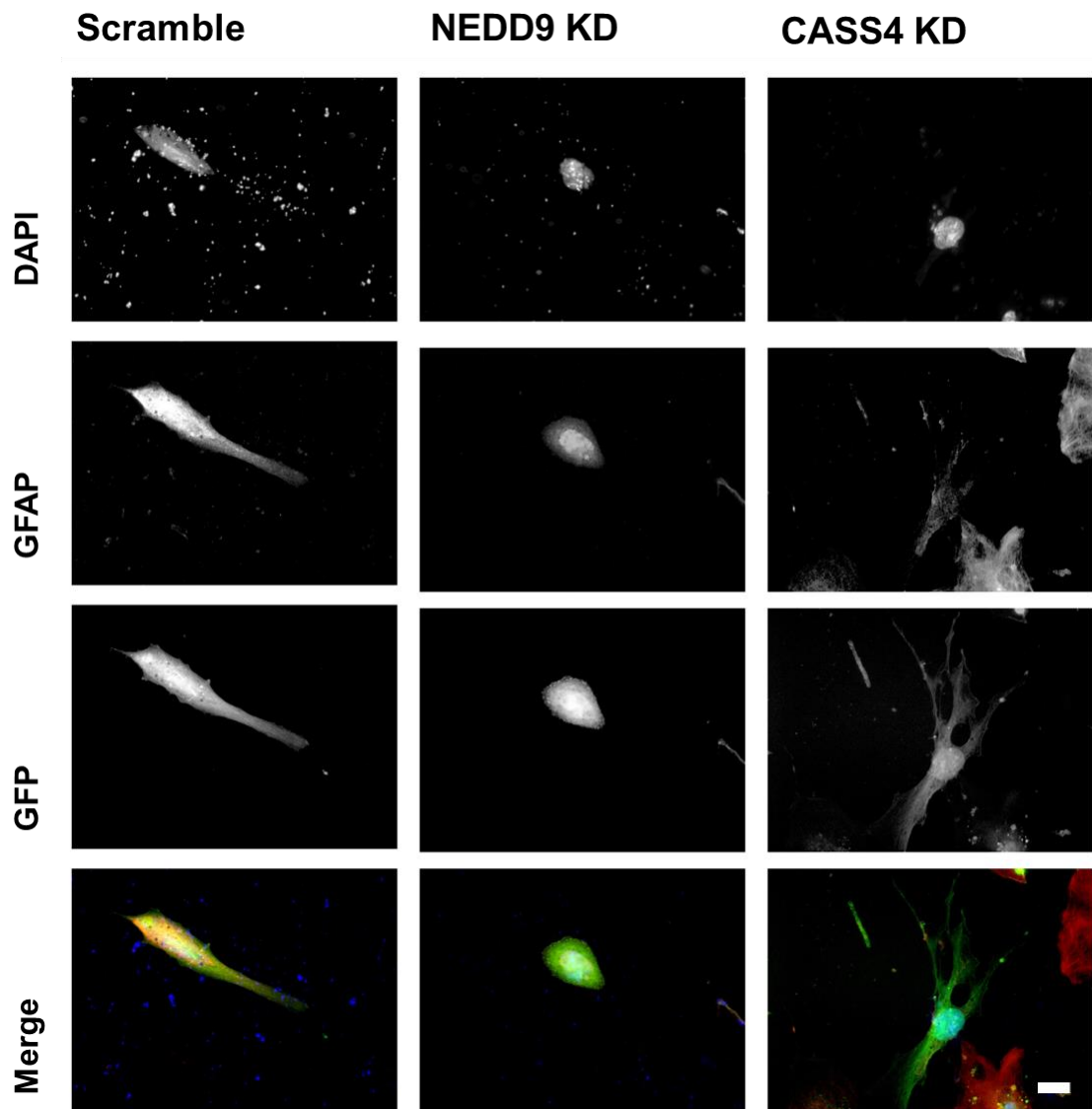
Figure 6.3 GFAP fluorescence is reduced in NHAs depleted of NEDD9 or CASS4

Fixed NHAs were stained using an anti-GFAP primary antibody, followed by Alexa Fluor 555 secondary antibody (red) revealing slightly striated staining throughout the cell in the control and reduced staining in the KD cells. GFP+ transfected cells, green N=3 donors. Scale bar = 20µm.

Initial observations seemed to indicate that GFAP fluorescence was less intense in the Cas-protein-depleted cells compared to the scramble control. Hence, quantification and comparison of fluorescence was undertaken (Figure 6.4). It should be noted that the method of quantification employed takes into account the size of each cell, such that there

is no bias against smaller cells. This analysis revealed a significant reduction of GFAP fluorescence in both the NEDD9 (137.87±6.34 a.u.) and CASS4 (133.62±3.28 a.u.) depleted cells compared to the scrambled control (970.97±40.18 a.u.), (ANOVA, $F_{(2,6)}$= 418.826, $P< 0.001$; Tukey *post hoc* $P< 0.001$ for both); indicating that depletion of either of the Cas-proteins induces reduced GFAP expression in primary human astrocytes *in vitro*.
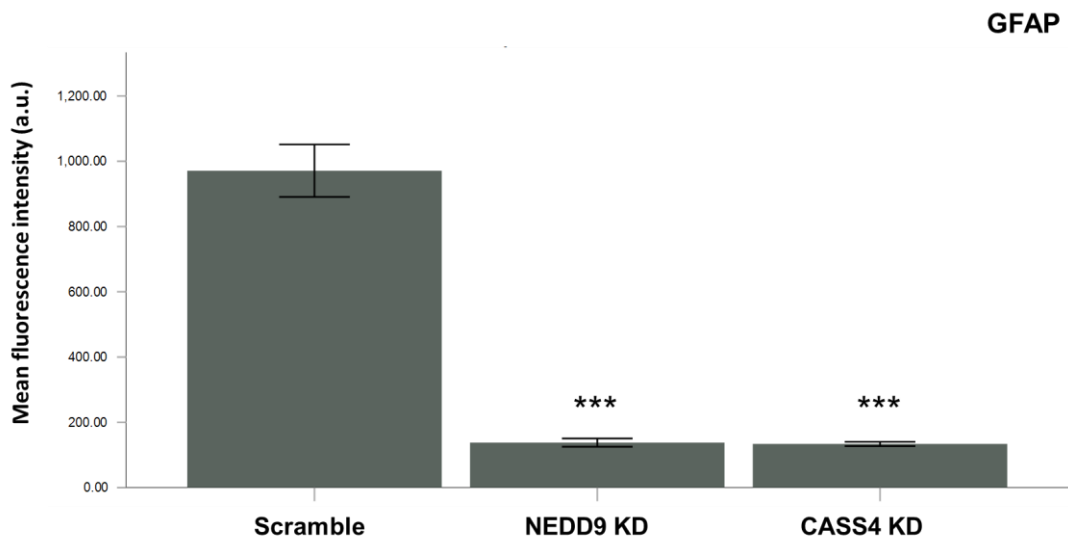
Figure 6.4 Knock-down of NEDD9 and CASS4 induces down regulation of GFAP

*Mean fluorescence intensity of GFAP in NEDD9- and CASS4-depleted NHAs in comparison to the scramble control. Error bars ± SEM. N=3 donors. *** p≤ 0.001*

6.2.2 S100 calcium-binding protein B

Fluorescence imaging of NHAs immunocytochemically treated with an anti-S100B antibody revealed staining throughout the cytosol, consistent with the expected localisation of S100B. As with GFAP, no difference of S100B localisation could be detected between the blank vector control and the NHAs, overexpressing either NEDD9 or CASS4. (Figure 6.5).
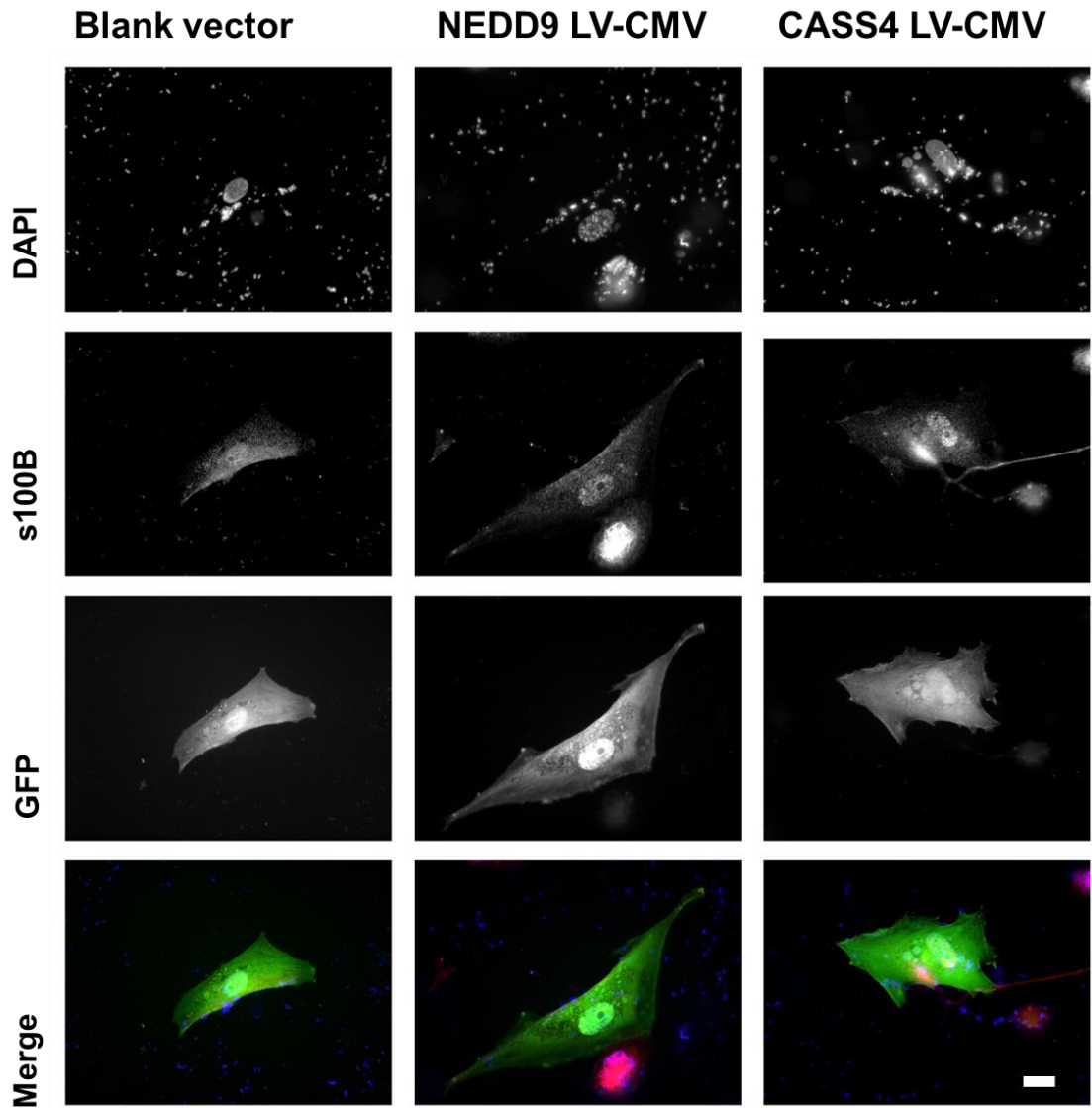
Figure 6.5 Overexpression of NEDD9 or CASS4 has no effect on S100B fluorescence or localisation

Fixed NHAs were stained using an anti-S100B primary antibody, followed by Alexa Fluor 555 secondary antibody (red) revealing slightly punctate staining throughout the cell under all transfection conditions. GFP+ transfected cells, green N=3 donors. Scale bar = 20µm.

Comparison of the S100B fluorescence between the blank vector control cells (656.35±17.96 a.u.) and cells overexpressing either NEDD9 (630.13±24.87 a.u.) or CASS4 (637.00±43.37 a.u.) revealed no significant difference (ANOVA, $F_{(2,6)}= 0.197$,

P= 0.827) of S100B fluorescence (Figure 6.6), suggesting that overexpression of the Cas-

protein has no effect on S100B expression in astrocytes.

Figure 6.6 Overexpression of NEDD9 or CASS4 has no effect on S100B expression

Mean fluorescence intensity of S100B in NEDD9 or CASS4 overexpressing NHAs in comparison to the blank vector control. Error bars ± SEM. N=3 donors. P=NS.

On the contrary, a marked reduction of S100B fluorescence was observed between the

scramble control cells and the NEDD9 KD or CASS4 KD population, presenting with a

reduction of S100B fluorescence in both KD populations (Figure 6.7).
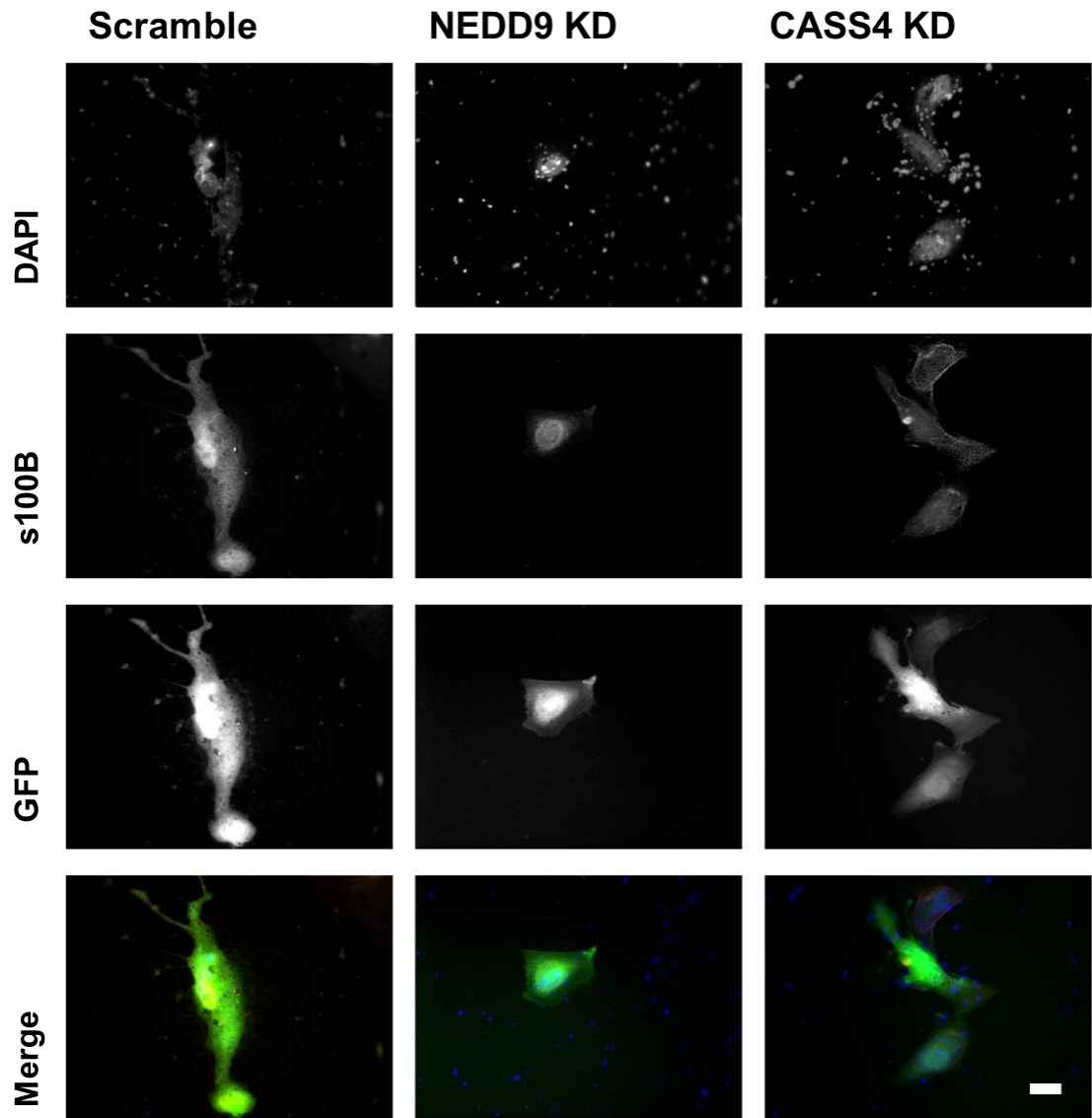
Figure 6.7 Knock-down of NEDD9 or CASS4 shows a reduction of S100B fluorescence

Fixed NHAs were stained using an anti-S100B primary antibody, followed by Alexa Fluor 555 secondary antibody (red) revealing slightly punctate staining throughout the cell under control conditions and staining adjacent to the nuclei in both KD populations. GFP+ transfected cells, green. N=3. Scale bar = 20μm.

Additionally, an unusual cellular localisation of S100B could be observed in both knock-down populations when observed by high-resolution confocal microscopy (Figure 6.8). S100B ordinarily localises throughout the cytosol, which could be observed in the NHAs

transfected with the scramble control (red, left panel). Yet in the cells depleted of NEDD9 or CASS4, S100B appears to localise in a distinctive ring shape around the nucleus (red, centre and right panels, respectively), suggesting that depletion of the Cas-proteins may induce re-localisation of the calcium binding protein, possibly to the nuclear envelope.
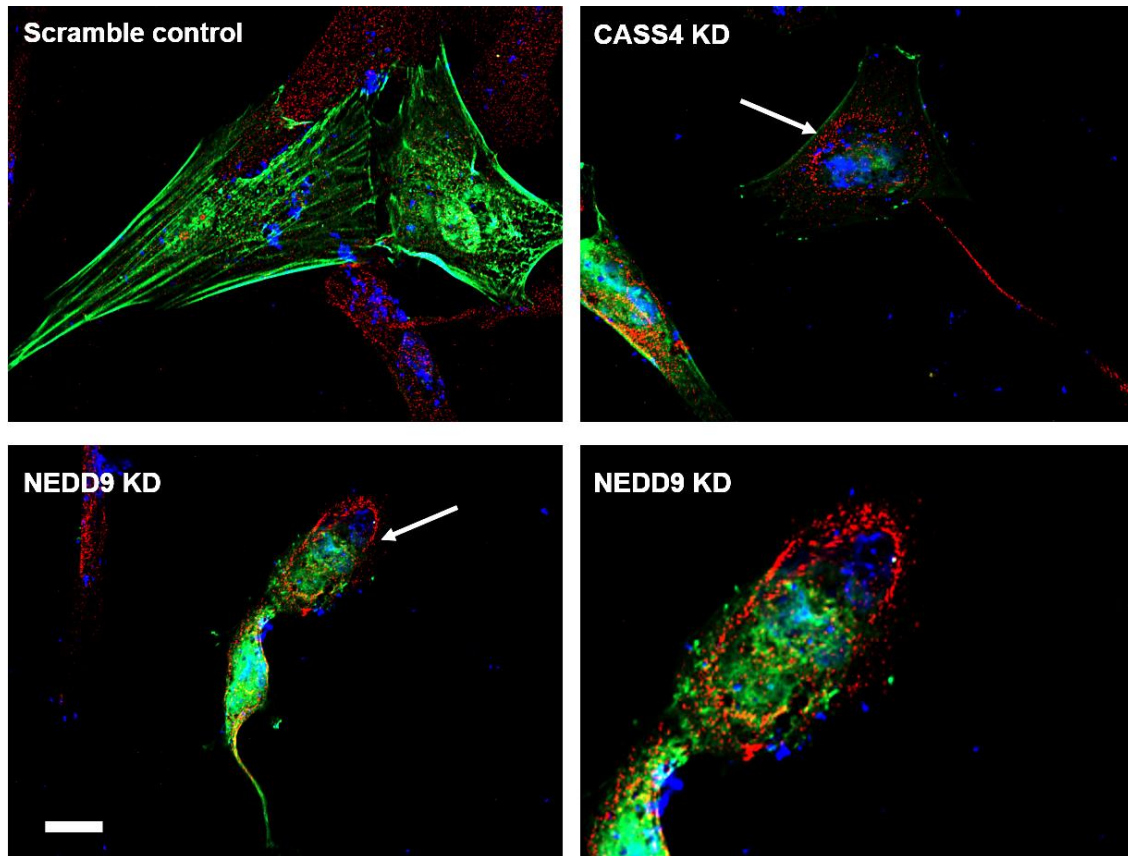
Figure 6.8 NEDD9 and CASS4 knock-out induce aberrant subcellular localisation of S100B

Fixed NHAs were stained using an anti-S100B primary antibody, followed by Alexa Fluor 555 secondary antibody (red) revealing punctate staining in the control and aberrant circular staining, adjacent to the nuclei (arrows) in both KD populations. GFP+ transfected cells, green. Scale bar = 10µm. N=3 donors.

Fluorescence intensities of S100B staining were quantified and compared between NHAs depleted of NEDD9 or CASS4 and the scramble control (Figure 6.9). A significant

reduction of S100B fluorescence was revealed in the NEDD9 (132.48±5.45 a.u.) and CASS4 knock-down (150.38±2.30 a.u.) NHAs compared to scrambled controls (675.16±5.97 a.u.), (ANOVA, $F_{(2,6)}= 4027.529$, $P< 0.001$; Tukey *post hoc* $P< 0.001$ for both), suggesting that KD of NEDD9 or CASS4 downregulates S100B expression in primary human astrocytes *in vitro*.
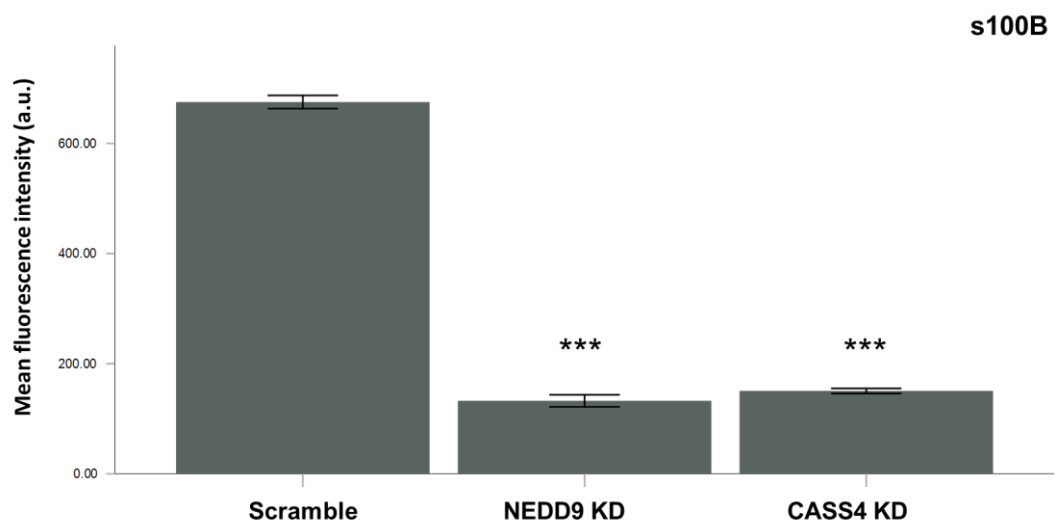
Figure 6.9 Knock-down of NEDD9 and CASS4 downregulates S100B expression

*Mean fluorescence intensity of S100B is significantly reduced in NEDD9 or CASS4 knock-down NHAs in comparison to the scramble control. Error bars ± 2 SEM. N=3 donors *** p≤ 0.001.*

6.2.3 Excitatory amino acid transporter 2

Fluorescence imaging of NHAs immunocytochemically stained for EAAT 2 revealed a slightly punctate pattern of staining throughout the cell, consistent with its expected localisation in the cytosol. No difference of subcellular localisation or fluorescence could

be observed between cells overexpressing NEDD9 or CASS4 in comparison to the blank

vector control (Figure 6.10).
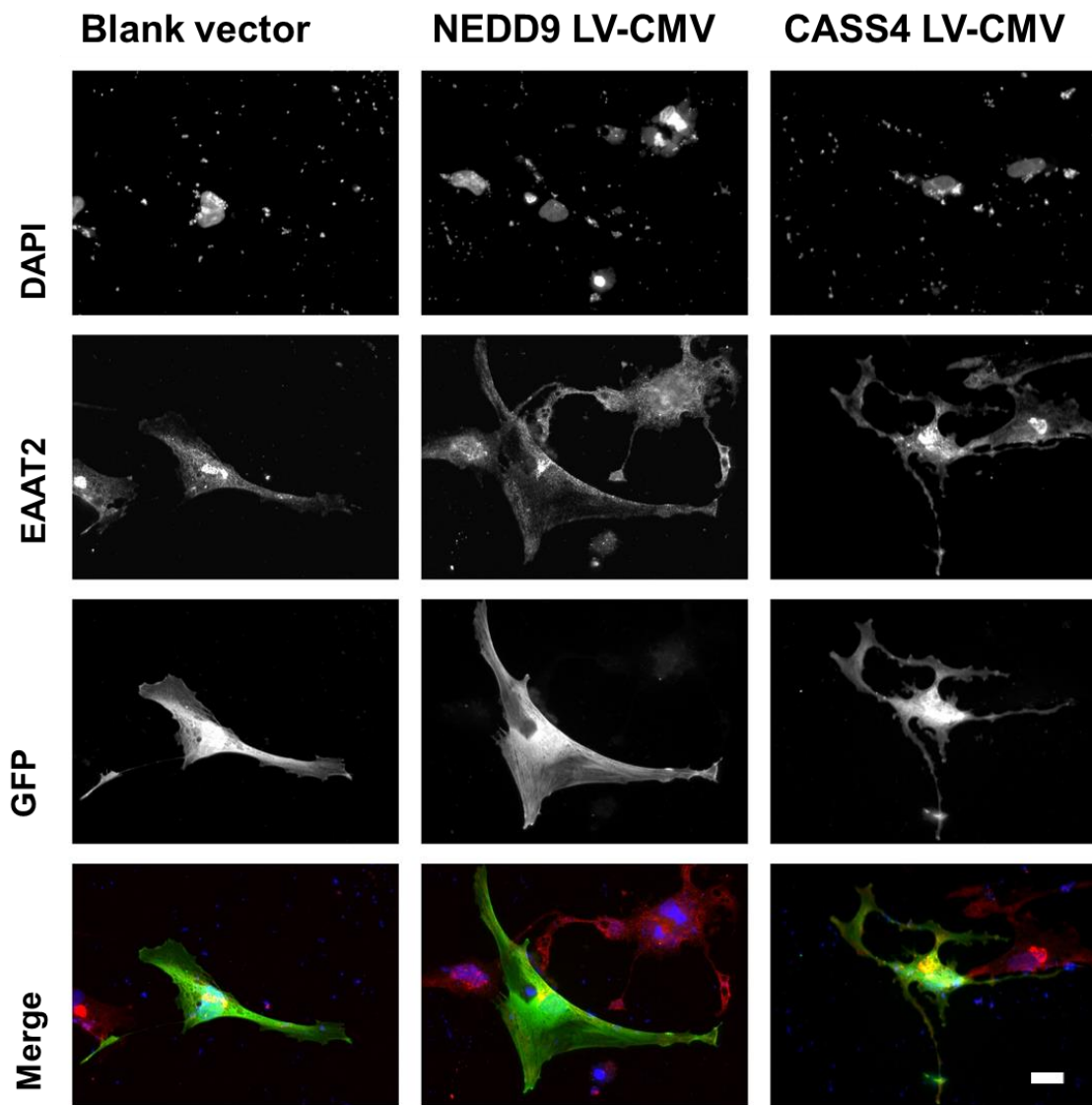
Figure 6.10 Overexpression of NEDD9 or CASS4 has no effect on EAAT2 fluorescence or localisation

Fixed NHAs were stained using an anti-EAAT2 primary antibody, followed by Alexa Fluor 555 secondary antibody (red) revealing staining throughout the cell. GFP+ transfected cells, green. N=3 donors. Scale bar = 20µm

Quantification and comparison of EAAT2 fluorescence revealed no significant difference between cells overexpressing either NEDD9 (262.67±4.89 a.u.) or CASS4 (249.79±1.27 a.u.) and the blank vector control (271.11±10.06 a.u.) (ANOVA, $F_{(2,6)}$= 5.422, P= 0.147), suggesting that overexpression of the Cas-proteins has no effect on EAAT2 expression in astrocytes (Figure 6.11).
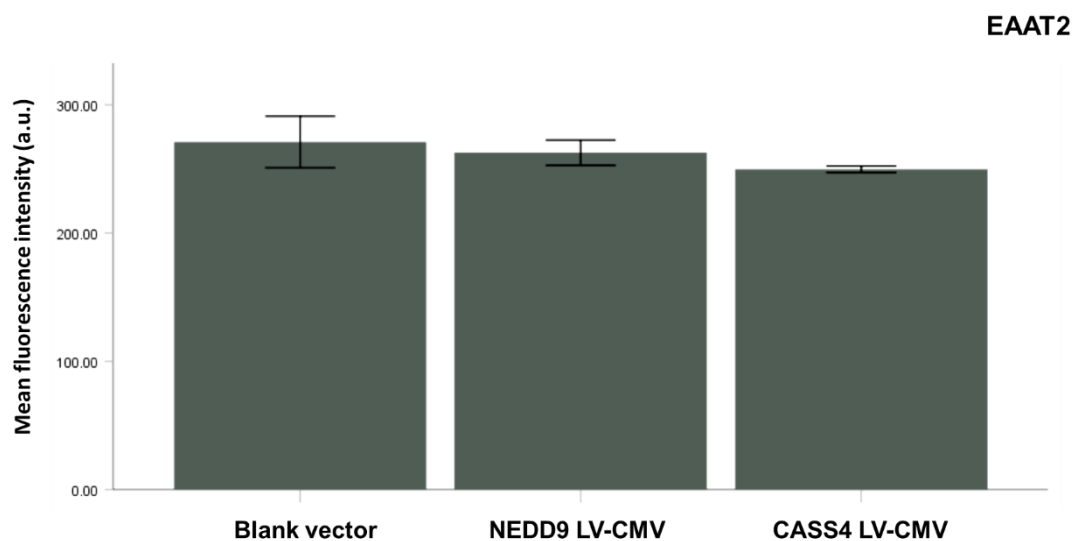
EAAT2

Figure 6.11 Overexpression of NEDD9 or CASS4 do not affect EAAT2 fluorescence

Mean fluorescence intensity of EAAT2 in NEDD9 and CASS4 overexpressing NHAs in comparison to the blank vector control. N=3 donors. Error bars ± 2 SEM. P=NS

In contrast to the overexpression model, a reduction of EAAT2 fluorescence could be observed in the NEDD9 (118.01±1.51 a.u.) or CASS4 (162.97±8.58 a.u.) knock-down NHAs when compared with the scramble control (263.40±5.29 a.u.), (Figure 6.12).
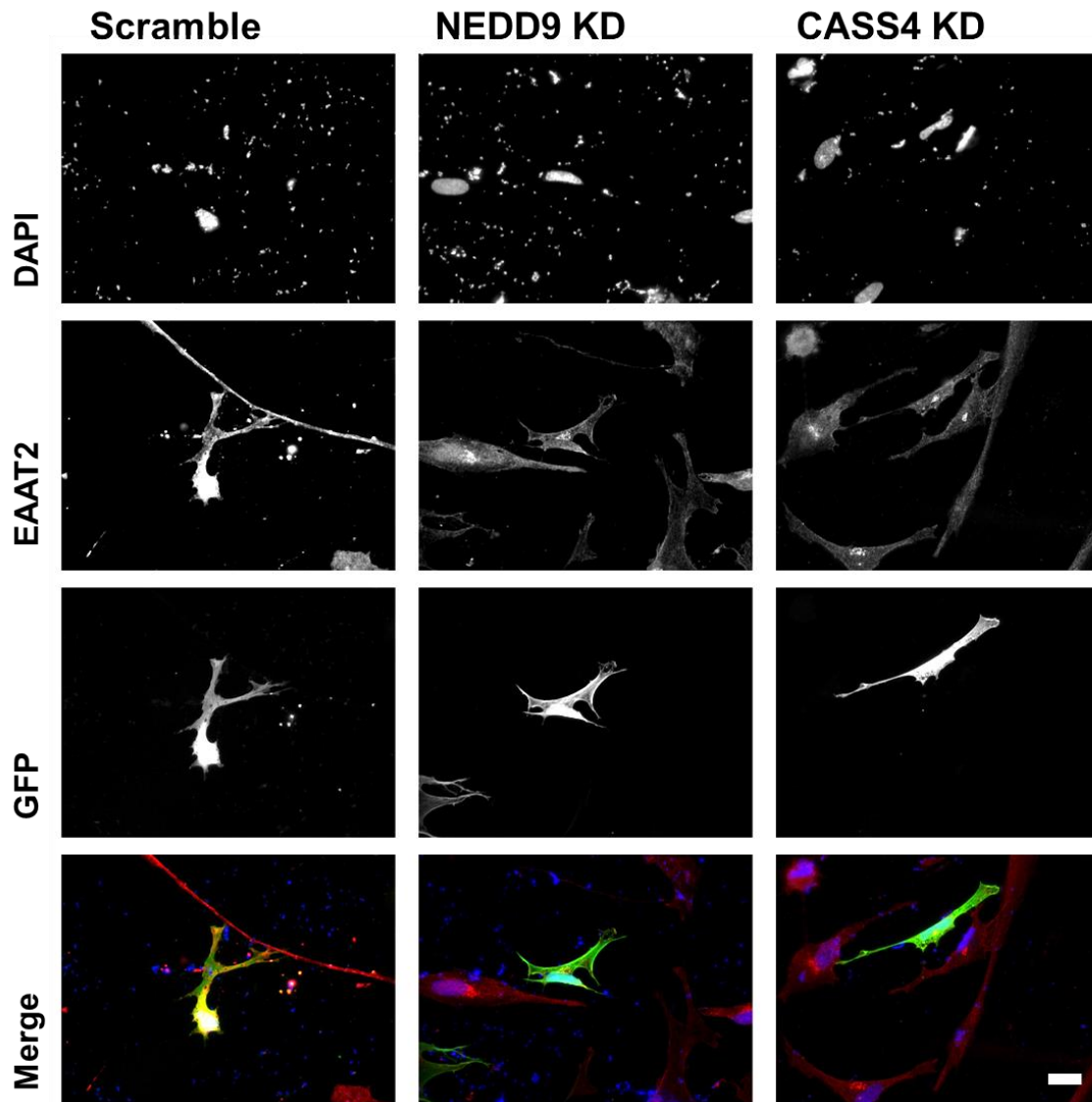
Figure 6.12 Knock-down of NEDD9 or CASS4 shows a reduction of EAAT2 fluorescence

Fixed NHA were stained using an anti-EAAT2 primary antibody, followed by Alexa Fluor 555 secondary antibody (red) revealing staining throughout the cell. GFP+ transfected cells, green. N=3 donors. Scale bar = 20μm.

Comparing measurements of EAAT2 fluorescence in these cells revealed that this reduction was statistically significant (Figure 6.13; ANOVA, $F_{(2,6)}= 159.709$, $P< 0.001$; Tukey *post hoc* $P< 0.001$ for both). This suggests that depletion of either of these Cas-proteins stimulates a downregulation of this glutamate transporter in human astrocytes *in vitro*.
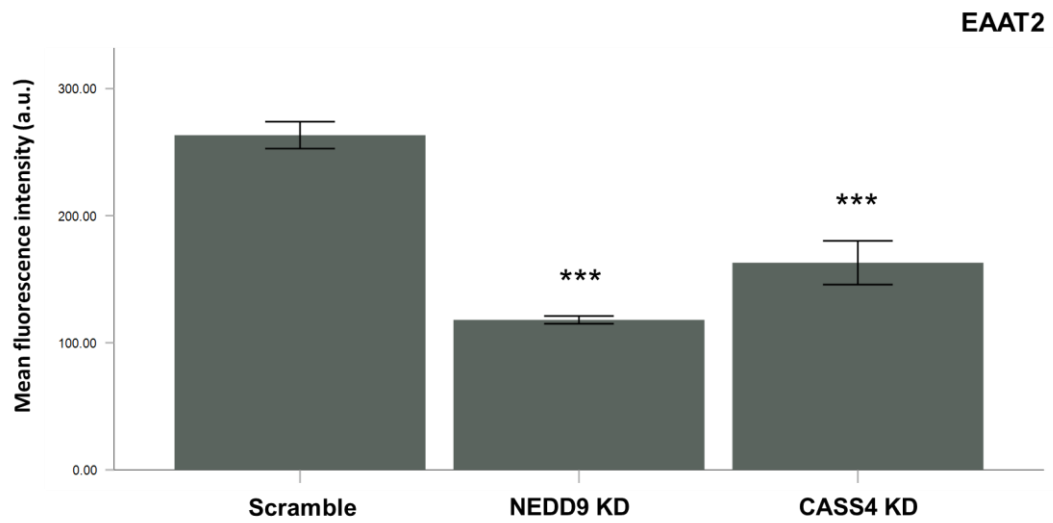
Figure 6.13 Knock-down of NEDD9 and CASS4 downregulates EAAT2 expression

Mean fluorescence intensity of EAAT2 is significantly reduced in NEDD9 and CASS4 knock-down NHAs in comparison to the scramble control. N=3 donors. Error bars ± 2 SEM. *** p≤ 0.001.

6.2.4   β Actin

Fluorescence imaging of NHAs stained for β-actin revealed striated staining throughout the cytosol and enriched in various stretches of the cell membrane, consistent with its cytoskeletal localisation (Figure 6.14). A difference of β-actin fluorescence or localisation could not be seen between the cells overexpressing NEDD9 or CASS4 and the blank vector control.
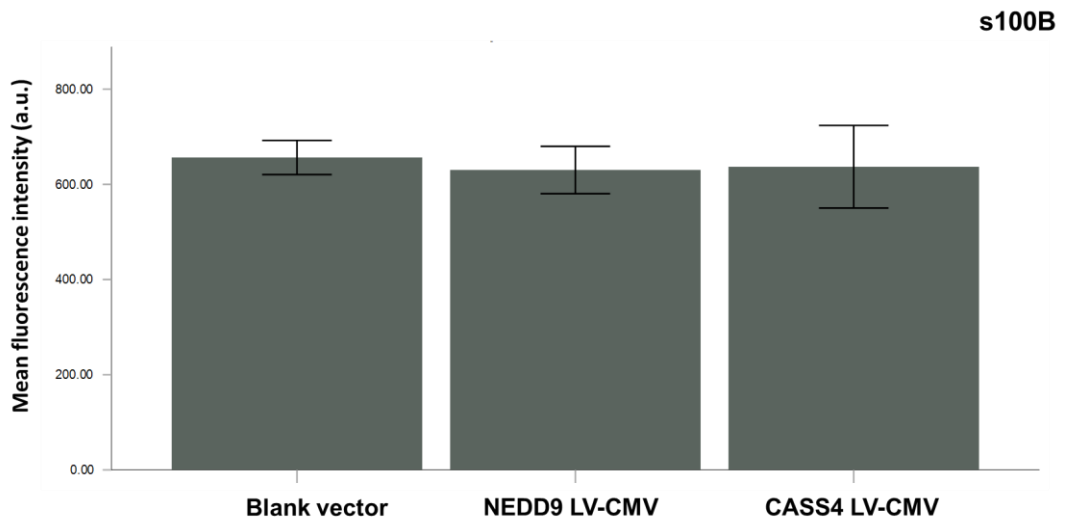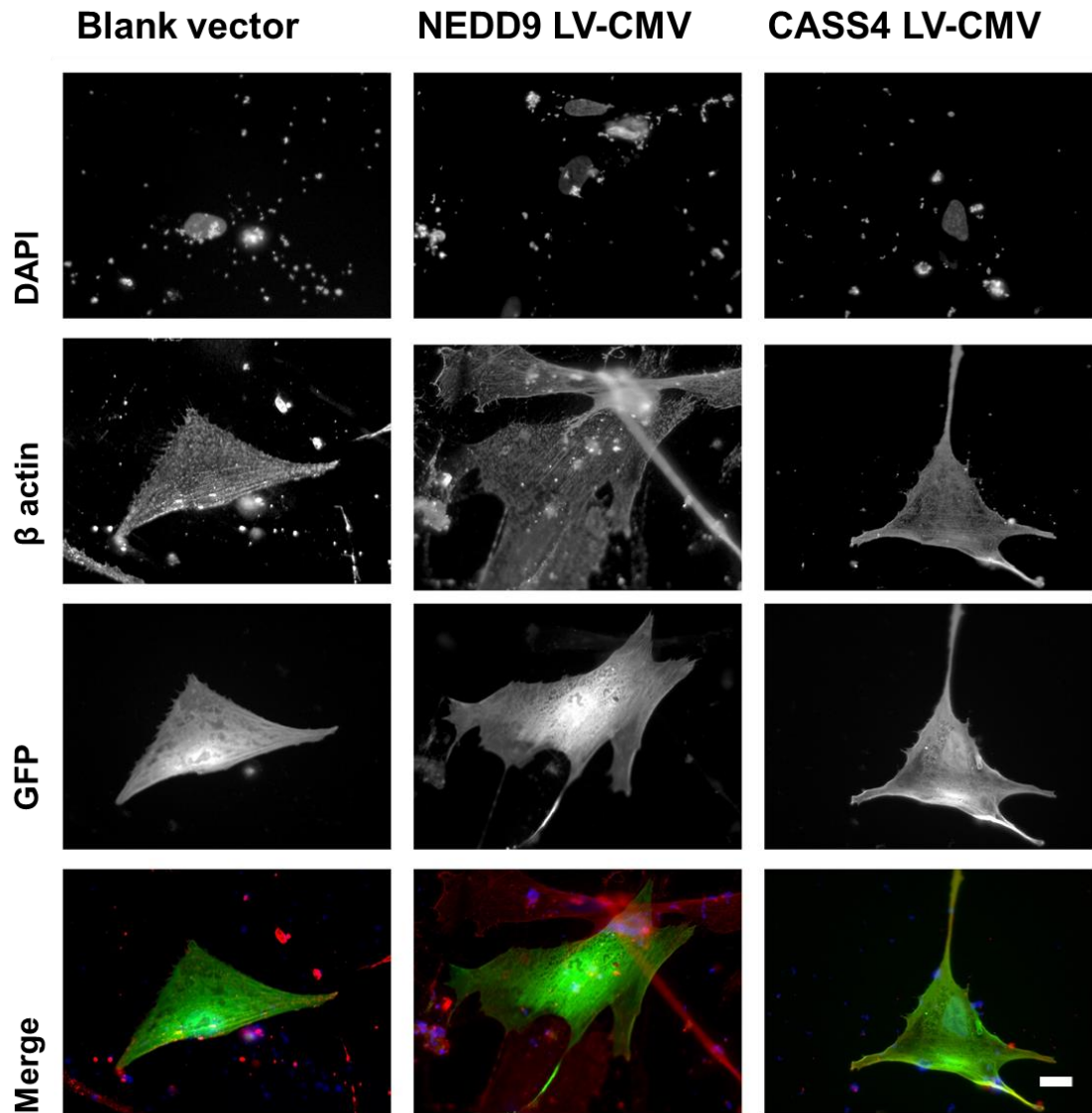
Figure 6.14 Overexpression of NEDD9 or CASS4 has no effect on βactin fluorescence or localisation

Fixed NHA were stained using an anti-βactin primary antibody, followed by Alexa Fluor 555 secondary antibody (red) revealing slightly striated staining throughout the cell. GFP+ transfected cells, green. N=3 donors. Scale bar = 20μm.

Quantification and comparison of β-actin fluorescence revealed no significant changes between the overexpressing population (NEDD9 217.42±19.46; CASS4 304.17±15.05 a.u.) and the control population (216.57±36.77 a.u.) of NHAs (Figure 6.15; ANOVA, $F_{(2,6)}$= 3.881, *P*= 0.083), suggesting that overexpression of the Cas-proteins does not influence expression of the actin filament.
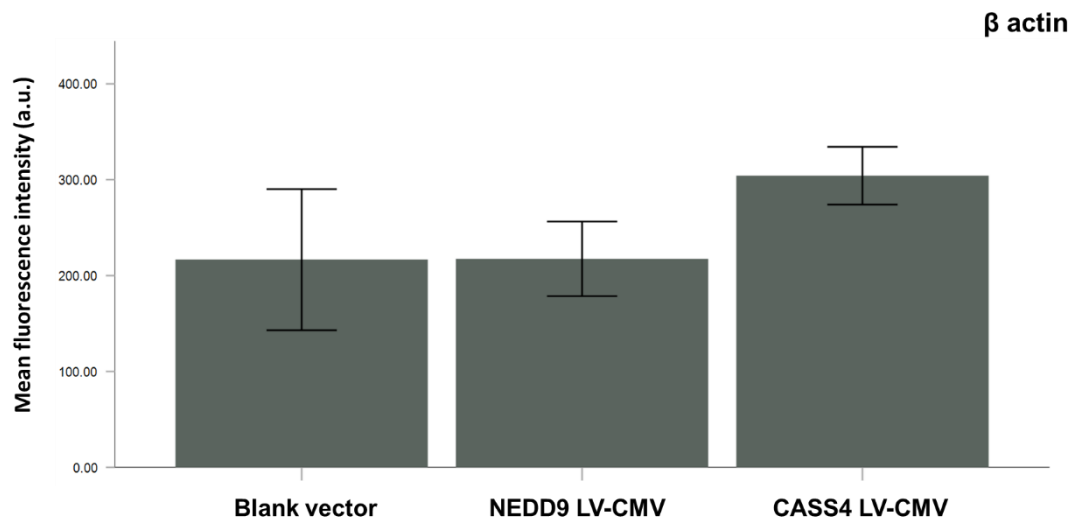
β actin

Figure 6.15 Overexpression of NEDD9 or CASS4 has no effect on βactin expression

Mean fluorescence intensity of β-actin in NEDD9 or CASS4 overexpressing cells in comparison to the blank vector control. Error bars ± 2 SEM. N=3 donors. P=NS.

As seen in the overexpression cells, NEDD9 or CASS4 KD did not appear to change β-actin fluorescence or cellular localisation in NHAs, depleted of either NEDD9 or CASS4 in comparison to the scramble control (Figure 6.16).
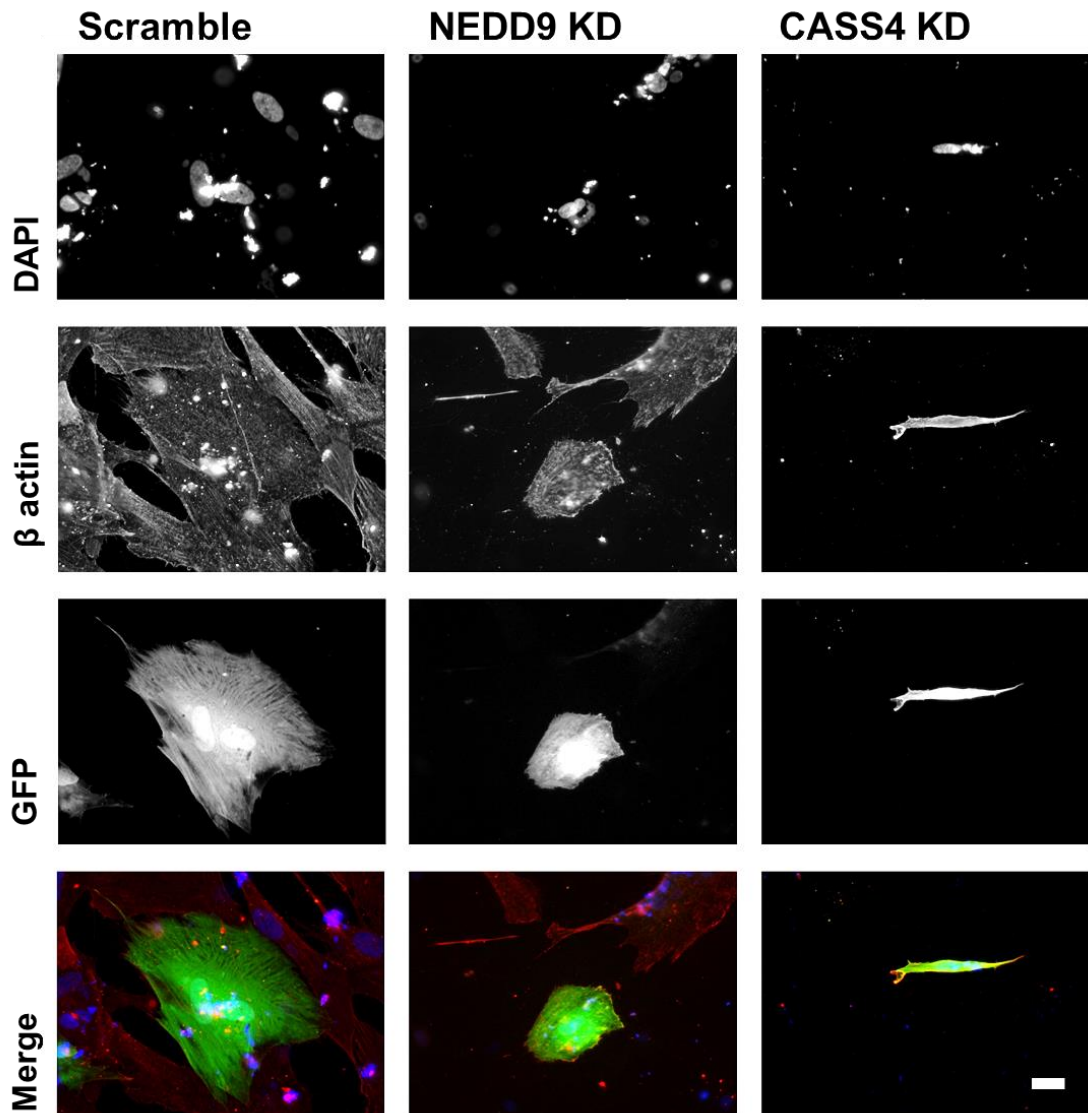
Figure 6.16 Knock-down of NEDD9 or CASS4 has no effect on βactin fluorescence or localisation

> *Fixed NHAs were stained using an anti-βactin primary antibody, followed by Alexa Fluor 555 secondary antibody (red) revealing slightly striated staining throughout the cell. GFP+ transfected cells, green. N=3 donors. Scale bar = 20µm.*

Comparing β-actin fluorescence of NHAs depleted of NEDD9 (242.57±43.30 a.u.) or CASS4 (214.13±31.73 a.u.) to the scramble control (272.72±4.064 a.u.) revealed no significant changes between these populations (Figure 6.17; ANOVA, $F_{(2,6)}$= 0.568, *P*= 0.595), suggesting that depletion of NEDD9 or CASS4 does not affect β-actin expression in these astrocytes.
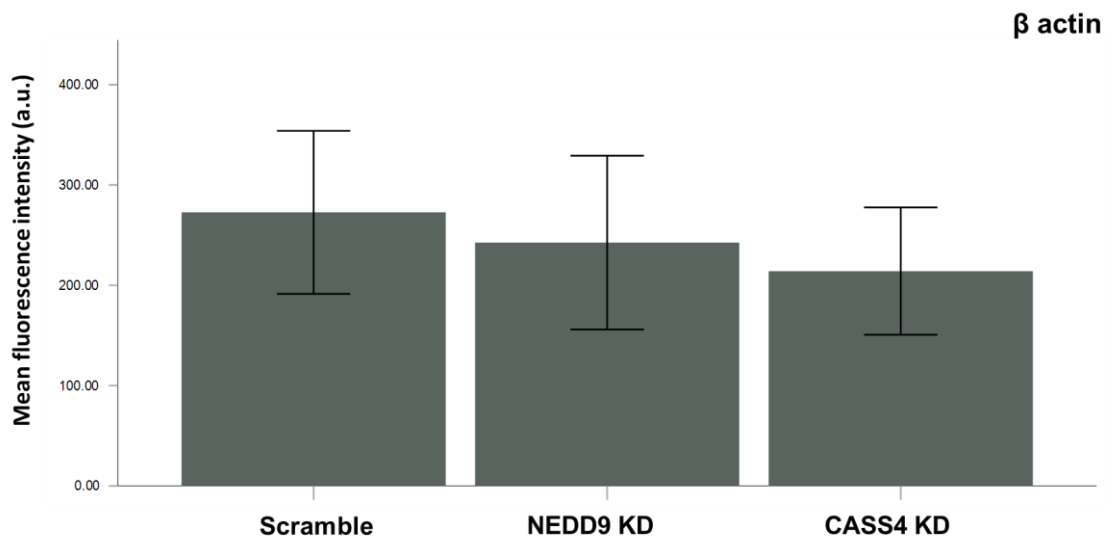
β actin

Figure 6.17 Knock-down of NEDD9 or CASS4 does not affect βactin fluorescence

Mean fluorescence intensity of β-actin in NEDD9 and CASS4 depleted NHAs in comparison to the blank vector control. Error bars ± SEM. N=3 donors

6.2.5 α Tubulin

Fluorescence imaging of NHAs immunocytochemically stained for α-tubulin revealed a striated pattern of staining, similar to β-actin, throughout the cytosol, consistent with the expected cytoskeletal localisation of this tubulin. Cells overexpressing NEDD9 or CASS4 appeared to display a slightly increased α-tubulin fluorescence in comparison to the blank vector control but with no apparent change in subcellular localisation (Figure 6.18).
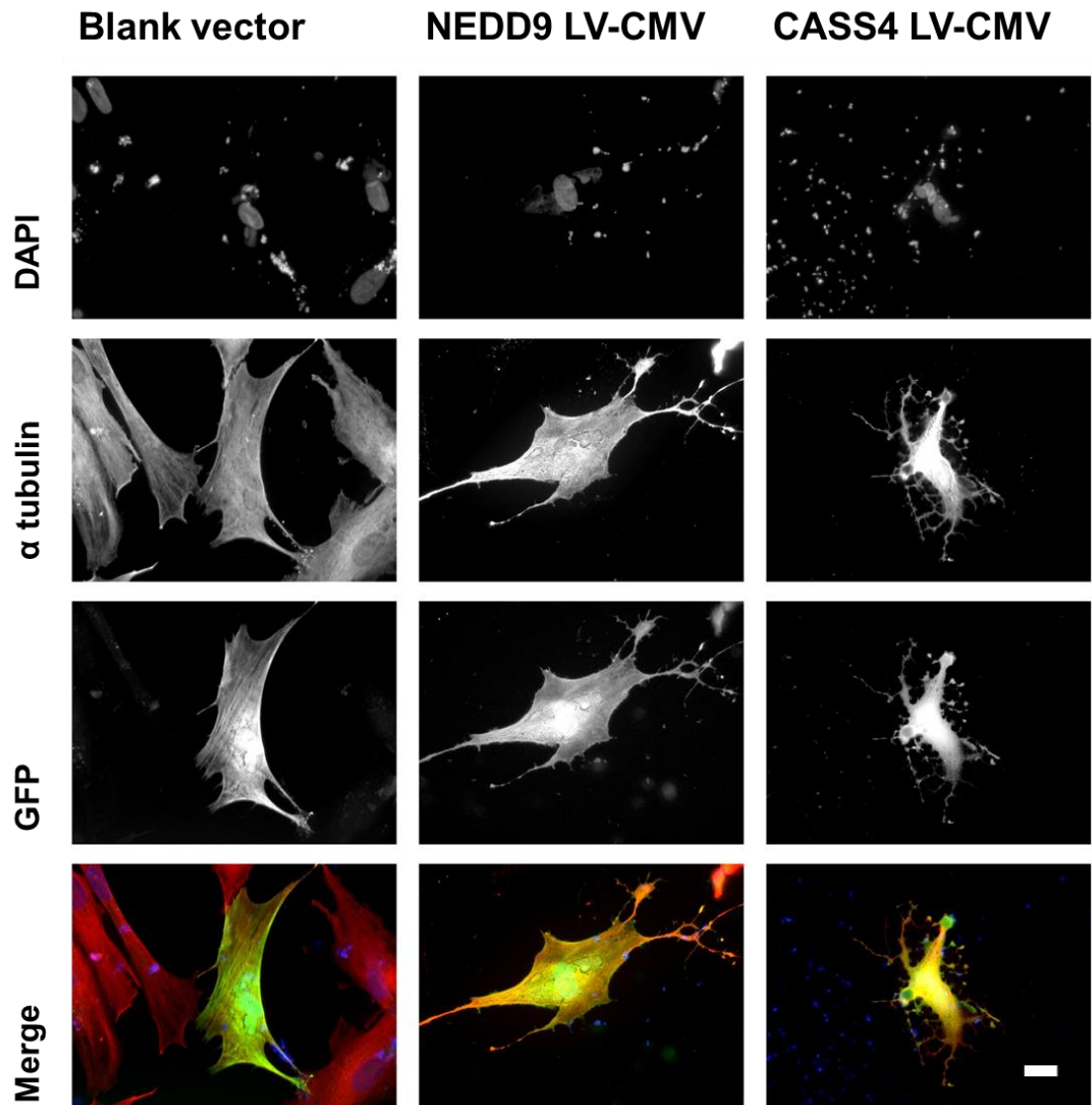
Figure 6.18 Overexpression of NEDD9 or CASS4 leads to an increase of α tubulin fluorescence

Fixed NHA were stained using an anti-tubulin primary antibody, followed by Alexa Fluor 555 secondary antibody (red) revealing slightly striated staining throughout the cell under all transfection conditions. GFP+ transfected cells, green. N=3 donors. Scale bar = 20μm.

Quantification and subsequent comparison of α-tubulin immunofluorescence revealed that the increase in fluorescence upon NEDD9 (2003.81±58.97 a.u.) or CASS4 (2290.29±45.53 a.u.) overexpression was statistically significant (Figure 6.19; ANOVA, $F_{(2,6)}= 68.184$, $P< 0.001$; Tukey *post hoc, P≤ 0.001*) in comparison to the blank vector

control (1537.32±31.32 a.u.) suggesting that both NEDD9 and CASS4 are influencing α tubulin expression in these NHAs.
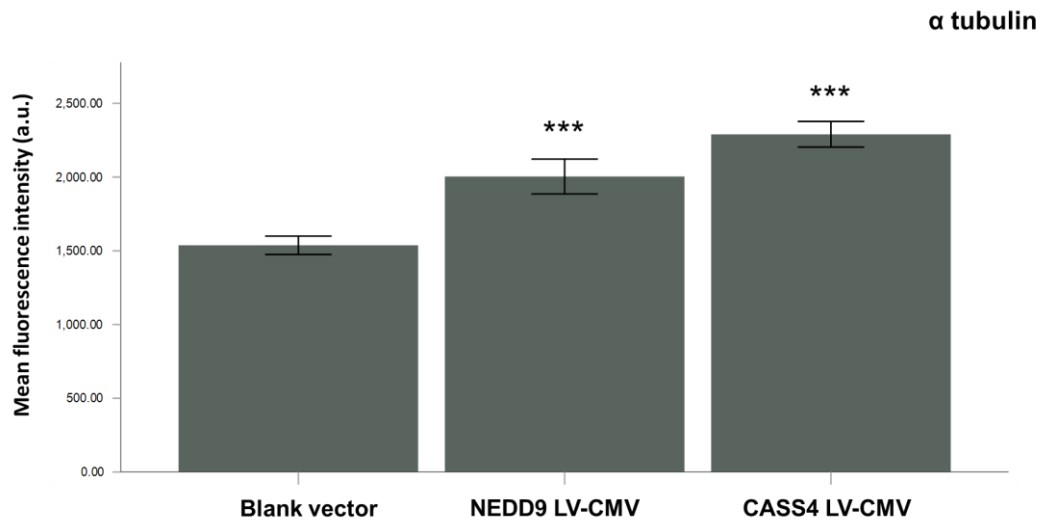
α tubulin

Figure 6.19 Overexpression of NEDD9 and CASS4 upregulates α tubulin expression

*Mean fluorescence intensity of α-tubulin is significantly increased in NEDD9 and CASS4 overexpressing NHAs in comparison to the blank vector control. N=3 donors. Error bars ± SEM. ** p≤ 0.01; *** p≤ 0.001*

Fluorescence imaging of the KD NHA groups stained for α tubulin revealed a slightly reduced fluorescence for the globular protein in cells, depleted of CASS4 in comparison to the cells depleted of NEDD9 and the scramble control (Figure 6.20).
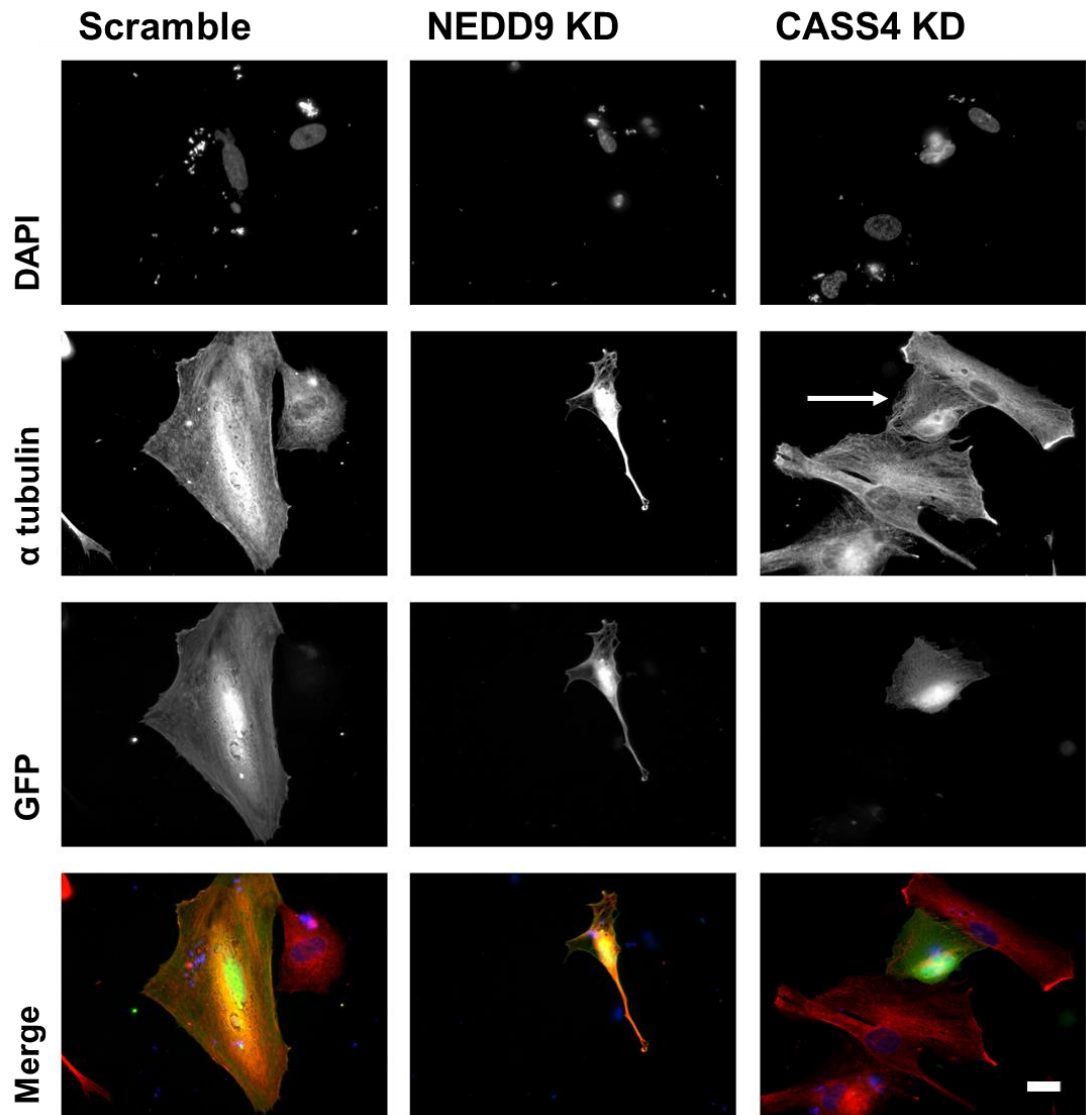
Figure 6.20 Knock-down of CASS4 shows a reduction of αtubulin fluorescence

Fixed NHAs were stained using an anti-αtubulin primary antibody, followed by Alexa Fluor 555 secondary antibody (red) revealing slightly striated staining throughout the cell and a reduction of α-tubulin in the CASS4 KD cells (arrow). GFP+ transfected cells, green. N=3. Scale bar = 20μm.

Comparison of the measured α-tubulin fluorescence confirmed that there was a significant reduction in fluorescence in the CASS4 (722.74±12.34 a.u.) depleted NHAs compared to scrambled controls (1507.65±248.88 a.u.) (ANOVA, $F_{(2,6)}$= 8.444, *P*= 0.018; Tukey *post hoc, P*= 0.024) but not for the NEDD9 knock-down (1457.98±81.11 a.u.) (Tukey

post hoc, P= 0.917) in comparison to the scramble control cells (Figure 6.21), indicating that only CASS4 has an effect on α tubulin expression when depleted.
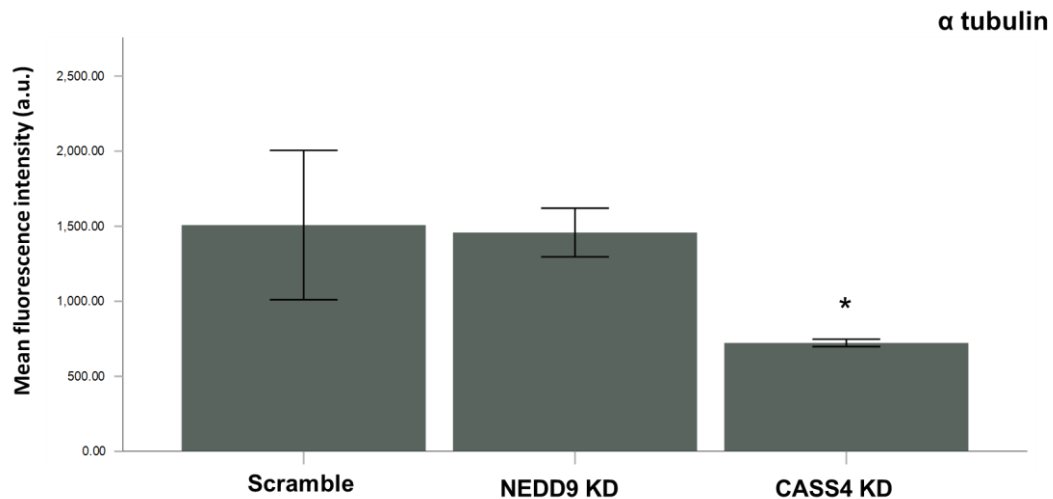
Figure 6.21 Knock-down of CASS4 downregulates αtubulin expression

*Mean fluorescence intensity of α-tubulin is significantly reduced in CASS4 depleted cells in comparison to the scramble control. NEDD9 knock-down NHAs show no change in α-tubulin levels. N=3 donors. Error bars ± 2 SEM. *p≤ 0.05.*

6.3 Discussion

As outlined previously, cell morphology and function are not separate entities but rather a unified system in which one influences the other. While overexpression of NEDD9 and CASS4 promoted an increase of cell volume and surface area; it had no effect on β-actin localisation or expression. Only α-tubulin was altered, with astrocytes overexpressing either NEDD9 or CASS4 experiencing increased expression of α-tubulin (although no change in subcellular distribution was evident). This may be in keeping with the earlier findings that the microtubule network, rather than actin filaments, play a particular role in morphological changes in astrocytes and glial cell lines (Ellenbroek *et al*., 2012,

Etienne-Manneville and Hall, 2001, Panopoulos *et al*., 2011). Development of the microtubule network is necessary for cells to increase in size (Lacroix *et al*., 2018). As one of the two major components of microtubules, enhanced expression of α-tubulin would be expected in larger cells. Moreover, changes of the microtubule network would be expected to occur due to the role of Cas-proteins in cytoskeletal arrangement: NEDD9 has been shown to regulate AURKA (Bargon *et al*., 2005), which in turn controls microtubule remodelling (Yamada *et al*., 2010); and both NEDD9 and CASS4 are also known to have roles in mediating integrin-dependent signalling, maintaining focal adhesion integrity and regulating cell spreading and migration (Singh *et al*., 2008). This finding suggests, that overexpression of the Cas-proteins promotes astrocyte process formation and could hence even have a protective role in synapse support. Process formation is vital for contact with pre- and postsynaptic membrane, building the tripartite synapse, enabling bidirectional communication between neurons and astrocytes (Zovkic *et al.*, 2013, Zorec *et al.*, 2015). To investigate the effects of the larger astrocytes and the upregulation of tubulin on neuronal function would require co-cultures. Measuring neuron function in presence of NEDD9/CASS4 overexpressing astrocytes could provide evidence for a protective or damaging role.

Interestingly, in the knock-down model, only depletion of CASS4 led to decreased levels of α-tubulin; NEDD9 depletion did not alter α-tubulin expression. This finding is somewhat at odds with reports that CASS4 may be less biologically active than NEDD9 in mediating integrin-dependent signalling (Singh *et al*., 2008), possibly due to reduced Src binding (Tachibana *et al*., 1997). The relative activities of the Cas-proteins in astrocytes have not yet been explored, however, so this could potentially be reflective of an astrocyte-specific preference. Decreased expression of tubulin coincides with the loss of processes seen in the KD model and may reflect the inability of these cells to maintain

the tripartite synapse and hence loss of synaptic support, which could contribute to synaptic loss in the early stages of AD.

Notably, overexpression of the Cas-proteins did not induce an increase of GFAP, suggesting that the increased cell size and process formation seen in the previous chapter was not due to an induction of reactivity, as outlined in the introduction, reactive/hypertrophic astrocytes present with increased GFAP expression and are a direct result to injury (Robinson *et al.,* 2016, Gonzales-Reyes *et al.,* 2017), such as amyloid plaques.

Depletion of NEDD9 and CASS4, on the other hand, induced a marked decrease in GFAP expression. Although upregulation of GFAP as part of the astroglial reactive response is a hallmark of several neurodegenerative diseases (Pekny and Pekna, 2004, Ross *et al.*, 2003, Yang and Wang, 2015, Verkhratsky *et al.*, 2013); in AD, reactive astrocytes are only evident during later symptomatic stages of the disease (Verkhratsky *et al.*, 2017). During the early, asymptomatic stages of AD, astrocytes exhibit atrophy and present with a decreased GFAP expression (Beauquis *et al.*, 2014, Jones *et al.*, 2017, Olabarria *et al.*, 2010). Hence, NEDD9- or CASS4-induced reduction in GFAP concurrent with decreased cell size and arborisation in NHAs mirrors the early AD astrocyte phenotype.

Neither overexpression of NEDD9 or CASS4 showed a significant difference in s100B or EAAT2 expression or localisation. Conversely, in Cas-protein-depleted cells, both of these markers were significantly downregulated. Reduced expression of the glutamate transporter EAAT2 could be a direct consequence of knock-down induced atrophy but may also be a result of reduced GFAP expression, as GFAP has previously been implicated as a regulator of EAAT2 (Hughes *et al.*, 2004, Simpson *et al.*, 2010). This is contrary to the finding that the mouse orthologue of EAAT2, GLT1, only displayed a slight, non-significant reduction in astrocytes of the prefrontal cortex in the 3xTg-AD

murine model (Kulijewicz-Nawrot *et al*., 2013), despite the pronounced atrophy evident in these cells (Kulijewicz-Nawrot *et al*., 2012). This disparity might be due to differences in the brain regions tested as the NHAs utilised herein being harvested from across the cortex, while Kulijewicz-Nawrot and colleagues specifically focused on the medial prefrontal cortex. Additionally, GFAP expression in 2D culture of astrocytes can vary greatly, depending on culture methods, from their counterparts *in vivo* (Lange *et al*., 2012). This is a limitation of cells in 2D culture but alternatively, it may simply be due to inherent differences between mouse and human astrocytes (Mohamet *et al*., 2018). Although *in vivo* models are generally superior to *in vitro*, murine astrocytes differ greatly to human astrocytes (Zhang *et al*., 2013, Vasile *et al*., 2017, Verkahratsky *et al.,* 2017), suggesting that primary astrocyte models are a more viable option for this investigation. Jones *et al*. (2017) previously reported reduced expression of another member of the EAAT family of glutamate transporters, EAAT1, in human astrocytes derived from AD patients. EAAT1 and EAAT2 share significant sequence homology (Arriza *et al*., 1994) and are both found almost exclusively on astrocyte processes which ensheath synapses, although they may exhibit some functional differences and brain region-specific expression variation (Valtcheva and Venance, 2019). Unfortunately, EAAT1 expression could not be tested in this thesis owing to the technical difficulties with the staining and a limited number of primary astrocytes available for optimisation. In the absence of any published literature suggesting otherwise, it is reasonable to speculate that the factors which impact upon the expression of one paralogue will have a similar effect on the other. Parallels may thus be drawn between the downregulation of EAAT1 seen in AD patient-derived astrocytes and the downregulation of EAAT2 induced by NEDD9 or CASS4 depletion. In both cases, loss of synapse-associated astrocytic glutamate transporters could be indicators of impaired synaptic glutamate homeostasis.

S100B was also significantly downregulated in NHAs depleted of either NEDD9 or CASS4. Reduced expression of s100B has previously been reported in iPSC-derived astrocytes of AD patients (both LOAD and EOAD) (Jones *et al*., 2017). The atrophic astrocytes also displayed a nuclear localisation of s100B, which was exclusively detected in the nucleolar region instead of the usual cytoplasmic subcellular localisation. A similar, though less extreme, mis-localisation of S100B was observed in the cells depleted of NEDD9 or CASS4, wherein the protein localised in a ring shape surrounding the nuclei with reduced prevalence in the cytoplasm. Nuclear accumulation of s100B has been reported in astrocytes previously, and also in adult oligodendrocyte progenitor cells, where those which exhibit nuclear S100B immunoreactivity go on to produce dense processes, while those which do not express S100B fail to achieve stellation (Deloulme *et al*., 2004). Depletion of s100B has previously been reported to result in a loss of typical morphology and the development of a fibroblast-like shape in the rat C6 glioma cell line and the GL15 astrocytoma cell lines, akin to that seen upon Cas-protein depletion (Brozzi *et al*., 2009, Selinfreund *et al*., 1991). Selinfreund and colleagues suggested that S100B might play a role maintaining proper astrocyte stellation through its interaction with Src kinase. As Src is a known binding partner of NEDD9 and CASS4, this might be another potential mechanism through which the Cas-proteins can exert influence on astrocyte morphology. Expression of s100B may also be linked to calcium signalling, but remains a limited aspect of such and further functional testing is required to determine the effects on calcium signalling in this model; this could be done with calcium labelling and live cell imaging. But s100B is also implicated in cell migration, proliferation and inflammatory response, whereby s100B downregulation reduces these effects (Xia *et al.,* 2018). Hence cells, depleted of s100B, are unable to respond to brain insults, suggesting,

that these astrocytes may not be able to deal with accumulating plaques and NFTs, leading to disease progression in AD.

Overall, the changes of astrocyte functional markers in the NEDD9/CASS4 overexpression model have been minimal and clearly coincide with the increased cell size, as cytoskeletal protein tubulin is expected to increase with increasing cell size and might even provide protective properties. Contrary to this, the KD model presented with drastic changes in functional markers, which as outlined above, suggests that the physiological functions of these cells are impaired. This is likely to lead to loss of the neuroprotective role of astrocytes to injury, such as plaques, and the role in homeostasis, such as clearing glutamate from the synaptic cleft. Protein aggregates, such as amyloid or tau, and loss of synapses are known AD pathologies and based on the above, atrophic astrocytes may be an early contributor to these manifestations. If further tests confirm NEDD9 and CASS4 as regulators of astrocyte atrophy in AD, the Cas-proteins could be used as therapeutic targets in the future.

Chapter 7

General discussion

7 Discussion

The overall aim of this thesis was to investigate whether altered expression of NEDD9 and CASS4 induce morpho-functional changes in astrocytes and to explore if the altered expression links to a role in astrocyte dystrophy in AD. Initially it was necessary to confirm endogenous expression of these proteins, as this had previously not been demonstrated. Robust expression of both NEDD9 and CASS4 was confirmed via immunocytochemistry and Western blotting in glial cell lines and in primary human cortical astrocytes. Ideally, expression would also have been determined in the human adult brain, which had only been demonstrated in one previous study (Li *et al*., 2008), as the primary astrocytes used for this thesis are derived from foetal sources. Notwithstanding, the NHAs employed did express mature astrocyte markers, including s100B which has been reported to be a marker for terminally differentiated cortical astrocytes (Raponi *et al*., 2007). Human brain tissue was not available for this investigation (although ethical approvals are being sought to undertake this work, see future directions section), however expression was confirmed in the entorhinal cortex of adult mice. As the whole brain homogenate contains all brain cell types, conclusions may not be drawn about astrocyte expression in isolation. Nonetheless, these data indicate that both Cas-proteins are expressed in the mature murine brain. Taken together with the data from individual primary astrocyte cultures, it is highly likely, that the proteins are expressed in mature astrocytes *in situ*.

Normal human astrocytes were selected as the model system in which to test the effects of the Cas-proteins. Although CASS4 isoforms were consistent across glial cell lines and the primary human astrocytes, blotting of whole cell lysates for NEDD9 revealed key differences in the expression of NEDD9 isoforms between the cell lines and primary

astrocytes. While cell lines expressed two cleaved forms of the full-length protein (55 kDa and 65 kDa), NHA lysates contained only one of these isoforms (55 kDa) together with two phosphorylated isoforms of the full-length protein (105 kDa and 115k Da) (Bradshaw *et al.*, 2011, Law *et al.*, 1998). It may be that these differences are part of the altered NEDD9 expression profiles in the cancer cells from which the cell lines are derived (Gabbasov *et al.*, 2018, Feng *et al.*, 2015, Li *et al.*, 2011, Izumchenko *et al.*, 2009). Although, as outlined in chapter four, primary cells are difficult to transfect (Alabdullah *et al.*, 2019, Gresch and Altrogge, 2012), it is likely that the different NEDD9 splice variants may serve different roles and might arise from cell type-specific post-translational modifications. These differences meant that the primary human astrocytes were a superior option on which to base the expression models to permit better translation of findings to humans. Hence, immortalised cell lines were omitted from further experiments.

When blotting cell lysates for CASS4, a band was never seen at the predicted size of 87 kDa in any cell type. Instead, the truncated isoform 2 (76 kDa) was evident, together with an unusually large band at 230 kDa was seen in all cell types. This large molecular weight species does not correlate with any known isoform of the protein; however, it was consistently observed in all lysates, including the cell lines, NHA and mouse brain, indicating that the band is representative of CASS4 expression. Additionally, as previously indicated, this heavier CASS4 band has also been observed in the laboratories of Dr Mahendra Singh and Prof Erica Golemis (personal correspondence), although they have never published this finding. Although Cas-proteins undergo extensive phosphorylation, the very large size makes this unlikely to explain this size difference. The protein may form homo- or heterodimers via the C-terminal domain, as has been previously reported for NEDD9 (Law *et al.*, 1999), although the size would be closer to

a trimerization, which has not been described for these proteins previously. Alternatively, this might represent a complex of CASS4 with one of its larger binding partners, such as Abl, which at 123 kDa would provide roughly the correct size band (Shagisultanova *et al*., 2015, Witte *et al*., 1980). Notwithstanding, this large molecular weight species resisted all attempts at disruption, including exposure to heat, additional reducing agents and chemical denaturants including urea. Interestingly, it was this band which was primarily enriched upon overexpression of CASS4 and knocked-down by siRNA; isoform 2 was largely unchanged in either case. This would indicate that a change in expression does not influence binding of CASS4 to its 'mysterious' binding partner. Identifying this binding partner may reveal new insights into CASS4-specific functions, since NEDD9 does not appear to form this same complex. Unfortunately, preliminary attempts at immunoprecipitation were unsuccessful and, since they were not a central objective of this thesis, will have to be left for future work.

The NEDD9 and CASS4 overexpression and knock-down models in NHAs were created via transient transfection. This was initially considered to provide a sufficient transfection efficiency for subsequent experiments including the planned morphometric analyses. Stable transfection of NHAs may have aided this work as a continuous stock could have been created, readily available for follow-up experiments and longer-term experiments could have been undertaken (although maintenance of primary cells in culture for extended periods is not recommended as they become 'culture adapted' and start to exhibit altered phenotypes (Hayflick, 1979). The procedures of viral design and establishing stable transfection, however, are time consuming and require specific safety requirements, which would have limited the scope of this project. The transfection efficiency was suitable for preliminary validation of overexpression and knock-down via

immunocytochemistry. Western blotting, however, is the gold-standard and most commonly used method to validate overexpression and knock-down (Kikuno *et al*., 2007, LaRocca *et al*., 2019, Liu *et al*., 2009, Zhao *et al*., 2018). A stable line may have been advantageous in this validation via Western blot, as the relatively low transfection efficiency generated by the transient transfections meant that endogenous expression of the Cas-proteins in the non-transfected cell pool masked the knock-down. This was overcome by enrichment via puromycin selection for 24 hours, which produced sufficient enrichment by killing off the non-transfected cells in the culture, permitting knock-down confirmation. Selection of transfected cells via fluorescence-activated cell sorting (FACS) was also trialled, however both the low total numbers of primary cells available and the larger-than-average size of the NHAs meant that this method was unsuccessful and without results. Given more time for optimisation, FACS would be a suitable method to further validate KD and overexpression and improve this model. Other means to confirm the knock-down could have included qRT-PCR to quantify NEDD9 or CASS4 mRNA levels; although this method only indicates the level of the transcript which, as described earlier, may not be a reliable indicator of the level of the protein product (Liu *et al*., 2016, Schwanhausser *et al*., 2011). Nevertheless, the combined results of confirmation via quantification of immunofluorescence and Western blot, combined with the observation of clear phenotypic changes in the transfected NHAs from three different donors, provided sufficient validation of Cas-protein overexpression and knock-down within the scope of this project. This thesis is the first study to create overexpression and knock-down models of the Cas-proteins in astrocytes as their effect on this cell type, or any neuronal cells, has not been tested to date. This permits a novel insight to regulation of morphology and physiology of astrocytes and a possible mechanism for astrocyte

atrophy in AD. Furthermore, it provides insights to the effect of GWAS identified risk variants on clinically relevant cells.

Overexpression and knock-down experiments provided clear evidence that both NEDD9 and CASS4 are capable of inducing morphological changes in astrocytes, achieving one of the main objectives of this thesis. Initial observation and visual binning of cells overexpressing either of the Cas-proteins showed a general shift towards a more stellate cell phenotype and a decrease in fibroblast-like morphologies. This is reflective of previous findings that upregulation of NEDD9 promotes process formation in epithelial cancer cells (Bargon *et al.*, 2005). The morphometric quantitative analysis revealed that overexpression of NEDD9 or CASS4 leads to generally larger cells, based on the measurements of volume and cell surface, but no significant difference in surface to volume ratio was found. This would indicate, however, that the cellular morphology is not necessarily more complex in the overexpressing cells, compared to the control group; a small soma with several processes would lead to a higher surface to volume ratio in comparison to cells of a less complex nature as fibroblast-like cells (Jones *et al.*, 2017). This discrepancy may be down to a number of factors. The method of visually assessing cell morphology is limited by subjectively categorising cell morphologies, whereas isosurface renders, used for morphometric analysis, are more quantitative and less prone to subjective influences. Moreover, despite best efforts at blinding when visually binning cell morphologies, the marked change in cell size was rather obvious to the observer, thus potentially compromising the blinding. However, the methodology used to image and render cells in 3D for the morphometric analysis could be considered less sensitive to detect finer processes. Such processes would contain limited amounts of GFP, making them relatively dim. Confocal microscopy (even the high-end systems with hybrid

detectors employed here) notoriously struggle to deal with low levels of fluorescence since the principles used to collect individual optical z-sections mean much of the light from the specimen fails to pass through the pinhole to the detector. A widefield fluorescence microscope of the sort used to conduct the visual binning experiments, however, collects all of the light from the specimen (even that which is out of focus) (Lichtman and Conchello, 2005). This combined with the cells being visualised using the human eye (which despite huge advances in the field is still considerably better dynamic range than a CCD camera or other digital detector) would offer a superior ability to identify fine, dim processes emanating from larger, brighter cell bodies. Alternatively, this difference may be the result of using a relatively crude measure of cellular complexity in the form of the surface area to volume ratio. It could be that a form of Sholl analysis, which was originally developed to quantify neuronal dendritic arborisation (Longair *et al*., 2011, Sholl, 1953), modified to take into account the thicker processes of astrocytes might provide a more sophisticated approach to quantifying such complex morphologies. Although a modified Sholl method has recently been applied to astrocytes, this was in mouse brain sections; where astrocytes exhibit native 3D conformations that include much finer processes emanating in all dimensions (Tavares *et al*., 2017). Attempts to apply the method to human astrocytes in culture during this thesis were unsuccessful, probably owing to differences in cellular morphology between the 2D culture system and the *in vivo* morphologies upon which the analysis method was based. Nonetheless, modification of this morphometric approach might prove beneficial to future studies on astrocytes in 2D culture.

Morphological analyses of the NEDD9 and CASS4 knock-down model presented a somewhat clearer picture; visual evaluation and binning cells into morphology types and morphometric analysis both revealed that astrocytes depleted of either of the Cas-proteins

exhibit an atrophic morphology. These cells presented with a decreased somata width and were process devoid. Similarly, morphometric analyses showed a significant decrease in cell surface area and volume and no difference in surface to volume ratio, indicating that depletion of NEDD9 and CASS4 promotes smaller cells. This is also in keeping with previous findings, were NEDD9 depletion has induced cell rounding in mouse embryo fibroblasts (Zhong *et al*., 2012) and is capable of inducing dendritic spine loss of hippocampal neurons in mice (Knutson *et al*., 2016).

Taken together these data indicate that depletion of NEDD9 and CASS4 can inhibit the formation and/or maintenance of membrane protrusions, such as processes, a phenomenon which has not previously been reported for CASS4 in any cell type.

The molecular mechanisms underlying Cas-protein-induced morphological changes were not explored as part of this thesis, however previous studies provide some insight. NEDD9 is known to be involved in several signalling pathways which could lead to morphological changes. NEDD9 regulates AURKA activity, which is essential for proper arrangement of the microtubule network (Mori *et al*., 2009, Pugacheva and Golemis, 2005). Microtubules, rather than the actin cytoskeleton, have previously been especially implicated in astrocyte morphogenesis (Ellenbroek *et al*., 2012, Etienne-Manneville and Hall, 2001, Panopoulos *et al*., 2011). During this process, phosphorylation of the 115 kDa NEDD9 isoform is increased (Sakai *et al*., 1994). This isoform was overexpressed in the NHAs transfected with NEDD9 LV-CMV and it is plausible that overexpression triggers a similar pathway in astrocytes, inducing process formation, discussed in in chapter 5. Additionally, the 115 kDa isoform was depleted in the KD cells and may inhibit such pathways, hence inhibit process formation. As cells depleted of CASS4 exhibit a similar phenotype, it is likely that the protein acts in the same manner as its paralogue.

Alternatively, these morphological changes might be mediated by s100B, whose levels appear to be influenced by the Cas-proteins via Src and has been reported to play an important role maintaining proper astrocyte stellation (Brozzi *et al*., 2009, Selinfreund *et al*., 1990).

One particularly interesting find was that the astrocytes depleted of NEDD9 or CASS4 mimic the atrophic phenotype of astrocytes found in both mouse and human models of AD (Jones *et al*., 2017, Kulijewicz-Nawrot *et al*., 2012 Olabarria *et al*., 2011, Yeh *et al*., 2011). Cell morphology in both models are characterised by soma shrinkage and complete loss of cellular processes, as was the morphological phenotype induced by Cas-protein depletion presented here. As astrocyte atrophy in AD remains unexplained and polymorphisms in both NEDD9 and CASS4 which likely alter expression have been linked to an increased risk of LOAD, it is reasonable to suggest that this might be a potential mechanism through which atrophy might manifest and requires further investigation. Atrophic, process-devoid astrocytes are likely unable to be in contact with synapses, hence losing the ability to support them. This could lead to an increase of toxins, such as glutamate, in the synaptic cleft and ultimately synaptic loss. Synaptic loss is a manifestation in AD, uncovering mechanisms leading to these hallmarks, such as Cas-protein induced atrophy, could aid the understanding of pathogenesis and identify new therapeutic targets in the future.

The change of astrocyte functional markers induced by Cas-protein depletion also correlated with findings from AD models. Jones *et al* (2017) have reported the downregulation of GFAP, s100B, EAAT1 and GS in their atrophic human iPSC-derived AD astrocytes. Here a reduction in GFAP and s100B accompanied NEDD9 or CASS4 knock-down. Crucially, overexpression of the Cas-proteins induced no change in GFAP

or s100B levels, indicating that the enlarged morphological phenotype induced was not due to astrocyte reactivity, which is associated with upregulation of both of these proteins (Pekny and Pekna, 2014). Depletion of s100B has previously been reported to result in a loss of typical morphology and the development of a fibroblast-like shape in glial cell lines (Brozzi *et al.*, 2009, Selinfreund *et al.*, 1990). Furthermore, downregulation of s100B has been shown to inhibit the inflammatory response in other cell types (Ohtaki *et al.*, 2007), suggesting that a decrease of s100B may hamper the ability of astrocytes to respond to brain insults, such as amyloid plaques or NFTs.

The downregulation of S100B and its aberrant cellular mis-localisation provided another parallel to the studies of atrophic astrocytes in AD, as a reduced expression was reported in 3xTg-AD mice and human iPSC-derived AD astrocytes (Jones *et al.*, 2017, Yeh *et al.*, 2011). The atrophic iPSC-derived AD astrocytes also displayed a mis-localisation of s100B, which was exclusively detected in the nuclei instead of the usual cytoplasmic subcellular localisation. A similar redistribution of s100B was observed in the NHAs depleted of NEDD9 or CASS4 here with the protein localising in a ring shape surrounding the nucleus. It remains unclear how the dysregulation and mis-localisation of s100B occurs. S100B binds to GFAP, hence the reduction of GFAP and aberrant cytoskeletal arrangement in the Cas-protein KD cells could potentially influence s100B localisation. To completely elucidate the morphological and functional changes induced by altered expression of the Cas-proteins will require additional research. Notwithstanding, NEDD9 or CASS4 depletion alone appears to induce a similar s100B cellular phenotype to that seen in AD models.

Downregulation of the astrocytic glutamate transporter EAAT2 was also reported upon depletion of either Cas-protein. Kulijewicz-Nawrot *et al.* (2013) also reported a slight

decrease in EAAT2 in astrocytes of the prefrontal cortex in the 3xTg-AD murine model, although this was deemed non-significant, and Jones and colleagues (2017) showed a downregulation of EAAT1, a related paralogue of EAAT1 (Arriza *et al*., 1994). Determination of EAAT1 levels in the overexpression and knock-down models was attempted, however it was not possible due to difficulties with the optimisation of the staining protocol and the limited number of primary cells. The same problem occurred for glutamine synthetase, which has also been reported to be reduced in AD (Jones *et al*., 2017, Kulijewicz-Nawrot *et al*., 2013, Rodriguez-Arellano *et al*., 2016). Notwithstanding, these data point to an impairment of astrocyte functional markers upon Cas-protein depletion, implying a key role for both NEDD9 and CASS4 in maintaining astroglial functions. For example, EAAT2 is responsible for the majority of glutamate uptake by astrocytes (Kim *et al*., 2011, Nedergaard *et al*., 2002) and hence a reliable marker of astrocytic function. Altered expression of the transporter as reported here would inevitably lead to unbalancing glutamate homeostasis in the brain. Indeed, altered expression has been linked to several neurological diseases, such as amyotrophic lateral sclerosis (Rattray and Bendotti, 2006), Huntington's disease (Arzberger *et al*., 1997) and AD (Garcia-Esparcia *et al*., 2018). The reduction of EAAT2 could be a direct consequence of KD-induced atrophy but may also be a result of reduced GFAP expression, as GFAP has previously been implicated as a regulator of EAAT2 (Hughes *et al*., 2004, Simpson *et al*., 2010). A downregulation of EAAT2 would indicate that glutamate transport of the KD cells is affected and may hence lead to unbalanced glutamate homeostasis and reduced uptake at the synapse, potentially exposing neurons to excitotoxic damage (Kim *et al*., 2011, Nedergaard *et al*., 2002). Collectively, the dysregulation, particularly the downregulation of functional markers in the KD astrocytes, give imply that the function of these cells is affected. This downregulation

mirrors the atrophic AD phenotype, identified in earlier studies (Jones *et al*., 2017), further implicating altered expression of the Cas-proteins as a possible mechanism in astrocyte atrophy in AD. However, immunocytochemistry alone is not sufficient and direct functional assessments, such as glutamate uptake assays, should be employed to validate these findings.

Collectively, the functions of atrophic astrocytes, such as the NEDD9/CASS4 KD model, are likely to be impaired and play a role in AD pathogenesis. The downregulation of glutamate transporters could ultimately lead to synaptic loss due to glutamate neurotoxicity, but the mechanisms by which early synaptic impairment is caused in AD remain elusive, however given the dependence of many synapses on close physical contact with astrocytes (Hama *et al*., 2004, Hennenberger *et al*., 2010), astroglial atrophy is likely be a contributing factor in synaptic dysfunction in AD. Furthermore, atrophic astrocytes are likely unable to deal with amyloid or NFT load, hence contributing to AD pathology. It remains unclear if atrophic astrocytes become reactive during later stages of the disease but are likely an independent early hallmark and hence playing a different, yet unknown role in disease progression.

While the mechanisms are not yet fully understood, this thesis demonstrates, that altered expression of the Cas-proteins, NEDD9 and CASS4 (implied by GWAS as a risk factor for AD) are capable of recapitulating many of the morphological and functional deficits seen in atrophic astrocytes in AD. These results build upon the astrocyte atrophy during early, asymptomatic AD stages, identified by Jones *et al*. (2017) and propose a new mechanism for this manifestation.

7.1 Concluding statement

In summary, this work provides valuable insights of how NEDD9 and CASS4 may be involved in astrocyte pathology and provides solid grounds for further research. This work confirms that altered expression of the Cas-proteins leads to morpho-functional changes in astrocytes, which may uncover mechanisms leading to astrocyte atrophy in AD. This thesis is a step towards elucidating pathologies in AD but harbours some limitations, such as the NHA model of foetal tissue origin. Although there are no adult astrocyte models available, testing human brain samples alongside the *in vitro* model could have improved this thesis. Furthermore, much time was spent on the validation of the models, particularly via FACS, when validation had already been achieved via IF and western blotting. This time could have been used to pursue functional tests, thus greatly enhanced the last result chapter. Due to the novelty of this work and lack of literature, much optimisation was required, which limited time for testing the model. Nonetheless, this thesis contributes to the understanding of astrocyte dystrophy in AD and could, with some additional work, unearth new therapeutic targets in the future.

Chapter 8

Future directions

8 Future directions

First of all, some work of this thesis could be refined, repeated and extended, such as the model validation or the investigation of functional markers, however, this is already outlined in the general discussion. The role of NEDD9 and CASS4 in AD development has previously not been studied. Based on this, there is copious future work which could build upon the findings of this thesis

A good starting point would be to genotype the NHAs, used in this thesis, as there is the possibility of the (NHA) donors carrying the SNPs indicated as LOAD risk factors. Although the SNPs are rare and the results have been congruent across all donors, it is a vital investigation, which was not possible due to lack of resources for this thesis.

Once the absence of the indicated SNPs is established, rescue studies should be employed to fully exclude the possibility of off-target effects and confirm that KD of *NEDD9* and *CASS4* is indeed the cause for the atrophic phenotype. This work would require the development of siRNA-resistant expression vectors which would be used to rescue the levels of each Cas-protein following knock-down. Although this would be vital to validate the KD, the low transfection efficiency may lead to difficulties as a second transfection with siRNA-resistant vectors is unlikely to be successful in all KD cells, if at all. This could be overcome with stable transfection, but as outlined in this thesis, is time consuming and may cause further off-target effects. Nonetheless, rescue experiments should be trialled, including crossover studie, to see if overexpression of CASS4 could rescue the phenotype induced by KD of NEDD9, and *vice versa*. In this way overlapping functions could be uncovered.

Next functional assessment of the astrocyte models should be undertaken. The findings of changed marker expression, particularly the downregulation in the KD model, points to aberrant function of these cells. To actually determine this, functional tests could be performed. The downregulation of the glutamate transporter EAAT2 is likely to affect glutamate homeostasis; a glutamate uptake assay would be a relatively simple but effective way to test if glutamate uptake is impaired in these cells. Furthermore, the dysregulation and mislocalisation of s100B indicates that calcium signalling may also be affected in these cells. To determine calcium signalling in this model, calcium immuno-labelling, such as Rhod-2, would be required for live cell imaging. Live cell imaging has not been undertaken, as the experiments of this thesis required fixed cells. The transient overexpression and knockdown would be time limiting but it would also show how these cells function over a, although short, time period.

As KD of NEDD9 or CASS4 leads to smaller cells which reflects the atrophic phenotype found in iPSC-derived astrocytes from EOAD and LOAD patients, it would be of great interest to determine the expression of the Cas-proteins in these cells. This would conclusively establish whether there, expression of the Cas-proteins is indeed reduced in AD. The same phenotype had been found in transgenic mouse models of AD, it would thus also be of interest to test the expression of the Cas-proteins in AD mouse brain tissues in comparison to a wild-type control.

Furthermore, NEDD9 and CASS4 knockout (KO) murine models would also be a valid path of investigation. It has previously been shown that mice null for NEDD9 display dendritic spine loss in neurons (Knutson *et al*., 2016), yet astrocytes were not investigated in this study and no such model exists for CASS4. Gaining access to brain tissues from the NEDD9 KO model and, in the longer term, establishing a CASS4 KO model would

provide significant insight to how altered expression of the Cas-proteins affects astrocytes (and other neural cells) *in vivo*.

There is little knowledge on how atrophic astrocytes affect neurons. To determine this, growing co-cultures of primary neurons alongside astrocytes with altered NEDD9/CASS4 expression could give some insight and follow-up testing of neuron morphology and function may provide vital clues on synaptic loss in AD.

Finally, it would be of interest to investigate the large CASS4 (230 kDa) band seen in WB and to establish its binding partner. This could be undertaken via immunoprecipitation followed by mass spectrometry. This may not relate directly to AD, but may yield more knowledge of the Cas-protein individual function, which would ultimately aid the investigation of its role in LOAD.

If the role of NEDD9 and CASS4 in LOAD can be confirmed, it would be of interest to test various compounds which may reverse the phenotype caused by dysregulation (possibly downregulation) of the Cas- protein expression. Drugs, known to stabilise the cytoskeleton, such as Paclitaxel (used in cancer treatment), could also be administered to see if they might aid the reverse to a healthy astrocyte phenotype.

Collectively, there is a myriad of future work which could be conducted based on the findings in this thesis which might provide insight into not only the specific functions of the Cas-proteins in astrocytes but also their role in the development of LOAD. Several steps must be undertaken to determine their role and definite function, but once achieved, the Cas-proteins could deliver new therapeutic targets for the treatment of LOAD. Furthermore, if the proteins indeed play a role in astrocyte atrophy during the asymptomatic stages of AD, they could even deliver targets for preventative measures in the future.

9 Appendices

9.1 Appendix 1 – Exemplar western blot including loading controls
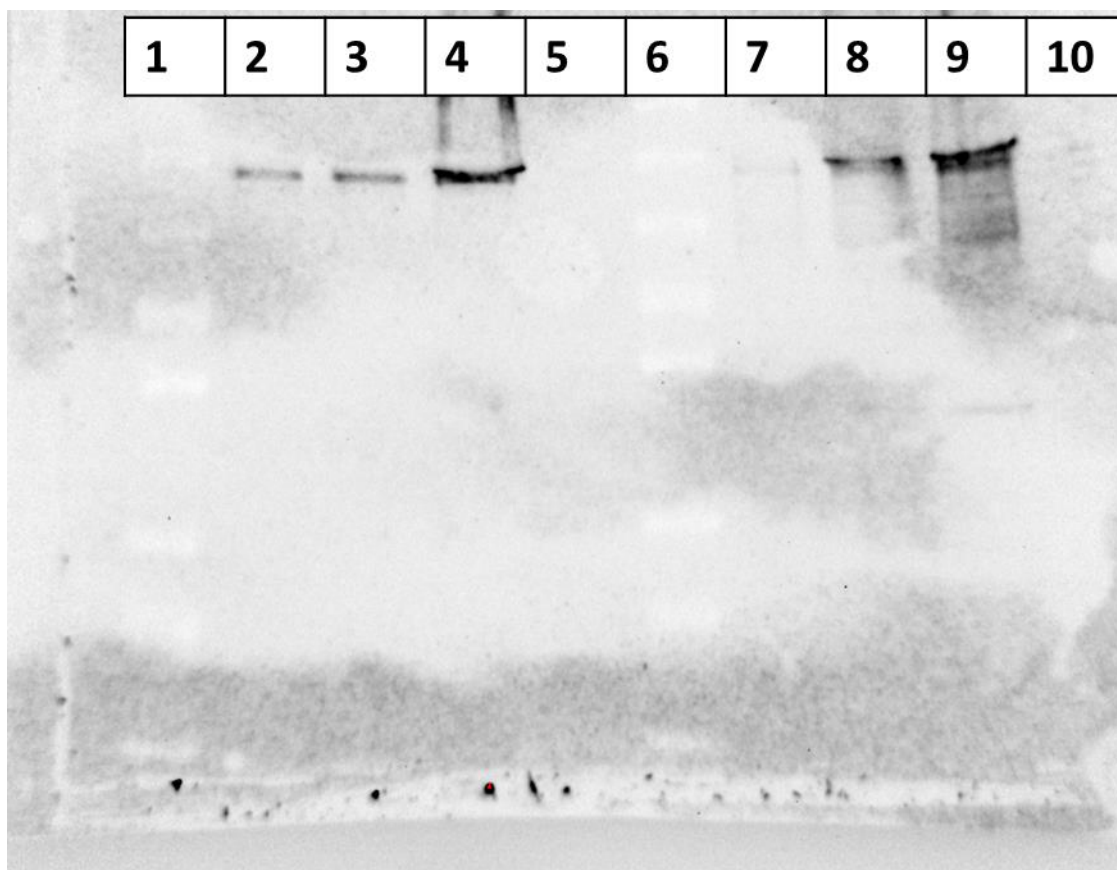
Figure 9.1 Exemplar western blot including lysis buffer controls

All ten lanes are shown. Lane 1, protein marker (ladder); Lane 2-4, NHA lysate; Lane 5 and 6, lysis and loading buffer only (RIPA); Lane 7-9, NHA lysate; Lane 10, loading buffer (Laemmli) only. Blot stained for CASS4, no visible staining in the lanes with lysis buffer or/and loading buffer.

References

10 References

ABRAMOV, A. Y., CANEVARI, L. & DUCHEN, M. R. 2003. Changes in intracellular calcium and glutathione in astrocytes as the primary mechanism of amyloid neurotoxicity. *J Neurosci,* 23**,** 5088-95.

ACAZ-FONSECA, E., ORTIZ-RODRIGUEZ, A., AZCOITIA, I., GARCIA-SEGURA, L. M. & AREVALO, M.-A. 2019. Notch signaling in astrocytes mediates their morphological response to an inflammatory challenge. *Cell Death Discovery,* 5, 85.

ALABDULLAH, A. A., AL-ABDULAZIZ, B., ALSALEM, H., MAGRASHI, A., PULICAT, S. M., ALMZROUA, A. A., ALMOHANNA, F., ASSIRI, A. M., AL TASSAN, N. A. & AL-MUBARAK, B. R. 2019. Estimating transfection efficiency in differentiated and undifferentiated neural cells. *BMC Res Notes,* 12**,** 225.

ALBERDI, E., WYSSENBACH, A., ALBERDI, M., SANCHEZ-GOMEZ, M. V., CAVALIERE, F., RODRIGUEZ, J. J., VERKHRATSKY, A. & MATUTE, C. 2013. Ca(2+) -dependent endoplasmic reticulum stress correlates with astrogliosis in oligomeric amyloid beta-treated astrocytes and in a model of Alzheimer's disease. *Aging Cell,* 12**,** 292-302.

ALBERINI, C. M., CRUZ, E., DESCALZI, G., BESSIERES, B. & GAO, V. 2018. Astrocyte glycogen and lactate: New insights into learning and memory mechanisms. *Glia,* 66**,** 1244-1262.

ALGE, C. S., HAUCK, S. M., PRIGLINGER, S. G., KAMPIK, A. & UEFFING, M. 2006. Differential protein profiling of primary versus immortalized human RPE cells identifies expression patterns associated with cytoskeletal remodeling and cell survival. *J Proteome Res,* 5**,** 862-78.

ALMEIDA, R. & ALLSHIRE, R. C. 2005. RNA silencing and genome regulation. *Trends Cell Biol,* 15**,** 251-8.

ALONSO, A. C., ZAIDI, T., GRUNDKE-IQBAL, I. & IQBAL, K. 1994. Role of abnormally phosphorylated tau in the breakdown of microtubules in Alzheimer disease. *Proceedings of the National Academy of Sciences, 91, 5562*.

ALTMAN, D. G. & BLAND, J. M. 2005. Standard deviations and standard errors. Bmj, 331, 903.

ALZHEIMER, A. 1910. *Beiträge zur Kenntnis der Pathologischen Neuroglia und ihrer Beziehungen zu den Abbauvorgängen im Nervengewebe*, G. Fischer.

ANTÚNEZ, C., BOADA, M., GONZÁLEZ-PÉREZ, A., GAYÁN, J., RAMÍREZ-LORCA, R., MARÍN, J., HERNÁNDEZ, I., MORENO-REY, C., MORÓN, F. J., LÓPEZ-ARRIETA, J., MAULEÓN, A., ROSENDE-ROCA, M., NOGUERA-PEREA, F., LEGAZ-GARCÍA, A., VIVANCOS-MOREAU, L., VELASCO, J., CARRASCO, J. M., ALEGRET, M., ANTEQUERA-TORRES, M., MANZANARES, S., ROMO, A., BLANCA, I., RUIZ, S., ESPINOSA, A., CASTAÑO, S., GARCÍA, B., MARTÍNEZ-HERRADA, B., VINYES, G., LAFUENTE, A., BECKER, J. T., GALÁN, J. J., SERRANO-RÍOS, M., ALZHEIMER'S DISEASE NEUROIMAGING, I., VÁZQUEZ, E., TÁRRAGA, L., SÁEZ, M. E., LÓPEZ, O. L., REAL, L. M. & RUIZ, A. 2011. The membrane-spanning 4-domains, subfamily A (MS4A) gene cluster contains a common variant associated with Alzheimer's disease. *Genome medicine,* 3**,** 33-33.

AQUINO, J. B., MARMIGERE, F., LALLEMEND, F., LUNDGREN, T. K., VILLAR, M. J., WEGNER, M. & ERNFORS, P. 2008. Differential expression and dynamic changes of murine NEDD9 in progenitor cells of diverse tissues. *Gene Expr Patterns,* 8**,** 217-26.

ARRIZA, J. L., FAIRMAN, W. A., WADICHE, J. I., MURDOCH, G. H., KAVANAUGH, M. P. & AMARA, S. G. 1994. Functional comparisons of three glutamate transporter subtypes cloned from human motor cortex. *J Neurosci,* 14**,** 5559-69.

ARZBERGER, T., KRAMPFL, K., LEIMGRUBER, S. & WEINDL, A. 1997. Changes of NMDA receptor subunit (NR1, NR2B) and glutamate transporter (GLT1) mRNA expression in Huntington's disease--an in situ hybridization study. *J Neuropathol Exp Neurol,* 56**,** 440-54.

BAGYINSZKY, E., YOUN, Y. C., AN, S. S. A. & KIM, S. 2016. Mutations, associated with early-onset Alzheimer's disease, discovered in Asian countries. *Clinical interventions in aging,* 11**,** 1467-1488.

BALDWIN, K. T. & EROGLU, C. 2018. Astrocytes "Chordinate" Synapse Maturation and Plasticity. *Neuron,* 100**,** 1010-1012.

BANCHER, C., BRUNNER, C., LASSMANN, H., BUDKA, H., JELLINGER, K., WICHE, G., SEITELBERGER, F., GRUNDKE-IQBAL, I., IQBAL, K. & WISNIEWSKI, H. M. 1989. Accumulation of abnormally phosphorylated tau precedes the formation of neurofibrillary tangles in Alzheimer's disease. *Brain Res,* 477, 90-9.

BARGON, S. D., GUNNING, P. W. & O'NEILL, G. M. 2005. The Cas family docking protein, HEF1, promotes the formation of neurite-like membrane extensions. *Biochim Biophys Acta,* 1746**,** 143-54.

BEAUQUIS, J., VINUESA, A., POMILIO, C., PAVIA, P., GALVAN, V. & SARAVIA, F. 2014. Neuronal and glial alterations, increased anxiety, and cognitive impairment before hippocampal amyloid deposition in PDAPP mice, model of Alzheimer's disease. *Hippocampus,* 24**,** 257-69.

BECK, T. N., NICOLAS, E., KOPP, M. C. & GOLEMIS, E. A. 2014. Adaptors for disorders of the brain? The cancer signaling proteins NEDD9, CASS4, and PTK2B in Alzheimer's disease. *Oncoscience,* 1**,** 486-503.

BEECHAM, G. W., HAMILTON, K., NAJ, A. C., MARTIN, E. R., HUENTELMAN, M., MYERS, A. J., CORNEVEAUX, J. J., HARDY, J., VONSATTEL, J.-P., YOUNKIN, S. G., BENNETT, D. A., DE JAGER, P. L., LARSON, E. B., CRANE, P. K., KAMBOH, M. I., KOFLER, J. K., MASH, D. C., DUQUE, L., GILBERT, J. R., GWIRTSMAN, H., BUXBAUM, J. D., KRAMER, P., DICKSON, D. W., FARRER, L. A., FROSCH, M. P., GHETTI, B., HAINES, J. L., HYMAN, B. T., KUKULL, W. A., MAYEUX, R. P., PERICAK-VANCE, M. A., SCHNEIDER, J. A., TROJANOWSKI, J. Q., REIMAN, E. M., ALZHEIMER'S DISEASE GENETICS, C., SCHELLENBERG, G. D. & MONTINE, T. J. 2014. Genome-wide association meta-analysis of neuropathologic features of Alzheimer's disease and related dementias. *PLoS genetics,* 10**,** e1004606-e1004606.

BEJANIN, A., SCHONHAUT, D. R., LA JOIE, R., KRAMER, J. H., BAKER, S. L., SOSA, N., AYAKTA, N., CANTWELL, A., JANABI, M., LAURIOLA, M., O'NEIL, J. P., GORNO-TEMPINI, M. L., MILLER, Z. A., ROSEN, H. J., MILLER, B. L., JAGUST, W. J. & RABINOVICI, G. D. 2017. Tau pathology and neurodegeneration contribute to cognitive impairment in Alzheimer's disease. *Brain,* 140**,** 3286-3300.

BENNINGER, F., GLAT, M. J., OFFEN, D. & STEINER, I. 2016. Glial fibrillary acidic protein as a marker of astrocytic activation in the cerebrospinal fluid of patients with amyotrophic lateral sclerosis. *Journal of Clinical Neuroscience,* 26**,** 75-78.

BERNARDINELLI, Y., MULLER, D. & NIKONENKO, I. 2014. Astrocyte-synapse structural plasticity. *Neural plasticity,* 2014**,** 232105-232105.

BERTRAM, L., LANGE, C., MULLIN, K., PARKINSON, M., HSIAO, M., HOGAN, M. F., SCHJEIDE, B. M., HOOLI, B., DIVITO, J., IONITA, I., JIANG, H., LAIRD, N., MOSCARILLO, T., OHLSEN, K. L., ELLIOTT, K., WANG, X., HU-LINCE, D., RYDER, M., MURPHY, A., WAGNER, S. L., BLACKER, D., BECKER, K. D. & TANZI, R. E. 2008. Genome-wide association analysis reveals putative Alzheimer's disease susceptibility loci in addition to APOE. *Am J Hum Genet,* 83**,** 623-32.

BOUCHET, B. P. & AKHMANOVA, A. 2017. Microtubules in 3D cell motility. *Journal of Cell Science,* 130**,** 39.

BRAAK, H. & BRAAK, E. 1991. Neuropathological stageing of Alzheimer-related changes. *Acta Neuropathol,* 82**,** 239-59.

BRAAK, H., BRAAK, E., BOHL, J. & LANG, W. 1989. Alzheimer's disease: amyloid plaques in the cerebellum. *J Neurol Sci,* 93**,** 277-87.

BRADSHAW, E. M., CHIBNIK, L. B., KEENAN, B. T., OTTOBONI, L., RAJ, T., TANG, A., ROSENKRANTZ, L. L., IMBOYWA, S., LEE, M., VON KORFF, A., MORRIS, M. C., EVANS, D. A., JOHNSON, K., SPERLING, R. A., SCHNEIDER, J. A., BENNETT, D. A. & DE JAGER, P. L. 2013. CD33 Alzheimer's disease locus: altered monocyte function and amyloid biology. *Nat Neurosci,* 16**,** 848-50.

BRADSHAW, L. N., ZHONG, J., BRADBURY, P., MAHMASSANI, M., SMITH, J. L., AMMIT, A. J. & O'NEILL, G. M. 2011. Estradiol stabilizes the 105-kDa phospho-form of the adhesion docking protein NEDD9 and suppresses NEDD9-dependent cell spreading in breast cancer cells. *Biochim Biophys Acta,* 1813**,** 340-5.

BRENNER, M. 1994. Structure and transcriptional regulation of the GFAP gene. *Brain Pathol,* 4**,** 245-57.

BRIKNAROVA, K., NASERTORABI, F., HAVERT, M. L., EGGLESTON, E., HOYT, D. W., LI, C., OLSON, A. J., VUORI, K. & ELY, K. R. 2005. The serine-rich domain from Crk-associated substrate (p130cas) is a four-helix bundle. *J Biol Chem,* 280**,** 21908-14.

BROZZI, F., ARCURI, C., GIAMBANCO, I. & DONATO, R. 2009. S100B Protein Regulates Astrocyte Shape and Migration via Interaction with Src Kinase: IMPLICATIONS FOR ASTROCYTE DEVELOPMENT, ACTIVATION, AND TUMOR GROWTH. *J Biol Chem,* 284**,** 8797-811.

BURNELL, S. E. A., SPENCER-HARTY, S., HOWARTH, S., BODGER, O., KYNASTON, H., MORGAN, C. & DOAK, S. H. 2018. STEAP2 Knockdown Reduces the Invasive Potential of Prostate Cancer Cells. *Scientific Reports*, 8, 6252.

BUSHONG, E. A., MARTONE, M. E. & ELLISMAN, M. H. 2004. Maturation of astrocyte morphology and the establishment of astrocyte domains during postnatal hippocampal development. *Int J Dev Neurosci,* 22**,** 73-86.

CAMPION, D., DUMANCHIN, C., HANNEQUIN, D., DUBOIS, B., BELLIARD, S., PUEL, M., THOMAS-ANTERION, C., MICHON, A., MARTIN, C., CHARBONNIER, F., RAUX, G., CAMUZAT, A., PENET, C., MESNAGE, V., MARTINEZ, M., CLERGET-DARPOUX, F., BRICE, A. & FREBOURG, T.

1999. Early-onset autosomal dominant Alzheimer disease: prevalence, genetic heterogeneity, and mutation spectrum. *Am J Hum Genet,* 65**,** 664-70.

CASLEY, C. S., LAKICS, V., LEE, H. G., BROAD, L. M., DAY, T. A., CLUETT, T., SMITH, M. A., O'NEILL, M. J. & KINGSTON, A. E. 2009. Up-regulation of astrocyte metabotropic glutamate receptor 5 by amyloid-beta peptide. *Brain Res,* 1260**,** 65-75.

CASSÉ, F., RICHETIN, K. & TONI, N. 2018. Astrocytes' Contribution to Adult Neurogenesis in Physiology and Alzheimer's Disease. *Frontiers in Cellular Neuroscience,* 12.

CASTELLO, M. A., JEPPSON, J. D. & SORIANO, S. 2014. Moving beyond anti-amyloid therapy for the prevention and treatment of Alzheimer's disease. *BMC Neurol,* 14**,** 169.

CHANG, J. X., GAO, F., ZHAO, G. Q. & ZHANG, G. J. 2012. Expression and clinical significance of NEDD9 in lung tissues. *Med Oncol,* 29**,** 2654-60.

CHAPUIS, J., HANSMANNEL, F., GISTELINCK, M., MOUNIER, A., VAN CAUWENBERGHE, C., KOLEN, K. V., GELLER, F., SOTTEJEAU, Y., HAROLD, D., DOURLEN, P., GRENIER-BOLEY, B., KAMATANI, Y., DELEPINE, B., DEMIAUTTE, F., ZELENIKA, D., ZOMMER, N., HAMDANE, M., BELLENGUEZ, C., DARTIGUES, J. F., HAUW, J. J., LETRONNE, F., AYRAL, A. M., SLEEGERS, K., SCHELLENS, A., BROECK, L. V., ENGELBORGHS, S., DE DEYN, P. P., VANDENBERGHE, R., O'DONOVAN, M., OWEN, M., EPELBAUM, J., MERCKEN, M., KARRAN, E., BANTSCHEFF, M., DREWES, G., JOBERTY, G., CAMPION, D., OCTAVE, J. N., BERR, C., LATHROP, M., CALLAERTS, P., MANN, D., WILLIAMS, J., BUEE, L., DEWACHTER, I., VAN BROECKHOVEN, C., AMOUYEL, P., MOECHARS, D., DERMAUT, B. & LAMBERT, J. C. 2013. Increased expression of BIN1 mediates Alzheimer genetic risk by modulating tau pathology. *Mol Psychiatry,* 18**,** 1225-34.

CHAPUIS, J., MOISAN, F., MELLICK, G., ELBAZ, A., SILBURN, P., PASQUIER, F., HANNEQUIN, D., LENDON, C., CAMPION, D., AMOUYEL, P. & LAMBERT, J.-C. 2008. Association study of the NEDD9 gene with the risk of developing Alzheimer's and Parkinson's disease. *Human Molecular Genetics,* 17**,** 2863-2867.

CHARTIER-HARLIN, M. C., PARFITT, M., LEGRAIN, S., PEREZ-TUR, J., BROUSSEAU, T., EVANS, A., BERR, C., VIDAL, O., ROQUES, P., GOURLET, V. & ET AL. 1994. Apolipoprotein E, epsilon 4 allele as a major risk factor for sporadic early and late-onset forms of Alzheimer's disease: analysis of the 19q13.2 chromosomal region. *Hum Mol Genet,* 3**,** 569-74.

CHAUDHRY, M., WANG, X., BAMNE, M. N., HASNAIN, S., DEMIRCI, F. Y., LOPEZ, O. L. & KAMBOH, M. I. 2015. Genetic variation in imprinted genes is associated with risk of late-onset Alzheimer's disease. *Journal of Alzheimer's disease* : JAD, 44, 989-994.

CHEN, G., CHEN, K. S., KNOX, J., INGLIS, J., BERNARD, A., MARTIN, S. J., JUSTICE, A., MCCONLOGUE, L., GAMES, D., FREEDMAN, S. B. & MORRIS, R. G. 2000. A learning deficit related to age and beta-amyloid plaques in a mouse model of Alzheimer's disease. *Nature,* 408**,** 975-9.

CHEN, H., WU, G., JIANG, Y., FENG, R., LIAO, M., ZHANG, L., MA, G., CHEN, Z., ZHAO, B., LI, K., YU, C. & LIU, G. 2015. Analyzing 54,936 Samples Supports the Association Between CD2AP rs9349407 Polymorphism and Alzheimer's Disease Susceptibility. *Mol Neurobiol,* 52**,** 1-7.

CHEUNG, G., SIBILLE, J., ZAPATA, J. & ROUACH, N. 2015. Activity-Dependent Plasticity of Astroglial Potassium and Glutamate Clearance. *Neural plasticity,* 2015**,** 109106-109106.

CLAVAGUERA, F., BOLMONT, T., CROWTHER, R. A., ABRAMOWSKI, D., FRANK, S., PROBST, A., FRASER, G., STALDER, A. K., BEIBEL, M., STAUFENBIEL, M., JUCKER, M., GOEDERT, M. & TOLNAY, M. 2009. Transmission and spreading of tauopathy in transgenic mouse brain. *Nat Cell Biol,* 11**,** 909-13.

COLANGELO, A. M., ALBERGHINA, L. & PAPA, M. 2014. Astrogliosis as a therapeutic target for neurodegenerative diseases. *Neuroscience Letters,* 565**,** 59-64.

CORDER, E. H., SAUNDERS, A. M., STRITTMATTER, W. J., SCHMECHEL, D. E., GASKELL, P. C., SMALL, G. W., ROSES, A. D., HAINES, J. L. & PERICAK-VANCE, M. A. 1993. Gene dose of apolipoprotein E type 4 allele and the risk of Alzheimer's disease in late onset families. *Science,* 261**,** 921-3.

CRUCHAGA, C., KARCH, C. M., JIN, S. C., BENITEZ, B. A., CAI, Y., GUERREIRO, R., HARARI, O., NORTON, J., BUDDE, J., BERTELSEN, S., JENG, A. T., COOPER, B., SKORUPA, T., CARRELL, D., LEVITCH, D., HSU, S., CHOI, J., RYTEN, M., SASSI, C., BRAS, J., GIBBS, R. J., HERNANDEZ, D. G., LUPTON, M. K., POWELL, J., FORABOSCO, P., RIDGE, P. G., CORCORAN, C. D., TSCHANZ, J. T., NORTON, M. C., MUNGER, R. G., SCHMUTZ, C., LEARY, M., DEMIRCI, F. Y., BAMNE, M. N., WANG, X., LOPEZ, O. L., GANGULI, M., MEDWAY, C., TURTON, J., LORD, J., BRAAE, A., BARBER, I., BROWN, K., PASTOR, P., LORENZO-BETANCOR, O., BRKANAC, Z., SCOTT, E., TOPOL, E., MORGAN, K., ROGAEVA, E., SINGLETON, A., HARDY, J., KAMBOH, M. I., GEORGE-HYSLOP, P. S., CAIRNS, N., MORRIS, J. C., KAUWE, J. S. K. & GOATE, A. M. 2014. Rare coding variants in the phospholipase D3 gene confer risk for Alzheimer's disease. *Nature,* 505**,** 550-554.

DADKE, D., JARNIK, M., PUGACHEVA, E. N., SINGH, M. K. & GOLEMIS, E. A. 2006. Deregulation of HEF1 impairs M-phase progression by disrupting the RhoA activation cycle. *Mol Biol Cell,* 17**,** 1204-17.

DAVIS, D. G., SCHMITT, F. A., WEKSTEIN, D. R. & MARKESBERY, W. R. 1999. Alzheimer neuropathologic alterations in aged cognitively normal subjects. *J Neuropathol Exp Neurol,* 58**,** 376-88.

DELOULME, J. C., RAPONI, E., GENTIL, B. J., BERTACCHI, N., MARKS, A., LABOURDETTE, G. & BAUDIER, J. 2004. Nuclear expression of S100B in oligodendrocyte progenitor cells correlates with differentiation toward the oligodendroglial lineage and modulates oligodendrocytes maturation. *Mol Cell Neurosci,* 27**,** 453-65.

DENEKA, A., KOROBEYNIKOV, V. & GOLEMIS, E. A. 2015. Embryonal Fyn-associated substrate (EFS) and CASS4: The lesser-known CAS protein family members. *Gene,* 570**,** 25-35.

DENG, B., SUN, Z., JASON, W. & YANG, P. 2013. Increased BCAR1 predicts poor outcomes of non-small cell lung cancer in multiple-center patients. *Ann Surg Oncol,* 20 Suppl 3**,** S701-8.

DENT, E. W. 2017. Of microtubules and memory: implications for microtubule dynamics in dendrites and spines. *Molecular biology of the cell,* 28**,** 1-8.

DINIZ, L. P., TORTELLI, V., MATIAS, I., MORGADO, J., BERGAMO ARAUJO, A. P., MELO, H. M., SEIXAS DA SILVA, G. S., ALVES-LEON, S. V., DE

SOUZA, J. M., FERREIRA, S. T., DE FELICE, F. G. & GOMES, F. C. A. 2017. Astrocyte Transforming Growth Factor Beta 1 Protects Synapses against Abeta Oligomers in Alzheimer's Disease Model. *J Neurosci, 37,* 6797-6809.

DONATO, R., CANNON, B. R., SORCI, G., RIUZZI, F., HSU, K., WEBER, D. J. & GECZY, C. L. 2013. Functions of S100 proteins. *Current molecular medicine, 13,* 24-57.

DOSSI, E., VASILE, F. & ROUACH, N. 2018. Human astrocytes in the diseased brain. *Brain Research Bulletin, 136,* 139-156.

DOURLEN, P., FERNANDEZ-GOMEZ, F. J., DUPONT, C., GRENIER-BOLEY, B., BELLENGUEZ, C., OBRIOT, H., CAILLIEREZ, R., SOTTEJEAU, Y., CHAPUIS, J., BRETTEVILLE, A., ABDELFETTAH, F., DELAY, C., MALMANCHE, N., SOININEN, H., HILTUNEN, M., GALAS, M. C., AMOUYEL, P., SERGEANT, N., BUÉE, L., LAMBERT, J. C. & DERMAUT, B. 2016. Functional screening of Alzheimer risk loci identifies PTK2B as an in vivo modulator and early marker of Tau pathology. *Molecular Psychiatry, 22,* 874.

ELLENBROEK, S. I., IDEN, S. & COLLARD, J. G. 2012. The Rac activator Tiam1 is required for polarized protrusional outgrowth of primary astrocytes by affecting the organization of the microtubule network. *Small GTPases, 3,* 4-14.

ERUSTES, A. G., STEFANI, F. Y., TERASHIMA, J. Y., STILHANO, R. S., MONTEFORTE, P. T., DA SILVA PEREIRA, G. J., HAN, S. W., CALGAROTTO, A. K., HSU, Y.-T., URESHINO, R. P., BINCOLETTO, C. & SMAILI, S. S. 2018. Overexpression of α-synuclein in an astrocyte cell line promotes autophagy inhibition and apoptosis. *Journal of Neuroscience Research, 96,* 160-171.

ETIENNE-MANNEVILLE, S. 2013. Microtubules in cell migration. *Annu Rev Cell Dev Biol, 29,* 471-99.

ETIENNE-MANNEVILLE, S. & HALL, A. 2001. Integrin-mediated activation of Cdc42 controls cell polarity in migrating astrocytes through PKCzeta. *Cell, 106,* 489-98.

FAGAN, A. M., MINTUN, M. A., SHAH, A. R., ALDEA, P., ROE, C. M., MACH, R. H., MARCUS, D., MORRIS, J. C. & HOLTZMAN, D. M. 2009. Cerebrospinal fluid tau and ptau(181) increase with cortical amyloid deposition in cognitively normal individuals: implications for future clinical trials of Alzheimer's disease. *EMBO Mol Med, 1,* 371-80.

FASHENA, S. J., EINARSON, M. B., O'NEILL, G. M., PATRIOTIS, C. & GOLEMIS, E. A. 2002. Dissection of HEF1-dependent functions in motility and transcriptional regulation. *J Cell Sci, 115,* 99-111.

FEIGIN , N. E., ALAM T, BANNICK MS, BEGHI E, BLAKE N, CULPEPPER WJ, DORSEY ER, ELBAZ A, ELLENBOGEN RG, FISHER JL, FITZMAURICE C, GIUSSANI G, GLENNIE L, JAMES SL, JOHNSON CO, KASSEBAUM NJ, LOGROSCINO G, MARIN B, MOUNTJOY-VENNING WC, NGUYEN M, OFORI-ASENSO R, PATEL AP, PICCININNI M, ROTH GA, STEINER TJ, STOVNER LJ, SZOEKE CEI, THEADOM A, VOLLSET SE, WALLIN MT, WRIGHT C, ZUNT JR, ABBASI N, ABD-ALLAH F, ABDELALIM A, ABDOLLAHPOUR I, ABOYANS V, ABRAHA HN, ACHARYA D, ADAMU AA, ADEBAYO OM, ADEOYE AM, ADSUAR JC, AFARIDEH M, AGRAWAL S, AHMADI A, AHMED MB, AICHOUR AN, AICHOUR I, AICHOUR MTE, AKINYEMI RO, AKSEER N, AL-EYADHY A, AL-SHAHI SALMAN R, ALAHDAB F, ALENE KA, ALJUNID SM, ALTIRKAWI K, ALVIS-GUZMAN N, ANBER NH, ANTONIO CAT, ARABLOO J, AREMU O,

ÄRNLÖV J, ASAYESH H, ASGHAR RJ, ATALAY HT, AWASTHI A, AYALA QUINTANILLA BP, AYUK TB, BADAWI A, BANACH M, BANOUB JAM, BARBOZA MA, BARKER-COLLO SL, BÄRNIGHAUSEN TW, BAUNE BT, BEDI N, BEHZADIFAR M, BEHZADIFAR M, BÉJOT Y, BEKELE BB, BELACHEW AB, BENNETT DA, BENSENOR IM, BERHANE A, BEURAN M, BHATTACHARYYA K, BHUTTA ZA, BIADGO B, BIJANI A, BILILIGN N, BIN SAYEED MS, BLAZES CK, BRAYNE C, BUTT ZA, CAMPOS-NONATO IR, CANTU-BRITO C, CAR M, CÁRDENAS R, CARRERO JJ, CARVALHO F, CASTAÑEDA-ORJUELA CA, CASTRO F, CATALÁ-LÓPEZ F, CERIN E, CHAIAH Y, CHANG JC, CHATZIRALLI I, CHIANG PP, CHRISTENSEN H, CHRISTOPHER DJ, COOPER C, CORTESI PA, COSTA VM, CRIQUI MH, CROWE CS, DAMASCENO AAM, DARYANI A, DE LA CRUZ-GÓNGORA V, DE LA HOZ FP, DE LEO D, DEMOZ GT, DERIBE K, DHARMARATNE SD, DIAZ D, DINBERU MT, DJALALINIA S, DOKU DT, DUBEY M, DUBLJANIN E, DUKEN EE, EDVARDSSON D, EL-KHATIB Z, ENDRES M, ENDRIES AY, ESKANDARIEH S, ESTEGHAMATI A, ESTEGHAMATI S, FARHADI F, FARO A, FARZADFAR F, FARZAEI MH, FATIMA B, FERESHTEHNEJAD SM, FERNANDES E, FEYISSA GT, FILIP I, FISCHER F, FUKUMOTO T, GANJI M, GANKPE FG, GARCIA-GORDILLO MA, GEBRE AK, GEBREMICHAEL TG, GELAW BK, GELEIJNSE JM, GEREMEW D, GEZAE KE, GHASEMI-KASMAN M, GIDEY MY, GILL PS, GILL TK, GIRMA ET, GNEDOVSKAYA EV, GOULART AC, GRADA A, GROSSO G, GUO Y, GUPTA R, GUPTA R, HAAGSMA JA, HAGOS TB, HAJ-MIRZAIAN A, HAJ-MIRZAIAN A, HAMADEH RR, HAMIDI S, HANKEY GJ, HAO Y, HARO JM, HASSANKHANI H, HASSEN HY, HAVMOELLER R, HAY SI, HEGAZY MI, HEIDARI B, HENOK A, HEYDARPOUR F, HOANG CL, HOLE MK, HOMAIE RAD E, HOSSEINI SM, HU G, IGUMBOR EU, ILESANMI OS, IRVANI SSN, ISLAM SMS, JAKOVLJEVIC M, JAVANBAKHT M, JHA RP, JOBANPUTRA YB, JONAS JB, JOZWIAK JJ, JÜRISSON M, KAHSAY A, KALANI R, KALKONDE Y, KAMIL TA, KANCHAN T, KARAMI M, KARCH A, KARIMI N, KASAEIAN A, KASSA TD, KASSA ZY, KAUL A, KEFALE AT, KEIYORO PN, KHADER YS, KHAFAIE MA, KHALIL IA, KHAN EA, KHANG YH, KHAZAIE H, KIADALIRI AA, KIIRITHIO DN, KIM AS, KIM D, KIM YE, KIM YJ, KISA A, KOKUBO Y, KOYANAGI A, KRISHNAMURTHI RV, KUATE DEFO B, KUCUK BICER B, KUMAR M, LACEY B, LAFRANCONI A, LANSINGH VC, LATIFI A, LESHARGIE CT, LI S, LIAO Y, LINN S, LO WD, LOPEZ JCF, LORKOWSKI S, LOTUFO PA, LUCAS RM, LUNEVICIUS R, MACKAY MT, MAHOTRA NB, MAJDAN M, MAJDZADEH R, MAJEED A, MALEKZADEH R, MALTA DC, MANAFI N, MANSOURNIA MA, MANTOVANI LG, MÄRZ W, MASHAMBA-THOMPSON TP, MASSENBURG BB, MATE KKV, MCALINDEN C, MCGRATH JJ, MEHTA V, MEIER T, MELES HG, MELESE A, MEMIAH PTN, MEMISH ZA, MENDOZA W, MENGISTU DT, MENGISTU G, MERETOJA A, MERETOJA TJ, MESTROVIC T, MIAZGOWSKI B, MIAZGOWSKI T, MILLER TR, MINI GK, MIRRAKHIMOV EM, MOAZEN B, MOHAJER B, MOHAMMAD GHOLI MEZERJI N, MOHAMMADI M, MOHAMMADI-KHANAPOSHTANI M, MOHAMMADIBAKHSH R, MOHAMMADNIA-AFROUZI M, MOHAMMED S, MOHEBI F, MOKDAD AH, MONASTA L, MONDELLO S, MOODLEY Y, MOOSAZADEH M,

MORADI G, MORADI-LAKEH M, MORADINAZAR M, MORAGA P, MORENO VELÁSQUEZ I, MORRISON SD, MOUSAVI SM, MUHAMMED OS, MURUET W, MUSA KI, MUSTAFA G, NADERI M, NAGEL G, NAHEED A, NAIK G, NAJAFI F, NANGIA V, NEGOI I, NEGOI RI, NEWTON CRJ, NGUNJIRI JW, NGUYEN CT, NGUYEN LH, NINGRUM DNA, NIRAYO YL, NIXON MR, NORRVING B, NOUBIAP JJ, NOUROLLAHPOUR SHIADEH M, NYASULU PS, OGAH OS, OH IH, OLAGUNJU AT, OLAGUNJU TO, OLIVARES PR, ONWUJEKWE OE, OREN E, OWOLABI MO, PA M, PAKPOUR AH, PAN WH, PANDA-JONAS S, PANDIAN JD, PATEL SK, PEREIRA DM, PETZOLD M, PILLAY JD, PIRADOV MA, POLANCZYK GV, POLINDER S, POSTMA MJ, POULTON R, POUSTCHI H, PRAKASH S, PRAKASH V, QORBANI M, RADFAR A, RAFAY A, RAFIEI A, RAHIM F, RAHIMI-MOVAGHAR V, RAHMAN M, RAHMAN MHU, RAHMAN MA, RAJATI F, RAM U, RANTA A, RAWAF DL, RAWAF S, REINIG N, REIS C, RENZAHO AMN, RESNIKOFF S, REZAEIAN S, REZAI MS, RIOS GONZÁLEZ CM, ROBERTS NLS, ROEVER L, RONFANI L, RORO EM, ROSHANDEL G, ROSTAMI A, SABBAGH P, SACCO RL, SACHDEV PS, SADDIK B, SAFARI H, SAFARI-FARAMANI R, SAFI S, SAFIRI S, SAGAR R, SAHATHEVAN R, SAHEBKAR A, SAHRAIAN MA, SALAMATI P, SALEHI ZAHABI S, SALIMI Y, SAMY AM, SANABRIA J, SANTOS IS, SANTRIC MILICEVIC MM, SARRAFZADEGAN N, SARTORIUS B, SARVI S, SATHIAN B, SATPATHY M, SAWANT AR, SAWHNEY M, SCHNEIDER IJC, SCHÖTTKER B, SCHWEBEL DC, SEEDAT S, SEPANLOU SG, SHABANINEJAD H, SHAFIEESABET A, SHAIKH MA, SHAKIR RA, SHAMS-BEYRANVAND M, SHAMSIZADEH M, SHARIF M, SHARIF-ALHOSEINI M, SHE J, SHEIKH A, SHETH KN, SHIGEMATSU M, SHIRI R, SHIRKOOHI R, SHIUE I, SIABANI S, SIDDIQI TJ, SIGFUSDOTTIR ID, SIGURVINSDOTTIR R, SILBERBERG DH, SILVA JP, SILVEIRA DGA, SINGH JA, SINHA DN, SKIADARESI E, SMITH M, SOBAIH BH, SOBHANI S, SOOFI M, SOYIRI IN, SPOSATO LA, STEIN DJ, STEIN MB, STOKES MA, SUFIYAN MB, SYKES BL, SYLAJA PN, TABARÉS-SEISDEDOS R, TE AO BJ, TEHRANI-BANIHASHEMI A, TEMSAH MH, TEMSAH O, THAKUR JS, THRIFT AG, TOPOR-MADRY R, TORTAJADA-GIRBÉS M, TOVANI-PALONE MR, TRAN BX, TRAN KB, TRUELSEN TC, TSADIK AG, TUDOR CAR L, UKWAJA KN, ULLAH I, USMAN MS, UTHMAN OA, VALDEZ PR, VASANKARI TJ, VASANTHAN R, VEISANI Y, VENKETASUBRAMANIAN N, VIOLANTE FS, VLASSOV V, VOSOUGHI K, VU GT, VUJCIC IS, WAGNEW FS, WAHEED Y, WANG YP, WEIDERPASS E, WEISS J, WHITEFORD HA, WIJERATNE T, WINKLER AS, WIYSONGE CS, WOLFE CDA, XU G, YADOLLAHPOUR A, YAMADA T, YANO Y, YASERI M, YATSUYA H, YIMER EM, YIP P, YISMA E, YONEMOTO N, YOUSEFIFARD M, YU C, ZAIDI Z, ZAMAN SB, ZAMANI M, ZANDIAN H, ZARE Z, ZHANG Y, ZODPEY S, NAGHAVI M, MURRAY CJL, VOS T 2019. Global, regional, and national burden of neurological disorders, 1990-2016: a systematic analysis for the Global Burden of Disease Study 2016. *Lancet Neurol,* 18**,** 459-480.

FENG, J., ZHAO, J., XIE, H., YIN, Y., LUO, G., ZHANG, J., FENG, Y. & LI, Z. 2015. Involvement of NEDD9 in the invasion and migration of gastric cancer. *Tumour Biol,* 36**,** 3621-8.

FIELDS, R. D., WOO, D. H. & BASSER, P. J. 2015. Glial Regulation of the Neuronal Connectome through Local and Long-Distant Communication. *Neuron,* 86**,** 374-86.

FU, Y., HE, F., TANG, N. L., TAM, C. W., LUI, V. W., CHIU, H. F. & LAM, L. C. 2012. NEDD9 gene polymorphism influences the risk of Alzheimer disease and cognitive function in Chinese older persons. *Alzheimer Dis Assoc Disord,* 26**,** 88-90.

GABBASOV, R., XIAO, F., HOWE, C. G., BICKEL, L. E., O'BRIEN, S. W., BENRUBI, D., DO, T. V., ZHOU, Y., NICOLAS, E., CAI, K. Q., LITWIN, S., SEO, S., GOLEMIS, E. A. & CONNOLLY, D. C. 2018. NEDD9 promotes oncogenic signaling, a stem/mesenchymal gene signature, and aggressive ovarian cancer growth in mice. *Oncogene,* 37**,** 4854-4870.

GAN, K. A., CARRASCO PRO, S., SEWELL, J. A. & FUXMAN BASS, J. I. 2018. Identification of Single Nucleotide Non-coding Driver Mutations in Cancer. *Frontiers in Genetics,* 9.

GANDY, S., SIMON, A. J., STEELE, J. W., LUBLIN, A. L., LAH, J. J., WALKER, L. C., LEVEY, A. I., KRAFFT, G. A., LEVY, E., CHECLER, F., GLABE, C., BILKER, W. B., ABEL, T., SCHMEIDLER, J. & EHRLICH, M. E. 2010. Days to criterion as an indicator of toxicity associated with human Alzheimer amyloid-beta oligomers. *Ann Neurol,* 68**,** 220-30.

GARCIA-ESPARCIA, P., DIAZ-LUCENA, D., AINCIBURU, M., TORREJÓN-ESCRIBANO, B., CARMONA, M., LLORENS, F. & FERRER, I. 2018. Glutamate Transporter GLT1 Expression in Alzheimer Disease and Dementia With Lewy Bodies. *Frontiers in Aging Neuroscience,* 10.

GLENNER, G. G., WONG, C. W., QUARANTA, V. & EANES, E. D. 1984. The amyloid deposits in Alzheimer's disease: their nature and pathogenesis. *Appl Pathol,* 2**,** 357-69.

GOEDERT, M. & SPILLANTINI, M. G. 2017. Propagation of Tau aggregates. *Mol Brain,* 10**,** 18.

GÖTZ, J., HALLIDAY, G. & NISBET, R. M. 2019. Molecular Pathogenesis of the Tauopathies. *Annual Review of Pathology: Mechanisms of Disease,* 14, 239-261.

GOLDE, T. E., SCHNEIDER, L. S. & KOO, E. H. 2011. Anti-abeta therapeutics in Alzheimer's disease: the need for a paradigm shift. *Neuron,* 69**,** 203-13.

GONZÁLEZ-REYES, R. E., NAVA-MESA, M. O., VARGAS-SÁNCHEZ, K., ARIZA-SALAMANCA, D. & MORA-MUÑOZ, L. 2017. Involvement of Astrocytes in Alzheimer's Disease from a Neuroinflammatory and Oxidative Stress Perspective. *Frontiers in molecular neuroscience,* 10**,** 427-427.

GREENBAUM, D., COLANGELO, C., WILLIAMS, K. & GERSTEIN, M. 2003. Comparing protein abundance and mRNA expression levels on a genomic scale. *Genome biology,* 4**,** 117-117.

GRESCH, O. & ALTROGGE, L. 2012. Transfection of difficult-to-transfect primary mammalian cells. *Methods Mol Biol,* 801**,** 65-74.

GROLLA, A. A., SIM, J. A., LIM, D., RODRIGUEZ, J. J., GENAZZANI, A. A. & VERKHRATSKY, A. 2013. Amyloid-beta and Alzheimer's disease type pathology differentially affects the calcium signalling toolkit in astrocytes from different brain regions. *Cell Death Dis,* 4**,** e623.

HAASS, C. & SELKOE, D. J. 2007. Soluble protein oligomers in neurodegeneration: lessons from the Alzheimer's amyloid beta-peptide. *Nat Rev Mol Cell Biol,* 8**,** 101-12.

HAMA, H., HARA, C., YAMAGUCHI, K. & MIYAWAKI, A. 2004. PKC signaling mediates global enhancement of excitatory synaptogenesis in neurons triggered by local contact with astrocytes. *Neuron,* 41**,** 405-15.

HANGER, D. P., BRION, J. P., GALLO, J. M., CAIRNS, N. J., LUTHERT, P. J. & ANDERTON, B. H. 1991. Tau in Alzheimer's disease and Down's syndrome is insoluble and abnormally phosphorylated. *Biochem J,* 275 (Pt 1), 99-104.

HARDY, J. & ALLSOP, D. 1991. Amyloid deposition as the central event in the aetiology of Alzheimer's disease. *Trends Pharmacol Sci,* 12**,** 383-8.

HARDY, J. & SELKOE, D. J. 2002. The amyloid hypothesis of Alzheimer's disease: progress and problems on the road to therapeutics. *Science,* 297**,** 353-6.

HAROLD, D., ABRAHAM, R., HOLLINGWORTH, P., SIMS, R., GERRISH, A., HAMSHERE, M. L., PAHWA, J. S., MOSKVINA, V., DOWZELL, K., WILLIAMS, A., JONES, N., THOMAS, C., STRETTON, A., MORGAN, A. R., LOVESTONE, S., POWELL, J., PROITSI, P., LUPTON, M. K., BRAYNE, C., RUBINSZTEIN, D. C., GILL, M., LAWLOR, B., LYNCH, A., MORGAN, K., BROWN, K. S., PASSMORE, P. A., CRAIG, D., MCGUINNESS, B., TODD, S., HOLMES, C., MANN, D., SMITH, A. D., LOVE, S., KEHOE, P. G., HARDY, J., MEAD, S., FOX, N., ROSSOR, M., COLLINGE, J., MAIER, W., JESSEN, F., SCHURMANN, B., HEUN, R., VAN DEN BUSSCHE, H., HEUSER, I., KORNHUBER, J., WILTFANG, J., DICHGANS, M., FROLICH, L., HAMPEL, H., HULL, M., RUJESCU, D., GOATE, A. M., KAUWE, J. S., CRUCHAGA, C., NOWOTNY, P., MORRIS, J. C., MAYO, K., SLEEGERS, K., BETTENS, K., ENGELBORGHS, S., DE DEYN, P. P., VAN BROECKHOVEN, C., LIVINGSTON, G., BASS, N. J., GURLING, H., MCQUILLIN, A., GWILLIAM, R., DELOUKAS, P., AL-CHALABI, A., SHAW, C. E., TSOLAKI, M., SINGLETON, A. B., GUERREIRO, R., MUHLEISEN, T. W., NOTHEN, M. M., MOEBUS, S., JOCKEL, K. H., KLOPP, N., WICHMANN, H. E., CARRASQUILLO, M. M., PANKRATZ, V. S., YOUNKIN, S. G., HOLMANS, P. A., O'DONOVAN, M., OWEN, M. J. & WILLIAMS, J. 2009. Genome-wide association study identifies variants at CLU and PICALM associated with Alzheimer's disease. *Nat Genet,* 41**,** 1088-93.

HASELEU, J., ANLAUF, E., BLAESS, S., ENDL, E. & DEROUICHE, A. 2013. Studying subcellular detail in fixed astrocytes: dissociation of morphologically intact glial cells (DIMIGs). *Frontiers in Cellular Neuroscience,* 7.

HASSAN, M., SHAHZADI, S., ALASHWAL, H., ZAKI, N., SEO, S. Y. & MOUSTAFA, A. A. 2018. Exploring the mechanistic insights of Cas scaffolding protein family member 4 with protein tyrosine kinase 2 in Alzheimer's disease by evaluating protein interactions through molecular docking and dynamic simulations. *Neurol Sci,* 39**,** 1361-1374.

HATTERMANN, K., FLUH, C., ENGEL, D., MEHDORN, H. M., SYNOWITZ, M., MENTLEIN, R. & HELD-FEINDT, J. 2016. Stem cell markers in glioma progression and recurrence. *Int J Oncol,* 49**,** 1899-1910.

HAYFLICK, L. 1979. The cell biology of aging. *J Invest Dermatol,* 73**,** 8-14.

HELLER, J. P. & RUSAKOV, D. A. 2015. Morphological plasticity of astroglia: Understanding synaptic microenvironment. *Glia,* 63**,** 2133-51.

HENNEBERGER, C., PAPOUIN, T., OLIET, S. H. & RUSAKOV, D. A. 2010. Long-term potentiation depends on release of D-serine from astrocytes. *Nature,* 463**,** 232-6.

HERTZ, L. 2013. The Glutamate-Glutamine (GABA) Cycle: Importance of Late Postnatal Development and Potential Reciprocal Interactions between Biosynthesis and Degradation. *Front Endocrinol (Lausanne),* 4**,** 59.

HIMMELSTEIN, D. S., WARD, S. M., LANCIA, J. K., PATTERSON, K. R. & BINDER, L. I. 2012. Tau as a therapeutic target in neurodegenerative disease. *Pharmacology & therapeutics,* 136**,** 8-22.

HOL, E. M. & PEKNY, M. 2015. Glial fibrillary acidic protein (GFAP) and the astrocyte intermediate filament system in diseases of the central nervous system. *Curr Opin Cell Biol,* 32**,** 121-30.

HOLLINGWORTH, P., HAROLD, D., SIMS, R., GERRISH, A., LAMBERT, J. C., CARRASQUILLO, M. M., ABRAHAM, R., HAMSHERE, M. L., PAHWA, J. S., MOSKVINA, V., DOWZELL, K., JONES, N., STRETTON, A., THOMAS, C., RICHARDS, A., IVANOV, D., WIDDOWSON, C., CHAPMAN, J., LOVESTONE, S., POWELL, J., PROITSI, P., LUPTON, M. K., BRAYNE, C., RUBINSZTEIN, D. C., GILL, M., LAWLOR, B., LYNCH, A., BROWN, K. S., PASSMORE, P. A., CRAIG, D., MCGUINNESS, B., TODD, S., HOLMES, C., MANN, D., SMITH, A. D., BEAUMONT, H., WARDEN, D., WILCOCK, G., LOVE, S., KEHOE, P. G., HOOPER, N. M., VARDY, E. R., HARDY, J., MEAD, S., FOX, N. C., ROSSOR, M., COLLINGE, J., MAIER, W., JESSEN, F., RUTHER, E., SCHURMANN, B., HEUN, R., KOLSCH, H., VAN DEN BUSSCHE, H., HEUSER, I., KORNHUBER, J., WILTFANG, J., DICHGANS, M., FROLICH, L., HAMPEL, H., GALLACHER, J., HULL, M., RUJESCU, D., GIEGLING, I., GOATE, A. M., KAUWE, J. S., CRUCHAGA, C., NOWOTNY, P., MORRIS, J. C., MAYO, K., SLEEGERS, K., BETTENS, K., ENGELBORGHS, S., DE DEYN, P. P., VAN BROECKHOVEN, C., LIVINGSTON, G., BASS, N. J., GURLING, H., MCQUILLIN, A., GWILLIAM, R., DELOUKAS, P., AL-CHALABI, A., SHAW, C. E., TSOLAKI, M., SINGLETON, A. B., GUERREIRO, R., MUHLEISEN, T. W., NOTHEN, M. M., MOEBUS, S., JOCKEL, K. H., KLOPP, N., WICHMANN, H. E., PANKRATZ, V. S., SANDO, S. B., AASLY, J. O., BARCIKOWSKA, M., WSZOLEK, Z. K., DICKSON, D. W., GRAFF-RADFORD, N. R., PETERSEN, R. C., et al. 2011. Common variants at ABCA7, MS4A6A/MS4A4E, EPHA1, CD33 and CD2AP are associated with Alzheimer's disease. *Nat Genet,* 43**,** 429-35.

HOLMBERG, J., HE, X., PEREDO, I., ORREGO, A., HESSELAGER, G., ERICSSON, C., HOVATTA, O., OBA-SHINJO, S. M., MARIE, S. K., NISTER, M. & MUHR, J. 2011. Activation of neural and pluripotent stem cell signatures correlates with increased malignancy in human glioma. *PLoS One,* 6**,** e18454.

HOLMSETH, S., SCOTT, H. A., REAL, K., LEHRE, K. P., LEERGAARD, T. B., BJAALIE, J. G. & DANBOLT, N. C. 2009. The concentrations and distributions of three C-terminal variants of the GLT1 (EAAT2; slc1a2) glutamate transporter protein in rat brain tissue suggest differential regulation. *Neuroscience,* 162**,** 1055-71.

HOLTZMAN, D. M., MORRIS, J. C. & GOATE, A. M. 2011. Alzheimer's disease: the challenge of the second century. *Sci Transl Med,* 3**,** 77sr1.

HSIAO, K., CHAPMAN, P., NILSEN, S., ECKMAN, C., HARIGAYA, Y., YOUNKIN, S., YANG, F. & COLE, G. 1996. Correlative memory deficits, Abeta elevation, and amyloid plaques in transgenic mice. *Science,* 274**,** 99-102.

HUANG, W., QIU, C., VON STRAUSS, E., WINBLAD, B. & FRATIGLIONI, L. 2004. APOE Genotype, Family History of Dementia, and Alzheimer Disease Risk: A 6-Year Follow-up Study. *JAMA Neurology,* 61**,** 1930-1934.

HUGHES, E. G., MAGUIRE, J. L., MCMINN, M. T., SCHOLZ, R. E. & SUTHERLAND, M. L. 2004. Loss of glial fibrillary acidic protein results in decreased glutamate transport and inhibition of PKA-induced EAAT2 cell surface trafficking. *Brain Res Mol Brain Res,* 124**,** 114-23.

IADECOLA, C. & NEDERGAARD, M. 2007. Glial regulation of the cerebral microvasculature. *Nat Neurosci,* 10**,** 1369-76.

ICE, R. J., MCLAUGHLIN, S. L., LIVENGOOD, R. H., CULP, M. V., EDDY, E. R., IVANOV, A. V. & PUGACHEVA, E. N. 2013. NEDD9 depletion destabilizes Aurora A kinase and heightens the efficacy of Aurora A inhibitors: implications for treatment of metastatic solid tumors. *Cancer research,* 73**,** 3168-3180.

ISHII, T., UEYAMA, T., SHIGYO, M., KOHTA, M., KONDOH, T., KUBOYAMA, T., UEBI, T., HAMADA, T., GUTMANN, D. H., AIBA, A., KOHMURA, E., TOHDA, C. & SAITO, N. 2017. A Novel Rac1-GSPT1 Signaling Pathway Controls Astrogliosis Following Central Nervous System Injury. *J Biol Chem,* 292**,** 1240-1250.

ISHINO, M., OHBA, T., SASAKI, H. & SASAKI, T. 1995. Molecular cloning of a cDNA encoding a phosphoprotein, Efs, which contains a Src homology 3 domain and associates with Fyn. *Oncogene,* 11**,** 2331-8.

IRWIN, D. J. 2016. Tauopathies as clinicopathological entities. *Parkinsonism & related disorders,* 22 Suppl 1, S29-S33.

IZUMCHENKO, E., SINGH, M. K., PLOTNIKOVA, O. V., TIKHMYANOVA, N., LITTLE, J. L., SEREBRIISKII, I. G., SEO, S., KUROKAWA, M., EGLESTON, B. L., KLEIN-SZANTO, A., PUGACHEVA, E. N., HARDY, R. R., WOLFSON, M., CONNOLLY, D. C. & GOLEMIS, E. A. 2009. NEDD9 promotes oncogenic signaling in mammary tumor development. *Cancer Res,* 69**,** 7198-206.

JANKE, A. L., DE ZUBICARAY, G., ROSE, S. E., GRIFFIN, M., CHALK, J. B. & GALLOWAY, G. J. 2001. 4D deformation modeling of cortical disease progression in Alzheimer's dementia. *Magn Reson Med,* 46**,** 661-6.

JOHNSON, K. A., SCHULTZ, A., BETENSKY, R. A., BECKER, J. A., SEPULCRE, J., RENTZ, D., MORMINO, E., CHHATWAL, J., AMARIGLIO, R., PAPP, K., MARSHALL, G., ALBERS, M., MAURO, S., PEPIN, L., ALVERIO, J., JUDGE, K., PHILIOSSAINT, M., SHOUP, T., YOKELL, D., DICKERSON, B., GOMEZ-ISLA, T., HYMAN, B., VASDEV, N. & SPERLING, R. 2016. Tau positron emission tomographic imaging in aging and early Alzheimer disease. *Ann Neurol,* 79**,** 110-9.

JOHNSTON-WILSON, N. L., SIMS, C. D., HOFMANN, J. P., ANDERSON, L., SHORE, A. D., TORREY, E. F. & YOLKEN, R. H. 2000. Disease-specific alterations in frontal cortex brain proteins in schizophrenia, bipolar disorder, and major depressive disorder. The Stanley Neuropathology Consortium. *Mol Psychiatry,* 5**,** 142-9.

JONES, V. C., ATKINSON-DELL, R., VERKHRATSKY, A. & MOHAMET, L. 2017. Aberrant iPSC-derived human astrocytes in Alzheimer's disease. *Cell Death &Amp; Disease,* 8**,** e2696.

JONSSON, T., STEFANSSON, H., STEINBERG, S., JONSDOTTIR, I., JONSSON, P. V., SNAEDAL, J., BJORNSSON, S., HUTTENLOCHER, J., LEVEY, A. I., LAH, J. J., RUJESCU, D., HAMPEL, H., GIEGLING, I., ANDREASSEN, O. A., ENGEDAL, K., ULSTEIN, I., DJUROVIC, S., IBRAHIM-VERBAAS, C., HOFMAN, A., IKRAM, M. A., VAN DUIJN, C. M., THORSTEINSDOTTIR, U., KONG, A. & STEFANSSON, K. 2013. Variant of TREM2 associated with the risk of Alzheimer's disease. *N Engl J Med,* 368**,** 107-16.

JURCIC, P., RADULOVIC, P., BALJA, M. P., MILOSEVIC, M. & KRUSLIN, B. 2019. E-cadherin and NEDD9 expression in primary colorectal cancer, metastatic lymph nodes and liver metastases. *Oncol Lett,* 17**,** 2881-2889.

K, T. C., LUNETTA, K. L., BALDWIN, C. T., MCKEE, A. C., GUO, J., CUPPLES, L. A., GREEN, R. C., ST GEORGE-HYSLOP, P. H., CHUI, H., DECARLI, C. & FARRER, L. A. 2008. Association of distinct variants in SORL1 with cerebrovascular and neurodegenerative changes related to Alzheimer disease. *Arch Neurol,* 65**,** 1640-8.

KAMANU, F., MEDVEDEVA, Y., SCHAEFER, U., JANKOVIC, B., ARCHER, J. & BAJIC, V. 2012. Mutations and Binding Sites of Human Transcription Factors. *Frontiers in Genetics,* 3.

KAMETANI, F. & HASEGAWA, M. 2018. Reconsideration of Amyloid Hypothesis and Tau Hypothesis in Alzheimer's Disease. *Frontiers in neuroscience,* 12**,** 25-25.

KARAS, G. B., SCHELTENS, P., ROMBOUTS, S. A., VISSER, P. J., VAN SCHIJNDEL, R. A., FOX, N. C. & BARKHOF, F. 2004. Global and local gray matter loss in mild cognitive impairment and Alzheimer's disease. *Neuroimage,* 23**,** 708-16.

KARCH, C. M. & GOATE, A. M. 2015. Alzheimer's disease risk genes and mechanisms of disease pathogenesis. *Biological psychiatry,* 77**,** 43-51.

KIKUNO, N., SHIINA, H., URAKAMI, S., KAWAMOTO, K., HIRATA, H., TANAKA, Y., PLACE, R. F., POOKOT, D., MAJID, S., IGAWA, M. & DAHIYA, R. 2007. Knockdown of astrocyte-elevated gene-1 inhibits prostate cancer progression through upregulation of FOXO3a activity. *Oncogene,* 26**,** 7647.

KIM, J., BASAK, J. M. & HOLTZMAN, D. M. 2009. The role of apolipoprotein E in Alzheimer's disease. *Neuron,* 63**,** 287-303.

KIM, K., LEE, S.-G., KEGELMAN, T. P., SU, Z.-Z., DAS, S. K., DASH, R., DASGUPTA, S., BARRAL, P. M., HEDVAT, M., DIAZ, P., REED, J. C., STEBBINS, J. L., PELLECCHIA, M., SARKAR, D. & FISHER, P. B. 2011. Role of excitatory amino acid transporter-2 (EAAT2) and glutamate in neurodegeneration: opportunities for developing novel therapeutics. *Journal of cellular physiology,* 226**,** 2484-2493.

KIM, M.-S., PINTO, S. M., GETNET, D., NIRUJOGI, R. S., MANDA, S. S., CHAERKADY, R., MADUGUNDU, A. K., KELKAR, D. S., ISSERLIN, R., JAIN, S., THOMAS, J. K., MUTHUSAMY, B., LEAL-ROJAS, P., KUMAR, P., SAHASRABUDDHE, N. A., BALAKRISHNAN, L., ADVANI, J., GEORGE, B., RENUSE, S., SELVAN, L. D. N., PATIL, A. H., NANJAPPA, V., RADHAKRISHNAN, A., PRASAD, S., SUBBANNAYYA, T., RAJU, R., KUMAR, M., SREENIVASAMURTHY, S. K., MARIMUTHU, A., SATHE, G. J., CHAVAN, S., DATTA, K. K., SUBBANNAYYA, Y., SAHU, A., YELAMANCHI, S. D., JAYARAM, S., RAJAGOPALAN, P., SHARMA, J., MURTHY, K. R., SYED, N., GOEL, R., KHAN, A. A., AHMAD, S., DEY, G., MUDGAL, K., CHATTERJEE, A., HUANG, T.-C., ZHONG, J., WU, X., SHAW, P. G., FREED, D., ZAHARI, M. S., MUKHERJEE, K. K., SHANKAR, S., MAHADEVAN, A., LAM, H., MITCHELL, C. J., SHANKAR, S. K., SATISHCHANDRA, P., SCHROEDER, J. T., SIRDESHMUKH, R., MAITRA, A., LEACH, S. D., DRAKE, C. G., HALUSHKA, M. K., PRASAD, T. S. K., HRUBAN, R. H., KERR, C. L., BADER, G. D., IACOBUZIO-DONAHUE, C. A., GOWDA, H. & PANDEY, A. 2014. A draft map of the human proteome. *Nature,* 509**,** 575-581.

KNUTSON, D. C., MITZEY, A. M., TALTON, L. E. & CLAGETT-DAME, M. 2016. Mice null for NEDD9 (HEF1alpha) display extensive hippocampal dendritic spine loss and cognitive impairment. *Brain Res,* 1632**,** 141-55.

KOHUTNICKA, M., LEWANDOWSKA, E., KURKOWSKA-JASTRZEBSKA, I., CZLONKOWSKI, A. & CZLONKOWSKA, A. 1998. Microglial and astrocytic involvement in a murine model of Parkinson's disease induced by 1-methyl-4-phenyl-1,2,3,6-tetrahydropyridine (MPTP). *Immunopharmacology,* 39**,** 167-80.

KOK, E. H., LUOTO, T., HAIKONEN, S., GOEBELER, S., HAAPASALO, H. & KARHUNEN, P. J. 2011. CLU, CR1 and PICALM genes associate with Alzheimer's-related senile plaques. *Alzheimers Res Ther,* 3**,** 12.

KOPKE, E., TUNG, Y. C., SHAIKH, S., ALONSO, A. C., IQBAL, K. & GRUNDKE-IQBAL, I. 1993. Microtubule-associated protein tau. Abnormal phosphorylation of a non-paired helical filament pool in Alzheimer disease. *J Biol Chem,* 268, 24374-84.

KONDO, S., IWATA, S., YAMADA, T., INOUE, Y., ICHIHARA, H., KICHIKAWA, Y., KATAYOSE, T., SOUTA-KURIBARA, A., YAMAZAKI, H., HOSONO, O., KAWASAKI, H., TANAKA, H., HAYASHI, Y., SAKAMOTO, M., KAMIYA, K., DANG, N. H. & MORIMOTO, C. 2012. Impact of the integrin signaling adaptor protein NEDD9 on prognosis and metastatic behavior of human lung cancer. *Clin Cancer Res,* 18**,** 6326-38.

KONG, C., WANG, C., WANG, L., MA, M., NIU, C., SUN, X., DU, J., DONG, Z., ZHU, S., LU, J. & HUANG, B. 2011. NEDD9 is a positive regulator of epithelial-mesenchymal transition and promotes invasion in aggressive breast cancer. *PLoS One,* 6**,** e22666.

KULIJEWICZ-NAWROT, M., SYKOVA, E., CHVATAL, A., VERKHRATSKY, A. & RODRIGUEZ, J. J. 2013. Astrocytes and glutamate homoeostasis in Alzheimer's disease: a decrease in glutamine synthetase, but not in glutamate transporter-1, in the prefrontal cortex. *ASN Neuro,* 5**,** 273-82.

KULIJEWICZ-NAWROT, M., VERKHRATSKY, A., CHVATAL, A., SYKOVA, E. & RODRIGUEZ, J. J. 2012. Astrocytic cytoskeletal atrophy in the medial prefrontal cortex of a triple transgenic mouse model of Alzheimer's disease. *J Anat,* 221**,** 252-62.

KUMAR, S., TOMOOKA, Y. & NODA, M. 1992. Identification of a set of genes with developmentally down-regulated expression in the mouse brain. *Biochem Biophys Res Commun,* 185**,** 1155-61.

LACROIX, B., LETORT, G., PITAYU, L., SALLE, J., STEFANUTTI, M., MATON, G., LADOUCEUR, A. M., CANMAN, J. C., MADDOX, P. S., MADDOX, A. S., MINC, N., NEDELEC, F. & DUMONT, J. 2018. Microtubule Dynamics Scale with Cell Size to Set Spindle Length and Assembly Timing. *Dev Cell,* 45**,** 496-511.e6.

LALO, U., PANKRATOV, Y., PARPURA, V. & VERKHRATSKY, A. 2011. Ionotropic receptors in neuronal-astroglial signalling: what is the role of "excitable" molecules in non-excitable cells. *Biochim Biophys Acta,* 1813**,** 992-1002.

LAMBERT, J.-C., IBRAHIM-VERBAAS, C. A., HAROLD, D., NAJ, A. C., SIMS, R., BELLENGUEZ, C., JUN, G., DESTEFANO, A. L., BIS, J. C., BEECHAM, G. W., GRENIER-BOLEY, B., RUSSO, G., THORNTON-WELLS, T. A., JONES, N., SMITH, A. V., CHOURAKI, V., THOMAS, C., IKRAM, M. A., ZELENIKA, D., VARDARAJAN, B. N., KAMATANI, Y., LIN, C.-F., GERRISH, A., SCHMIDT, H., KUNKLE, B., DUNSTAN, M. L., RUIZ, A., BIHOREAU, M.-T., CHOI, S.-H., REITZ, C., PASQUIER, F., HOLLINGWORTH, P.,

RAMIREZ, A., HANON, O., FITZPATRICK, A. L., BUXBAUM, J. D., CAMPION, D., CRANE, P. K., BALDWIN, C., BECKER, T., GUDNASON, V., CRUCHAGA, C., CRAIG, D., AMIN, N., BERR, C., LOPEZ, O. L., HUENTELMAN, M. J., LOVE, S., HARDY, J., POWELL, J. F. & EUROPEAN ALZHEIMER'S DISEASE, I. 2013. Meta-analysis of 74,046 individuals identifies 11 new susceptibility loci for Alzheimer's disease. *Nature Genetics*.

LANOISELEE, H. M., NICOLAS, G., WALLON, D., ROVELET-LECRUX, A., LACOUR, M., ROUSSEAU, S., RICHARD, A. C., PASQUIER, F., ROLLIN-SILLAIRE, A., MARTINAUD, O., QUILLARD-MURAINE, M., DE LA SAYETTE, V., BOUTOLEAU-BRETONNIERE, C., ETCHARRY-BOUYX, F., CHAUVIRE, V., SARAZIN, M., LE BER, I., EPELBAUM, S., JONVEAUX, T., ROUAUD, O., CECCALDI, M., FELICIAN, O., GODEFROY, O., FORMAGLIO, M., CROISILE, B., AURIACOMBE, S., CHAMARD, L., VINCENT, J. L., SAUVEE, M., MARELLI-TOSI, C., GABELLE, A., OZSANCAK, C., PARIENTE, J., PAQUET, C., HANNEQUIN, D. & CAMPION, D. 2017. APP, PSEN1, and PSEN2 mutations in early-onset Alzheimer disease: A genetic screening study of familial and sporadic cases. *PLoS Med,* 14, e1002270.

LAROCCA, T. J., MARIANI, A., WATKINS, L. R. & LINK, C. D. 2019. TDP-43 knockdown causes innate immune activation via protein kinase R in astrocytes. *Neurobiology of Disease*, 104514.

LAUMET, G., CHOURAKI, V., GRENIER-BOLEY, B., LEGRY, V., HEATH, S., ZELENIKA, D., FIEVET, N., HANNEQUIN, D., DELEPINE, M., PASQUIER, F., HANON, O., BRICE, A., EPELBAUM, J., BERR, C., DARTIGUES, J. F., TZOURIO, C., CAMPION, D., LATHROP, M., BERTRAM, L., AMOUYEL, P. & LAMBERT, J. C. 2010. Systematic analysis of candidate genes for Alzheimer's disease in a French, genome-wide association study. *J Alzheimers Dis,* 20, 1181-8.

LAW, S. F., ESTOJAK, J., WANG, B., MYSLIWIEC, T., KRUH, G. & GOLEMIS, E. A. 1996. Human enhancer of filamentation 1, a novel p130cas-like docking protein, associates with focal adhesion kinase and induces pseudohyphal growth in Saccharomyces cerevisiae. *Mol Cell Biol,* 16, 3327-37.

LAW, S. F., NEILL, G. M., FASHENA, S. J., EINARSON, M. B. & GOLEMIS, E. A. 2000. The Docking Protein HEF1 Is an Apoptotic Mediator at Focal Adhesion Sites. *Molecular and Cellular Biology,* 20, 5184.

LAW, S. F., ZHANG, Y. Z., FASHENA, S. J., TOBY, G., ESTOJAK, J. & GOLEMIS, E. A. 1999. Dimerization of the docking/adaptor protein HEF1 via a carboxy-terminal helix-loop-helix domain. *Exp Cell Res,* 252, 224-35.

LAW, S. F., ZHANG, Y. Z., KLEIN-SZANTO, A. J. & GOLEMIS, E. A. 1998. Cell cycle-regulated processing of HEF1 to multiple protein forms differentially targeted to multiple subcellular compartments. *Mol Cell Biol,* 18, 3540-51.

LI, A., ZHANG, W., XIA, H., MIAO, Y., ZHOU, H., ZHANG, X., DONG, Q., LI, Q., QIU, X. & WANG, E. 2016. Overexpression of CASS4 promotes invasion in non-small cell lung cancer by activating the AKT signaling pathway and inhibiting E-cadherin expression. *Tumour Biol,* 37, 15157-15164.

LI, Y., BAVARVA, J. H., WANG, Z., GUO, J., QIAN, C., THIBODEAU, S. N., GOLEMIS, E. A. & LIU, W. 2011. HEF1, a novel target of Wnt signaling, promotes colonic cell migration and cancer progression. *Oncogene,* 30, 2633-43.

LI, Y., GRUPE, A., ROWLAND, C., HOLMANS, P., SEGURADO, R., ABRAHAM, R., JONES, L., CATANESE, J., ROSS, D., MAYO, K., MARTINEZ, M.,

HOLLINGWORTH, P., GOATE, A., CAIRNS, N. J., RACETTE, B. A., PERLMUTTER, J. S., O'DONOVAN, M. C., MORRIS, J. C., BRAYNE, C., RUBINSZTEIN, D. C., LOVESTONE, S., THAL, L. J., OWEN, M. J. & WILLIAMS, J. 2008. Evidence that common variation in NEDD9 is associated with susceptibility to late-onset Alzheimer's and Parkinson's disease. *Hum Mol Genet,* 17**,** 759-67.

LICHTMAN, J. W. & CONCHELLO, J. A. 2005. Fluorescence microscopy. *Nat Methods,* 2**,** 910-9.

LIDDELOW, S. A., GUTTENPLAN, K. A., CLARKE, L. E., BENNETT, F. C., BOHLEN, C. J., SCHIRMER, L., BENNETT, M. L., MUNCH, A. E., CHUNG, W. S., PETERSON, T. C., WILTON, D. K., FROUIN, A., NAPIER, B. A., PANICKER, N., KUMAR, M., BUCKWALTER, M. S., ROWITCH, D. H., DAWSON, V. L., DAWSON, T. M., STEVENS, B. & BARRES, B. A. 2017. Neurotoxic reactive astrocytes are induced by activated microglia. *Nature,* 541**,** 481-487.

LIN, J., YANG, Q., WILDER, P. T., CARRIER, F. & WEBER, D. J. 2010. The calcium-binding protein S100B down-regulates p53 and apoptosis in malignant melanoma. *J Biol Chem,* 285**,** 27487-98.

LINDWALL, G. & COLE, R. D. 1984. Phosphorylation affects the ability of tau protein to promote microtubule assembly. *J Biol Chem,* 259, 5301-5.

LIU, H., SONG, X., LIU, C., XIE, L., WEI, L. & SUN, R. 2009. Knockdown of astrocyte elevated gene-1 inhibits proliferation and enhancing chemo-sensitivity to cisplatin or doxorubicin in neuroblastoma cells. *Journal of Experimental & Clinical Cancer Research,* 28**,** 19.

LIU, Y., BEYER, A. & AEBERSOLD, R. 2016. On the Dependency of Cellular Protein Levels on mRNA Abundance. *Cell,* 165**,** 535-50.

LONGAIR, M. H., BAKER, D. A. & ARMSTRONG, J. D. 2011. Simple Neurite Tracer: open source software for reconstruction, visualization and analysis of neuronal processes. *Bioinformatics,* 27**,** 2453-4.

LUBLIN, A. L. & GANDY, S. 2010. Amyloid-beta oligomers: possible roles as key neurotoxins in Alzheimer's Disease. *Mt Sinai J Med,* 77**,** 43-9.

MAKELA, M., KAIVOLA, K., VALORI, M., PAETAU, A., POLVIKOSKI, T., SINGLETON, A. B., TRAYNOR, B. J., STONE, D. J., PEURALINNA, T., TIENARI, P. J., TANSKANEN, M. & MYLLYKANGAS, L. 2018. Alzheimer risk loci and associated neuropathology in a population-based study (Vantaa 85+). *Neurol Genet,* 4**,** e211.

MANIE, S. N., BECK, A. R., ASTIER, A., LAW, S. F., CANTY, T., HIRAI, H., DRUKER, B. J., AVRAHAM, H., HAGHAYEGHI, N., SATTLER, M., SALGIA, R., GRIFFIN, J. D., GOLEMIS, E. A. & FREEDMAN, A. S. 1997. Involvement of p130(Cas) and p105(HEF1), a novel Cas-like docking protein, in a cytoskeleton-dependent signaling pathway initiated by ligation of integrin or antigen receptor on human B cells. *J Biol Chem,* 272**,** 4230-6.

MARTINEAU, M., PARPURA, V. & MOTHET, J.-P. 2014. Cell-type specific mechanisms of D-serine uptake and release in the brain. *Frontiers in synaptic neuroscience,* 6**,** 12-12.

MARTINEZ-CORIA, H., YEUNG, S. T., AGER, R. R., RODRIGUEZ-ORTIZ, C. J., BAGLIETTO-VARGAS, D. & LAFERLA, F. M. 2015. Repeated cognitive stimulation alleviates memory impairments in an Alzheimer's disease mouse model. *Brain Res Bull,* 117**,** 10-5.

MASTERS, C. L., SIMMS, G., WEINMAN, N. A., MULTHAUP, G., MCDONALD, B. L. & BEYREUTHER, K. 1985. Amyloid plaque core protein in Alzheimer disease and Down syndrome. *Proc Natl Acad Sci U S A,* 82**,** 4245-9.

MATIAS, I., MORGADO, J. & GOMES, F. C. A. 2019. Astrocyte Heterogeneity: Impact to Brain Aging and Disease. *Frontiers in Aging Neuroscience,* 11.

MATYASH, V. & KETTENMANN, H. 2010. Heterogeneity in astrocyte morphology and physiology. *Brain Research Reviews,* 63**,** 2-10.

MCLAUGHLIN, S. L., ICE, R. J., RAJULAPATI, A., KOZYULINA, P. Y., LIVENGOOD, R. H., KOZYREVA, V. K., LOSKUTOV, Y. V., CULP, M. V., WEED, S. A., IVANOV, A. V. & PUGACHEVA, E. N. 2014. NEDD9 depletion leads to MMP14 inactivation by TIMP2 and prevents invasion and metastasis. *Mol Cancer Res,* 12**,** 69-81.

MEISTER, G., LANDTHALER, M., PATKANIOWSKA, A., DORSETT, Y., TENG, G. & TUSCHL, T. 2004. Human Argonaute2 mediates RNA cleavage targeted by miRNAs and siRNAs. *Mol Cell,* 15**,** 185-97.

MERRILL, R. A., SEE, A. W., WERTHEIM, M. L. & CLAGETT-DAME, M. 2004. Crk-associated substrate (Cas) family member, NEDD9, is regulated in human neuroblastoma cells and in the embryonic hindbrain by all-trans retinoic acid. *Dev Dyn,* 231**,** 564-75.

MIAO, Y., WANG, L., LIU, Y., LI, A. L., LIU, S. L., CAO, H. Y., ZHANG, X. P., JIANG, G. Y., LIU, D. & WANG, E. H. 2013. Overexpression and cytoplasmic accumulation of Hepl is associated with clinicopathological parameters and poor prognosis in non-small cell lung cancer. *Tumour Biol,* 34**,** 107-14.

MILLER, S. J. 2018. Astrocyte Heterogeneity in the Adult Central Nervous System. *Frontiers in Cellular Neuroscience,* 12.

MINEGISHI, M., TACHIBANA, K., SATO, T., IWATA, S., NOJIMA, Y. & MORIMOTO, C. 1996. Structure and function of Cas-L, a 105-kD Crk-associated substrate-related protein that is involved in beta 1 integrin-mediated signaling in lymphocytes. *The Journal of experimental medicine,* 184**,** 1365-1375.

MOCELLIN, S. & PROVENZANO, M. 2004. RNA interference: learning gene knock-down from cell physiology. *J Transl Med,* 2, 39.

MOHAMET, L., JONES, V. C., DAYANITHI, G. & VERKHRATSKY, A. 2018. Pathological human astroglia in Alzheimer's disease: opening new horizons with stem cell technology. *Future Neurology,* 13**,** 87-99.

MOON, Y., KIM, H. J., KIM, J. Y., KIM, H., KIM, W. R. & SUN, W. 2011. Different expression of human GFAP promoter-derived GFP in different subsets of astrocytes in the mouse brain. *Animal Cells and Systems,* 15**,** 268-273.

MORENO-TREVIÑO, M. G., CASTILLO-LÓPEZ, J. & MEESTER, I. 2015. Moving away from amyloid Beta to move on in Alzheimer research. *Frontiers in aging neuroscience,* 7**,** 2-2.

MORI, D., YAMADA, M., MIMORI-KIYOSUE, Y., SHIRAI, Y., SUZUKI, A., OHNO, S., SAYA, H., WYNSHAW-BORIS, A. & HIROTSUNE, S. 2009. An essential role of the aPKC-Aurora A-NDEL1 pathway in neurite elongation by modulation of microtubule dynamics. *Nat Cell Biol,* 11**,** 1057-68.

MORRIS, J. C., ROE, C. M., XIONG, C., FAGAN, A. M., GOATE, A. M., HOLTZMAN, D. M. & MINTUN, M. A. 2010. APOE predicts amyloid-beta but not tau Alzheimer pathology in cognitively normal aging. *Ann Neurol,* 67**,** 122-31.

NAJ, A. C., JUN, G., BEECHAM, G. W., WANG, L. S., VARDARAJAN, B. N., BUROS, J., GALLINS, P. J., BUXBAUM, J. D., JARVIK, G. P., CRANE, P. K.,

LARSON, E. B., BIRD, T. D., BOEVE, B. F., GRAFF-RADFORD, N. R., DE JAGER, P. L., EVANS, D., SCHNEIDER, J. A., CARRASQUILLO, M. M., ERTEKIN-TANER, N., YOUNKIN, S. G., CRUCHAGA, C., KAUWE, J. S., NOWOTNY, P., KRAMER, P., HARDY, J., HUENTELMAN, M. J., MYERS, A. J., BARMADA, M. M., DEMIRCI, F. Y., BALDWIN, C. T., GREEN, R. C., ROGAEVA, E., ST GEORGE-HYSLOP, P., ARNOLD, S. E., BARBER, R., BEACH, T., BIGIO, E. H., BOWEN, J. D., BOXER, A., BURKE, J. R., CAIRNS, N. J., CARLSON, C. S., CARNEY, R. M., CARROLL, S. L., CHUI, H. C., CLARK, D. G., CORNEVEAUX, J., COTMAN, C. W., CUMMINGS, J. L., DECARLI, C., DEKOSKY, S. T., DIAZ-ARRASTIA, R., DICK, M., DICKSON, D. W., ELLIS, W. G., FABER, K. M., FALLON, K. B., FARLOW, M. R., FERRIS, S., FROSCH, M. P., GALASKO, D. R., GANGULI, M., GEARING, M., GESCHWIND, D. H., GHETTI, B., GILBERT, J. R., GILMAN, S., GIORDANI, B., GLASS, J. D., GROWDON, J. H., HAMILTON, R. L., HARRELL, L. E., HEAD, E., HONIG, L. S., HULETTE, C. M., HYMAN, B. T., JICHA, G. A., JIN, L. W., JOHNSON, N., KARLAWISH, J., KARYDAS, A., KAYE, J. A., KIM, R., KOO, E. H., KOWALL, N. W., LAH, J. J., LEVEY, A. I., LIEBERMAN, A. P., LOPEZ, O. L., MACK, W. J., MARSON, D. C., MARTINIUK, F., MASH, D. C., MASLIAH, E., MCCORMICK, W. C., MCCURRY, S. M., MCDAVID, A. N., MCKEE, A. C., MESULAM, M., MILLER, B. L., et al. 2011. Common variants at MS4A4/MS4A6E, CD2AP, CD33 and EPHA1 are associated with late-onset Alzheimer's disease. *Nat Genet,* 43**,** 436-41.

NEDERGAARD, M., TAKANO, T. & HANSEN, A. J. 2002. Beyond the role of glutamate as a neurotransmitter. *Nat Rev Neurosci,* 3**,** 748-55.

NIKONOVA, A. S., ASTSATUROV, I., SEREBRIISKII, I. G., DUNBRACK, R. L., JR. & GOLEMIS, E. A. 2013. Aurora A kinase (AURKA) in normal and pathological cell division. *Cellular and molecular life sciences : CMLS,* 70**,** 661-687.

NISHIDA, H. & OKABE, S. 2007. Direct astrocytic contacts regulate local maturation of dendritic spines. *J Neurosci,* 27**,** 331-40.

NONAKA, T., WATANABE, S. T., IWATSUBO, T. & HASEGAWA, M. 2010. Seeded aggregation and toxicity of {alpha}-synuclein and tau: cellular models of neurodegenerative diseases. *J Biol Chem,* 285**,** 34885-98.

O'NEILL, G. M. & GOLEMIS, E. A. 2001. Proteolysis of the docking protein HEF1 and implications for focal adhesion dynamics. *Mol Cell Biol,* 21**,** 5094-108.

OBERHEIM, N. A., TAKANO, T., HAN, X., HE, W., LIN, J. H., WANG, F., XU, Q., WYATT, J. D., PILCHER, W., OJEMANN, J. G., RANSOM, B. R., GOLDMAN, S. A. & NEDERGAARD, M. 2009. Uniquely hominid features of adult human astrocytes. *J Neurosci,* 29**,** 3276-87.

OHTAKI, N., KAMITANI, W., WATANABE, Y., HAYASHI, Y., YANAI, H., IKUTA, K. & TOMONAGA, K. 2007. Downregulation of an astrocyte-derived inflammatory protein, S100B, reduces vascular inflammatory responses in brains persistently infected with Borna disease virus. *Journal of virology*, 81, 5940-5948.

OLABARRIA, M., NORISTANI, H. N., VERKHRATSKY, A. & RODRIGUEZ, J. J. 2010. Concomitant astroglial atrophy and astrogliosis in a triple transgenic animal model of Alzheimer's disease. *Glia,* 58**,** 831-8.

OLUDE, M. A., MUSTAPHA, O. A., ADEROUNMU, O. A., OLOPADE, J. O. & IHUNWO, A. O. 2015. Astrocyte morphology, heterogeneity, and density in the developing African giant rat (Cricetomys gambianus). *Frontiers in Neuroanatomy,* 9.

217

OSBORN, L. M., KAMPHUIS, W., WADMAN, W. J. & HOL, E. M. 2016. Astrogliosis: An integral player in the pathogenesis of Alzheimer's disease. *Prog Neurobiol,* 144**,** 121-41.

PACHERNEGG, S., EILEBRECHT, S., EILEBRECHT, E., SCHÖNEBORN, H., NEUMANN, S., BENECKE, A. G. & HOLLMANN, M. 2018. The siRNA-mediated knockdown of GluN3A in 46C-derived neural stem cells affects mRNA expression levels of neural genes, including known iGluR interactors. *PloS one,* 13, e0192242-e0192242.

PAN, C., KUMAR, C., BOHL, S., KLINGMUELLER, U. & MANN, M. 2009. Comparative proteomic phenotyping of cell lines and primary cells to assess preservation of cell type-specific functions. *Mol Cell Proteomics,* 8**,** 443-50.

PANOPOULOS, A., HOWELL, M., FOTEDAR, R. & MARGOLIS, R. L. 2011. Glioblastoma motility occurs in the absence of actin polymer. *Mol Biol Cell,* 22**,** 2212-20.

PARPURA, V., HENEKA, M. T., MONTANA, V., OLIET, S. H., SCHOUSBOE, A., HAYDON, P. G., STOUT, R. F., JR., SPRAY, D. C., REICHENBACH, A., PANNICKE, T., PEKNY, M., PEKNA, M., ZOREC, R. & VERKHRATSKY, A. 2012. Glial cells in (patho)physiology. *J Neurochem,* 121**,** 4-27.

PARSONS, B. D., SCHINDLER, A., EVANS, D. H. & FOLEY, E. 2009. A direct phenotypic comparison of siRNA pools and multiple individual duplexes in a functional assay. *PLoS One,* 4**,** e8471.

PATTERSON, C. 2018. World Alzheimer Report.

PEHAR, M., HARLAN, B. A., KILLOY, K. M. & VARGAS, M. R. 2017. Role and Therapeutic Potential of Astrocytes in Amyotrophic Lateral Sclerosis. *Current pharmaceutical design,* 23**,** 5010-5021.

PEKNY, M. & PEKNA, M. 2004. Astrocyte intermediate filaments in CNS pathologies and regeneration. *J Pathol,* 204**,** 428-37.

PEREA, G., NAVARRETE, M. & ARAQUE, A. 2009. Tripartite synapses: astrocytes process and control synaptic information. *Trends Neurosci,* 32**,** 421-31.

PEREZ-ALVAREZ, A., NAVARRETE, M., COVELO, A., MARTIN, E. D. & ARAQUE, A. 2014. Structural and functional plasticity of astrocyte processes and dendritic spine interactions. *J Neurosci,* 34**,** 12738-44.

PEREZ-NIEVAS, B. G. & SERRANO-POZO, A. 2018. Deciphering the Astrocyte Reaction in Alzheimer's Disease. *Frontiers in Aging Neuroscience,* 10.

PIACERI, I., NACMIAS, B. & SORBI, S. 2013. Genetics of familial and sporadic Alzheimer's disease. *Front Biosci (Elite Ed),* 5**,** 167-77.

POLLARD, T. D. & BORISY, G. G. 2003. Cellular motility driven by assembly and disassembly of actin filaments. *Cell,* 112**,** 453-65.

POMILIO, C., PAVIA, P., GOROJOD, R. M., VINUESA, A., ALAIMO, A., GALVAN, V., KOTLER, M. L., BEAUQUIS, J. & SARAVIA, F. 2016. Glial alterations from early to late stages in a model of Alzheimer's disease: Evidence of autophagy involvement in Aβ internalization. *Hippocampus,* 26**,** 194-210.

PUGACHEVA, E. N. & GOLEMIS, E. A. 2005. The focal adhesion scaffolding protein HEF1 regulates activation of the Aurora-A and Nek2 kinases at the centrosome. *Nat Cell Biol,* 7**,** 937-46.

PUGACHEVA, E. N., JABLONSKI, S. A., HARTMAN, T. R., HENSKE, E. P. & GOLEMIS, E. A. 2007. HEF1-dependent Aurora A activation induces disassembly of the primary cilium. *Cell,* 129**,** 1351-63.

RAPONI, E., AGENES, F., DELPHIN, C., ASSARD, N., BAUDIER, J., LEGRAVEREND, C. & DELOULME, J. C. 2007. S100B expression defines a

state in which GFAP-expressing cells lose their neural stem cell potential and acquire a more mature developmental stage. *Glia,* 55**,** 165-77.

RATTRAY, M. & BENDOTTI, C. 2006. Does excitotoxic cell death of motor neurons in ALS arise from glutamate transporter and glutamate receptor abnormalities? *Exp Neurol,* 201**,** 15-23.

ROBINSON, C., APGAR, C. & SHAPIRO, L. A. 2016. Astrocyte Hypertrophy Contributes to Aberrant Neurogenesis after Traumatic Brain Injury. *Neural Plast,* 2016**,** 1347987.

RODRIGUEZ-ARELLANO, J. J., PARPURA, V., ZOREC, R. & VERKHRATSKY, A. 2016. Astrocytes in physiological aging and Alzheimer's disease. *Neuroscience,* 323**,** 170-82.

RODRIGUEZ, J. J., YEH, C. Y., TERZIEVA, S., OLABARRIA, M., KULIJEWICZ-NAWROT, M. & VERKHRATSKY, A. 2014. Complex and region-specific changes in astroglial markers in the aging brain. *Neurobiol Aging,* 35**,** 15-23.

ROSELLI, S., WALLEZ, Y., WANG, L., VERVOORT, V. & PASQUALE, E. B. 2010. The SH2 domain protein Shep1 regulates the in vivo signaling function of the scaffolding protein Cas. *Cellular signalling,* 22**,** 1745-1752.

ROSENTHAL, S. L. & KAMBOH, M. I. 2014. Late-Onset Alzheimer's Disease Genes and the Potentially Implicated Pathways. *Current genetic medicine reports,* 2**,** 85-101.

ROSS, G. W., O'CALLAGHAN, J. P., SHARP, D. S., PETROVITCH, H., MILLER, D. B., ABBOTT, R. D., NELSON, J., LAUNER, L. J., FOLEY, D. J., BURCHFIEL, C. M., HARDMAN, J. & WHITE, L. R. 2003. Quantification of regional glial fibrillary acidic protein levels in Alzheimer's disease. *Acta Neurol Scand,* 107**,** 318-23.

ROUSSEAU, B., JACQUOT, C., LE PALABE, J., MALLETER, M., TOMASONI, C., BOUTARD, T., SAKANYAN, V. & ROUSSAKIS, C. 2015. TP53 transcription factor for the NEDD9/HEF1/Cas-L gene: potential targets in Non-Small Cell Lung Cancer treatment. *Sci Rep,* 5**,** 10356.

RYGIEL, K. 2016. Novel strategies for Alzheimer's disease treatment: An overview of anti-amyloid beta monoclonal antibodies. *Indian journal of pharmacology,* 48**,** 629-636.

SAKAI, R., IWAMATSU, A., HIRANO, N., OGAWA, S., TANAKA, T., NISHIDA, J., YAZAKI, Y. & HIRAI, H. 1994. Characterization, partial purification, and peptide sequencing of p130,the main phosphoprotein associated with v-Crk oncoprotein. *J Biol Chem,* 269**,** 32740-6.

SANTELLO, M., TONI, N. & VOLTERRA, A. 2019. Astrocyte function from information processing to cognition and cognitive impairment. *Nature Neuroscience,* 22**,** 154-166.

SATHE, K., MAETZLER, W., LANG, J. D., MOUNSEY, R. B., FLECKENSTEIN, C., MARTIN, H. L., SCHULTE, C., MUSTAFA, S., SYNOFZIK, M., VUKOVIC, Z., ITOHARA, S., BERG, D. & TEISMANN, P. 2012. S100B is increased in Parkinson's disease and ablation protects against MPTP-induced toxicity through the RAGE and TNF-alpha pathway. *Brain,* 135**,** 3336-47.

SATO, J., HORIBE, S., KAWAUCHI, S., SASAKI, N., HIRATA, K.-I. & RIKITAKE, Y. 2018. Involvement of aquaporin-4 in laminin-enhanced process formation of mouse astrocytes in 2D culture: Roles of dystroglycan and α-syntrophin in aquaporin-4 expression. *Journal of Neurochemistry,* 147**,** 495-513.

SAWADA, Y., TAMADA, M., DUBIN-THALER, B. J., CHERNIAVSKAYA, O., SAKAI, R., TANAKA, S. & SHEETZ, M. P. 2006. Force sensing by mechanical extension of the Src family kinase substrate p130Cas. *Cell,* 127**,** 1015-26.

SCHITINE, C., NOGAROLI, L., COSTA, M. R. & HEDIN-PEREIRA, C. 2015. Astrocyte heterogeneity in the brain: from development to disease. *Frontiers in Cellular Neuroscience,* 9.

SCHIWECK, J., EICKHOLT, B. J. & MURK, K. 2018a. Important Shapeshifter: Mechanisms Allowing Astrocytes to Respond to the Changing Nervous System During Development, Injury and Disease. *Frontiers in cellular neuroscience,* 12**,** 261-261.

SCHIWECK, J., EICKHOLT, B. J. & MURK, K. 2018b. Important Shapeshifter: Mechanisms Allowing Astrocytes to Respond to the Changing Nervous System During Development, Injury and Disease. *Frontiers in Cellular Neuroscience,* 12.

SCHWANHAUSSER, B., BUSSE, D., LI, N., DITTMAR, G., SCHUCHHARDT, J., WOLF, J., CHEN, W. & SELBACH, M. 2011. Global quantification of mammalian gene expression control. *Nature,* 473**,** 337-42.

SELINFREUND, R. H., BARGER, S. W., PLEDGER, W. J. & VAN ELDIK, L. J. 1991. Neurotrophic protein S100 beta stimulates glial cell proliferation. *Proceedings of the National Academy of Sciences of the United States of America,* 88**,** 3554-3558.

SELINFREUND, R. H., BARGER, S. W., WELSH, M. J. & VAN ELDIK, L. J. 1990. Antisense inhibition of glial S100 beta production results in alterations in cell morphology, cytoskeletal organization, and cell proliferation. *J Cell Biol,* 111**,** 2021-8.

SERGEANT, N., DELACOURTE, A. & BUEE, L. 2005. Tau protein as a differential biomarker of tauopathies. *Biochim Biophys Acta*, 1739, 179-97.

SHAGISULTANOVA, E., GAPONOVA, A. V., GABBASOV, R., NICOLAS, E. & GOLEMIS, E. A. 2015. Preclinical and clinical studies of the NEDD9 scaffold protein in cancer and other diseases. *Gene,* 567**,** 1-11.

SHERRINGTON, R., ROGAEV, E. I., LIANG, Y., ROGAEVA, E. A., LEVESQUE, G., IKEDA, M., CHI, H., LIN, C., LI, G., HOLMAN, K., TSUDA, T., MAR, L., FONCIN, J. F., BRUNI, A. C., MONTESI, M. P., SORBI, S., RAINERO, I., PINESSI, L., NEE, L., CHUMAKOV, I., POLLEN, D., BROOKES, A., SANSEAU, P., POLINSKY, R. J., WASCO, W., DA SILVA, H. A., HAINES, J. L., PERKICAK-VANCE, M. A., TANZI, R. E., ROSES, A. D., FRASER, P. E., ROMMENS, J. M. & ST GEORGE-HYSLOP, P. H. 1995. Cloning of a gene bearing missense mutations in early-onset familial Alzheimer's disease. *Nature,* 375**,** 754-60.

SHOLL, D. A. 1953. Dendritic organization in the neurons of the visual and motor cortices of the cat. *Journal of anatomy,* 87**,** 387-406.

SIMA, N., CHENG, X., YE, F., MA, D., XIE, X. & LU, W. 2013. The overexpression of scaffolding protein NEDD9 promotes migration and invasion in cervical cancer via tyrosine phosphorylated FAK and SRC. *PLoS One,* 8**,** e74594.

SIMIC, G., BABIC LEKO, M., WRAY, S., HARRINGTON, C., DELALLE, I., JOVANOV-MILOSEVIC, N., BAZADONA, D., BUEE, L., DE SILVA, R., DI GIOVANNI, G., WISCHIK, C. & HOF, P. R. 2016. Tau Protein Hyperphosphorylation and Aggregation in Alzheimer's Disease and Other Tauopathies, and Possible Neuroprotective Strategies. *Biomolecules,* 6, 6.

SIMPSON, J. E., INCE, P. G., LACE, G., FORSTER, G., SHAW, P. J., MATTHEWS, F., SAVVA, G., BRAYNE, C. & WHARTON, S. B. 2010. Astrocyte phenotype

in relation to Alzheimer-type pathology in the ageing brain. *Neurobiol Aging,* 31**,** 578-90.

SINGH, M., COWELL, L., SEO, S., O'NEILL, G. & GOLEMIS, E. 2007. Molecular basis for HEF1/NEDD9/Cas-L action as a multifunctional co-ordinator of invasion, apoptosis and cell cycle. *Cell Biochem Biophys,* 48**,** 54-72.

SINGH, M. K., DADKE, D., NICOLAS, E., SEREBRIISKII, I. G., APOSTOLOU, S., CANUTESCU, A., EGLESTON, B. L. & GOLEMIS, E. A. 2008. A novel Cas family member, HEPL, regulates FAK and cell spreading. *Mol Biol Cell,* 19**,** 1627-36.

SKENE, N. G. & GRANT, S. G. 2016. Identification of Vulnerable Cell Types in Major Brain Disorders Using Single Cell Transcriptomes and Expression Weighted Cell Type Enrichment. *Front Neurosci,* 10**,** 16.

SOFRONIEW, M. V. & VINTERS, H. V. 2010. Astrocytes: biology and pathology. *Acta Neuropathol,* 119**,** 7-35.

SPERANZA, M. C., FRATTINI, V., PISATI, F., KAPETIS, D., PORRATI, P., EOLI, M., PELLEGATTA, S. & FINOCCHIARO, G. 2012. NEDD9, a novel target of miR-145, increases the invasiveness of glioblastoma. *Oncotarget,* 3**,** 723-734.

STIMMELL, A. C., BAGLIETTO-VARGAS, D., MOSELEY, S. C., LAPOINTE, V., THOMPSON, L. M., LAFERLA, F. M., MCNAUGHTON, B. L. & WILBER, A. A. 2019. Impaired Spatial Reorientation in the 3xTg-AD Mouse Model of Alzheimer's Disease. *Sci Rep,* 9**,** 1311.

STRUBLE, R. G., ALA, T., PATRYLO, P. R., BREWER, G. J. & YAN, X.-X. 2010. Is brain amyloid production a cause or a result of dementia of the Alzheimer's type? *Journal of Alzheimer's disease : JAD,* 22**,** 393-399.

TACHIBANA, K., URANO, T., FUJITA, H., OHASHI, Y., KAMIGUCHI, K., IWATA, S., HIRAI, H. & MORIMOTO, C. 1997. Tyrosine phosphorylation of Crk-associated substrates by focal adhesion kinase. A putative mechanism for the integrin-mediated tyrosine phosphorylation of Crk-associated substrates. *J Biol Chem,* 272**,** 29083-90.

TAMADA, M., SHEETZ, M. P. & SAWADA, Y. 2004. Activation of a signaling cascade by cytoskeleton stretch. *Dev Cell,* 7**,** 709-18.

TANG, S.-S., WANG, H.-F., ZHANG, W., KONG, L.-L., ZHENG, Z.-J., TAN, M.-S., TAN, C.-C., WANG, Z.-X., TAN, L., JIANG, T., YU, J.-T. & TAN, L. 2016. MEF2C rs190982 polymorphism with late-onset Alzheimer's disease in Han Chinese: A replication study and meta-analyses. *Oncotarget,* 7**,** 39136-39142.

TAVARES, G., MARTINS, M., CORREIA, J. S., SARDINHA, V. M., GUERRA-GOMES, S., DAS NEVES, S. P., MARQUES, F., SOUSA, N. & OLIVEIRA, J. F. 2017. Employing an open-source tool to assess astrocyte tridimensional structure. *Brain Struct Funct,* 222**,** 1989-1999.

TERRY, R. D. 1996. The pathogenesis of Alzheimer disease: an alternative to the amyloid hypothesis. *J Neuropathol Exp Neurol*, 55, 1023-5.

THOMPSON, P. M., HAYASHI, K. M., DE ZUBICARAY, G., JANKE, A. L., ROSE, S. E., SEMPLE, J., HERMAN, D., HONG, M. S., DITTMER, S. S., DODDRELL, D. M. & TOGA, A. W. 2003. Dynamics of gray matter loss in Alzheimer's disease. *J Neurosci,* 23**,** 994-1005.

TIKHMYANOVA, N., LITTLE, J. L. & GOLEMIS, E. A. 2010. CAS proteins in normal and pathological cell growth control. *Cellular and molecular life sciences : CMLS,* 67**,** 1025-1048.

TOIVARI, E., MANNINEN, T., NAHATA, A. K., JALONEN, T. O. & LINNE, M. L. 2011. Effects of transmitters and amyloid-beta peptide on calcium signals in rat

cortical astrocytes: Fura-2AM measurements and stochastic model simulations. *PLoS One,* 6**,** e17914.

TONG, J., ANG, L. C., WILLIAMS, B., FURUKAWA, Y., FITZMAURICE, P., GUTTMAN, M., BOILEAU, I., HORNYKIEWICZ, O. & KISH, S. J. 2015. Low levels of astroglial markers in Parkinson's disease: relationship to alpha-synuclein accumulation. *Neurobiol Dis,* 82**,** 243-253.

TUGRUL, M., PAIXAO, T., BARTON, N. H. & TKACIK, G. 2015. Dynamics of Transcription Factor Binding Site Evolution. *PLoS Genet,* 11**,** e1005639.

VALTCHEVA, S. & VENANCE, L. 2019. Control of Long-Term Plasticity by Glutamate Transporters. *Frontiers in Synaptic Neuroscience,* 11.

VAN ELDIK, L. J. & WAINWRIGHT, M. S. 2003. The Janus face of glial-derived S100B: beneficial and detrimental functions in the brain. *Restor Neurol Neurosci,* 21**,** 97-108.

VASILE, F., DOSSI, E. & ROUACH, N. 2017. Human astrocytes: structure and functions in the healthy brain. *Brain Structure and Function*, 222, 2017-2029.

VERKHRATSKY, A. & NEDERGAARD, M. 2018. Physiology of Astroglia. *Physiol Rev,* 98**,** 239-389.

VERKHRATSKY, A., OLABARRIA, M., NORISTANI, H. N., YEH, C. Y. & RODRIGUEZ, J. J. 2010. Astrocytes in Alzheimer's disease. *Neurotherapeutics,* 7**,** 399-412.

VERKHRATSKY, A., PARPURA, V., PEKNA, M., PEKNY, M. & SOFRONIEW, M. 2014. Glia in the pathogenesis of neurodegenerative diseases. *Biochem Soc Trans,* 42**,** 1291-301.

VERKHRATSKY, A., RODRÍGUEZ, J. J. & PARPURA, V. 2013. Astroglia in neurological diseases. *Future neurology,* 8**,** 149-158.

VERKHRATSKY, A., ZOREC, R., RODRIGUEZ, J. J. & PARPURA, V. 2016. PATHOBIOLOGY OF NEURODEGENERATION: THE ROLE FOR ASTROGLIA. *Opera Med Physiol,* 1**,** 13-22.

VERKHRATSKY, A., ZOREC, R., RODRIGUEZ, J. J. & PARPURA, V. 2017. Neuroglia: Functional Paralysis and Reactivity in Alzheimer's Disease and Other Neurodegenerative Pathologies. *Adv Neurobiol,* 15**,** 427-449.

VIJAYAN, V. K., GEDDES, J. W., ANDERSON, K. J., CHANG-CHUI, H., ELLIS, W. G. & COTMAN, C. W. 1991a. Astrocyte hypertrophy in the Alzheimer's disease hippocampal formation. *Exp Neurol,* 112**,** 72-8.

VIJAYAN, V. K., GEDES, J. W., ANDERSON, K. J., CHANG-CHUI, H., ELLIS, W. G. & COTMAN, C. W. 1991b. Astrocyte hypertrophy in the Alzheimer's disease hippocampal formation. *Experimental Neurology,* 112**,** 72-78.

VUORI, K., HIRAI, H., AIZAWA, S. & RUOSLAHTI, E. 1996. Introduction of p130cas signaling complex formation upon integrin-mediated cell adhesion: a role for Src family kinases. *Mol Cell Biol,* 16**,** 2606-13.

WAKASA, S., SHIIYA, N., TACHIBANA, T., OOKA, T. & MATSUI, Y. 2009. A semiquantitative analysis of reactive astrogliosis demonstrates its correlation with the number of intact motor neurons after transient spinal cord ischemia. *J Thorac Cardiovasc Surg,* 137**,** 983-90.

WALZ, W. 2000. Role of astrocytes in the clearance of excess extracellular potassium. *Neurochem Int,* 36**,** 291-300.

WANG, J., WANG, S., LUAN, Y., ZHANG, W., SUN, C., CHENG, G., LI, K., XIN, Q., LIN, Z., QI, T. & KONG, F. 2017. Overexpression of NEDD9 in renal cell carcinoma is associated with tumor migration and invasion. *Oncol Lett,* 14**,** 8021-8027.

WANG, X., LOPEZ, O. L., SWEET, R. A., BECKER, J. T., DEKOSKY, S. T., BARMADA, M. M., DEMIRCI, F. Y. & KAMBOH, M. I. 2015. Genetic determinants of disease progression in Alzheimer's disease. *J Alzheimers Dis,* 43**,** 649-55.

WANG, Y., BI, L., WANG, H., LI, Y., DI, Q., XU, W. & QIAN, Y. 2012. NEDD9 rs760678 polymorphism and the risk of Alzheimer's disease: a meta-analysis. *Neurosci Lett,* 527**,** 121-5.

WEINGARTEN, M. D., LOCKWOOD, A. H., HWO, S. Y. & KIRSCHNER, M. W. 1975. A protein factor essential for microtubule assembly. *Proceedings of the National Academy of Sciences of the United States of America,* 72, 1858-1862.

WITTE, O. N., DASGUPTA, A. & BALTIMORE, D. 1980. Abelson murine leukaemia virus protein is phosphorylated in vitro to form phosphotyrosine. *Nature,* 283**,** 826-31.

WRAY, S., SAXTON, M., ANDERTON, B. H. & HANGER, D. P. 2008. Direct analysis of tau from PSP brain identifies new phosphorylation sites and a major fragment of N-terminally cleaved tau containing four microtubule-binding repeats. *J Neurochem,* 105, 2343-52.

WU, W., HODGES, E., REDELIUS, J. & HOOG, C. 2004. A novel approach for evaluating the efficiency of siRNAs on protein levels in cultured cells. *Nucleic Acids Res*, 32, e17.

XING, Y. Y., YU, J. T., YAN, W. J., CHEN, W., ZHONG, X. L., JIANG, H., WANG, P. & TAN, L. 2011. NEDD9 is genetically associated with Alzheimer's disease in a Han Chinese population. *Brain Res,* 1369**,** 230-4.

XIA, C., BRAUNSTEIN, Z., TOOMEY, A. C., ZHONG, J. & RAO, X. 2017. S100 Proteins As an Important Regulator of Macrophage Inflammation. *Front Immunol,* 8, 1908.

XU, W., LU, J., ZHAO, Q., WU, J., SUN, J., HAN, B., ZHAO, X. & KANG, Y. 2019. Genome-Wide Plasma Cell-Free DNA Methylation Profiling Identifies Potential Biomarkers for Lung Cancer. *Dis Markers,* 2019**,** 4108474.

YAMADA, M., HIROTSUNE, S. & WYNSHAW-BORIS, A. 2010. The essential role of LIS1, NDEL1 and Aurora-A in polarity formation and microtubule organization during neurogensis. *Cell Adh Migr,* 4**,** 180-4.

YAMANAKA, K. & KOMINE, O. 2018. The multi-dimensional roles of astrocytes in ALS. *Neurosci Res,* 126**,** 31-38.

YANG, Z. & WANG, K. K. 2015. Glial fibrillary acidic protein: from intermediate filament assembly and gliosis to neurobiomarker. *Trends Neurosci,* 38**,** 364-74.

YARDAN, T., ERENLER, A. K., BAYDIN, A., AYDIN, K. & COKLUK, C. 2011. Usefulness of S100B protein in neurological disorders. *J Pak Med Assoc,* 61**,** 276-81.

YEH, C. Y., VADHWANA, B., VERKHRATSKY, A. & RODRIGUEZ, J. J. 2011. Early astrocytic atrophy in the entorhinal cortex of a triple transgenic animal model of Alzheimer's disease. *ASN Neuro,* 3**,** 271-9.

YOUN, G. S., JU, S. M., CHOI, S. Y. & PARK, J. 2015. HDAC6 mediates HIV-1 tat-induced proinflammatory responses by regulating MAPK-NF-kappaB/AP-1 pathways in astrocytes. *Glia,* 63**,** 1953-1965.

ZHANG, H., KOLB, F. A., JASKIEWICZ, L., WESTHOF, E. & FILIPOWICZ, W. 2004. Single processing center models for human Dicer and bacterial RNase III. *Cell,* 118**,** 57-68.

ZHANG, S., WU, M., PENG, C., ZHAO, G. & GU, R. 2017. GFAP expression in injured astrocytes in rats. *Experimental and therapeutic medicine,* 14, 1905-1908.

ZHANG, Y., SLOAN, S. A., CLARKE, L. E., CANEDA, C., PLAZA, C. A., BLUMENTHAL, P. D., VOGEL, H., STEINBERG, G. K., EDWARDS, M. S. B., LI, G., DUNCAN, J. A., 3RD, CHESHIER, S. H., SHUER, L. M., CHANG, E. F., GRANT, G. A., GEPHART, M. G. H. & BARRES, B. A. 2016. Purification and Characterization of Progenitor and Mature Human Astrocytes Reveals Transcriptional and Functional Differences with Mouse. *Neuron*, 89, 37-53.

ZHAO, X., ZHOU, K.-S., LI, Z.-H., NAN, W., WANG, J., XIA, Y.-Y. & ZHANG, H.-H. 2018. Knockdown of Ski decreased the reactive astrocytes proliferation in vitro induced by oxygen-glucose deprivation/reoxygenation. *Journal of Cellular Biochemistry,* 119**,** 4548-4558.

ZHONG, J., BACH, C. T., SHUM, M. S. & O'NEILL, G. M. 2014. NEDD9 regulates 3D migratory activity independent of the Rac1 morphology switch in glioma and neuroblastoma. *Mol Cancer Res,* 12**,** 264-73.

ZHONG, J., BAQUIRAN, J. B., BONAKDAR, N., LEES, J., CHING, Y. W., PUGACHEVA, E., FABRY, B. & O'NEILL, G. M. 2012. NEDD9 stabilizes focal adhesions, increases binding to the extra-cellular matrix and differentially effects 2D versus 3D cell migration. *PLoS One,* 7**,** e35058.

ZHOU, B., ZUO, Y. X. & JIANG, R. T. 2019. Astrocyte morphology: Diversity, plasticity, and role in neurological diseases. *CNS Neurosci Ther,* 25**,** 665-673.

ZHOU, S., XU, M., SHEN, J., LIU, X., CHEN, M. & CAI, X. 2017. Overexpression of NEDD9 promotes cell invasion and metastasis in hepatocellular carcinoma. *Clin Res Hepatol Gastroenterol,* 41**,** 677-686.

ZOREC, R., HORVAT, A., VARDJAN, N. & VERKHRATSKY, A. 2015. Memory Formation Shaped by Astroglia. *Frontiers in Integrative Neuroscience,* 9.

ZOVKIC, I. B., GUZMAN-KARLSSON, M. C. & SWEATT, J. D. 2013. Epigenetic regulation of memory formation and maintenance. *Learn Mem,* 20, 61-74.